# Exploring the potential of novel Pellino2-targeted compounds to control pathways and cells that drive inflammation and cancer

by

**XINYUAN WANG**

A thesis presented to Maynooth University

for the degree of Doctor of Philosophy

Kathleen Lonsdale Institute for Human Health Research

Department of Biology

Maynooth University


June 2023

Research Supervisor: Prof. Paul Moynagh

Head of Department: Prof. Paul Moynagh

# Declaration

This thesis has not been previously submitted to this or any other university for examination for a higher degree. The work presented here is entirely my own except where otherwise acknowledged. This thesis maybe available for consultation within the university library. It may be copied or lent to other libraries for purpose of consultation.

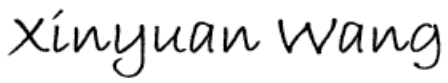

---

XINYUAN WANG

# Contents

# Acknowledgement

Firstly, I would like to express my sincere gratitude to Paul for his unwavering patience and continuous support throughout this entire journey. I am truly thankful for the invaluable opportunity you have provided me with to pursue my PhD degree. Your consistent attention to my experimental developments and insightful advice have been instrumental in guiding me and enabling timely adjustments to the direction of my experiments. Furthermore, your meticulous review and corrections have played a pivotal role in the successful completion of my PhD thesis.

I would like to extend my appreciation to Nezira. Thanks for your hard work and dedication, the laboratory is able to function in a proper and orderly manner. Additionally, I am deeply grateful for the care you have extended towards me over the past four years, greatly facilitating my integration into Irish life. Thanks, my “Irish mom”.

A special thank you goes out to everyone in the Molecular Immunology Lab. To Lu Yang, Thank you for all your help over the past four years. your assistance over the past four years has been invaluable. Your guidance has greatly contributed to the seamless execution of my experiments, and your active involvement in discussing the direction of my projects has provided me with valuable insights. You have been instrumental in teaching me to approach problems from different perspectives, inspiring my research thinking along the way. To Devlin, Dr. Coughlan, my homie, my dawg, my dear friend, I cannot thank you enough for your assistance with my experiments and thesis writing.

Moreover, I am grateful for the joyous experiences we have shared, exploring the breathtaking landscapes of various parts of Ireland. Can not say anything more to show my love to you, bro. I would also like to thank to Jian Li, Linan Xu and Karyn, for your unwavering support in helping me overcome the challenges I encountered along this journey.

I would also like to express my heartfelt gratitude to my parents, my mother Hong Zhang and my father Jun Wang. Your unwavering respect for my choices and unwavering support in my studies have been truly remarkable. Throughout my 20 years of education, you have provided me with boundless care, attention, and understanding. Your constant presence and unwavering support have been my pillars of strength. I will forever cherish and love you both.

Lastly, I would like to thank myself for doing all these hard work. I would like to thank myself for not settling for mediocrity at every crossroad during my educational journey. I would like to thank myself for never giving up, even during moments of occasional procrastination. I would like to thank myself for my enduring curiosity that kept me engaged in countless days and nights spent in the lab. I would like to thank myself for my fearless attitude towards the unknown and my unwavering desire to explore new horizons. I would like to thank to myself for my resilient spirit, never succumbing to loneliness, self-doubt, and always maintaining faith that tomorrow will bring better opportunities. I would also like to thank myself for prioritizing physical fitness, abandoning the detrimental habit of smoking, and adhering to a healthy diet and routine to ensure my physical well-being. (Regrettably, I must admit that I may not be able to forsake sweets for the rest of my life.)

# Abstract

Small molecule drugs have emerged as valuable therapeutic agents in the treatment of inflammation and cancer. However, there is still a need to identify additional molecular targets amenable to therapeutic exploitation. Pellino proteins form a three-membered family of E3 ubiquitin ligases, and an understanding of their crucial roles in regulating innate immunity and cancer is emerging. This understanding is largely gleaned from the use of experimental models, ranging from over-expression studies and gene knockdown/knockout approaches in cell models and the use of Pellino-deficient mice in disease models. Despite this, the potential to pharmacologically target Pellino proteins for therapeutic application in the treatment of inflammatory diseases or cancer remains largely unexplored. No candidate molecules have been described to date that effectively mimic or promote their function. However, recent work from my host laboratory has led to the design of two novel compounds intended to target Pellino proteins, especially Pellino2. This body of work aimed to investigate the regulatory effects of these novel compounds on the pathways and cells that drive inflammation, inflammatory diseases, and colorectal cancer. Initial studies identified that both compounds effectively inhibit inflammatory responses by targeting and facilitating the degradation of IRAK1. This led to the down-regulation of the NF-κB signaling pathway and the suppression of the expression of pro-inflammatory cytokines (e.g., IL-1β, IL-6, and TNFα) in a Pellino2-dependent manner. These effects were manifested at non-cytotoxic concentrations. Further studies supported a novel role for Pellino2 in protecting against pro-tumorigenic effects in colorectal cancer. The research revealed a down-regulation of human *Pellino2* mRNA in colorectal cancer patients and cells, and

a deletion of the Pellino2 gene in mice led to an increased tumor burden in preclinical models of colorectal cancer. The studies also demonstrated that human Pellino2 suppresses the growth and proliferation of colorectal cancer cells by promoting cell apoptosis. In promoting this pro-apoptotic effect, Pellino2 was shown to target the ubiquitination and degradation of Bcl-xL. Interestingly, while neither of the novel compounds designed to target Pellino2 consistently inhibited colorectal cancer cell growth, they did enhance the sensitivity of colorectal cancer cells to the cytotoxic effects of the chemotherapeutic agent Cisplatin in a Pellino2-dependent manner. Overall, this work reveals the promising potential of these novel compounds in targeting the pathways and cells that drive inflammatory diseases and colorectal cancer. It also highlights Pellino proteins as potential therapeutic targets in the development of innovative anti-inflammatory and anti-cancer therapeutics.

# Abbreviations

| | |
|---|---|
| APC | Antigen presenting cells |
| AP-1 | Activator protein 1 |
| APPs | Acute phase proteins |
| AIF | Apoptosis inducing factor |
| APS | Ammonium persulfate |
| AKT | Protein kinase B |
| ASC | Apoptosis-associated Speck-like Protein |
| ATP | Adenosine 5′-triphosphate |
| Bcl-2 | B-cell lymphoma-2 |
| Bcl-xL | B-cell lymphoma-extra-large |
| BIM | Bcl-2 Interacting Mediator |
| BID | BH3 Interacting Domain |
| BMDM | Bone marrow-derived macrophage |
| BCA | Bicinchoninic acid |
| BSA | Bovine Serum Albumin |
| CRP | C-reactive protein |
| CLRs | C-type lectin receptors |
| COX1/2 | Cyclooxygenase1/2 |
| CRC | Colorectal cancer |
| CIN | Chromosomal instability |
| CD | Crohn's disease |
| cDNA | Complementary DNA |

| | |
|---|---|
| Co-IP | Co-Immunoprecipitation |
| DAMPs | Damage-associated molecular patterns |
| DNA | Deoxyribonucleic acid |
| DMSO | Dimethyl sulfoxide |
| DTT | Dithiothreitol |
| DIABLO | Direct IAP Binding protein with Low pI |
| DISC | Death-Inducing Signaling Complex |
| ERK | Extracellular signal-regulated kinase |
| EAE | Experimental autoimmune encephalomyelitis |
| EMT | Epithelial–mesenchymal transition |
| ELISA | Enzyme-linked immunosorbent assay |
| EDTA | Ethylenediaminetetraacetic acid |
| *E.coli* | *Escherichia* |
| EV | Empty vector |
| FHA | Forkhead-associated |
| FBS | Fetal bovine serum |
| GIT | Gastrointestinal tract |
| g | Gravitation |
| HIF-1α | Hypoxia-inducible factor 1α |
| HtrA2 | Omi/high temperature requirement protein A |
| h | Hour |
| HEK | Human embryonic kidney |
| HPRT | Hypoxanthine-guanine phosphoribosyltransferase |
| HRP | Horseradish-peroxidase |
| IB | Immunoblot |
| IL-1β | Interleukin-1β |
| IL-6 | Interleukin-6 |
| IRAK4/2/1 | IL-1 receptor-associated kinase 4/2/1 |
| IKKs | IκB kinases |

| | |
|---|---|
| IκB | Inhibitor of κB |
| kD | Kilodalton |
| IAPs | Inhibitors of apoptosis |
| IC50 | Half-maximal inhibitory concentration |
| IP | Immunoprecipitation |
| IBD | Inflammatory bowel disease |
| IRF3 | Interferon regulatory factor 3 |
| JNK | c-Jun N-terminal kinase |
| LRRs | Leucine-rich repeats |
| LPS | Lipopolysaccharides |
| LDH | Lactate dehydrogenase |
| MD-2 | Myeloid differentiation factor 2 |
| MAC | Membrane attack complex |
| MHC | Major Histocompatibility Complex |
| MEFs | Mouse embryonic fibroblasts |
| MyD88 | Myeloid differentiation factor 88 |
| MAPK | Mitogen-activated protein kinase |
| MSI | Microsatellite instability |
| M-CSF | Macrophage colony-stimulating factor |
| MTT | 3-(4,5-Dimethylthiazol-2-yl)-2,5-Diphenyltetrazolium Bromide |
| min | Minute |
| ml | Milliliter |
| mRNA | Messenger RNA |
| $Na_3VO_4$ | Sodium orthovanadate |
| NaCl | Sodium chloride |
| NLRs | Nucleotide-binding oligomerization domain (NOD)-like receptors |
| NF-κB | Nuclear factor-kappa B |
| NSAIDs | Non-steroidal anti-inflammatory drugs |

| | |
|---|---|
| NLRP3 | Intracellular "NOD-like" receptor (NLR) protein 3 |
| ng | Nanogram |
| OD | Optical density |
| PAMP | Pathogen-associated molecular patterns |
| PRRs | Pattern recognition receptors |
| PYHIN | Pyrin and HIN domain-containing protein |
| PTC | Papillary thyroid cancer |
| PS | Phosphatidylserine |
| PUMA | p53 upregulated modulator of apoptosis protein |
| PBS | Phosphate buffered saline |
| PCR | Polymerase chain reaction |
| PMSF | Phenylmethylsulphonyl fluoride |
| PI | propidium iodide |
| PAGE | Polyacrylamide gel electrophoresis |
| PARP | Poly (ADP-ribose) polymerase |
| PELI1/2/3 | Pellino1/2/3 |
| RLRs | Retinoic acid-inducible gene I (RIG-I)-like receptors |
| RIP2 | Receptor-interacting-serine/threonine-protein kinase 2 |
| RIPA lysis buffer | Radioimmunoprecipitation lysis buffer |
| SAA | Serum amyloid A |
| Smac | Second mitochondria-derived activator of caspase |
| Slug | Zinc finger protein |
| Snail | Zinc finger protein SNAI1 |
| shRNA | Short hairpin RNA |
| SDS | Sodium Dodecyl Sulfate |
| sec | Second |
| TLRs | Toll-like receptors |
| TNFα | Tumor necrosis factor α |
| TRAF6 | Tumor necrosis factor receptor-associated factor 6 |

| | |
|---|---|
| TAK1 | Growth factor (TGF)-β-activated kinase 1 |
| TAB1/4 | TAK-binding proteins1/4 |
| TRIF | TIR-domain-containing adapter-inducing interferon-β |
| TEMED | Tetramethyl ethylenediamine |
| TBS | tris-buffered saline |
| TMB | 3,3′,5,5′-Tetramethylbenzidine |
| TAE | Tris-acetate-EDTA |
| UC | Ulcerative colitis |
| v | Volume |
| µg | Microgram |
| µl | Microliter |
| µM | Micromolar |

# Chapter 1: Introduction

## 1.1 Immune system

The immune system is a complex and dynamic network comprising diverse molecules, cells, and organs that collaborate to carry out specialized functions in protecting the host from pathogenic invaders and infections. Early research has demonstrated that the response of the immune system can be divided into two separate phases: the innate (natural) response and the acquired (adaptive) response (Delves and Roitt 2000). The innate immune response primarily operates quickly in the face of pathogenic threats, involves a diverse set of phagocytic cells such as macrophages, neutrophils, mast cells, dendritic cells, and monocytes, as well as cells that secrete inflammatory mediators including basophils, and eosinophils. These effector cells are involved in the recognition of specific conserved pathogenic components, allowing for a broad range of pathogenic targets to be rapidly neutralized by natural killer cells and other innate immune components. (Gasteiger et al. 2017). In addition, the innate immune response also involves a large number of molecular components including complement, acute-phase proteins and cytokines such as Interleukin-1β (IL-1β), Tumor necrosis factor alpha (TNFα), Interleukin-6 (IL-6) and interferons (Strieter, Belperio, and Keane 2002b; Lacy and Stow 2011). In contrast to the rapidly and non-specific nature of innate immune responses, acquired immune responses are mediated by antigen-specific B- and T-lymphocytes that undergo proliferation and clonal expansion, resulting in a delayed response to the pathogenic challenge. The activation of these cells occurs through the recognition of the antigen by the surface receptors on lymphocytes, a

process that initiates a series of complex signaling events, resulting in the production of highly specialized effector cells with the ability to specifically target and eliminate the pathogenic invader (Chaplin 2010). The T-cell response needs specialized cells, called antigen presenting cells (APCs), such as macrophages and dendritic cells (Braciale, Sun, and Kim 2012), to present the antigen to the T-cells and react with T-cells for differentiation, polarization and activation (Kaech, Wherry, and Ahmed 2002; Luckheeram et al. 2012; Mahnke et al. 2013; Mittrucker, Visekruna, and Huber 2014). After the activation of T-cells, the activated T-cells assist the B-cells to start to produce (Hoffman, Lakkis, and Chalasani 2016) and secrete immunoglobulins, the antigen-specific antibodies responsible for eliminating extracellular microorganisms (Akkaya, Kwak, and Pierce 2020; Cyster and Allen 2019). Activated T-cells can also help clear the intracellular pathogens by activating macrophages and by killing virally infected cells (Hilhorst et al. 2014; Roberts, Dickinson, and Taams 2015; Underhill et al. 1999). As the body of research in this field has expanded, it has become clear that the traditional classification between the innate and acquired immune responses is no longer applicable to current research. Rather than functioning independently, these two different immune responses engage in a complex communication and coordination to eliminate pathogenic threats. This crosstalk and interaction between the innate and acquired immune responses is important for the effective resolution of infections, and represents a key area of ongoing investigation in the field of immunology.

### 1.1.1 Innate immune system

The innate immune system represents an ancient component of the body's defense system and is the first line of defense against a variety of pathogenic threats. This system provides rapid and non-specific protection against a broad range of potential pathogens, including bacteria, viruses, fungi, and parasites, that are able to penetrate the physical barriers of the skin and mucous membranes and invade the body's internal environment (Chaplin 2010; Coates, Blanchard, and MacLeod 2018; Delves and Roitt 2000; Nigam et al. 2012). The innate immune system has conventionally been defined

as consisting of all immune defenses that do not exhibit immunological memory. However, recent research has introduced the concept of "Trained Immunity" to describe and reference memory-like characteristics within the innate immune system. Upon exposure to specific stimuli, innate immune cells exhibit the capacity to adapt their responses to subsequent challenges. This adaptive process leads to an amplified reaction when faced with previously encountered infectious agents (Gasteiger et al. 2017).

#### 1.1.1.1 Cellular components of innate immune responses

The cellular component is a fundamental and important part of the innate immune response, in which different types of cell act in concert to provide a rapid and effective defense against invading pathogens. These cellular effectors play an important role in detecting, neutralizing, and eliminating pathogenic agents from the body, while also activating and modulating the adaptive immune response for a coordinated and effective defense (Gasteiger et al. 2017).

Phagocytes is a collective term for a range of cells in the innate immune system and includes cells such as neutrophils (Rosales 2018; Burn et al. 2021) and monocytes (Kapellos et al. 2019; Guilliams, Mildner, and Yona 2018). Upon recognition of a pathogenic invader, a phagocyte performs a process known as phagocytosis to engulf the foreign pathogen. Following phagocytosis, the pathogen is subjected to a range of antimicrobial substances, such as enzymes and reactive oxygen species, which help to digest and destroy the invader. Ultimately, the phagocyte clears away debris from the pathogen, thus effectively eliminating the threat to the body (Underhill and Goodridge 2012; Gordon 2016). In addition, phagocytes play a role in activating the complement system, a series of proteins that enhance the innate immune response by marking pathogens for destruction and increasing the potency of phagocytes (Dunkelberger and Song 2010).

Macrophages are derived from blood-borne monocytes. They are present in virtually all tissues and capable of recognizing and engulfing pathogens, as well as removing self-cellular debris and dead cells. Once a macrophage has engulfed a pathogen, it uses degradative enzymes and lysosomes to break down the invader and subsequently present peptide fragments on its cell surface to activate the response from the adaptive immune system (Mosser and Edwards 2008; Murray and Wynn 2011; Wynn, Chawla, and Pollard 2013). In the context of macrophage biology, it is evident that macrophages exhibit remarkable adaptability in response to stimulations, thereby manifesting a dynamic spectrum of polarization states, defined by the M1 and M2. M1 macrophages are renowned for their pro-inflammatory attributes, typified by their heightened phagocytic and cytotoxic capabilities. These M1 macrophages can be distinguished by the expression of discernible markers, including major histocompatibility complex (MHC) Class II, cluster of differentiation (CD)15, CD80/CD86, CD38, and inducible nitric oxide synthase (iNOS). Notably, M1 macrophages are robustly producers of pro-inflammatory cytokines such as IL-6, IL-12, IL-1β, and TNF-α, as well as chemokines such as CCL2 and CCL5. This unique cytokine production ability plays important roles in the recruitment and sustained activation of various immune cell types, notably T cells and B cells, to sites of infection and inflammation. Conversely, M2 macrophages exhibit distinct functional properties, primarily directed towards the resolution of inflammatory processes and active participation in tissue repair pathways. These M2 macrophages are characterized by the presence of specific cell surface markers, namely CD36, CD206, and CD163, which underscore their unique regulatory and reparative functions in the context of tissue homeostasis and repair. (Murray and Stow 2014; Stow et al. 2009; Xu et al. 2022).

Dendritic cells (DC cells) represent a distinct population of antigen-presenting cells that possess the special capacity to detect and process pathogenic antigens and then present these molecules to the adaptive immune system. This function of DC cells establishes a critical bridge between the innate and adaptive immune responses. DC cells recognize the invading pathogen, phagocytose the foreign invader and subsequently processes its

associated antigens. These processed antigens are then displayed on the surface of DC cells, where they are ready to be recognized by T and B lymphocytes, the central effectors of the adaptive immune response (Galamb, Molnar, and Tulassay 2003; Ardavin, Amigorena, and Reis e Sousa 2004; Mohty and Gaugler 2003; Thomson et al. 2002).

Natural Killer (NK) cells are capable of killing infected and malignant cells through a process that does not require advanced sensitization or activation by antigens (Delves and Roitt 2000). NK cells express a range of receptors that allow them to detect changes on infected cells by a mix of inhibitory and activating receptors on their surface. The inhibitory receptors like KIR (Killer-cell immunoglobulin-like receptor) and CD94-NKG2A heterodimer on the surface of NK cells bind to MHC class I molecules on normal healthy cells, signaling to the NK cell that the target cell is not infected. On the other hand, when MHC class I expression is lost or reduced on the surface of infected or abnormal cells, activating receptors NCRs (Natural cytotoxicity receptors) and NKG2D on the surface of the NK cell binds to these cells and recognize these cells are potential targets (Lanier 2005; Abel et al. 2018). NK cells also use other receptors to recognize infected or abnormal cells. These receptors can recognize specific viral antigens, changes in cell surface markers, or the release of cytokines or other signals associated with cellular stress or injury. Once an infected cell is detected, the NK cell releases cytokines and other effector molecules to induce cell death (Lanier 2005).

Mast cells respond to pathogens by releasing a range of mediators, including histamine, proteases, and cytokines. These substances work to eliminate the invading pathogens and coordinate the innate immune response. Mast cells have also been linked to atopic allergies, such as eczema, hay fever, and asthma. In addition to their innate immune functions, mast cells can also activate the adaptive immune response by attracting and stimulating antigen-presenting cells, such as dendritic cells (Krystel-Whittemore, Dileepan, and Wood 2015).

#### 1.1.1.2 Soluble factors in the innate immune response

The soluble factors involved in the innate immune response are a range of proteins and other molecules that are released by immune cells and play an important role in the response to pathogens. These factors can act on their own or work with other immune cells to help eliminate pathogens and promote tissue repair.

Complement is a series of proteins that are activated in response to the presence of pathogens and by a number of different mechanisms, including the binding of antibodies to pathogens, the binding of specific pattern recognition receptors on immune cells to pathogen-associated molecular patterns (PAMPs), and the direct binding of complement proteins to pathogens. Once complement has been activated, the complement proteins form a cascade of reactions that result in the formation of the membrane attack complex (MAC), a complex of proteins that destroy the membrane of the pathogen and induces lysis. The complement system can also promote phagocytosis of pathogens by attracting phagocytes to the site of infection and by marking pathogens for destruction. In addition to these direct effects on pathogens, the complement system can also directly regulate the strength of the immune response (Dunkelberger and Song 2010; Sarma and Ward 2011; Merle, Church, et al. 2015; Merle, Noe, et al. 2015).

Cytokines constitute another group of soluble mediators in the innate immune response. They are produced by a variety of immune cells, including macrophages (Arango Duque and Descoteaux 2014; Lacy and Stow 2011; Murray and Stow 2014), dendritic cells (Blanco et al. 2008), and mast cells (Mukai et al. 2018). Cytokines are multifunctional signaling molecules that mediate the connection between the immune system and other physiological systems and regulating the immune response. These molecules act as central organizers within the immune system, creating a complex network involved in immune response regulation. Cytokines perform a range of different activities in immune response. Primarily, cytokines demonstrate the capability to facilitate immune cell recruitment. It has been substantiated through research that

TNF has the potential to induce vasodilation and enhance vascular permeability, thereby fostering the infiltration of lymphocytes, neutrophils, and monocytes. This process is pivotal in recruiting these immune cells to sites of inflammation, and it is achieved through the regulation of chemokine release (Griffin et al. 2012). Additionally, IL-6 trans signaling has been observed to play a role in the recruitment of monocytes to sites of inflammation. IL-6 trans signaling not only aids in monocyte recruitment but also supports the maintenance of Th17 cells while inhibiting T cell apoptosis and the development of regulatory T cells (Scheller et al. 2011). Cytokines also play a crucial role in the regulation of immune cells. For example, serves as a chemoattractant for granulocytes and is involved in the expansion and differentiation of CD4 T cells (Arango Duque and Descoteaux 2014). Similarly, has been identified to trigger the expression of chemokines, such as CXCL1, CXCL2, and CXCL5, which attract neutrophils (Griffin et al. 2012) and also augments the expression of cell adhesion molecules that facilitate diapedesis, the process of immune cell migration through blood vessel walls (Vieira et al. 2009). Furthermore, cytokines are pivotal in initiating and modulating the inflammatory response as well as regulating the immune response. research has indicated that IL-1β induces the release of histamine in mast cells, leading to vasodilation and localized inflammation. IL-1β also stimulates the production of acute phase proteins from the liver and acts on the central nervous system to induce fever and prostaglandin secretion (Arango Duque and Descoteaux 2014). In a separate study, IL-12 was found to promote cell-mediated immunity by stimulating Th1 cells. IL-12 synergizes with TNF and other proinflammatory cytokines, thus enhancing interferon-gamma (IFN-γ) production and the cytotoxicity of natural killer (NK) cells and CD8 T cells (Arango Duque and Descoteaux 2014; Blanco et al. 2008; Strieter, Belperio, and Keane 2002a; Miller et al. 2011). Cytokines can be pro-inflammatory or anti-inflammatory in function, depending on their role in the inflammatory response. Pro-inflammatory cytokines, such as IL-1β, IL-6 and TNFα, play a role in driving the inflammatory process in the immune response while anti-inflammatory cytokines like IL-4, IL-10 and IL-13 counteract the effects of pro-inflammatory cytokines and promote resolution of inflammation (Dodoo et al. 2002). These two types of cytokines

regulate each other to maintain the balance of immune response intensity.

Acute phase proteins (APPs) are a group of proteins produced by the liver and are highly expressed in the blood in response to inflammation or infection, helping to defend the host against pathogens and by regulating the immune response. APPs include proteins such as the C-reactive protein (CRP), serum amyloid A (SAA), and ferritin (Mantovani and Garlanda 2023; Sander et al. 2010).

### 1.1.2 Pattern recognition receptors (PRRs)

Pattern recognition receptors (PRRs) are a class of proteins located on the surface of immune cells that are responsible for recognizing pathogen-associated molecular patterns (PAMPs) of invading pathogens, including those of bacterial, viral, fungal, and parasitic origin, and drive innate immune responses that aim to efficiently remove the pathogen. PRRs can also recognize molecules called damage-associated molecular patterns (DAMPs) (Amarante-Mendes et al. 2018). PRRs distinguishes between self and non-self molecules and initiates the innate immune response. There are five major sub-families of PRRs described to date (Li and Wu 2021): Toll-like receptors (TLRs), nucleotide-binding oligomerization domain (NOD)-like receptors (NLRs), Retinoic acid-inducible gene I (RIG-I)-like receptors (RLRs), Pyrin and HIN domain-containing protein (PYHIN) family and C-type lectin receptors (CLRs). Each family consists of several members and all recognizing a range of PAMPs and DAMPs. Once the pathogen or molecules that released by damage cells is recognized by PRRs, it triggers a series of complex signaling cascades that lead to the activation of the immune cells. This results in the production of cytokines including interferons and interleukins. These cytokines help to activate other immune cells and initiate the innate immune response to effect the elimination of the pathogen (Broz and Monack 2013).

### 1.1.3 Toll-like receptors (TLRs)

Toll-like receptors were the first family of PRRs to be discovered. Their discovery arose from early studies showing that mutations in a Drosophila gene called *Toll* led to a reduced ability of the fly to fight infections (Rock et al. 1998). This then led to the discovery of a mammalian homologue of Toll that was termed Toll-like receptor (TLR) (now known as TLR4) and subsequently a family of these receptors known as TLRs (Govind 2008; Wu, Zhang, and Huang 2010; O'Neill, Golenbock, and Bowie 2013). TLRs are transmembrane proteins that are expressed on the surface of immune cells or in endosomal compartments. TLRs consist of extracellular leucine-rich repeats (LRRs), a cytosolic Toll/IL-1R (TIR) domain, a transmembrane domain and a cytoplasmic tail (Fig1.1). The repeating LRR sequences form a characteristic "basket-like" structure that is responsible for recognizing and binding the PAMPs, the membrane spanning component anchors the TLRs to the cell membrane and separates the extracellular and intracellular domains. The TIR domain is responsible for transmitting the signal from the extracellular domain to the intracellular signaling pathways and the cytoplasmic tail contains various binding sites for intracellular signaling molecules that are involved in the initiation and regulation of the innate immune response (Ohto 2016; Medzhitov 2001). There are 10 human TLRs (12 mice TLRs) that have been identified to date, These TLRs all recognize unique pathogens while there is also cross-linking between their functions (Medzhitov 2001).

TLR4 was the first TLR to be discovered and acts as the receptor for lipopolysaccharides (LPS), a component of the cell wall of gram-negative bacteria (Medzhitov 2001). Mutations in the *TLR4* gene results in impaired LPS recognition (Heine et al. 1999). LPS is a large, complex molecule that is found on the outer surface of the cell wall of Gram-negative bacteria. It is composed of a lipid portion (lipid A) and a polysaccharide portion. The lipid A portion is responsible for the toxic effects of LPS like sepsis, endocarditis, and meningitis and makes LPS and its signaling an important area of research (Bertani and Ruiz 2018). When LPS binds to TLR4, it leads

to a signaling cascade that results in the activation of immune cells and the production of cytokines and other signaling molecules (Medzhitov 2001; Li and Wu 2021). This initiation of the innate immune response helps to prevent the spread of bacterial infections. However, over-activation of TLR4 can also lead to an excessive and chronic immune response, which can result in sepsis and other inflammatory disorders (Miller, Ernst, and Bader 2005; Molteni, Gemma, and Rossetti 2016). For these reasons, the regulation of TLR4 signaling is critical for maintaining a healthy immune response and preventing the development of immune-mediated conditions.

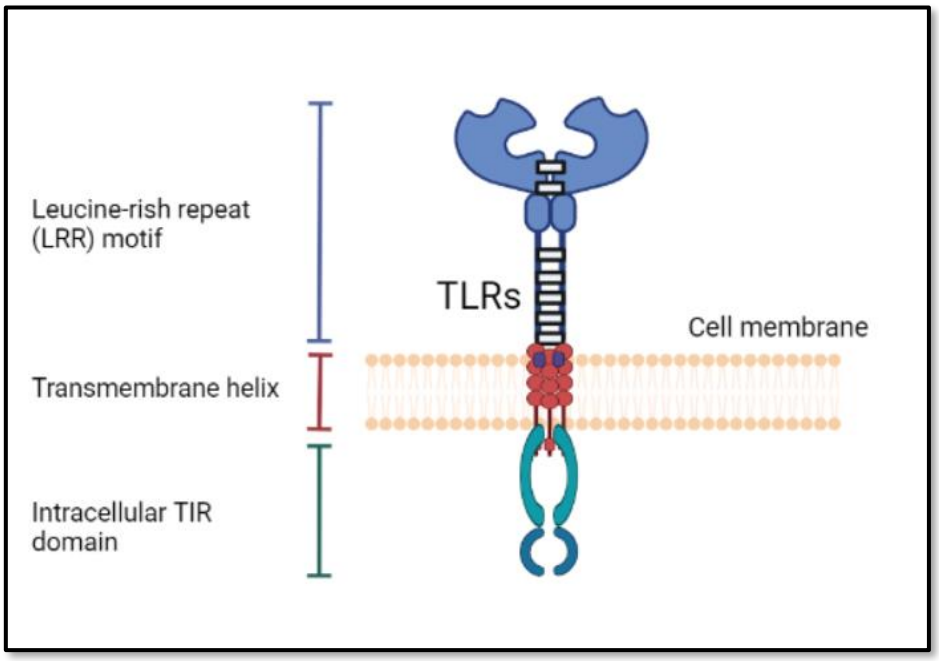


**Fig1.1 Schematic TLR receptors structure**

**TLRs consist of extracellular leucine-rich repeats (LRRs), a cytosolic Toll/IL-1R (TIR) domain and a transmembrane domain.**

### 1.1.4 LPS/TLR4 signal transduction

#### 1.1.4.1 Signaling pathways activation

LPS-induced signal transduction is a complex network involving adaptor proteins, protein kinases and transcription factors (Akira, Takeda, and Kaisho 2001; Lu, Yeh, and Ohashi 2008; Medzhitov 2001; Ohto 2016; Park and Lee 2013). These signaling pathways are geared towards activation of transcription factors that will drive the transcription of a plethora of genes, such as pro-inflammatory cytokines IL-1β, IL-6, TNFα and IFN.

One of the most important transcription factors activation by TLR4 is Nuclear factor-kappa B (NF-κB) so named after it was first discovered to be involved in the transcription of B cell κ chain genes (Sen and Baltimore 1986). NF-κB is a heterodimer composed of two molecules, the most common of which are p50 and p65 (Urban and Baeuerle 1991; Giridharan and Srinivasan 2018), NF-κB is present in the cytoplasm in an inactive form and is complexed to the inhibitory protein known as IκBs under normal conditions (P A Baeuerle and Henkel 1994). After LPS binds to the TLR4 and its co-receptor MD-2, myeloid differentiation factor 88 (MyD88) is rapidly recruited to the receptor via interaction of Toll/IL-1R (TIR) domains which are present in both MyD88 and TLR4 (Moynagh 2014). IL-1 receptor-associated kinase 4 (IRAK4) is also recruited to the receptor complex through a death domain interaction with MyD88 followed by recruitment of IRAK1 and IRAK2 (Motshwene et al. 2009; Li et al. 2002). This is followed by recruitment of an E3 ubiquitin ligase called tumor necrosis factor receptor-associated factor 6 (TRAF6) to form a complex with transforming growth factor (TGF)-β-activated kinase 1 (TAK1) and TAK-binding proteins (TAB1 and TAB4) (Wi et al. 2014; Dong et al. 2006). TRAF6 is degraded due to its own ubiquitination (Zhou et al. 2010; Zhao et al. 2012; Lin et al. 2013)and the TAK1-TAB1-TAB4 complex activates the IκB kinases (IKKs) through phosphorylation. Activated IKKs phosphorylates IκBs, leading to their ubiquitination and degradation (Chen 2012;

Emmerich et al. 2013). NF-κB is released and translocates to the nucleus, thereby regulating the transcription of inflammatory genes involved in the production of pro-inflammatory cytokines and chemokines, such as TNFα, IL-1β, and IL-6, which trigger an inflammatory response and help to eliminate invading pathogens (Cerretti et al. 1992; Ghayur et al. 1997; Pu and Wang 2014). TLR4 can also use a MyD88 independent way to trigger downstream activation of NF-κB (Kuriakose et al. 2019). When LPS binds to the TLR4, it can recruit another TIR domain-containing protein called TIR-domain-containing adapter-inducing interferon-β (TRIF) to trigger activation of NF-κB in a receptor-interacting serine/threonine-protein kinase 1 (RIP1) dependent manner (Kawai and Akira 2007). TRIF can also activate members of the interferon regulatory factor (IRF) family of transcription factors including interferon regulatory factor 3 (IRF3) that can induce antiviral cytokines such as interferons (Fig 1.2) (Tong et al. 2020).

In addition to the NF-κB signaling pathway, TLR4 can also active the mitogen-activated protein kinase (MAPK) pathway. MAPKs is a group of serine-threonine proteins kinases that can be activated by different extracellular stimulation (Soares-Silva et al. 2016). Three main subsets have been identified and well-studied: Extracellular signal-regulated kinase (ERK), c-Jun N-terminal kinase (JNK)/SAPK and P38 MAPK. When LPS binds to TLR4, IRAK1 is activated by phosphorylation and interacts with TRAF6, and as well as activating the IKK complex, it can also activate the MAPKs. In addition, MAPK signaling pathways can also be activated by the MyD88 independent way (Fig 1.2) (Moynagh 2005).

Activated MAPKs can activate transcription factors, such as c-Fos and activator protein 1 (AP-1), that bind to specific DNA sequences in the promoter region of target genes, leading to the transcription of genes involved in the production of pro-inflammatory cytokines and chemokines. NF-κB and MAPK signaling pathways can integrate and work together to trigger the production of a large array of pro-inflammatory proteins in response to LPS stimulation (Frigo et al. 2004; Whitmarsh and Davis 1996; Karin 1996).

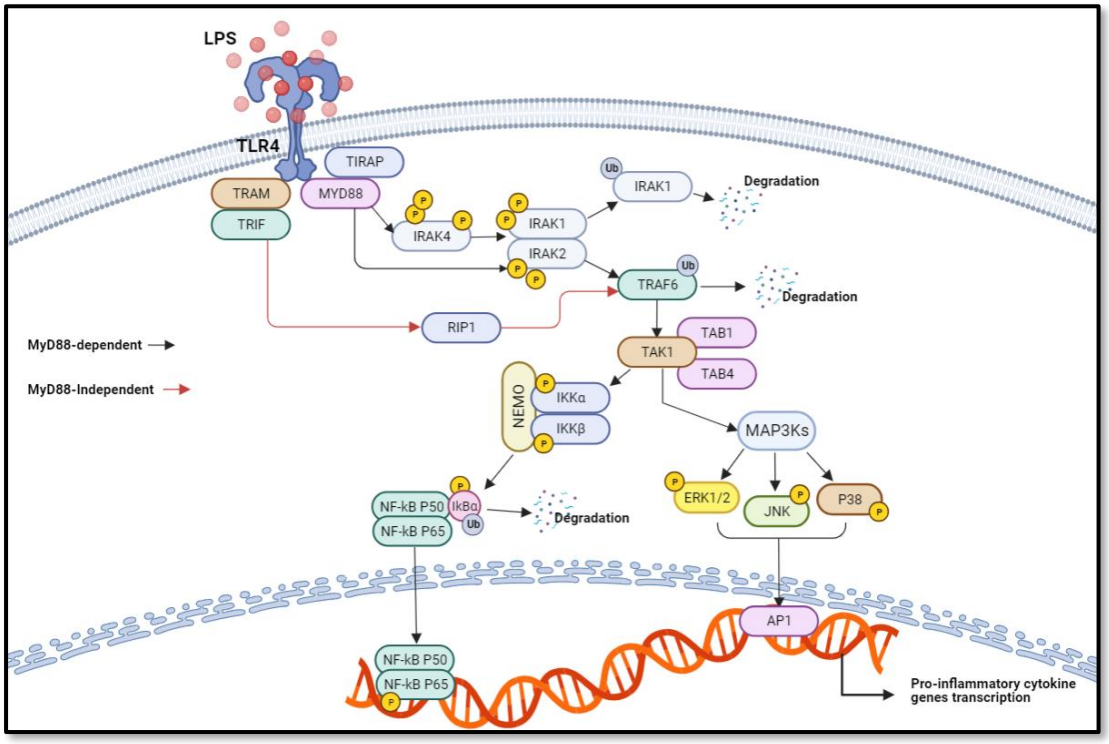


**Fig1.2 Signaling pathways activated by LPS/TLR4**

**Described in detail in section 1.14, LPS binds to TLR4 to activate the NF-κB and MAPKs signaling pathway through the MyD88-dependent and inpdepedent mechanisms ultramately leading to the activation of pro-inflammatory cytokine genes transcription.**

### 1.1.4.2 The role of IRAK1 in LPS/TLR4-induced NF-κB activation

Interleukin-1 receptors-associated kinase 1 (IRAK1) is a member of IRAKs protein family and plays an important kinase in the LPS-induced assembly of myeloid differentiation factor 88 (MyD88) complex and downstream activation of NF-κB. Upon LPS binding to TLR4, MyD88 is rapidly recruited to the receptor and IRAK1 is also recruited to the receptor complex by directly-interacting with MyD88. Binding to MyD88 leads to phosphorylation of IRAK1 at Thr-209 and Thr-387. This results in the activation of IRAK1 kinase activity. Then phosphorylated IRAK1 disengages from the MyD88 complex, and forms a cytosolic IRAK1-TRAF6 complex, TRAF6 then interacts with TAK1 and TAB, resulting in eventual activation of the NF-κB. With the

activation of NF-κB, IRAK1 is modified by K48-linked ubiquitination (The elucidation of ubiquitination is expounded upon in Chapter1.3) that tagged it for degradation by the proteasome, creating a negative feedback regulation of NF-κB activation, so the expression level of IRAK1 and activation of NF-κB are positively correlated (Gottipati, Rao, and Fung-Leung 2008; Yu et al. 2020). The degradation of IRAK1 is contingent upon both IRAK1 kinase activity and its auto-phosphorylation. This phenomenon has been demonstrated by inhibiting IRAK1 kinase activity and using a kinase inhibitor. The loss of IRAK1 protein is due to proteasome mediated degradation as demonstrated by studies using proteasome inhibitors(Yamin and Miller 1997). Nevertheless, it is important to note that LPS/TLR4 signaling can also induce K63-linked ubiquitination of IRAK1. This K63-linked ubiquitination does not to tag IRAK1 for degradation but rather serves a crucial role in LPS/TLR-mediated activation of NF-κB (Gottipati, Rao, and Fung-Leung 2008; Yu et al. 2020). Several reports highlight the involvement of K63-linked ubiquitinated IRAK1 in this process, elucidating that it functions as a molecular scaffold. K63-linked ubiquitinated IRAK1 recruits an IκB kinase (IKK) complex comprising catalytic IKKα and IKKβ, along with their regulatory subunit IKKγ. Notably, IKKγ lacks catalytic activity but is essential for activation of NF-kB (Gottipati, Rao, and Fung-Leung 2008; Yu et al. 2020). It contains a ubiquitin-binding domain that specifically recognizes K63-linked ubiquitinated IRAK1, thus, facilitating IKK–IRAK complex formation as part of TLR and IL-1R signaling (Gottipati, Rao, and Fung-Leung 2008; Yu et al. 2020). These studies indicate a model in which TAK1 is recruited to K63-linked ubiquitin chains on TRAF6 and the IKK complex is recruited to K63-linked polyubiquitin chains on IRAK1. Furthermore, as research progresses, a number of specific E3 ubiquitin ligases responsible for IRAK1 ubiquitination have been identified. Notably, Pellino proteins, recognized as pivotal E3 ubiquitin ligases, have been shown to play a pivotal role in IRAK1 ubiquitination (A comprehensive exploration of Pellino proteins and their relationship with IRAK1 is provided in Chapter 1.3).

### 1.1.5 NLRP3 Inflammasome

The secretion of the pro-inflammatory cytokine IL-1β is subject to tight regulation due to its capacity to induce systemic inflammation. Initially, IL-1β is synthesized as an inactive precursor (pro-IL-1β) and confined to the cytoplasm. Subsequently, it undergoes cleavage and activation mediated by the inflammasome complex, a process which enables its secretion from the cells (van de Veerdonk et al. 2011).

Inflammasomes are large multi-protein complex, located within the cytosol of immune cells, first proposed in 2002. The inflammasome is assembled following the detection of PAMPs and DAMPs, and plays a pivotal role in immune responses. Inflammasome consists of three main components: cytoplasmic sensor proteins (cytoplasmic PRRs), adapter proteins (Apoptosis-associated speck-like protein) and effector caspases (pro-Caspase-1). Inflammasome are classified into various types based on the different sensors proteins. Each type of inflammasome is capable of recognizing different classes of triggers and includes subsets like NLRP1, NLRP3, NLRC4, AIM2, and Pyrin (Broz and Dixit 2016; Zheng, Liwinski, and Elinav 2020).

NLRP3 is the most well-studied subset of the inflammasome. NLRP3 activation takes place in two steps: The first signal (Priming signal) triggers the expression of NLRP3 and pro-IL-1β. This priming step is initiated by the recognition of PAMPs or DAMPs by TLRs or other PPRs. Upon recognition, these receptors trigger the NF-κB signaling pathway, leading to the transcription and translation of NLRP3 and pro-IL-1β. The second signal (Activation signal) directly activates the NLRP3 inflammasome. To date, it's known that a variety of stimuli can serve as the second signal, including ATP, toxins, crystalline substances such as uric acid or cholesterol, amyloid-beta, as well as environmental irritants like silica or asbestos. Once the inflammasome is activated, it recruits and activates Caspase-1. Caspase-1 then processes the precursor forms pro-IL-1β and pro-IL-18, into their active forms, which are then secreted from the cell and contribute to the inflammatory response (van de Veerdonk et al. 2011).

Meanwhile, activated Caspase-1 can also cleave a protein known as gasdermin D (GSDMS) (Liu, Wang, et al. 2020). Once cleaved by Caspase-1, GSDMS forms two fragments, an N-terminal and a C-terminal fragment. The N-terminal fragment is the active form of GSDMD and it targets the cell membrane. This fragment can change the integrity of membrane and form the large pores as the direct gateway for the release of the mature IL-1β and IL-18 (He et al. 2015). Besides that, these large pores in the membrane permit the unimpeded flow of ions in and out of the cell, leading to a substantial disruption in ion balance. Furthermore, another effect of this disruption is the massive influx of water into the cell. As water rushes into the cell due to osmotic pressure, it causes the cell to swell rapidly. This rapid swelling compromises the structural integrity of the cell. Ultimately, severe swelling and ions imbalance leads to the rupture of the cell membrane and the complete lysis of the cell (Burdette et al. 2021).

This kind of cell death, characterized by the release of pro-inflammatory contents into the surrounding environment, is named pyroptosis (Tan et al. 2021; Yu et al. 2021), a highly inflammatory form of programmed cell death distinct from apoptosis. Notably, this type of cell death is a double-edged sword. While it can eliminate infected cells and aid in the control of infection, excessive or dysregulated pyroptosis can cause excessive inflammation and tissue damage, contributing to the pathogenesis of various inflammatory diseases.

## 1.2 Colorectal cancer and inflammation

Cancer is a significant challenge to global public health, as it is the primary cause of death and a major barrier to increasing life expectancy in all countries around the world. The 2019 survey report from the World Health Organization (WHO), describes cancer to be the first or second leading cause of death before age 70 in 112 of 183 countries, and the third or fourth leading cause of death in another 23 countries. Over 19.3 million new cancer cases and almost 10.0 million cancer deaths occurred in 2020, and this

number has been rising since 2000 (Siegel et al. 2022; Sung et al. 2021).

Colorectal cancer (CRC) is the third most commonly diagnosed cancer (over 1.1 million new cases were diagnosed as CRC) and second leading cause of cancer-related death (over half million new death) in 2020. It is estimated that by the year 2035, the total number of deaths from rectal and colon cancer will increase by 60% and 71.5% (Douaiher et al. 2017), respectively. In Ireland, according to the report from Irish Cancer society, CRC is the second most common cancer both in men and women. Over 2500 cases are diagnosed each year. And from 1994 to 2017, the incidence rate of CRC is stable at 7 per 10 thousand persons.

Various factors have been implicated that are associated with the development of CRC. Individuals with a history of cancer (Win et al. 2012; Kolligs 2016; Rawla, Sunkara, and Barsouk 2019), inflammatory bowel diseases (Rawla, Sunkara, and Barsouk 2019), colon polyps (Shussman and Wexner 2014), diabetes mellitus (Ma et al. 2018; Pang et al. 2018; Yu et al. 2022), or cholecystectomy (Jiang et al. 2022; Ma et al. 2022; Qin et al. 2022) are at an increased risk for CRC. But the majority of CRC cases and deaths can be traced to the modifiable lifestyle risk factors, such as inappropriate diet (Guo et al. 2022; Vallis and Wang 2022), excessive alcohol consumption (Fujiyoshi et al. 2022; Seol et al. 2020; Mohr et al. 2017), cigarette smoking (Li et al. 2023; Ugai et al. 2022; Fujiyoshi et al. 2020), sedentary behavior (Namasivayam and Lim 2017; Yu et al. 2014), and obesity (Ramadan et al. 2022; Ulanja et al. 2023; Bou Malhab and Abdel-Rahman 2022). Moreover, age, gender, race, socio-economic status, and gut microbiome are additional factors that have been found to influence the development of CRC (Fig1.3) (Ulanja et al. 2023; Sawicki et al. 2021).

Colorectal cancer is usually staged using the TNM system, which stands for tumor, nodes and metastases (Banias et al. 2022). the TNM system considers the size and location of the primary tumor (T), whether the cancer has spread to nearby lymph nodes (N) and whether it has spread (metastasized) to other parts of the body (M) (Doescher,

Veit, and Hoffmann 2017; Hari et al. 2013). In most cases of CRC carcinogenesis, the formation of benign precursor lesions, referred to as polyps, is a crucial component. As growth progresses, the polyp becomes malignant, resulting in the development of a malignant polyp in the pre-cancer stage. Stage I follows the pre-cancer stage, characterized by the presence of abnormal cells in the inner lining of the colon or rectum, and the formation of a small tumor that has not yet penetrated the entire intestinal wall. As tumor growth continues, the tumor size increases and penetrates the entire intestinal wall, but has not yet spread to local lymph node glands or distant sites, which is stage II. In stage III, cancer has spread to the nearby lymph nodes or to areas of fat near the lymph nodes, but not to the nodes themselves, and has not yet spread to distant sites. Stage IV is defined as when the cancer has spread to other organs, such as the liver and lungs, or to distant lymph nodes (Chakrabarti et al. 2020; Yuan et al. 2017; Gallo et al. 2019; Venderbosch et al. 2011).

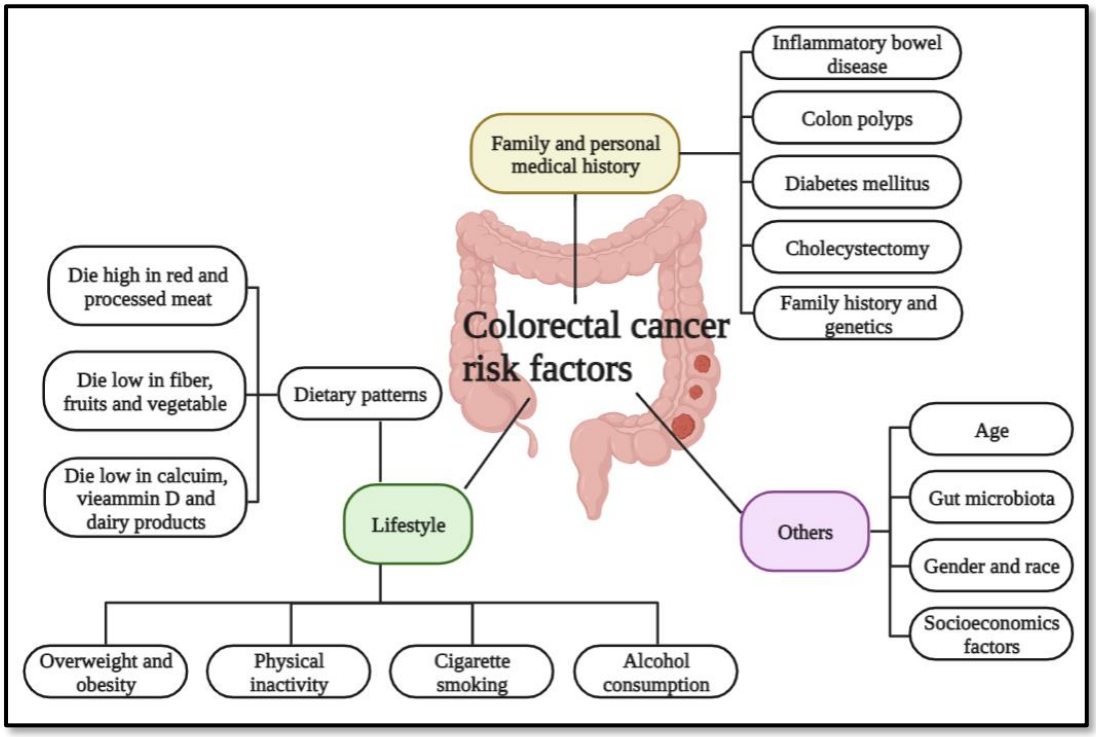


**Fig1.3 The main risk factors associated with Colorectal cancer**

**Described in detail in section 1.2, colorectal cancer is associated with several risk factors including age, gender, gut microbiota, family and personal medical history. In addition, the majority of CRC cases are potentially attributable to the inappropriate lifestyle chose.**

The connection between inflammation and cancer has been recognized for over two centuries, and several studies have established a functional relationship between these processes (Khandia and Munjal 2020; Maccio and Madeddu 2020; Qian, Golubnitschaja, and Zhan 2019). The link between inflammation and cancer was firstly recognized through a variety of observations, which have highlighted the complex molecular and cellular interactions underlying this relationship. A specific subset of CRC arise from chronic inflammation caused by inflammatory bowel disease (IBD) (Lichtenstern et al. 2020; Long, Lundsmith, and Hamilton 2017; Seyedian, Nokhostin, and Malamir 2019). IBD constitutes a number of immune-mediated advanced inflammatory conditions of the gastrointestinal tract (GIT) with the two most common being ulcerative colitis (UC) and Crohn's disease (CD) (Seyedian, Nokhostin, and

Malamir 2019). The association between IBD and CRC was first described by Burrill Crohn in 1925. Further case reports subsequently described the occurrence of CRC in patients with CD. In the early 1980s, attempts were made to compare cancer incidences directly in CD and UC. Studies reported a similar extent of parity between the relative risks of colon cancer in CD and left-sided UC. As a result, it was suggested that when cases of ulcerative and Crohn's colitis with similar anatomic extent are followed for similar durations, the two diseases may ultimately demonstrate similar increases in the risk for CRC. Both CD and UC are characterized by chronic, relapsing inflammation of the intestines, and chronic inflammation is assumed to be a causative factor in the development of cancer (Kraus and Arber 2009). Chronic inflammation in the colon can lead to changes in the cells lining the colon, making them more susceptible to the development of tumorigenesis (Qian, Golubnitschaja, and Zhan 2019). This is thought to be due to the inflammatory cells producing reactive oxygen species, pro-inflammatory cytokines, and growth factors, which can promote cell proliferation, inhibit apoptosis (programmed cell death), and lead to DNA damage, mutations and genomic instability (Rubin, Shaker, and Levin 2012).

## 1.3 The Pellino protein family

Ubiquitination is the process by which small proteins called ubiquitin are attached to other proteins in a cellular process known as protein modification. This process serves several important functions, including regulation of protein activity, localization, and degradation (Swatek and Komander 2016). The ubiquitination of a target protein requires 3 separate enzymes to be involved: an E1-ubiquitin-activating enzyme, an E2 ubiquitin-conjugating enzyme and an E3 ubiquitin-protein ligase (Neutzner and Neutzner 2012). For humans, there are two E1 activating enzymes called Uba6 and Ube1 (Schulman and Harper 2009). These two enzymes bind to ubiquitin and activates it by adenylation, creating a high-energy intermediate that is then transferred to the ubiquitin-conjugating E2 conjugating enzyme. E2 then transfers the activated ubiquitin

to a specific lysine residue on the target protein through a reaction catalyzed by an E3 ligase. There are approximately 40 active E2 enzymes in human and hundreds of E3 ligases. E3 proteins are a large and diverse group, due to their requirement to bind to a large variety of targets (Neutzner and Neutzner 2012).

The Pellino family of proteins were first discovered as a component of the Dorsal/Cactus signaling complex in *Drosophila melanogaster*. Drosophila Pellino being identified as a protein interaction partner of the IRAK (Grosshans, Schnorrer, and Nusslein-Volhard 1999). Three mammalian Pellino proteins have been identified and genetically mapped: Pellino1, Pellino2 and Pellino3 (Butler, Hanly, and Moynagh 2005; Jiang et al. 2003; Yu et al. 2002). The Pellino1 and Pellino2 proteins are encoded by the genes *PELI1* and *PELI2* and map to chromosomes 2p14 and 14q22.3 in human. Pellino3 protein is encoded by the gene *PELI3* and locates to chromosomes 11q13.2 in humans. Pellino3 has two splice variants, the large one called Pellino3a while the shorter one is called Pellino3b.

Early research indicated that there is a conserved RING-like finger motif on the carboxyl termini of Pellino proteins and this RING-like domain is a feature of a sub-family of E3 ubiquitin ligases, suggesting that this RING-like domain may have the E3 ubiquitin ligase activity (Rich et al. 2000). Indeed, Pellino proteins (Pellino1, 2 and 3) were shown to ubiquitinate IRAK1 in a RING-like domain-dependent manner (Butler, Hanly, and Moynagh 2007). All members of Pellino family proteins contain a N-terminal cryptic phosphothreonine-binding forkhead-associated (FHA) domain with two inserts that form a ‘wing’ or appendage packed closely to the FHA domain that facilitates its interaction with IRAK1 (Lin et al. 2008). The core FHA domain and wing structures are conserved across the Pellino family and so the FHA-mediated recognition of phosphorylated target proteins is likely to be a family trait (Fig1.4). Compared to Pellino1 and Pellino2, Pellino3 protein shares an amino acid identity of 84% and 85%, respectively. Pellino3 also has a longer amino-terminal domain by 27 and 25 amino acid compared with Pellino1 and Pellino2.

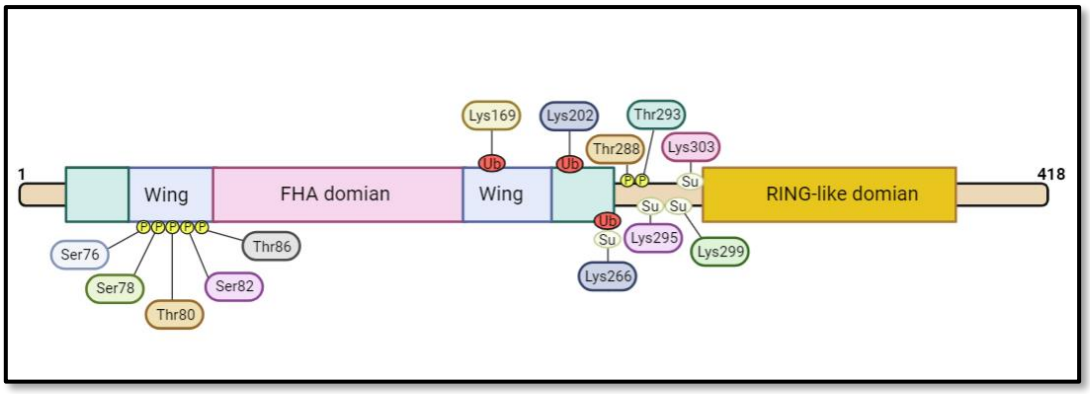


**Fig1.4 Molecular features of Pellino proteins**

**Pellino proteins contain a core forkhead-associated (FHA) domain with two inserts that form a "wing" or appendage packed closely to the FHA domain. They also contain a RING-like domain with the indicated pattern of cysteine and histidine amino acids.**

### 1.3.1 Pellino proteins and inflammation

In the context of inflammation, Pellino1 has been shown to be involved in the regulation of different types of inflammation and inflammation-associated disease. Pellino1-deficient mice have revealed a specialized function of Pellino1 in the TL3 and TL4 signaling pathways. Pellino1 knockout mice showed higher resistance to the TLR3 or TLR4 ligand-induced septic shock, and also showed down-regulation of NF-κB activation and with reduced expression of pro-inflammatory genes. RIP1 and Pellino1 are recruited by TLR3 and TLR4 through TRIF. Pellino1 is phosphorylate and activated and facilitates the ubiquitination of RIP1, which is a crucial step in TRIF-dependent activation of NF-κB (Also known as MyD88-independent). Thus, Pellino1 is an important intermediary molecule in the TRIF-dependent NF-κB activation (Chang, Jin, and Sun 2009). IL-1 is a pro-inflammatory cytokines that also the signal through the IL-1 receptor to activation the MyD88, and knockdown Pellino1 impairs the IL-1-induced activation of NF-κB in cell lines. But different results are observed from knock-in mice, in that knock-in of Pellino1 doesn't affect the IL-R signaling to the NF-κB and MAPKs. Also, mouse embryonic fibroblasts (MEFs) from Pellino 1-deficient mice

show normal responsiveness to IL-1β. Thus the role of Pellino1 in IL-1R signaling awaits resolution (Choi et al. 2006). Pellino1 knockout mice also showed reduced severity of experimental autoimmune encephalomyelitis (EAE) by suppressing the production of pro-inflammatory and chemokine gene expression, inhibiting the recruitment of T cells into the central nervous system. This effect is mediated through the regulation of c-IAP-TRAF3 signaling axis, a critical component for the activation of MAPK signaling pathway via the MyD88-dependent route. c-IAP is recognized as an E3 ubiquitin ligase, which can be activated by TLR signals. Upon activation, c-IAP mediates Lys-48 linked ubiquitination and degradation of TRAF3, an event that is essential for the activation of the MAPK pathway (Xiao et al. 2013). In addition, up-regulation of spinal Pellino1 is essential for the pathogenesis of neuropathic pain through Pellino1-dependent mobilization of spinal cord microglia by the activation of MAPK/NF-κB signaling and the production of pro-inflammation cytokines (Wang et al. 2020). This also indicated that Pellino1 may serve as a potential target for the treatment of neuropathic pain. Pellino1 is also involved in the viral sensing pathways. Research showed that Pellino1 regulated the TLR3 pathway and responses to airway viruses. Conditional knockout of Pellino1 in lung resulted in increased production of IL-6 and TNFα upon viral infection, accompanied by enhanced recruitment of immune cells to the airways (Marsh et al. 2020). Meanwhile, Pellino1 knockout mice succumb to systemic disease and develop larger zosteriform skin lesions along affected dermatomes by the infection of herpes simplex virus, and the virus also spread extensively through the epidermis and follicular infundibulum into sebaceous glands. Also, Pellino1 knockout mice showed delayed recruitment of myeloid and T cells to the infected epidermis (Cai et al. 2023).

Knock down of Pellino2 in cells has been shown to inhibit the LPS-induced and IL-1β-induced activation of NF-κB (Kim et al. 2012). Also, over-expression Pellino2 leads to the activation of ERK and JNK MAPK signaling pathway (Jensen and Whitehead 2003a) while knock down Pellino2 expression attenuates the IL-1β-induced and LPS-induced activation of these kinases (Kim et al. 2012). Pellino2 directly associates with

threonine-phosphorylated IRAK1, facilitating the subsequent ubiquitination of IRAK1. This interaction enhances IRAK1's kinase activity, consequently influencing cellular signaling. Notably, this modulatory effect is dependent on the FHA domain(Humphries et al. 2018; Lin et al. 2008). Pellino2 knockout leads to the down-regulation of LPS-induced IL-1β expression through suppressing the activation of NLRP3 inflammasome by impairing the ubiquitination of NLRP3 during the priming phase of activation (Humphries et al. 2018). This role of Pellino2 in modulating NLRP3 has also been observed in the context of pediatric pneumonia. Both mRNA and protein expression levels of Pellino2 were found to be diminished in patients and murine models alike. Notably, Pellino2 was found to be positively associated with pulmonary injury and augmented inflammation, as well as pyroptotic events in lung tissue specimens from pediatric pneumonia cases (Liu, Lin, and Yin 2022). These outcomes are attributable to Pellino2's function in mediating the ubiquitination and activation of NLRP3. DCs from Pellino2-deficient mice show impaired production of type I IFN following endosomal TLR9 activation, and it partly mediates a feed-forward loop of IFNβ that promotes IL-12 production in DCs. Also, Pellino2 in murine DCs is downregulated following TLR9 stimulation, and its overexpression induces upregulation of both IFN-b and IL-12, demonstrating the sufficiency of Pellino2 in driving these responses (Oleszycka et al. 2021).

Early work about the function of Pellino3 focused on its role in TLR and IL-1 signaling due to the finding of the interaction between Pellino3 and IRAK1. It was originally shown that Pellino3 could activate both c-jun and Elk-1, but not NF-κB (Jensen and Whitehead 2003b). It was hypothesized that differential levels of expressed Pellino3 in tissues could direct a cellular response towards either a MAPK dependent response in the case of high Pellino3 expression or a NF-κB response in tissues exhibiting low Pellino3 expression (Jensen and Whitehead 2003b). Over-expression of Pellino3 can activate ERK, JNK and P38 MAPKs signaling pathway and the activation of cAMP response element-binding protein (CREB) to induce expression of IL-10 (Butler, Hanly, and Moynagh 2005). Subsequent studies have found that the smaller splice variant

Pellino3b could negatively regulate the IL-1β-induced NF-κB activation through inhibiting the degradation of IRAK1 by promoting its Lys63-linked polyubiquitination (Xiao et al. 2008). Pellino3 also been found to have a role in the LPS-induced pro-inflammatory cytokine production by promoting the degradation of the adaptor protein MyD88. Following research showing low expression level of Pellino3 in human abdominal adipose tissue from obese subjects. Our research group demonstrated that Pellino3 deficiency mice showed exacerbation of inflammation, higher IL-1β expression, and stronger insulin resistance when induced by high-fat-diet. We demonstrated that Pellino3 negatively regulates the expression hypoxia-inducible factor 1α (HIF-1α) to suppress the expression of IL-1β (Yang et al. 2014). In addition, Pellino3 is also an important mediator in the Nod2 signaling pathway by ubiquitinating the critical Nod2 signaling intermediate receptor-interacting- serine/threonine-protein kinase 2 (RIP2) and promoting downstream protective effects in colitis. Pellino3 knockout mice had less induction of cytokines after engagement of Nod2. Interestingly, the expression of Pellino3 was lower in the colons of patients with Crohn's disease and this is consistent with Pellino3 having a protective effect in intestinal homeostasis (Yang et al. 2013).

### 1.3.2 Pellino and cancer

The first literature reported on the relationship between Pellino protein and cancer was published in 2014 (Park et al. 2014). Human Pellino1 knock-in mice were found to have shorter lifespan due to lymphoid and solid tumor formation. Constitutive expression of human Pellino1 resulted in ligand-independent hyper-activation of B cells and facilitated the development of a wide range of lymphoid tumors, with prominent B cell infiltration observed across multiple organs. In this study, Pellino1 was shown to interact with the oncoprotein BCL-6 and induced its Lys-63 specific polyubiquitination (Park et al. 2014). Subsequently, more studies began to explore the relationship between Pellino proteins and cancer. Pellino1 is highly expressed in human lung cancer cell lines and could increase the chemo-resistance in these cell lines by up-regulating the

expression level of the anti-apoptotic protein cIAP2 via its Lys-63 mediated polyubiquitination (Jeon et al. 2016). Pellino-1 over-expression also activated PI3K/Akt and ERK signaling pathways and elicited an epithelial–mesenchymal transition (EMT) phenotype of lung adenocarcinoma cells. Pellino1-mediated EMT was facilitated by stabilization of the Zinc finger protein SNAI2 (Slug) and Zinc finger protein SNAI1 (Snail) proteins through Lys-63 mediated polyubiquitination (Jeon et al. 2017). Similar effects of Pellino1 on Slug and Snail proteins were also found in the triple-negative breast cancer. Research showed that Resistomycin treatment leads to the down-regulated expression of Pellino1 and induced the degradation of Slug and Snail proteins (Liu, Qi, et al. 2020). Pellino1 is also elevated in papillary thyroid cancer (PTC) tissue, and over-expression Pellino1 was positively correlated with more intense tumor size and lymph node metastases. Pellino1 silencing significantly suppressed PTC growth both *in vitro* and *in vivo* accompanied with reduced expression of Ki-67 and matrix metallopeptidase 2 (MMP-2). Mechanistically, PI3K/AKT pathway was identified as the downstream target of Pellino1, and mediated the functional influence of PELI1 in PTC cells (Zheng et al. 2022). In addition to the direct effects on the tumor self, Pellino1 also attenuated tumor growth by inhibiting M2c polarization of macrophages through increasing STAT1 phosphorylation via Lys-63-linked ubiquitination of IRAK1 (Kim et al. 2019). Also, Pellino1 inhibits homeostatic regulation of the mitotic cell cycle and checkpoints and contributes to the initiation and progression of the neoplastic chromosome aneuploidy through ubiquitination-mediated downregulation budding uninhibited by benzimidazoles related1 (BubR1) (Park et al. 2017). All of these studies suggest Pellino1 to be a pro-tumorigenic factor.

In contrast, higher levels of Pellino2 are positively correlated to better prognosis in multiple myeloma patients and is responsible for proteasome inhibitor treatment-induced cell death in cell lines *in vitro* assay. Indeed Pellino2 was described to be a predictor for multiple myeloma responsiveness to proteasome inhibitor treatment in the clinic (Masuda et al. 2022). Further unpublished work from our laboratory shows that low expression levels of Pellino2 are associated with CRC. In addition, the deletion of

*Peli2* gene was found to exacerbate tumor load and overall disease burden in AOM/DSS-induced colorectal cancer models. This finding suggests a potential protective role of Pellino2 in the pathogenesis of CRC. To date, we are still unaware of any literature reports on Pellino3 and cancer.

## 1.4 Apoptosis

Cancer arises when the balance between cell survival and proliferation versus cell death is lost. One of the most important forms of cell death in this regard is apoptosis. This is a fundamental biological process characterized by an ordered sequence of cellular events that ultimately lead to programmed cell death (Elmore 2007). Apoptosis has been widely acknowledged as a prominent form of "programmed" cell death, in which the genetically regulated elimination of cells takes place (Obeng 2021). Nevertheless, it is very important to recognize that the other forms of programmed cell death have been identified, and it is possible that additional modes of programmed cell death remain to be discovered. Serval studies demonstrate that apoptosis occurs during the development, aging and several disease as a homeostasis balance factor to balance cell proliferation and cell death in tissues. Also, apoptosis will be triggered by several signals including abnormal cell proliferation, radiation, DNA damage, immune reaction or as a result of cell damaged by some disease or cytotoxicity agents (Lopez and Tait 2015; Zaman, Wang, and Gandhi 2014; Elmore 2007).

### 1.4.1 Cell changes in apoptosis

During the process of apoptosis, apoptotic cells undergo a series of changes, which can be mainly divided into morphological and biochemical changes (Obeng 2021). Morphological changes of apoptosis occur in both the nucleus and the cytoplasm, and their features are very similar across cell types and species. The morphological hallmarks in the nucleus are DNA fragmentation and chromatin condensation (Kroemer

et al. 2009). Chromatin condensation starts at the periphery of the nuclear envelope, then gives rise to a crescent or ring-shaped configuration that progressively increases in density until its fragmentation within cells with an intact nuclear membrane, a morphological trait commonly referred to as karyorrhexis (Majno and Joris 1995). At the same time, morphological changes begin to appear in the cytoplasm, including cell rounding, reduction of cellular volume and retraction of pseudopods, then membrane bleaching, ultrastructural change of cytoplasmic organelles and a loss of membrane integrity will happen at the later phase of apoptosis (Kroemer et al. 2009). In addition, the most important and easily recognizable morphological feature of apoptosis is the formation of apoptotic bodies. Apoptotic bodies appear as a result of the contraction of the cell membrane, which shrinks and forms small protrusions on its surface called blebs. These blebs are eventually separation from the cell to form apoptotic bodies, which are surrounded by the plasma membrane. The apoptotic bodies contain fragments of the cytoplasm, organelles, and nuclear material, including fragmented DNA. The plasma membrane that surrounds the apoptotic bodies prevents their contents from leaking into the extracellular space, thus preventing inflammation and damage to neighboring cells (Ziegler and Groscurth 2004).

There are three main types of biochemical changes in apoptosis: activation of Caspases, DNA and protein breakdown, membrane changes and recognition by phagocytic cells like macrophage and parenchyma (Wong 2011). At the early phase of apoptosis, there is appearance of phosphatidylserine (PS) in the outer leaflet of the plasma membrane bilayer, which has been “flipped out” from the inner layers. The PS in the out layer is the marker for the recognition of cell uptake by macrophages to prevent the release of pro-inflammatory cellular components (Hengartner 2001). DNA fragments into large 50 to 300 kilobase pieces and then cleaved into small fragments about 180-200 base pairs by DNA endonucleases (Wong 2011). And the final specific biochemical characteristic of apoptosis, also the final execution step of the cell is the activation of a group enzymes belonging to the cysteine protease family named Caspases (Wong 2011). Caspases are cysteine-dependent aspartate-specific proteases that cleave after specific

aspartic residue upon activation (McIlwain, Berger, and Mak 2015). They are initially produced as inactive proenzymes and on activation, they start a protease cascade by cleaving other pro-Caspases. And the apoptosis-associated Caspase could be group into two types: initiator Caspase (such as Caspase-2,-8,-9,-10) and executioner Caspase (such as Caspase-3, -6 and -7). Upon activation, Caspases can cleave numerous essential intracellular proteins, resulting in the breakdown of the nuclear scaffold and cytoskeleton. Additionally, they stimulate DNase activity, leading to the further degradation of small DNA fragments (McIlwain, Berger, and Mak 2015; Obeng 2021).

### 1.4.2 Mechanisms of apoptosis

Understanding the complex mechanisms of apoptosis is very important for investigating the pathogenesis of diseases caused by dysregulated apoptosis. This knowledge can be used to develop pharmacological agents that target specific genes or pathways involved in apoptosis. The Caspase system can be activated through three main pathways: the intrinsic mitochondrial pathway, extrinsic pathway, and intrinsic endoplasmic reticulum pathway (Fig1.5) (O'Brien and Kirby 2008). Both the intrinsic mitochondrial and extrinsic pathways eventually converge into the common pathway to activate apoptosis, while the intrinsic endoplasmic reticulum pathway is less well-known but is believed to be activated in response to endoplasmic reticulum stress, leading to the release of calcium and the activation of downstream Caspases (O'Brien and Kirby 2008).

The intrinsic mitochondrial pathway of apoptosis derives its name from the fact that it is triggered from within the cell. Endogenous stimulation, such as irreparable genetic damage, hypoxia, excessive cytosolic $Ca^{2+}$ concentrations, and severe oxidative stress, will finally lead to the activation of this pathway (Wong 2011). During the intrinsic mitochondrial pathway, an elevation in mitochondrial permeability leads to the release of pro-apoptotic proteins, including cytochrome c, from the intermembrane space into the cytosol (Danial and Korsmeyer 2004). Subsequently, the binding of cytochrome c

to Apaf-1 and Caspase 9 in the cytosol forms a complex known as the "apoptosome" while the apoptosome leads to the cleavage and activation of Caspase3 (Danial and Korsmeyer 2004). This pathway is well controlled and regulated by a group of proteins belonging to the Bcl-2 protein family. These protein can be categorized into two types: the pro-apoptotic proteins, including Bak, Bcl-10, Bax, Bad, Bid, Bim, Bik, Hrk or the anti-apoptotic proteins like Bcl-2, Bcl-x, Bcl-w, Bcl-XL, B-XS, BAG (Singh, Letai, and Sarosiek 2019). The balance of these pro- and anti-apoptotic proteins determine whether apoptosis should be started. Additional apoptotic factors that are co-released with cytochrome c from the mitochondria to the cytoplasm are apoptosis inducing factor (AIF), direct IAP Binding protein with Low pI (DIABLO), second mitochondria-derived activator of Caspase (Smac), and Omi/high temperature requirement protein A (HtrA2) (Kroemer, Galluzzi, and Brenner 2007). The promotion of Caspase activation by the Smac/DIABLO and Omi/HtrA2 complexes occurs through their binding to the inhibitor of apoptosis proteins (IAPs), thereby destroying the inhibitory interaction between IAPs and Caspase3 or Caspase9 (Kroemer, Galluzzi, and Brenner 2007).

The extrinsic pathway, as its name implies, begins when death ligands (TNF ligands, Fas ligands and TNF-related apoptosis inducing ligands) bind to the death receptors (TNF receptors, Fas receptor) (Hengartner 2001). The binding of death domain/adapter proteins to receptor ligand complexes enables the recruitment of an initiator Caspase 8 or 10, which contains a death effector domain (DED), to form an active complex known as the Death-Inducing Signaling Complex (DISC). This activation facilitates the relay of the death signal to an execution Caspase, ultimately resulting in apoptosis (O'Brien and Kirby 2008; Schneider and Tschopp 2000).

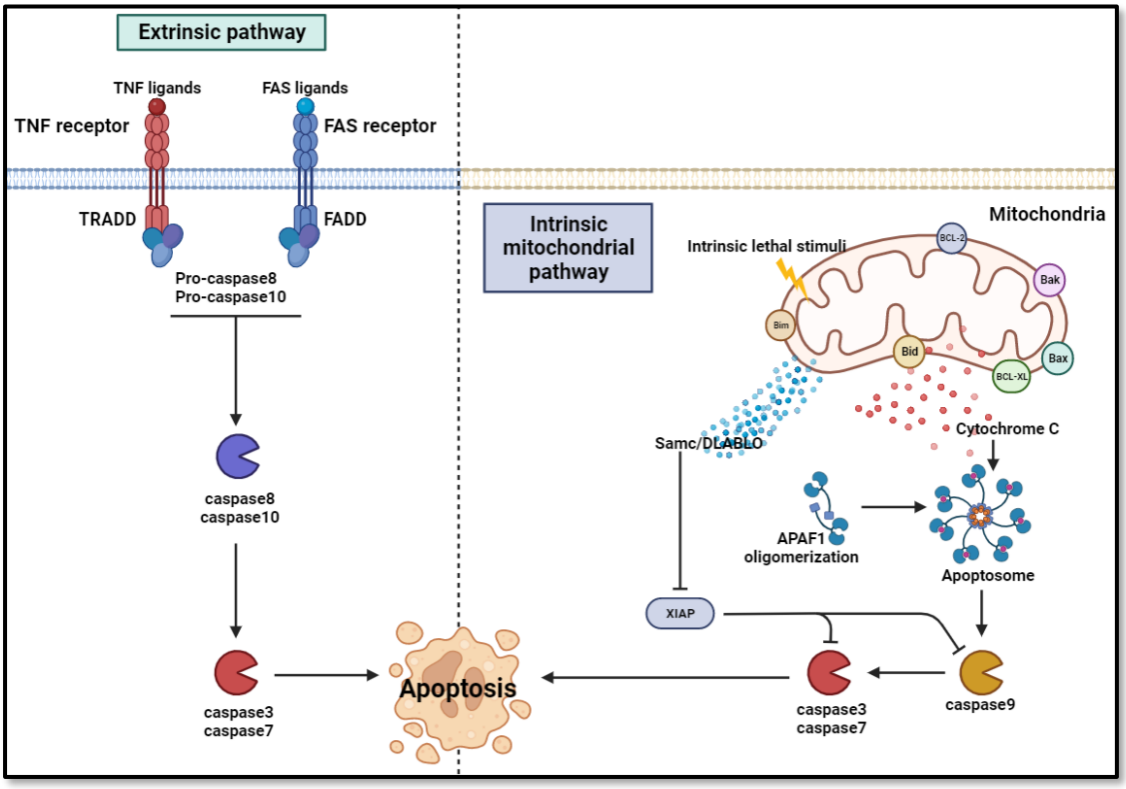


**Fig1.5 The intrinsic and extrinsic pathways of apoptosis**

**As detailed in Section 1.4.2, there are three pathways that can activate the Caspase system. The intrinsic pathway and extrinsic pathway are the two most commonly described initiation pathways, while the less well-known third pathway is the endoplasmic reticulum pathway.**

The upstream Caspase of intrinsic mitochondrial pathway is Caspase9 while the initiator Caspase of extrinsic pathway is Caspase8. Both of these two pathway will trigger the execution phase that involves the activation of Caspase3. The activated Caspase3 then cleaves the inhibitor of the Caspase-activated deoxyribonuclease, which is responsible for nuclear changes of apoptosis (Ghobrial, Witzig, and Adjei 2005). Caspases3 also plays an important role in inducing the cleavage of protein kinases, DNA repair proteins, cytoskeletal proteins and inhibitory subunits of endonucleases family. These events affect various cellular processes such as the cytoskeleton, cell cycle, and signaling pathways, collectively leading to the characteristic morphological changes associated with apoptosis (Ghobrial, Witzig, and Adjei 2005).

### 1.4.3 the Bcl-XL protein in apoptosis

B-cell lymphoma-extra-large (Bcl-xL), encoded by the *BCL2-like 1* gene, is the member of the Bcl-2 protein family that act as an anti-apoptosis protein and locates on the outer mitochondrial membrane. Bcl-xL was discovered to have similar anti-apoptotic function to Bcl-2 (Fiebig et al. 2006). Bcl-xL and Bcl-2 exhibit 43% similarity in their amino acid sequences and share common sequence motifs as well as a C-terminal hydrophobic region that is essential for their localization to membranes (Muchmore et al. 1996; Petros et al. 2001).

Bcl-xL is classified as an anti-apoptotic protein as it functions to inhibit the mitochondrial intrinsic pathway of apoptosis. In its natural state, Bcl-xL acts by stabilizing the outer mitochondrial membrane, thus preventing the release of pro-apoptotic proteins such as cytochrome c from the mitochondria (Thuduppathy et al. 2006). By doing so, Bcl-xL inhibits the formation of the apoptosome complex, which is essential for the activation of Caspase 9, a key mediator of the intrinsic pathway.

During apoptosis, Bxl-xL protein can undergo degradation via various mechanisms, depending on the apoptotic pathway involved. In the intrinsic pathway, BH3-only proteins can directly bind to and inhibit Bxl-xL, leading to its degradation. Bcl-2 Interacting Mediator (BIM) and BH3 Interacting Domain (BID) can interact with Bxl-xL and facilitate its ubiquitination and proteasomal degradation (Lomonosova and Chinnadurai 2008). Moreover, the transcriptional level also regulates Bxl-xL degradation. The tumor suppressor protein p53 can induce the expression of pro-apoptotic proteins such as p53 upregulated modulator of apoptosis protein (PUMA), which can bind and inhibit Bxl-xL, promoting its degradation (Bharatham, Chi, and Yoon 2011). Other transcription factors and signaling pathways such as NF-κB, STAT3, PI3K/AKT signaling pathway, and JAK/STAT signaling pathway also contribute to the regulation of the expression of Bxl-xL and other proteins involved in apoptosis (Zhuang et al. 2007; Sun et al. 2008; Lee et al. 2008; Alfano, Iaccarino, and Stoppelli 2006).

## 1.5 Development of novel molecules to target inflammation and cancer

This thesis focuses on the characterization of small molecules as potential regulators of inflammation and cancer. Inflammation is a term used to describe a range of biologic mechanisms, involving multiple systems of the organisms to contain and clear the invasive pathogens and resolve injuries, as well as repair tissue damage, by activating innate and adaptive immune responses. In order to maintain homeostasis, the immune system is required to recognize pathogens, respond to the pathogenic burden, and ultimately return to a balanced state. Achieving an appropriate inflammatory response needs a balance between producing sufficient cytokines to eliminate the pathogen and avoiding excessive inflammation, as an excess of cytokines can result in clinically significant collateral damage (Cicchese et al. 2018; Dodoo et al. 2002). Cytokines as a group of soluble mediators, play an important role in coordinating antimicrobial effector cells and providing regulatory signals that direct, amplify and resolve the immune response (Strieter, Belperio, and Keane 2002b; Stow et al. 2009). These molecules are characterized by a short half-life, which allows for rapid adaptation to changing conditions, as well as fine-tuned control of the intensity and duration of immune response and inflammation. The production of cytokines is tightly controlled. but in some cases, this regulation is broken and leads to immune hyperactivation and the production of large quantities of cytokines, resulting in a "cytokine storm" that can cause tissue damage (Morgan et al. 2010; Fajgenbaum and June 2020). Therefore, precisely and effectively controlling cytokine production, particularly the production of “pro-inflammatory cytokines” is a vital element in restoring the body to homeostasis.

However, there are three cytokines IL-1β, IL-6 and TNFα that have probably received most attention as key and critical drivers of inflammation. The increasing attention on regulating the production of the three pro-inflammatory cytokines has prompted the exploration of various strategies to intervene in their production and action and so

identify effective anti-inflammatory strategies (Brebner et al. 2000; Schuerwegh et al. 2003; Umare et al. 2014).

Anti-inflammatory drug can be divided into large biomacromolecules or small molecules (Warner, Hajdin, and Weeks 2018; Childs-Disney et al. 2022; Beck et al. 2022; Jahangirian et al. 2019). Small molecules can have the advantage of greater bioavailability, in that they are easily absorbed into the bloodstream and can effectively reach their target site in the body to achieve the effect. Small molecule drugs are also generally less toxic than larger biologic drugs, such as monoclonal antibodies, due to their smaller size and lower likelihood of causing immune reactions. Additionally, small molecule drugs can be administered via oral or injectable routes, making them convenient for patients and allowing for greater adherence of treatment (Beck et al. 2022; Arkin, Tang, and Wells 2014).

The development of anti-inflammatory drug-like small molecules involves several critical steps. Target identification is the first step and researchers must first identify the specific molecular pathways involved in inflammation that they want to target. Once a target is identified, researchers may screen a library of chemical compounds to find those that can inhibit that target, or work with it to enhance its function and potentially act as an anti-inflammatory agent. Thereafter, the lead optimization will be performed. The most promising compounds from lead discovery are then further optimized through chemical synthesis and structural modifications to improve their efficacy and specificity. Meanwhile, the mechanisms by which selected compounds exert their anti-inflammatory effects will also be investigated. This then progresses to pre-clinical testing their efficacy and safety and deciding whether they should progress to clinical trials. The research area of identifying novel small molecule anti-inflammatory drugs is one of great interest (Wang, Smith, and Yin 2013).

In the field of anti-inflammatory small molecule development, numerous core structures including pyrazole, indole, chalcone, and pyridine have been modified and

re-structured to produce diverse compounds with anti-inflammatory properties. As the NF-κB and MAPK signaling pathways play a crucial role in the inflammatory response, researchers have increasingly focused on developing small molecule inhibitors to target these pathways. Small molecules can be subdivided into different categories based on their mechanism of action. The first category is the inhibitor of protein kinases, which block the activation of IKK proteins (Kapahi et al. 2000; Kwok et al. 2001), target the functional domains of NF-κB proteins (Demarchi et al. 2003; Schwabe and Brenner 2002), or target specific proteins that influence the protein kinases of signaling pathways (Vanden Berghe et al. 1998; Ravi and Bedi 2004; Sanchez-Duffhues et al. 2009). The second category is the inhibitor of protein phosphatases, which suppress the phosphorylation of signaling pathway proteins and inhibit their transformation into the activation form, such as dephosphorylation of MAPKs and IκB protein (Arbibe et al. 2007; Sreenivasan, Sarkar, and Manna 2003). Similar to the inhibitor of protein kinases, the inhibitor of protein phosphatases can also target specific proteins that influence the protein phosphatases of signaling pathways (Singh and Aggarwal 1995). The third category is proteasome inhibitors, which inhibit the degradation of proteins such as IκB that impair the activation of NF-κB (Zhou et al. 2005; Yaron et al. 1997; Tang et al. 2005; Shembade, Ma, and Harhaj 2010). The fourth category involves the blockage of NF-κB nuclear translocation. An important step in the activation of transcription factors by NF-κB protein is the translocation from cytoplasm to nucleus, which can be blocked using small peptides that cross the cell membrane. For instance, SN50 is a synthetic peptide that contains a nuclear localization sequence of NF-κB p50 and a hydrophobic membrane-translocating region, which competitively inhibits LPS-induced and TNFα-induced NF-κB nucleus translocation (Lin et al. 1995). In addition to above, there are still many small molecules that inhibit the activation of NF-κB and MAPK signaling pathways through other different mechanisms, like inhibiting P65 acetylation, blocking methyltransferases, suppressing NF-κB protein binds to DNA and so on (Park et al. 2007; Sung et al. 2008).

## 1.6 Project aims

The above literature review captures the complexity of the biological processes and pathways regulating inflammation and cancer. It also highlights the potential for targeting these pathways in the development of new therapeutic strategies for the treatment of inflammatory diseases and cancer. Pellino proteins are emerging as key players in innate immunity and cancer. With this in mind, the overarching objective of my research was to evaluate the potential of exploiting the mediatory roles of Pellino proteins in these pathways and explore their therapeutic targeting for beneficial effects.

Recent work in our laboratory has involved the design and development of small molecule compounds targeting Pellino2. The specific aims of this study were to investigate their regulatory effects on the pathways involved in inflammation and cancer. More specifically, my research aimed to:

- To characterize the effect of Pellino-targeted molecules on inflammatory signaling pathways.

- To explore the functional, cellular and molecular roles of Pellino2 in colorectal cancer.

- To characterize the effects of Pellino-targeted molecules on cellular pathways driving colorectal cancer.

# Chapter 2: Material and Method

## 2.1 Materials

### 2.1.1 Reagents

| Reagents | Supplier |
|---|---|
| Agar | Sigma-Aldrich |
| Agarose | Promega |
| Ampicillin | Sigma-Aldrich |
| ATP | Invitrogen |
| Acetic Acid | Fisher-Scientific |
| BSA | Sigma-Aldrich |
| Bromophenol Blue | Sigma-Aldrich |
| Chloroform | Sigma-Aldrich |
| CLO75 | Invitrogen |
| CLO97 | Invitrogen |
| CpG type A ODN 1585 | Invitrogen |
| CpG type B ODN 1666 | Invitrogen |
| DirectPCR Lysis Buffer | Viagen Biotech |
| DMEM high glucose medium | Gibco™ |
| DMSO | Sigma-Aldrich |
| DTT | Fisher-Scientific |
| DNA ladder & Loading dye | Promega |

| | |
|---|---|
| E.coli-TOP10 competent cells | Invitrogen |
| EDTA | Sigma-Aldrich |
| Ethidium bromide | Sigma-Aldrich |
| FBS | Sigma-Aldrich |
| Flagellin | Invitrogen |
| Glycerol | Sigma-Aldrich |
| Glycine | Sigma-Aldrich |
| HEPES | Sigma-Aldrich |
| HCl | Merck |
| Isopropanol | Sigma-Aldrich |
| Kanamycin | Sigma-Aldrich |
| Lipofectamine 2000 | Invitrogen |
| LPS | Enzo Life Sciences |
| Luminata Forte Western HRP Substrate | Fisher-Scientific |
| LB | Sigma-Aldrich |
| Magnesium Chloride | Sigma-Aldrich |
| Methanol | BDH |
| Molecular biology grade water (RNase and DNase free) | Sigma-Aldrich |
| Pam2CSK4 | Invitrogen |
| Pam3CSK4 | Invitrogen |
| PBS | Sigma-Aldrich |
| Penicillin/Streptomycin | Invitrogen |
| PMSF | Sigma-Aldrich |
| Poly(I:C) | Invitrogen |
| Pre-stained molecular weight marker | Invitrogen |
| Protease inhibitor cocktail | Roche |
| Protein A/G-agarose binds | Santa Cruz |
| Proteinase K | Qiagen |
| Protogel | National Diagnostics |

| | |
|---|---|
| Puromycin | Sigma-Aldrich |
| Random primers | Invitrogen |
| RPMI-1640 medium | Gibco™ |
| Sucrose | Sigma-Aldrich |
| SDS | Sigma-Aldrich |
| Milk powder | Sigma-Aldrich |
| NaF | Sigma-Aldrich |
| NaCl | Sigma-Aldrich |
| NaOH | Sigma-Aldrich |
| $Na_3VO_4$ | Sigma-Aldrich |
| $Na_3PO_4$ | Sigma-Aldrich |
| $H_2SO_4$ | Sigma-Aldrich |
| TEMED | Sigma-Aldrich |
| TMB | Sigma-Aldrich |
| Tris-base | Sigma-Aldrich |
| Tris-HCl | Sigma-Aldrich |
| Triton-X-100 | Sigma-Aldrich |
| Trypsin/EDTA | Sigma-Aldrich |
| Trypsin/EDTA free | Sigma-Aldrich |
| Tween-20 | Sigma-Aldrich |
| Zymosan | Invitrogen |
| 2-Mercaptoethanol | Gibco™ |

### 2.1.2 Kits

| Kit | Supplier |
|---|---|
| Murine IL-1β ELISA Kit | R&D system |
| Murine IL-6 ELISA Kit | R&D system |
| Murine TNF-α ELISA Kit | R&D system |
| Murine CXCL1 ELISA Kit | R&D system |
| Murine RANTES ELISA Kit | R&D system |
| Plasmid Plus mini Kit | Qiagen |
| qScript$^{TM}$ cDNA Synthesis Kit | Qiagen |
| PerfeCTa® SYBG® Green FastMix® ROX Kit | Qiagen |

### 2.1.3 Buffers

| | |
|---|---|
| Lysis Buffer (RIPA) | 50mM Tris-HCl (pH=7.5)<br>150mM NaCl<br>0.5% (v/v) IGEPAL<br>50mM NaF<br>1mM $Na_3VO_4$<br>1mM DTT<br>1mM PMSF<br>Complete Mini EDTA-free Protease inhibitor cocktail tables, 1tablet in 10ml |
| 4x Sample Buffer | 0.25m Tris-HCl (pH=6.8)<br>6% (w/v) SDS<br>40% (w/v) Sucrose<br>0.04% (w/v) Bromophenol Blue<br>20% (v/v) 2-Mercaptoethanol |
| 4x Laemmli Lower Tris Buffer | 1.5M Tri-base |

| | |
|---|---|
| | 0.4%(w/v) SDS<br>Adjust pH to 8.8 with HCl |
| 4x laemmli Upper Tris Buffer | 1.5M Tris-base<br>0.4%(w/v) SDS<br>Adjust pH to 6.8 with HCl |
| SDS Running Buffer | 25mM Tris-base<br>192mM Glycine<br>0.1% (w/v) SDS<br>Adjust pH to 8.3 with NaOH |
| Transfer Buffer | 25mM Tris-base<br>192mM Glycine<br>15% (v/v) Methanol |
| Blocking Buffer<br>for Immunoblotting | TBS with<br>0.1% (v/v) Tween-20<br>5% (w/v) BSA or non-fat dry milk powder |
| Blocking Buffer for ELISA | PBS with<br>0.1% (v/v) Tween-20<br>1% (w/v) BSA |
| Tris-buffered saline (TBS) | 25mM Tris-base<br>0.14M NaCl<br>Adjust pH to 7.4 with HCl |
| Annexin Binding Buffer | 0.01M Hepes<br>0.14M NaCl<br>2.5mM $CaCl_2$<br>Adjust pH to 7.4 and filter with a 0.2µm sterile filter |

## 2.2 Cell culture

### 2.2.1 L-929 Cell line culture for production of M-CSF containing conditioned medium (M-CSF CM)

L-929 cells were cultured in RPMI-1640 medium supplemented with 10% (v/v) FBS100µg/ml Penicillin and 100µg/ml Streptomycin in a 37°C humidified chamber under a 5% $CO_2$ atmosphere. Cell morphology and confluence were monitored every two days. Once cells reached approximately 80% confluence, adherent cells were passaged using a cell scraper with PBS. For the generation of M-CSF CM, cells were counted using a hemocytometer and plated at $5x10^5$ cells/ml with 40 ml RPMI-1640 medium in a $T175^2$ culture flask for 7 days. Thereafter, the supernatant was removed from the cells and was centrifuged at 600g for 5min. After centrifugation, the supernatant was removed to a new 50ml falcon tube and stored at -80°C for up to 6 months. Cells were cultured for a maximum of 30 passages to avoid excessive genetic drift.

### 2.2.2 Culture of HEK293T Cells

HEK293T cells were cultured in DMEM High-Glucose medium supplemented with 10% (v/v) FBS, 100µg/ml Penicillin and 100µg/ml Streptomycin in a 37°C humidified chamber under a 5% $CO_2$ atmosphere. Cell morphology and confluence were monitored every two days. Once cells reached approximately 80% confluence, adherent cells were passaged using a 1% (w/v) Trypsin (without EDTA) solution in PBS. Cells were cultured for a maximum of 30 passages to avoid excessive genetic drift.

### 2.2.3 Bone marrow-derived macrophages (BMDMs)

Age (8-12 weeks) and gender-matched WT and Peli2$^{-/-}$ mice were sacrificed by cervical dislocation. Mice were first sterilized with 70% ethanol before removal of the femur and tibia under aseptic conditions in a laminar flow hood. Bone marrow was removed by flushing the bones with a 27 $^{3}/_{4}$ gauge needle containing 10ml PBS. Cells were then pelleted by centrifugation at 600g for 5min. 1ml Red blood cell lysis was carried out by resuspending the pellets and incubated at room temperature for 1min. Lysis was terminated by the addition of 20ml RPMI-1640 medium supplemented with 10% (v/v) FBS, 100µg/ml Penicillin and 100µg/ml Streptomycin and cells were centrifuged again at 600 g for 5 min. Pellets were re-suspended in 10ml RPMI-1640 and then cells were plated with 24ml RPMI-1640 medium in a T175$^{2}$ culture flask. 6ml M-CSF conditioned medium was added to a final concentration of 20% (v/v). Cells were cultured in a 37°C humidified chamber under a 5% $CO_2$ atmosphere. After 3 days of culture, the supernatant was carefully removed without displacing adherent cells. 25ml fresh RPMI-1640 medium supplemented with 20% M-CSF (w/v) was gently added and cells were cultured for a further 4 days. Optimal cell growth was determined by examining cell morphology. Differentiated BMDM cells were collected by cell scraping and plated in M-CSF free medium for further use.

### 2.2.4 Colorectal cancer cell lines and normal colon epithelial cell line

The human colorectal cancer cell lines SW480 and SW620 were purchased from ATCC. SW480 and SW620 were both established in 1978 from a primary adenocarcinoma of a 50-year-old male colorectal cancer patient and these two cell lines have subsequently been used worldwide as a model for colorectal cancer research. The human colorectal cancer cell lines DLD-1, HCT116, HT29 and LoVo were gifted by Prof. Daniel Longley (Queen's University Belfast). DLD-1 was derived in 1977 by D·L·Dexter from a primary adenocarcinoma of a colorectal cancer patient and has been shown to have a common genetic with HCT-15 and HRT-18 colorectal cancer cell lines. HCT116 was

isolated from the colon of an adult male colorectal cancer patient, it has a mutation in codon 13 of the Ras proto-oncogene. DLD-1 and HCT116 have been used for investigating treatment options and conducting drug screens. HT29 was isolated in 1964 from a primary adenocarcinoma of a 44-year-old female colorectal patient with epithelial morphology. LoVo was isolated in 1971 from the large intestine of a 56-year-old male with grade IV Dukes C colorectal cancer patient. The normal colon epithelial cell line NCM460D was gifted from the Wenjing Zhu group (The City Vocational College of Jiangsu in China). NCM460D was derived in 1996 from the normal colon of a 68-year-old Hispanic male. This cell line was not infected or transfected with any exogenous genetic information and is non-tumorigenic, and is used as a control cell line to colorectal cancer lines in colorectal cancer research.

The SW480, SW620, DLD-1 and NCM460D cell lines were cultured in DMEM High-Glucose medium supplemented with 10% (v/v) FBS, 100µg/ml Penicillin and 100µg/ml Streptomycin. The HCT116 and HT29 cell lines were cultured in RPMI-1640 medium supplemented with 10% (v/v) FBS, 100µg/ml Penicillin and 100µg/ml Streptomycin. The LoVo cell line was cultured in DMEM/F12 medium supplemented with 10% (v/v) FBS, 100µg/ml Penicillin and 100µg/ml Streptomycin. All cells above were cultured in a 37°C humidified chamber under a 5% $CO_2$ atmosphere.

## 2.3 Molecular biological methods

### 2.3.1 DNA Isolation for Genotyping

1-week-old mice were ear-punched and the tissue sample was placed in a sterile Eppendorf tube. Crude DNA samples were prepared by adding 70µl of DirectPCR$^{TM}$ Lysis Reagent containing 1µl Proteinase K (0.4 mg/ml) and incubated at 55°C for 4h at least. Proteinase K was inactivated by incubating at 85°C for 45 min. Extracted DNA was then diluted 1:10 in DNase-free water before being used as the template for

genotyping PCR reactions.

### 2.3.2 RNA isolation

To avoid contamination of RNA samples, all reagents and labware used were certified as RNase-free. All surfaces were decontaminated with 70% (v/v) ethanol. BMDM cells were plated at $1x10^6$ cells/ml (1ml medium) in 12-well plates for all mRNA analysis experiments. Colorectal cancer cell lines were plated at $0.5x10^6$ cells/ml (1ml medium) in 12-well plates for all mRNA analysis experiments. Harvesting for RNA was carried out by first washing cells with PBS, removing the PBS and adding 500µl Trizol into the well, Trizol and cells were mixed by pipetting multiple times using and incubated on the ice for 5min to ensure full homogenization. The Trizol-treated samples were transferred into a new RNase-free Eppendorf tube, 100µl of chloroform was added and the mixture was first inverted and then vortexed for 5sec. Samples were incubated at 4°C for 10min, during which time phase separation begins. This is completed by centrifugation at 12000g for 15min at 4°C. 200µl of the upper aqueous phase was transferred to a new RNase-free Eppendorf tube, avoiding contamination with the red phenol-chloroform phase or the interphase. 200µl of isopropanol was added to the aqueous phase and the mixture was first inverted and then vortexed for 5sec. Samples were incubated at 4°C for 5min, followed by centrifugation at 12000g for 15min at 4°C. The isopropanol was carefully removed without disturbing the precipitated RNA pellet. 900µl of 75% (w/v) ethanol was added to the pellet and vortexed briefly. Samples were centrifuged at 6000g for 5min at 4°C, after which the ethanol was removed and the RNA pellets were air dried in a laminar flow hood for 10min at least. The RNA pellet was re-suspended in 20µl of RNase-free water and incubated at 60°C for 10min. A Nanodrop™ spectrophotometer was used to quantify the concentration of RNA in each sample. The ratio of the absorbance at 260 and 280nm was used to assess the purity of the RNA sample, where a ratio of 1.8-2.0 indicated pure RNA. RNA samples were stored at -80°C for further use.

### 2.3.3 cDNA synthesis from RNA

1000ng RNA was converted into cDNA by using the qScript™ cDNA Synthesis Kit according to the manufacturer's instructions. 4µl of 5X qScript™ Reaction Buffer and 1µl of qScript™ reverse Transcriptase enzyme were added to 1000ng RNA, and nuclease-free water was added into the tube for a final volume of 20µl. Samples were gently mixed and then placed in a PCR machine. Samples were incubated at 25℃ for 10min, 42℃ for 5min, 85℃ for 5min and then held at 4℃ before retrieval. cDNA samples were stored at -20℃ for further use.

### 2.3.4 Real-time PCR

The real-time PCR was performed on cDNA by using the PerfeCTa® SYBG® Green FastMix® ROX. The mix used for quantification of the target genes included 10µl of the SYB® Green FastMix®, 2µl of primers (forward and reverse), 4µl of diluted cDNA and water was added up to a final volume of 20µl. The sequence and Tm of the primers used are shown in Table 2.1. The PCR cycling conditions are shown in Table 2.2, The annealing temperature was selected based on the primer set being used and was generally 20℃ less than the lower Tm value. Real-time PCR was performed on a StepOnePlus Real-Time PCR System (Applied Biosystems) using MicroAmp Fast 96-well reaction plates. All Real-time PCR experiments included a negative control to ensure the absence of contaminating DNA.

The data were analyzed by using the $2^{-\Delta\Delta CT}$ method. Initially, the target gene's Ct values were subjected to normalization through various Housekeeping Genes, such as HPRT, β-actin, and GAPDH, to obtain the △CT value. This was accomplished by subtracting the target gene Ct value from the housekeeping gene Ct value. Secondly, the △CT value for all samples was normalized to the △CT value of the control samples, resulting in the △△CT value (△△CT = △CT value of sample - △CT value of control sample). Finally, the fold change in expression level of the target gene was

calculated using the following formula: Change Fold = $2^{-\Delta\Delta CT}$.

| Specificity | Primer sequence (5'-3') | Tm(°C) |
|---|---|---|
| h*PELI2* | Forward: GTCAACACAGTATATCCTACAC | 53.81 |
| | Reverse: CCTGAAACATATCCGTATCC | 52.97 |
| m*PELI2* | Forward: ACAGCCACGACGGAGCA | 61.33 |
| | Reverse: TACACTCCCATCCCGAAAACG | 60.07 |
| m*RANTES* | Forward: ATCATCCTCACTGCAGCCCC | 61.99 |
| | Reverse: TGCTGGTGTAGAAATACTCC | 54.48 |
| m*IL-1β* | Forward: GGATGATGATGATAACCTGC | 53.61 |
| | Reverse: CATGGAGAATATCACTTGTTGG | 54.88 |
| m*IL-6* | Forward: TCCACGATTTCCCAGAGAACA | 59.03 |
| | Reverse: ACAACCACGGCCTTCCCTAC | 62.12 |
| m*TNFα* | Forward: TGGGAGTAGACAAGGTAC | 51.9 |
| | Reverse: CATCTTCTCAAAATTCGAGTGA | 60.8 |
| m*CXCL1* | Forward: CACCCGCTCGCTTCTCTGT | 62.29 |
| | Reverse: CACCTCAAGAACATCCAGAGC | 58.65 |
| m*HPRT* | Forward: AGGGATTTGAATCACGTT | 53.25 |
| | Reverse: TTTACTGGCAACATCAACAG | 54.11 |
| h*β-actin* | Forward: CACCATTGGCAATGAGCGGTTC | 62.90 |
| | Reverse: AGGTCTTTGCGGATGTCCACGT | 64.46 |

**Table 2.1 Primers for Real-time PCR, correspondent sequence and melting temperature (Tm)**

| Step | Temperature | Time | Number of cycles |
|---|---|---|---|
| Initial denaturation | 95℃ | 10min | 1 |
| Denaturation | 95℃ | 15s | |
| Annealing | 52-63℃ | 1min | 40 |
| Extension | 72℃ | 15s | |

**Table 2.2 Thermal cycling protocol was followed for real-time PCR experiments.**

### 2.3.5 Lentiviral hPELI2 over-expression or shRNA knockdown model construction in colorectal cancer cell lines.

$1x10^6$ HEK293T cells were plated into 6-well plates with 3ml medium to reach a confluency of 70-80% for next-day transfection. 3µl Lipofectamine2000 (Invitrogen) were diluted into 250µl Opti-MEM and different plasmid combinations were also diluted into another 250µl Opti-MEM (Table 2.3 and Table 2.4), both incubated at room temperature for 5min. A diluted plasmid combination was added into diluted Lipofectamine2000 with a 1:1 ratio, mixed with pipetting multiple times and incubated at room temperature for 15min. After the incubation, the plasmid-lipid complex was gently added to the cell culture medium.

| Packaging plasmid | | hPELI2 overexpression plasmid |
|---|---|---|
| psPAX2 | pMD2.G | hPELI2-strep pcDNA3.1 |
| 1µg | 1µg | 2µg |

**Table 2.3 Plasmid dosage for lentiviral Peli2 over-expression packaging**

| Packaging plasmid | | hPELI2 shRNA knockdown plasmid |
|---|---|---|
| psPAX2 | pMD2.G | hPELI2 shRNA pGIPZ plasmid (A3 or B7) |
| 1μg | 1μg | 2μg |

**Table 2.4 Plasmid dosage for lentiviral hPELI2 shRNA knockdown packaging**

The control group utilized either an empty vector plasmid (pcDNA3.1) or a non-targeting shRNA vector (Non-silencing shRNA pGIPZ). Following transfection, the medium was replaced with fresh medium after 4h and incubated for an additional 48h. Subsequently, the lentivirus-containing medium was collected and centrifuged at 1200g for 5min before transferring to falcon tubes for long-term storage at -80℃. To transduce cells, $1x10^6$ cells were plated into 6-well plates with 3ml of medium and incubated overnight. On the second day, at a confluency of approximately 70%, cells were transduced with 3ml of medium consisting of a 1 to 1 mixture of lentivirus-containing medium and fresh medium, containing hexadimethrine bromide (final concentration of 8mg/ml). After 48h, the medium was removed and replaced with fresh medium supplemented with the selective agent puromycin (10μg/ml). After 2 or 3 cell passages and puromycin selection, h*PELI2* mRNA and hPELI2 protein expression levels were assessed through quantitative real-time PCR and western blotting.

### 2.3.6 Transient transfection of cell

Between $5x10^5$ to $1x10^6$ cells were plated in 6-well plates with 3ml medium to attain a confluency of 70-80% for transfection the following day. On the second day, 3μl of Lipofectamine2000 (Invitrogen) was diluted into 250μl Opti-MEM, and 2500ng of target plasmid or a combination of plasmids was diluted into another 250μl Opti-MEM. Both mixtures were incubated at room temperature for 5min. The diluted plasmid or

plasmid combinations were combined with the diluted Lipofectamine2000 in a 1:1 ratio, thoroughly mixed with pipetting, and incubated at room temperature for 15 min. After incubation, the plasmid-lipid complex was gently added to the cell culture medium. The medium was replaced with fresh medium after 4h of transfection for continued incubation.

## 2.4 Cellular biological methods

### 2.4.1 MTT assay

#### 2.4.1.1 Cell proliferation assay

Cells (4 x$10^3$) were plated into 96-well plates with 200µl medium. After 12h, 24h, 48h and 72h, MTT solution (10µl, 5mg/ml) was added into the wells and the plate was returned to the 37℃ humidified chamber under a 5% $CO_2$ atmosphere for 4h. The medium was removed and DMSO (150µl) was added into wells to dissolve the crystals. Absorbance was measured at a wavelength of 490nm by using a microplate reader.

#### 2.4.1.2 Cell viability assay

Cells (4000) were plated into 96-well plates with 200µl medium for next-day treatment. After culture overnight, cells were treated with indicated concentrations of Dmx1/10 and/or chemotherapy drug Cisplatin for 48h. MTT solution (10µl, 5mg/ml) was added into the wells and the plate was returned to the 37℃ humidified chamber under a 5% $CO_2$ atmosphere for 4h. The medium was removed and DMSO (150µl) was added into wells to dissolve the crystals. Absorbance was measured at a wavelength of 490nm by using a microplate reader. The half maximal inhibitory concentration (IC50) of Dmx1/10 and/or Cisplatin to the cell viability was determined by interpolation from dose-response curves.

### 2.4.2 Colony formation assay

Cells (500) were plated into 6-well plates at 600 cells/well (HCT116 and HT29) or 900 cells/well (DLD-1, SW480 and SW620) with 3ml medium. After 5 days, cells were exposed to indicated specific treatment. On the day7, medium was removed and wells were gently washed with PBS. Colonies were then fixed in 2ml methanol for 5min. Methanol was removed and colonies were stained with 0.5% (v/v) Crystal Violet diluted in 20% methanol. Colony number in each wells was counted by using the OpenCFU software.

### 2.4.3 3D spheroid assays

Cells (500) were seeded in 96-well U-bottom ultra-low attachment plate with 200µl medium. Spheroids were allowed to develop for 24h, and then imaged at 4X magnification (Optika Vision Pro) and the diameter was measured (Olympus EP50) under a microscope using EP-view software to record spheroid diameter and marked as Day 1. Spheroids were returned to the 37℃ humidified chamber under a 5% $CO_2$ atmosphere for 4 days with spheroids being imaged and the diameter measured on Day 3 and Day 5, and the specific treatments were applied on Day 3 after being imaged. Day 1 diameter was subtracted from the Day 3 or Day 5 measurement to determine spheroid progression.

### 2.4.4 Flow cytometry

Cells ($5x10^5$) were plated into 6-well plates with 3ml medium to reach a confluency of 70-80% for next-day treatment. On the second day, cells were treated with 5µM Dmx1/10 and/or indicated concentrations of Cisplatin for 24h. And then adherent cells were harvested by trypsin treatment and suspension cells were pellet by 800g centrifugation for 5min. All the cells were mixed, and cells were twice washed with 1ml cold PBS and once with 1x Annexin binding buffer. Then cells were re-suspended

in 1000µl 1x Annexin binding buffer. 100µl cell suspensions were transferred into a new Eppendorf tube, 1x Annexin binding buffer (400µl), Annexin V (5µl, 90µg/ml) and propidium iodide (PI) (10µl, 1mg/ml) were added into the tube. The components were mixed by pipetting multiple times and incubated at room temperature for 15min, then the cells were evaluated by flow cytometry (BD Accuri$^{TM}$ C6). At least 10,000 cells were counted, single live cells were selected and the apoptosis rate and apoptosis stage were determined by using Annexin V as the X-axis coordinate and PI as the Y-axis coordinate. The unstained sample, Annexin V alone stain sample and PI alone stain sample were used as controls to delineate the different intervals.

## 2.5 Biochemical methods

### 2.5.1 Protein Extraction

Cells were plated into 6-well or 12-well plates to reach a confluency of 70-80% for next-day treatment. The details for each experiment are described in the correspondent results section and figure legends. When harvesting the cell lysates, to avoid protein degradation, all equipment was pre-chilled and all steps in the extraction process were carried out on ice unless otherwise stated. Medium was removed (for some experiments, the medium was transferred into a falcon tube and centrifuged at 6000g for 10min at 4℃ to pellet the cells) and the cells were gently washed with PBS. Then cells were scraped in PBS and transferred into the Eppendorf tubes. Samples were centrifuged at 6000g for 10min at 4℃, after that PBS was removed and cells were re-suspended in cold RIPA lysis buffer and incubated on ice for at least 30min. Lysate was then subjected to centrifugation at 12000g for 10min at 4℃, The supernatants were transferred into new Eppendorf tubes and the appropriate amount of 6x Sample buffer was added to make the final concentration 1x. Samples were then boiled for 10min at 95℃ and stored at -20℃ for further use.

### 2.5.2 Protein Immunoprecipitation

#### 2.5.2.1 Co-Immunoprecipitation to investigate protein-protein interactions

Cells were plated into 6-well plates with 3ml medium to reach a confluency of 70-80% for next-day treatment. The details for each experiment are described in the correspondent results section and figure legends. Cells were placed on ice and the media was removed. Cells were gently washed with cold PBS before being scraped into 1ml cold PBS. Cell suspensions were transferred to Eppendorf tubes and subjected to centrifugation at 6500g for 5min at 4℃. Excess PBS was removed without disturbing the pellet which was then re-suspended in 200µl ice-cold NP-40 lysis buffer or RIPA buffer and incubated on ice for at least 30min. Lysates were then subjected to centrifugation at 12000g for 10min at 4℃. lysate supernatants (20µl) were transferred into a new Eppendorf tube and 4µl of 6x sample buffer was added to make the final concentration 1x. Samples were then boiled for 10min at 95℃ and stored at -20℃ as an input whole cell lysate control. The remaining lysate was removed from the insoluble pellet and transferred to a fresh 1.5 ml Eppendorf tube. The volume of the sample was increased to 1ml using ice-cold lysis buffer. Immunoprecipitation of the protein of interest was then carried out by the addition of a respective antibody to each tube with an appropriate dilution ratio (Table 2.5). Samples were incubated overnight at 4℃ under constant agitation using a sample rocker.

| Antibody | Dilution ratio |
|---|---|
| IRAK1 | 1:300 |
| Myc | 1:1000 |
| Bcl-xL | 1:300 |

**Table 2.5 Antibody dilution ratio of Co-Immunoprecipitation**

On the following day, 40µl of protein A/G plus-agarose beads were added to each sample followed by a further incubation at 4°C for 4h under constant agitation. Samples were centrifuged at 6000g for 10min at 4°C and the supernatant was removed. 1ml of Co-IP lysis buffer was added to the bead pellet followed by several inversions of the tube. Samples were once again subjected to centrifugation and the wash step was repeated three more times. After the final wash step, all the supernatant was removed and 40µl of 2x sample buffer was added to the beads. Samples were boiled for 5min. Samples were then boiled for 10min at 95°C and stored at -20°C for further use.

#### 2.5.2.2 Immunoprecipitation of denatured proteins

Cells were plated into 6-well plates with 3ml medium to reach a confluency of 70-80% for next-day treatment. The details for each experiments are described in the correspondent results section and figure legends. Cells were placed on ice and the media was removed. Cells were gently washed with cold PBS prior to being scraped into 1ml cold PBS. Cell suspensions were transferred to Eppendorf tubes and subjected to centrifugation at 6500g for 5min at 4°C. Excess PBS was removed without disturbing the pellet which was then re-suspended in 200µl ice-cold RIPA lysis buffer and incubated on ice for at least 30min. Lysates were then subjected to centrifugation at 12000g for 10min at 4°C. Lysate supernatants (20µl) were transferred into a new Eppendorf tube and 4µl of 6x sample buffer was added to make the final concentration 1x. Samples were then boiled for 10min at 95°C and stored at -20°C as an input whole cell lysate control. The remaining 180µl lysate was removed from the insoluble pellet and transferred to a fresh 1.5 ml Eppendorf tube and 10% (w/v) SDS solution (20µl) was added into the lysate. Samples were mixed and boiled for 10min at 95°C to facilitate complete disassociation of proteins. After the heat, samples were cold on the ice for 10min and add 800µl ice-cold RIPA buffer to dilute SDS. Immunoprecipitation of the protein of interest was then carried out by the addition of a respective antibody to each tube with an appropriate dilution ratio. Samples were incubated overnight at 4°C under constant agitation using a sample rocker.

| Antibody | Dilution ratio |
|---|---|
| IRAK1 | 1:300 |
| Bcl-xL | 1:300 |

**Table 2.6 Antibody dilution ratio of Immunoprecipitation**

On the following day, 40µl of protein A/G plus-agarose beads were added to each sample followed by a further incubation at 4℃ for 4h under constant agitation. Samples were centrifuged at 6000g for 10min at 4℃ and the supernatant was removed. 1000µl of cold RIPA buffer was added to the bead pellet followed by several inversions of the tube. Samples were once again subjected to centrifugation and the wash step was repeated three more times. After the final wash step, all the supernatant was removed and 40µl of 2x sample buffer was added to the beads. Samples were boiled for 5min. Samples were then boiled for 10min at 95℃ and stored at -20℃ for further use.

### 2.5.3 BCA protein assay

BCA protein assay were performed to quantitate protein concentration. A known concentration of BSA standards and samples were diluted according to the manufacturer's instructions. The aliquots (5µl) of standards and diluted samples were added into wells of 96-well plates and 100µl of working reagent were mixed with samples, and the plate was incubated at 37℃ for 30min. The OD value of each well was measured at wavelength 600nm. AEL×800$^{TM}$ microplate reader with Gen5 Data Analysis Software was used to carry out the reading. The sample concentrations were determined by interpolating the sample absorbance from the known concentrations of the standard curve. Standards were assayed in duplicate while samples were analyzed in triplicate. Data and analysis were carried out using Excel and GraphPad.

### 2.5.4 SDS-Polyacrylamide gel electrophoresis (SDS-PAGE)

SDS-PAGE was conducted in a Biorad MiniProtean® Tetra System, according to the method of Laemmli (Laemmli, 1970), as modified by Studier (Studier, 1973). Typically, 10% SDS polyacrylamide gels were used with alterations made depending on the size of the protein of interest. Details about the preparation of all gels are displayed in Table 2.5. Electrophoresis was performed at a constant 90V through a 5% stacking gel, followed by 120V through the resolving gel for between 2h-3h depending on the size of your interest targeted protein.

**Lower Resolving Gels**

| **% Total Acrylamide** | **8%** | **10%** | **12%** | **15%** | |
|---|---|---|---|---|---|
| $H_2O$ | 12.1 | 10.5 | 8.75 | 6.25 | ml |
| 4X Lower Tris Buffer | 6.25 | 6.25 | 6.25 | 6.25 | ml |
| Protogel | 6.67 | 8.35 | 10 | 12.5 | ml |
| 10% (w/v) APS | 130 | 130 | 130 | 130 | µl |
| TEMED | 15 | 15 | 15 | 15 | µl |
| Total Volume | 25 | 25 | 25 | 25 | ml |

**Upper Stacking Gel**

| % Total Acrylamide | 5% | |
|---|---|---|
| $H_2O$ | 5.8 | ml |
| 4X Lower Tris Buffer | 2.5 | ml |
| Protogel | 1.7 | ml |
| 10% (w/v) APS | 40 | µl |
| TEMED | 20 | µl |
| | | |
| Total Volume | 10 | ml |

**Table 2.7 Composition of polyacrylamide gels used**

### 2.5.5 Immunoblotting

Following separation by electrophoresis, the migrated proteins were transferred electrophoretically to 0.2µm pore size nitrocellulose membranes by an Owl™ VEP-2 Mini Tank Electroblotting System. Electrical current (Amps) and transfer times varied depending on the size of the protein of interest between 15kDa to 250kDa. Pre-cut Whatmann paper and nitrocellulose membranes were equilibrated with Transfer Buffer 10min prior to use. 3 layers of Whatmann paper were placed on the bottom surface of the transfer unit followed by a single layer of nitrocellulose. The resolving gel was washed briefly in transfer buffer before being placed on the nitrocellulose while avoiding bubbles. 3 more layers of Whatmann paper were placed on top and the unit was closed. The transfer was carried out at 90mA/gel (4 gels maximum, corresponding to 360mA) for 90min. At the end of the transfer, the membranes were quickly washed in TBST buffer and incubation with TBST buffer containing 5% (w/v) Bovine Serum Albumin (BSA) for 1h on an orbital shaker at room temperature to inhibit non-specific antibody binding. Membranes were then incubated with appropriate primary antibodies

diluted in 5% (w/v) BSA-TBST buffer at 4℃ overnight. The specificity and dilutions used for the various antibodies are listed in Table 2.8.

After overnight incubation, membranes were washed in TBST buffer for 15min and repeated two more times. Following washing, the membranes were incubated with an HRP-conjugated secondary antibody or Licor-conjugated secondary antibody specific to the primary antibody in 5% (w/v) BSA-TBST buffer at room temperature for 1h (the secondary antibodies are listed in Table 2.9). The membranes were finally washed with TBST buffer for 5min and repeated two times. Protein bands were then visualized using the Odyssey infrared imaging system from Licor Biosciences or using enhanced chemiluminescence (ECL).

| **Primary antibody** | **Brand** | **Dilution** | **Source** |
|---|---|---|---|
| β-actin | Sigma | 1: 5000 | Mouse |
| IRAK1 | Cell Signaling | 1: 1000 | Rabbit |
| IκBα | Santa Cruz | 1: 500 | Rabbit |
| p-IκBα | Cell Signaling | 1: 500 | Mouse |
| IKKα/β | Cell Signaling | 1: 1000 | Rabbit |
| p-IKKα/β | Cell Signaling | 1: 1000 | Rabbit |
| P65 | Cell Signaling | 1: 1000 | Rabbit |
| p-P65 | Cell Signaling | 1: 1000 | Rabbit |
| AKT | Cell Signaling | 1: 3000 | Rabbit |
| p-AKT (Ser473) | Cell Signaling | 1: 1000 | Rabbit |
| p-AKT (Thr308) | Cell Signaling | 1: 1000 | Rabbit |
| ERK | Cell Signaling | 1: 3000 | Rabbit |
| p-ERK | Cell Signaling | 1: 1000 | Rabbit |
| JNK | Cell Signaling | 1: 1000 | Rabbit |
| p-JNK | Cell Signaling | 1: 1000 | Rabbit |
| P38 | Cell Signaling | 1: 3000 | Rabbit |

| | | | |
|---|---|---|---|
| p-P38 | Cell Signaling | 1: 1000 | Rabbit |
| IL-1β | R&D | 1: 1000 | Rabbit |
| Caspase1 | Adipogen | 1: 1000 | Rabbit |
| Caspase3 | Cell Signaling | 1: 1000 | Rabbit |
| Cleaved-Caspase3 | Cell Signaling | 1: 1000 | Rabbit |
| Caspase9 | Cell Signaling | 1: 1000 | Rabbit |
| NLRP3 | Cell Signaling | 1: 1000 | Rabbit |
| ASC | Adipogen | 1: 1000 | Rabbit |
| Bcl-xL | Cell Signaling | 1: 1000 | Rabbit |
| Bax | Cell Signaling | 1: 1000 | Rabbit |
| PARP | Cell Signaling | 1: 1000 | Rabbit |
| Ubiquitin | Millipore | 1: 500 | Rabbit |
| Lys48-Ubiquitin | Millipore | 1:500 | Rabbit |
| Lys63-Ubiquitin | Millipore | 1:500 | Rabbit |
| Myc-Tag | Cell Signaling | 1: 3000 | Mouse |
| Strep-Tag II | Cell Signaling | 1: 3000 | Rabbit |

**Table 2.8 Specificity, brand, dilution and source of all primary antibodies used.**

| Secondary Antibody | Brand | Dilution | Source |
|---|---|---|---|
| IRDye® 680RD Goat anti-Mouse | Li-cor | 1: 3000 | Goat |
| IRDye® 680RD Goat anti-Rabbit | Li-cor | 1: 3000 | Goat |
| IRDye® 680RD Donkey anti-Goat | Li-cor | 1: 3000 | Donkey |
| HRP-linked Goat anti-Rabbit | Cell Signaling | 1: 3000 | Goat |
| HRP-linked Goat anti-Mouse | Cell Signaling | 1: 3000 | Goat |

**Table 2.9 Specificity, brand, dilution and source of all secondary antibodies used.**

### 2.5.6 Enzyme-linked immunosorbent assay (ELISA)

Cell supernatants or serum samples were collected and stored at -20℃ prior to analysis. 96-well NUNC "Maxisorb" plates were coated with 30µl of capture antibody diluted to a working concentration in PBS according to the manufacturer's instructions. Plates were covered to avoid evaporation and placed on an orbital shaker at 4℃ for overnight.

Diluted Antibody was aspirated from the plate and each well was washed with PBST (0.05% Tween20 in PBS) buffer for three times. After the wash, then the plates were blocked by adding 100µl of block buffer (1% (w/v) BSA in PBS) at room temperature for 2h. After the block, plates were washed with PBST three times again, then samples were diluted appropriately with block buffer and 30µl diluted samples were added to

each well. Standards were diluted in block buffer along a seven-point standard curve using 2-fold serial dilutions with a top standard of 1000pg/ml. Plates were covered to avoid evaporation and placed on an orbital shaker at 4°C for overnight.

Plates were washed as above and 30µl of detection antibody was diluted to a working concentration in block buffer according to the manufacturer's instructions. Plates were incubated for 2h at room temperature and the wash steps were repeated. Streptavidin-HRP conjugate was diluted in block buffer according to the manufacturer's instructions and 30µl was added to each well. Plates were incubated in the dark for 30min at room temperature and the wash step was repeated after the incubation. 30µl TMB (1.25 mM/l) solution was added to each well and the plates were covered and incubated at room temperature for different periods of time depending on the intensity of the colour exhibited by the samples and standards. 10µl stop solution (1 N $H_2SO_4$) was added to stop the reaction. The optical density (OD) value of each well was measured at 450nm with a correction at 590nm. A ELx800$^{TM}$ microplate reader with GenS Data Analysis Software was used to carry out the reading. The sample concentrations were determined by interpolating the sample absorbance from the known concentrations of the standard curve. Standards were assayed in duplicate while samples were analyzed in triplicate. Data presentation and analysis were carried out using GraphPad Prism 5 software.

### 2.5.7 LDH assay to detect cell cytotoxicity

LDH release from cells was determined using a CytoTox 96® Non-Radio Cytotoxicity Assay Kit. 10x Lysis Buffer was added to untreated cells 45min prior to harvest to act as the maximum LDH activity control while RPMI-1640 medium was used as a background signal in the detection phase of the assay. 50µl of supernatant samples were collected from cells and transferred to a flat bottom 96-well plates followed by addition of 50µl of the CytoTox 96® Reagent. The plate was covered with foil to protect it from light and incubated at room temperature for 30min. 50µl of stop solution was added to each well to stop the reaction and the OD value of each well was measured at a

wavelength 490nm within 1h after adding the stop solution.

## 2.6 *In vivo* studies

WT mice were bred from the BRU facility of Maynooth University with a C57BL/6 mice colony. Peli2$^{-/-}$ mice were generated by Taconic Artemis using proprietary technology. To generate constitutive Peli2$^{-/-}$ mice, mice that were heterozygous for the targeted allele were bred with mice containing a Flpe transgene (C57BL/6-Tg (CAG-Flpe)2Arte). This resulted in the deletion of exon 2–6 and loss of function of the *Peli2* gene. The Flpe transgene was removed by breeding the resulting Peli2$^{+/-}$ mice with C57BL/6 mice during colony expansion. Mice were genotyped by PCR analysis of DNA isolated from ear punches using primers "a" GCCTCTACAGGATGCTCATTT; "b," GGACAGTCATGCTAGTCTGAGG; "c," GAGACTCTGGCTACTCATCC; and "d," CCTTCAGCAAGAGCTGGGGAC.

All animal experiments were performed under licenses of the Health Products Regulatory Authority (HPRA) of Ireland with all protocols being approved by the Research Ethics committees of Maynooth University

### 2.6.1 LPS-induced sepsis model

Age (8-10 weeks), weight and sex-matched mice were rehoused in pairs and allowed to acclimatize to the new surroundings for 3days or more to avoid stress. Mice were weighed again prior to injection to determine the normalized Dmx10 and LPS dosage. Injection of either 10 or 20mg/kg Dmx10, 10mg/kg ultrapure LPS was carried out i.p. using a 27g needle. Dmx10 were accurately weighted and subsequently dissolved in PBS at a final concentration of 2mg/ml, with DMSO included at 1:1000 (v/v) ratio. The resulting Dmx10 solution, along with a vehicle control consisting of an equivalent volume of PBS (including 1:1000 (v/v) DMSO), was administered to mice via

intraperitoneal injection. Over a period of 3h, the mice were vigilantly monitored every 1h, and their well-being was assessed and documented at hourly intervals using an animal welfare scoring system. Subsequently, mice were injected by i.p. injection with PBS-diluted LPS, with an equivalent volume of PBS serving as a vehicle control. On the second day, mice were sacrificed by cervical dislocation and blood was extracted by cardiac puncture into the Eppendorf tube. Whole blood samples were incubated at room temperature for 30min to allow clotting then centrifugation at 2000g for 10min at 4℃. The serum supernatant samples were removed to a new Eppendorf tube and stored at -80℃ for further use.

### 2.6.2 AOM/DSS-induced colorectal cancer model

Age (6-8 weeks), weight and sex-matched mice were rehouse in pairs and allowed to acclimatize to the new surroundings for 3days or more to avoid stress. Mice were weighed again prior to injection to determine the normalized AOM dosage. Injection of 10mg/kg AOM was carried out i.p. using a 27g needle. After one week, 2% DSS was administered in the drinking water for one week, followed by regular water for two weeks. The DSS-drinking were repeated for three cycles. Throughout the study, body weight, stool consistency and presence of hematochezia were continuously monitored every 3days until the mice were sacrificed at the $9^{th}$ week by cervical dislocation. Visible tumors on the colorectal mucous were counted, and tumor loads were measured.

# Chapter 3: Investigating the effects of novel compounds targeting Pellino2 in LPS-induced inflammation

## 3.1 Introduction

The innate immune system is equipped with various pattern recognition receptors (PRRs) to effectively eliminate pathogens (Li and Wu 2021; O'Neill, Golenbock, and Bowie 2013). PRRs are a category of proteins located on the surface of immune cells, responsible for detecting pathogen-associated molecular patterns (PAMPs) originating from invading pathogens (Amarante-Mendes et al. 2018). Toll-like receptors (TLRs), as the prototypical PRRs, are essential components of immune cells that respond to invading pathogens (Lester and Li 2014; Maslinska, Laure-Kamionowska, and Maslinska 2012; Medzhitov 2001). Nevertheless, dysregulated TLR activation has the potential to cause inflammatory ailments and autoimmune conditions in humans, such as septicemia (Kumar 2020), bronchial asthma (Zakeri and Russo 2018), rheumatoid arthritis (Huang and Pope 2009), and multiple sclerosis (Zheng et al. 2019). Recognition of microbial components like LPS by TLR4 initiates a signaling cascade that activates immune cells, triggering subsequent inflammatory events (Lu, Yeh, and Ohashi 2008; Park and Lee 2013; Pu and Wang 2014). This process involves the recruitment of the MyD88 adaptor protein, which subsequently recruits and activates IRAK4. This, in turn, associates with IRAK1, promoting its hyperphosphorylation. IRAK1 subsequently interacts with TRAF6, TAK1, TAB1, and TAB4 to form a complex that leads to the activation and relocation of the NF-κB transcription factor to the nucleus (Akira, Takeda, and Kaisho 2001; Lu, Yeh, and Ohashi 2008; Park and Lee

2013), this pathway also triggers the downstream activation of downstream MAPKs, including ERK, P38, and JNK (Kuriakose et al. 2019; Tong et al. 2020). These signaling pathways ultimately result in the transcription of inflammation-associated genes and the production of pro-inflammatory cytokines, such as IL-1β, IL-6, and TNFα (Pu and Wang 2014). Excessive activation of TLR4/NF-κB and MAPKs signaling pathways is closely linked to the development of inflammatory diseases. In addition, dysregulated production of pro-inflammatory cytokines may lead to the onset of a severe condition called a "Cytokine storm" (Fajgenbaum and June 2020) which can cause significant harm to the body. Therefore, maintaining precise regulation of cytokine production at the cellular level is crucial to ensure proper homeostasis in the body.

Protein ubiquitination is a critical post-transcriptional modification that regulates the intensity of cell signaling pathways (Swatek and Komander 2016). Specifically, lysine 48 (Lys48)-linked protein ubiquitination facilitates protein degradation via the ubiquitin-proteasome system (Tai and Schuman 2008; Gu et al. 2023). Conversely, lysine 63 (Lys63)-linked protein ubiquitination does not target proteins for proteasomal degradation. Instead, the function of Lys63-linked protein ubiquitination is to serve as a platform that links signaling proteins upstream and downstream (Jacobson et al. 2009). Ubiquitination plays a crucial role in regulating the activation of NF-κB and MAPKs signaling pathways. For instance, MyD88 recruits IRAK1 to further activate TRAF6. This process is followed by Lys48-specific ubiquitination and proteasomal degradation of IRAK1, which leads to the negative regulation of the signaling pathway (Chen 2012; Muroi and Tanamoto 2012). Additionally, IRAK1 can undergo ubiquitination at Lys63, which regulates its function during the activation of signaling pathway (Gottipati, Rao, and Fung-Leung 2008). The activation of the NF-κB signaling pathway is also critically dependent on the Lys63-specific ubiquitination of TRAF6 (Chen 2012). In contrast, recent research has shown that TRAF6 can also undergo ubiquitination at Lys48, which promotes its degradation (Muroi and Tanamoto 2012). The ubiquitination of target proteins requires the involvement of three distinct enzymes: E1 ubiquitin-activating enzyme, E2 ubiquitin-conjugating enzyme, and E3 ubiquitin-protein ligase (Ebner,

Versteeg, and Ikeda 2017). Due to the need to bind and ubiquitinate a wide variety of target proteins, humans have hundreds of E3 ubiquitin ligases.

Pellino proteins, including Pellino1, Pellino2, and Pellino3, are a family of E3 ubiquitin ligases that play diverse regulatory roles in innate immune signaling pathways (Moynagh 2014). Pellino proteins were first discovered as a component of the Dorsal/Cactus signaling complex in *Drosophila melanogaster* and have been identified as IRAK protein interaction partners. Each member possesses an N-terminal forkhead-associated (FHA) domain, recognizing phosphothreonine residues and enabling association with IRAK1. Additionally, the C-terminal RING-like domain provides these proteins with E3 ubiquitin ligase activity, catalyzing the Lys63-linked polyubiquitination of target proteins, including IRAKs (Yu et al. 2002; Jiang et al. 2003; Jensen and Whitehead 2003b). Pellino proteins are involved in various roles in immune signaling pathways. For example, Pellino1 has been implicated in suppressing T cell activation, driving neuroinflammation, and promoting lymphomagenesis and lung carcinogenesis through its involvement in TLR3 and TLR4 signaling pathways (Chang, Jin, and Sun 2009). Pellino2 is involved in the activation of NF-κB and MAPK signaling pathways induced by LPS and IL-1β, and has been shown to promote ubiquitination of NLRP3 to regulate inflammasome priming (Humphries et al. 2018). Pellino3, on the other hand, has been reported to suppress TLR3 signaling and TNF-induced cell death, as well as serve as an essential modulator of obesity-induced IL-1β expression and insulin resistance through its mediation of NOD2 signaling (Yang et al. 2013). Targeting Pellino proteins may represent a promising therapeutic strategy for regulating the activation of TLR4-mediated NF-κB and MAPKs signaling pathways and suppressing excessive inflammatory responses. However, despite the promising potential of targeting Pellino proteins to treat inflammatory diseases, no candidate molecules have been developed that effectively mimic or promote their function. Therefore, the development of a compound that targets and mimics the function of Pellino proteins presents an opportunity for treating these diseases.

Small molecule drugs have shown advantages over biomacromolecules in terms of greater specificity, bioavailability, and lower cytotoxicity (Beck et al. 2022; Jahangirian et al. 2019). In this study, we aimed to characterize the regulatory effects of two novel proprietary compounds, that were designed in our laboratory with the aim of targeting Pellino proteins, on inflammatory signaling pathways. We employed a ligand-based pharmacophore approach for drug design targeting Pellino proteins, utilizing protein structure information was available from the x-ray crystal structure of Pellino2 (Lin et al. 2008). Pharmacophore modeling was conducted based on a peptide sequence from Pellino proteins that our laboratory previous work had shown to be important for function. The resulting pharmacophore was employed for virtual screening of a compound library. Following this, we synthesized lead compounds based on the profiled virtual hits from the in silico screen. Through this process, we identified ten candidate compounds, namely, Dmx1 to Dmx10. The detailed process used in designing the pharmacophore, the in silico screening and subsequent medicinal chemical chemistry is the subject of an invention disclosure to Maynooth University and likely patent application. In this chapter we aimed to characterize the potential regulatory effects of these compounds on inflammatory signaling pathways and to explore the mechanistic basis to any such effects.

## 3.2 Results

### 3.2.1 Dmx1 and Dmx10 inhibit LPS-induced expression of the pro-inflammatory cytokine IL-1β independently of any cytotoxic effects

The compounds were designed based on x-ray crystal structure information from Pellino2. Given that our laboratory previous work has shown that Pellino2 promotes induction of the pro-inflammatory cytokines IL-1β, the potential anti-inflammatory properties of newly synthesized compounds were initially examined by assessing their regulatory effects on LPS-induced expression of IL-1β. To this end, wild-type (WT) bone marrow-derived macrophages (BMDMs) were pre-treated with the panel of compounds (5μM) (DMSO as a vehicle control) for 1h and then stimulated with the TLR4 ligand LPS (100ng/ml) for 24h and assessed for protein levels of the pro-inflammatory cytokine IL-1β. LPS-induced expression of IL-1β and pre-treatment with compounds Dmx1, Dmx5, Dmx7 and Dmx10, inhibited the expression of IL-1β to varying levels (Fig3.1). The other compounds failed to affect the LPS response.

The specificity of the inhibitory effects of Dmx1, 5, 7 and 10 on IL-1β expression, was then examined by investigating any general cytotoxic effects, as measured by cellular release of lactate dehydrogenase (LDH). LDH is a stable cytosolic enzyme released upon cell lysis and its release is a measure of cell damage and necrosis (Kumar, Nagarajan, and Uchil 2018; Chan, Moriwaki, and De Rosa 2013). WT BMDMs were treated with Dmx1, 5, 7 and Dmx10 (5μM) for 24h (DMSO as a vehicle control) and LDH content from supernatants was measured. Results showed that Dmx1 and Dmx10 did not cause any additional release of LDH beyond the vehicle control indicating that their inhibitory effects were independent of cytotoxicity (Fig3.2). In contrast, Dmx5 and Dmx7 showed a tendency to promote the LDH release, indicating potential cytotoxic effects. These two compounds were not further explored in my study.

The dose-dependent effects of Dmx1 and Dmx10 were next studied. Cells were treated

with Dmx1 or Dmx10 (5μM and10μM) (DMSO as a vehicle control) for 24h or 48h and the levels of IL-1β and LDH were measured. Results showed that the inhibitory effects on IL-1β expression of Dmx1 and Dmx10 exhibit concentration-dependency (Fig3.3a) without affecting LDH release (Fig3.3b).

Dmx1 and Dmx10 was next examined for any direct effects on cell viability. Viability was assessed using the MTT assay. This is a colorimetric assay that measures cell metabolic activity via the reduction of the tetrazolium dye MTT to insoluble purple formazan crystals (Buranaamnuay 2021). WT BMDMs were plated in 96-well plates, cells were treated with indicated concentrations Dmx1 or Dmx10 for 24h (DMSO as a vehicle control) and the MTT assay was performed to directly measure the effects of Dmx1 and Dmx10 on cell viability. Both compounds showed effects on cell viability at higher concentration with the IC50 of Dmx1 being 47.49μM while the IC50 of Dmx10 was 36.45μM (Fig3.4). At concentrations of 10μM or less that affect expression of LPS-responsive IL-1β, Dmx1 and Dmx10 do not impair macrophage cell viability. These data indicated that the inhibitory effects of Dmx1 and Dmx10 on LPS-induced expression of the pro-inflammatory cytokine IL-1β are independent of any cytotoxic effects.

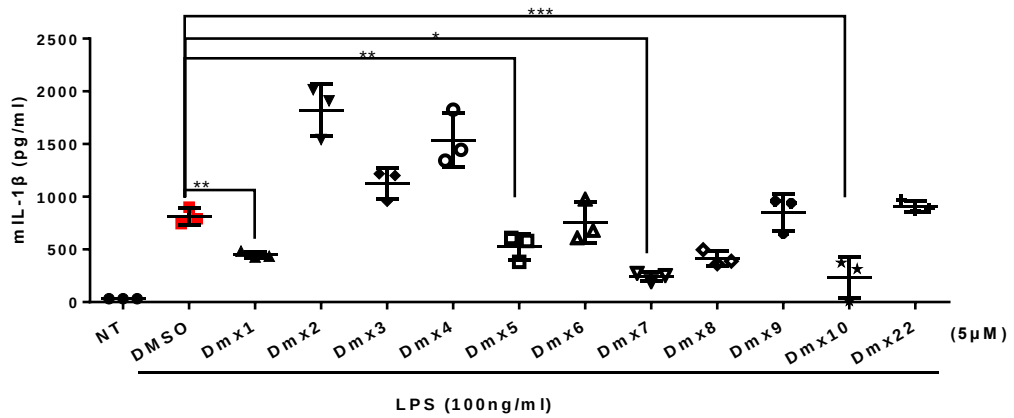


**Fig3.1 Screening the regulatory effects of proprietary Pellino-targeted small molecules on LPS-induced expression of IL-1β**

WT BMDMs (2 x$10^5$) were plated in 96-well plates. Cells were left untreated (NT) or treated for 1h with various compounds at a final concentration of 5μM. Control cells were treated with DMSO vehicle. Cells were stimulated with LPS (100ng/ml) for 24h. Supernatants were assayed by ELISA for levels of IL-1β. Data are shown from an experiment that is representative of three independent experiments. Statistical analysis was performed by using the paired Student t-test. Statistically significant differences are indicated by the asterisks: *, $P<0.05$; **, $P<0.01$; ***, $P<0.001$.

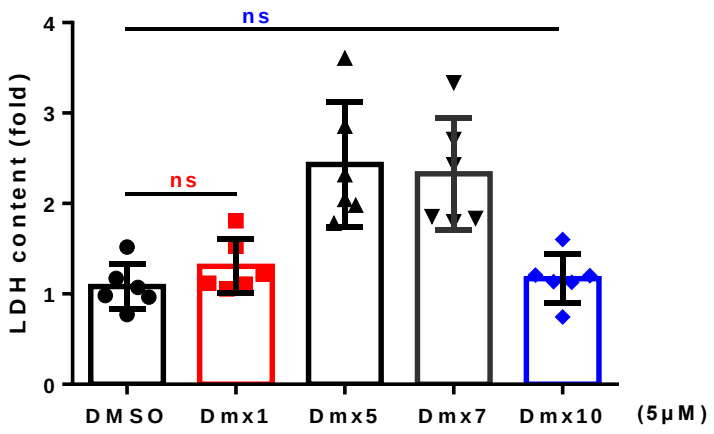


**Fig3.2 Use of LDH assay to evaluate potential cytotoxic effects of novel compounds**

WT BMDMs (2 x$10^5$) were plated in 96-well plates. Cells were treated with indicated compounds at a final concentration of 5µM for 24h. Control cells were treated with DMSO vehicle. Supernatants were assayed for levels of LDH. The cytotoxicity of the compounds was evaluated by relating the LDH content in the supernatant of compounds-treated cells with supernatants from DMSO treated cells. Data are shown from an experiment with six independent sample replicates that is representative of three independent experiments. Statistical analysis was performed by using the paired Student t-test. Statistically significant differences are indicated by the asterisks: ns, P>0.05.

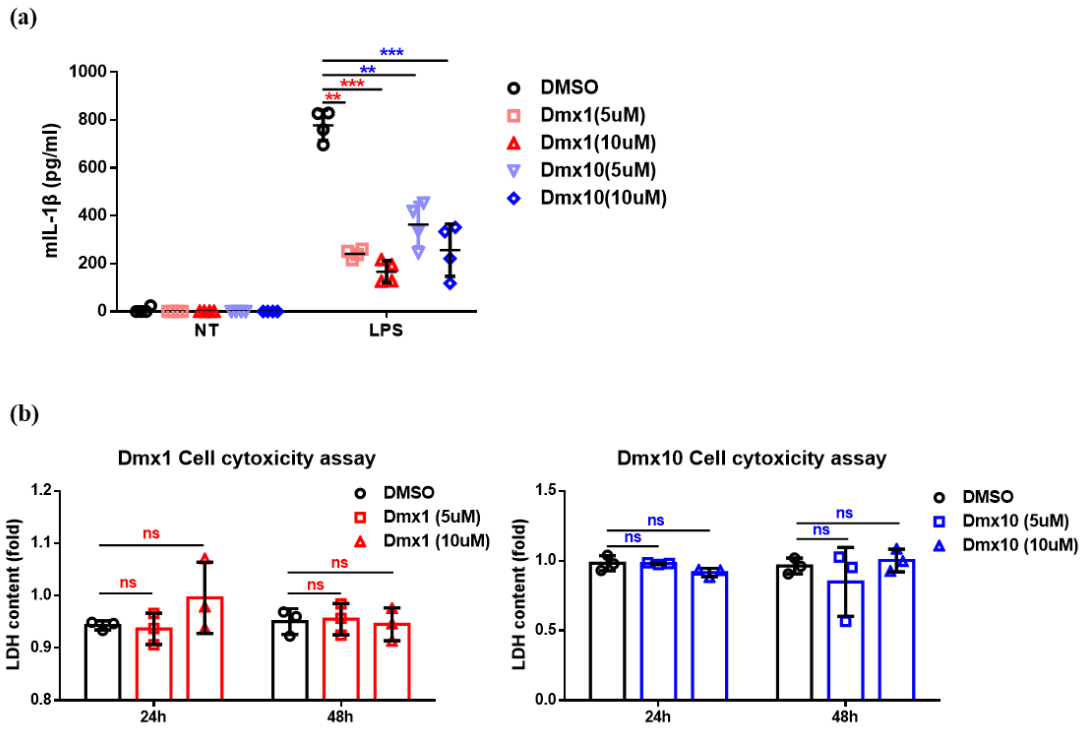


**Fig3.3 Dmx1 and Dmx10 exhibit concentration-dependent inhibition of IL-1β expression independently of cytotoxicity**

WT BMDMs (2 x$10^5$) were plated in 96-well plates. (a) Cells were pre-treated with Dmx1 or Dmx10 (5μM or 10μM) for 1h. Control cells were treated with DMSO vehicle. Cells were stimulated with LPS (100ng/ml) for 24h. Supernatants were assayed by ELISA for levels of IL-1β. (b) Cells were treated with Dmx1 or Dmx10 (5μM or 10μM) for 24h and 48h. Control cells were treated with DMSO vehicle. Supernatants were assayed by LDH release assay. The cytotoxicity of the compounds was evaluated by relating the LDH content in the supernatant of compounds-treated cells with supernatants from DMSO treated cells. Data are shown from an experiment that is representative of three independent experiments. Statistical analysis was performed by using the paired Student t-test. Statistically significant differences are indicated by the asterisks: ns, P>0.05; **, P<0.01; ***, P<0.001.

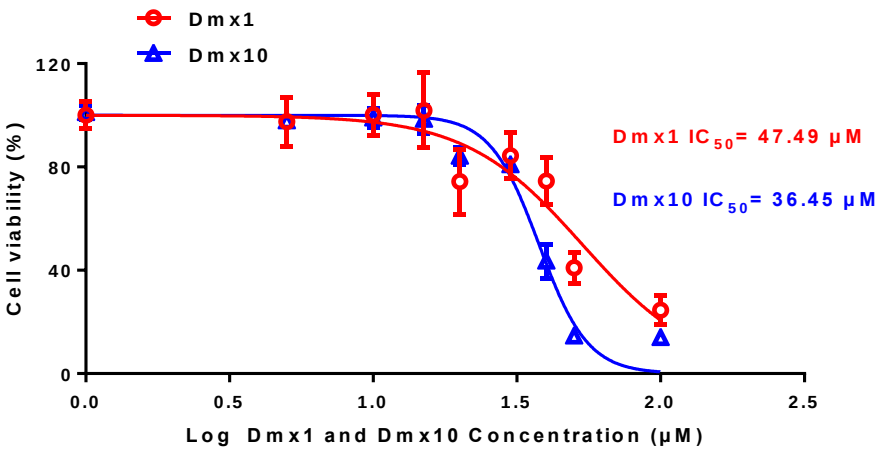


**Fig3.4 Effects of Dmx1 and Dmx10 on Macrophage cell viability**

WT BMDMs (2 x$10^5$) were plated in 96-well plates. Cells were treated with indicated concentrations of Dmx1 or Dmx10 for 24h. Control cells were treated with DMSO vehicle. 3-(4,5-dimethylthiazol-2-yl)-2,5-diphenyltetrazolium bromide (MTT) (50μg) was added into wells and incubated at 37°C for 4h. The medium was removed and DMSO (150μl) was added into wells to dissolve the crystals. Absorbance was measured at a wavelength of 490nm by using a microplate reader. Cell viabilities were normalized against DMSO vehicle control samples and the half maximal inhibitory concentration (IC50) of cell viabilities were calculated by Prism Graphpad. Data are shown from an experiment with quadruplicates that is representative of three independent experiments.

### 3.2.2 Dmx1 and Dmx10 suppress the expression of pro-IL-1β but do not affect the activation of NLRP3 inflammasome

The above data suggest that Dmx1 and Dmx10 suppress LPS-induced expression of the pro-inflammatory cytokine IL-1β. IL-1β is a cytokine whose secretion is regulated differently from other cytokines. Initially, IL-1β is translated in a precursor pro-IL-1β form that lacks a leader sequence and does not enter the classical secretory pathway upon upregulation. Instead, a secondary signal is required to allow its activation from an inactive to an active form (Lopez-Castejon and Brough 2011). The assembly of an inflammasome is responsible for processing pro-IL-1β into its mature and bioactive form, with the NLRP3 inflammasome being the most extensively studied for these IL-1β secretion processes (Humphries et al. 2018).

The role of Dmx1 and Dmx10 in NLRP3 inflammasome activation and processing of IL-1β was examined next. WT BMDMs were pre-treated with Dmx1 or Dmx10 (5μM) for 1h (DMSO as a vehicle control) and then stimulated with LPS (100ng/ml) for 4h and ATP (20ug/ml) which leads to the functional assembly of NLRP3 inflammasome for 30min. Dmx1 (Fig3.5a) and Dmx10 (Fig3.5b) strongly reduced the levels of processed and released IL-1β in the supernatant as well as the levels of pro-IL-1β in the cell lysate, but did not influence the levels of other key proteins involved in the assembly of NLRP3 inflammasome, including NLRP3, ASC and Caspase-1 (Fig3.5a and Fig3.5b). These data suggested that the compounds Dmx1 and Dmx10 may target the induction of pro-IL-1β and not the NLRP3 inflammasome activation.

We next examined if compounds could target IL-1β expression at the transcriptional level by measuring the effects of Dmx1 and Dmx10 on LPS-induced expression of *IL-1β* mRNA. WT BMDMs were pre-treated with Dmx1 or Dmx10 (10μM) (DMSO as a vehicle control) for 1h and then stimulated with LPS (100ng/ml) for indicated times and *IL-1β* mRNA was measured by quantitative real-time PCR. Dmx1 and Dmx10 treatment significantly inhibited the LPS-induced activation of *IL-1β* mRNA

transcription (Fig3.6). These data strongly suggested that both Dmx1 and Dmx10 down-regulate pro-inflammatory IL-1β by inhibiting *IL-1β* mRNA transcription and pro-IL-1β expression.

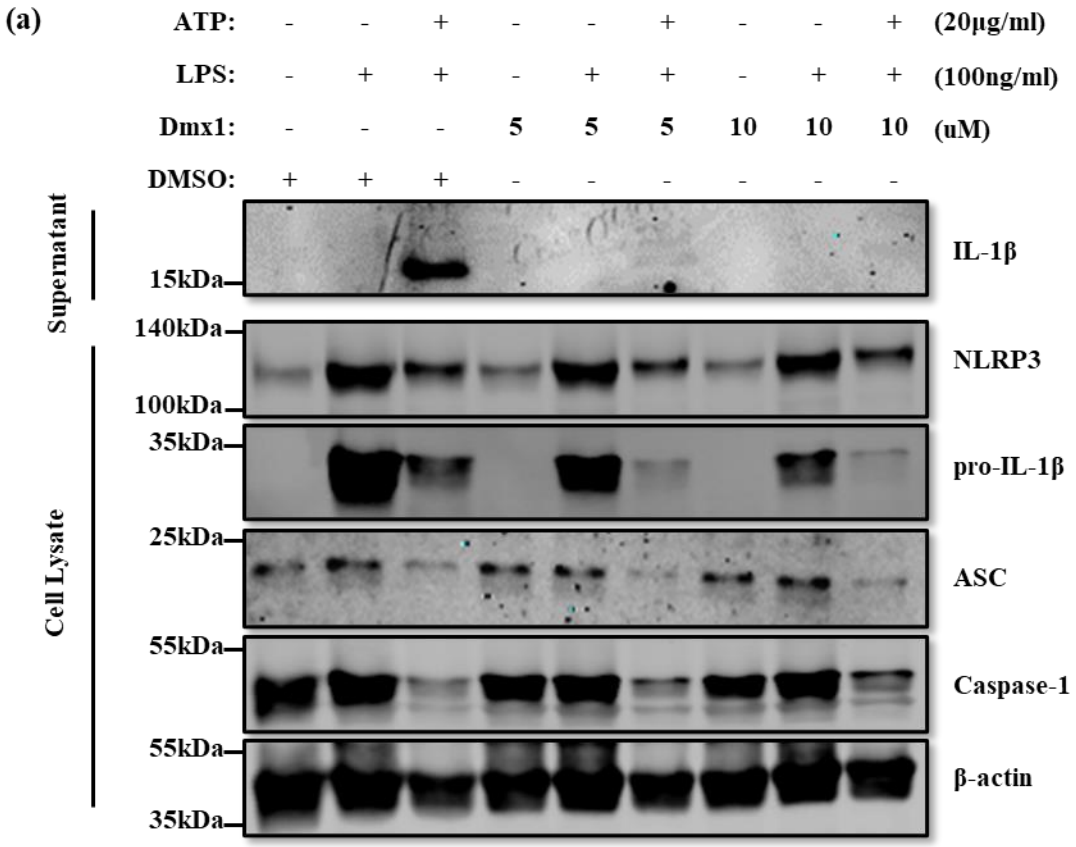

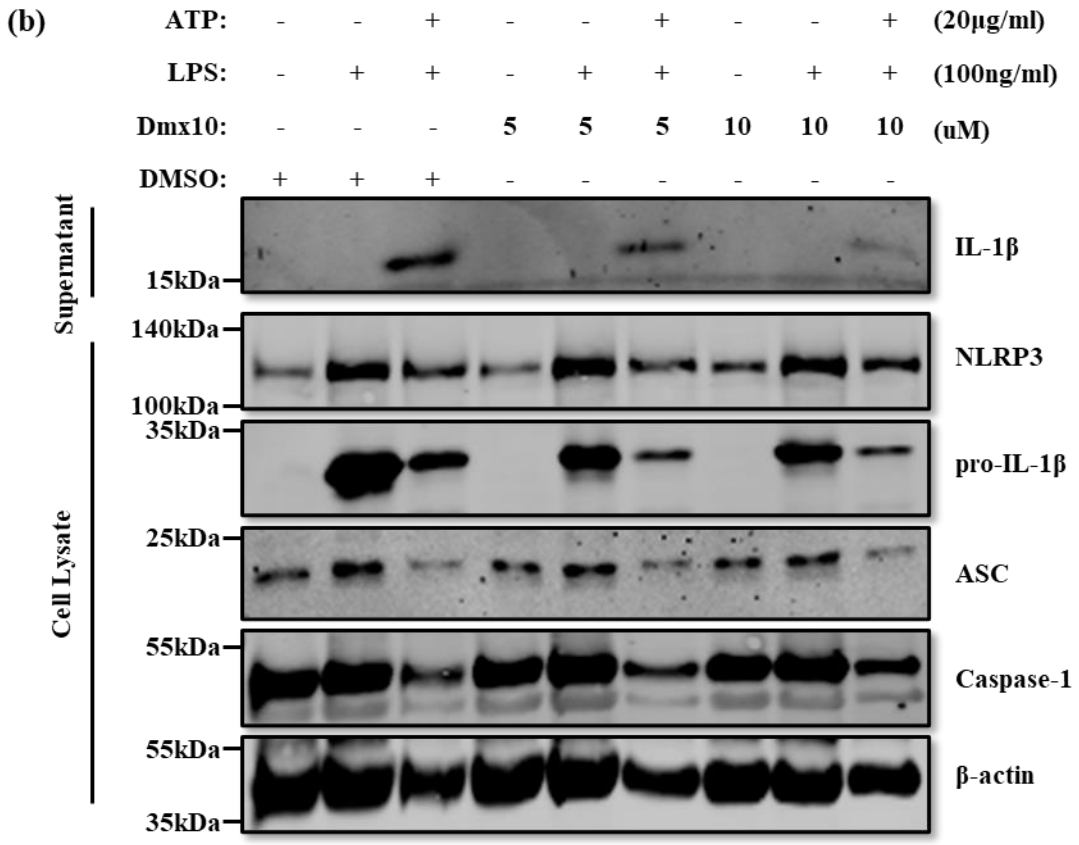


**Fig3.5 Dmx1 and Dmx10 suppress pro-IL-1β expression but do not affect the activation of NLRP3 inflammasome**

WT BMDMs (1 x$10^6$) were plated in 12-well plates. Cells were pre-treated with (a) Dmx1 or (b) Dmx10 (5μM or 10μM ) for 1h. Control cells were treated with DMSO vehicle. Cells were stimulated with LPS (100ng/ml) for 4h and ATP (20μg/ml ) for 30min. Supernatants and cell lysates were harvested in 2x loading buffer and subjected to Western Blotting. Supernatants were probed with antibody against cleaved-IL-1β. Cell lysate samples were probed with antibodies against pro-IL-1β, NLRP3, Caspase-1, ASC and β-actin. Data are shown from an experiment that is representative of three independent experiments.

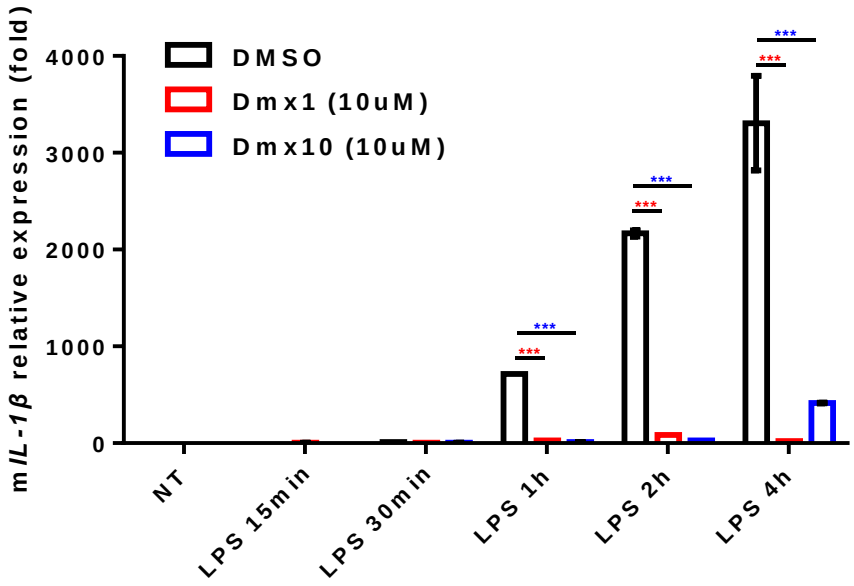


**Fig3.6 Dmx1 and Dmx10 inhibit the LPS-induced expression of *IL-1β* mRNA**

WT BMDMs (1 x$10^6$) were plated in 12-well plates. Cells were pre-treated with Dmx1 or Dmx10 (10μM ) for 1h, control cells were treated with DMSO vehicle. Cells were stimulated with LPS (100ng/ml) for indicated time points. Cells were harvested in TriZol and RNA was isolated and subsequently subjected to reverse transcription. *IL-1β* mRNA was measured by quantitative real-time PCR and normalized against *HPRT* mRNA. Data are shown from an experiment with duplicate samples that is representative of three independent experiments. Statistical analysis was performed by using the paired Student t-test. Statistically significant differences are indicated by the asterisks: ***, P<0.001.

Since the pathway upregulating IL-1β can also induce transcription of other pro-inflammatory genes such as IL-6 and TNFα, we then examined the effects of the compounds on the expression of IL-6 and TNFα at protein and mRNA levels. Results showed that Dmx1 and Dmx10 inhibited the LPS-induced expression of *IL-6* (Fig3.7a) and *TNFα* (Fig3.7b) mRNA at the transcriptional level, and also inhibited the expression of IL-6 (Fig3.8a) and TNFα (Fig3.8b) at the protein level. These results demonstrated that Dmx1 and Dmx10 inhibit LPS-induced expression of pro-inflammatory cytokines by likely suppressing transcription of their encoding genes.

**(a)**

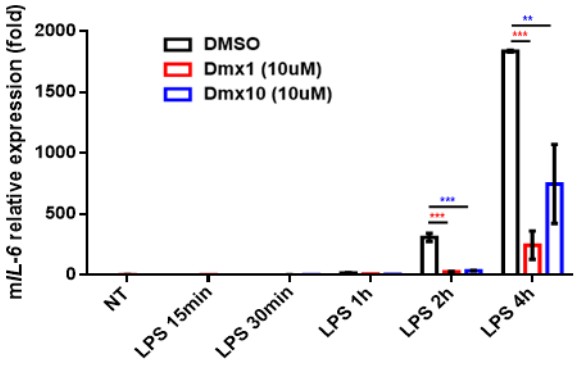


**(b)**

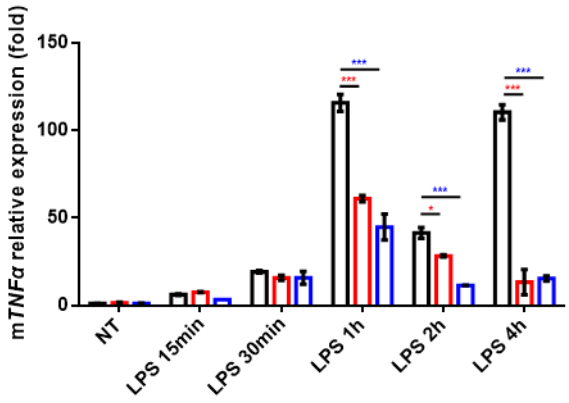


**Fig3.7 Dmx1 and Dmx10 inhibit the LPS-induced expression of *IL-6* and *TNFα* mRNA**

WT BMDMs (1 x$10^6$) were plated in 12-well plates. Cells were pre-treated with Dmx1 or Dmx10 (10μM ) for 1h, control cells were treated with DMSO vehicle. Cells were stimulated with LPS (100ng/ml) for indicated time points. Cells were harvested in TriZol and RNA was isolated and subsequently subjected to reverse transcription. *IL-6* and *TNFα* mRNA was measured by quantitative real-time PCR and normalized against *HPRT* mRNA. Data are shown from an experiment with duplicate samples that is representative of three independent experiments. Statistical analysis was performed by using the paired Student t-test. Statistically significant differences are indicated by the asterisks: **, P<0.01; ***, P<0.001.

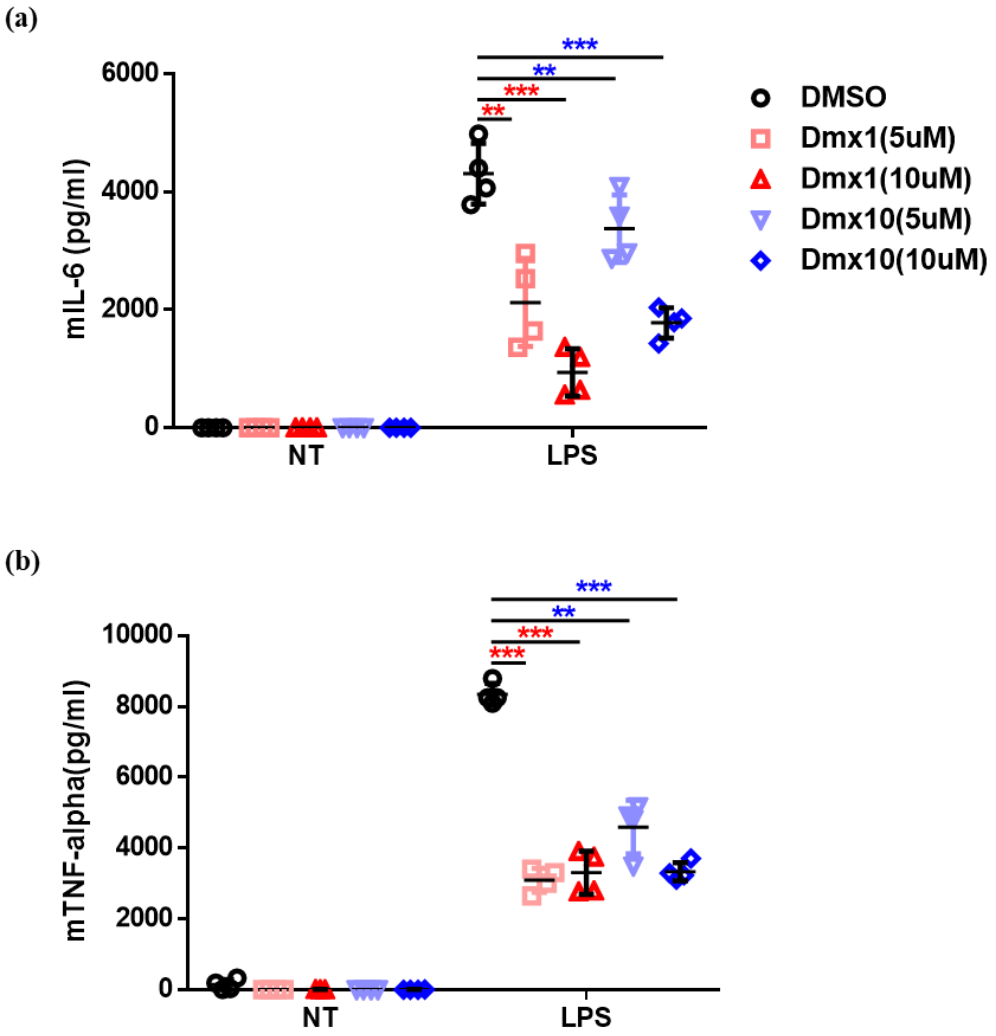


**Fig3.8 Dmx1 and Dmx10 inhibit the LPS-induced expression of IL-6 and TNFα**

WT BMDMs (2 x$10^5$) were plated in 96-well plates. Cells were pre-treated with Dmx1 or Dmx10 (5μM or 10μM) for 1h. Control cells were treated with DMSO vehicle. Cells were then stimulated with LPS (100ng/ml) for 24h. Supernatants were assayed by ELISA for levels of (a) IL-6 and (b) TNFα. Data are shown from an experiment that is representative of three independent experiments. Statistical analysis was performed by using the paired Student t-test. Statistically significant differences are indicated by the asterisks: **, P<0.01; ***, P<0.001.

### 3.2.3 Regulatory effects of Dmx1 and Dmx10 on TLRs pathways

To extend our research and given that Pellino proteins have been shown to affect TLR signaling, we next decided to perform a screen to comprehensively elucidate the regulatory effects of Dmx1 and 10 on various TLR signaling pathways. To this end, WT BMDMs were pre-treated with Dmx1 or Dmx10 (10μM) (DMSO as a vehicle control) for 1h and then stimulated for 24h with ligands for TLR2/6 (Pam2CSk4), TLR2/ (PamiCSK4), TLR/Dectine-1 (Zymosan), TLR3 (Poly(I: C)), TLR4 (LPS), TLR5 (Flagellin), TLR8 (CLO75), TLR7/8 (CLO97) and TLR9 (CpG) and assessed for IL-1β, IL-6 and TNFα expression.

As before, Dmx1 and Dmx10 effectively inhibited LPS-induced expression of IL-1β (Fig3.9a), IL-6 (Fig3.9b) and TNFα (Fig3.9c). Dmx1 showed some inhibitory effects on the expression of these pro-inflammatory cytokines induced by Pam2CSK, Pam3CSK, and Zymosan, whereas Dmx10 was without effect. Notably, neither Dmx1 nor Dmx10 exhibited anti-inflammatory effects when cell were stimulated with Poly(I: C), CLO75, CLO97, and CpG (Fig3.9). These data indicated that Dmx1 and Dmx10 showed some selectivity for inhibiting the LPS/TLR4 pathway.

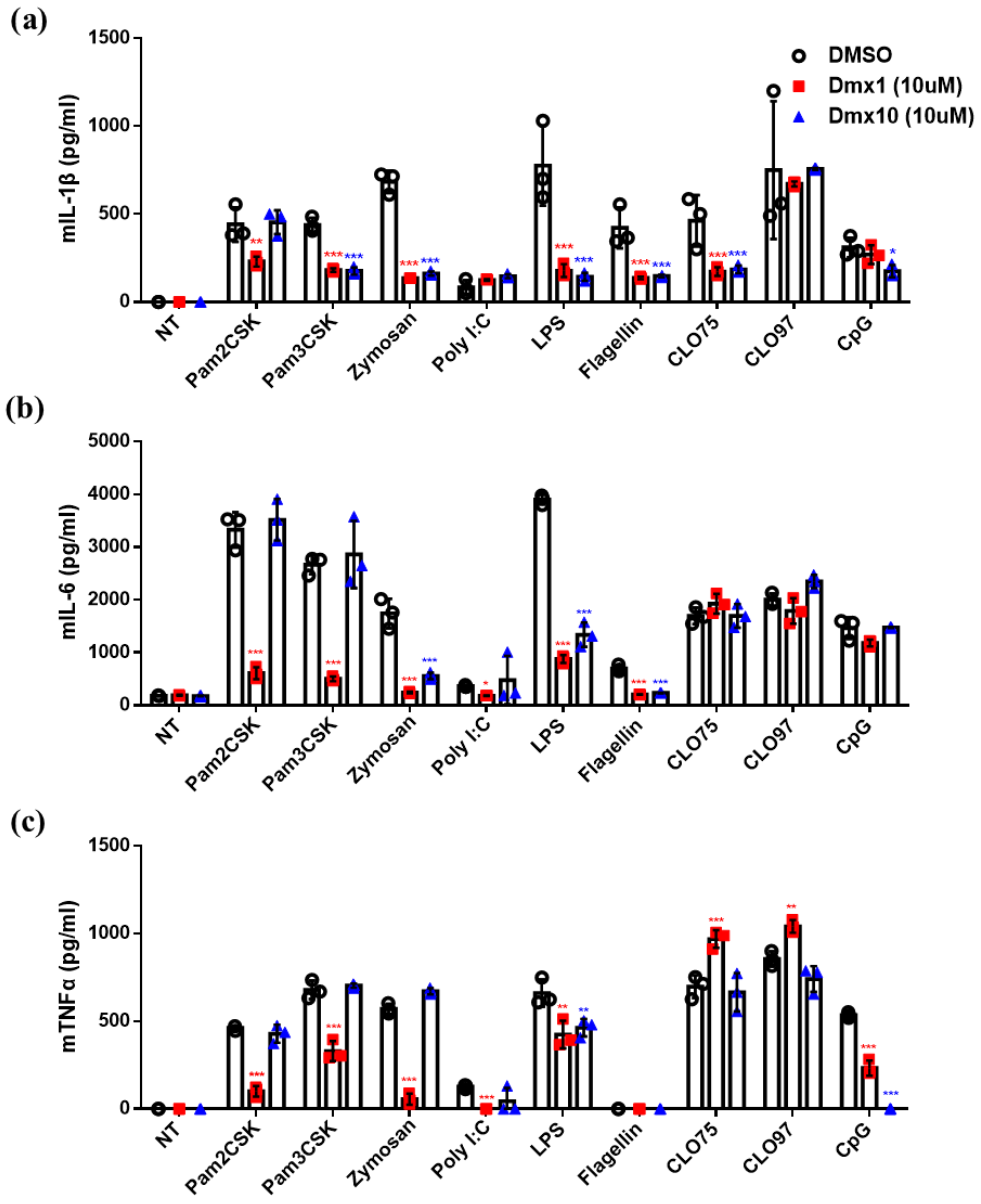


**Fig3.9 Regulation of TLR signaling pathways by Dmx1 and Dmx10**

WT BMDMs (2 x$10^5$) were plated in 96-well plates. Cells were pre-treated with Dmx1 or Dmx10 (5μM or 10μM) for 1h. Control cells were treated with DMSO vehicle. Cells were stimulated with Pam2CSK4 (10ng/ml), Pam3CKS4 (10ng/ml), Zymosan (5μg/ml), Poly(I: C) (25μg/ml), LPS (100ng/ml), Flagellin (5μg/ml), CLO75 (5μg/ml), CLO97 (5μg/ml), CpG (5μM) for 24h. Supernatants were assayed by ELISA for levels of (a) IL-1β, (b) IL-6 and (c) TNFα. Data are shown from an experiment that is representative of three independent experiments. Statistical analysis was performed by using the paired Student t-test. Statistically significant differences are indicated by the asterisks: *, P<0.05; **, P<0.01; ***, P<0.001.

### 3.2.4 Dmx1 and Dmx10 target the activation of the NF-κB signaling pathway

The molecular and mechanistic basis for the regulatory effects of Dmx1 and Dmx10 on the mRNA expression of the *IL-1β*, *IL-6* and *TNFα* were next investigated. The activation of NF-κB signaling pathway has previously been implicated in the transcriptional up-regulation of these genes (Pande and Ramos 2005). Pellino2 protein has also been reported to influence the activation of the NF-κB signaling pathway (Humphries et al. 2018; Liu et al. 2004). Since Dmx1 and Dmx10 are designed and synthesized based on the Pellino protein sequence and structure, the effects of Dmx1 and Dmx10 on the activation of NF-κB signaling pathway were first explored. The phosphorylation of IκBα is a key indicator of NF-κB signaling. During the activation of NF-κB signaling pathway, IκBα is rapidly phosphorylated and ubiquitinated, leading to degradation by the proteasome and nuclear translocation of NF-κB from the cytoplasm to the nucleus, so we decided to detect the phosphorylation and degradation of IκBα as a measure of NF-κB activation. WT BMDMs were pre-treated with Dmx1 or Dmx10 (5μM) for 1h (DMSO as a vehicle control) and then stimulated with LPS (100ng/ml) for indicated time points. Results showed that Dmx1 (Fig3.10a) and Dmx10 (Fig3.10b) treatment inhibited the LPS-induced phosphorylation of IκBα at 8h post-LPS stimulation, and also reduced the degradation of IκBα by LPS stimulation. Since the phosphorylation of IκBα is catalysed by IKK proteins, the effects of Dmx1 and Dmx10 on the activation of IKK proteins were next examined by measuring the phosphorylation of IKKs as an index of activation. We found the phosphorylation of IKKα/β is stimulated by LPS but is not affected by either compounds treatment but the expression level of total-IKKα/β is decreased with Dmx1 or Dmx10 treatment after 15min of LPS stimulation (Fig3.10). These data suggested Dmx1 and Dmx10 can down-regulate the activation of NF-κB signaling pathway.

We next examined the effects of Dmx1 and Dmx10 on the activation of the MAPKs signaling pathway since they are important regulators of pro-inflammatory gene transcription and are also controlled by Pellino proteins (Jensen and Whitehead 2003a).

The phosphorylation of JNK, ERK and p38 all showed similar temporal profiles of activation in response to LPS. Phosphorylation was observed 15 and 30 min after LPS stimulation and was subsequently lost. However, Dmx1 or Dmx10 had no effects on LPS-induced phosphorylation in the various MAPKs (Fig3.11). These results indicated that Dmx1 and Dmx10 have no role in regulating the activation of MAPKs. Instead, our data suggested that Dmx1 and Dmx10 may selectively down-regulate the activation of NF-κB signaling pathway to suppress the expression of pro-inflammatory cytokines IL-1β, IL-6 and TNFα.

**(a)**

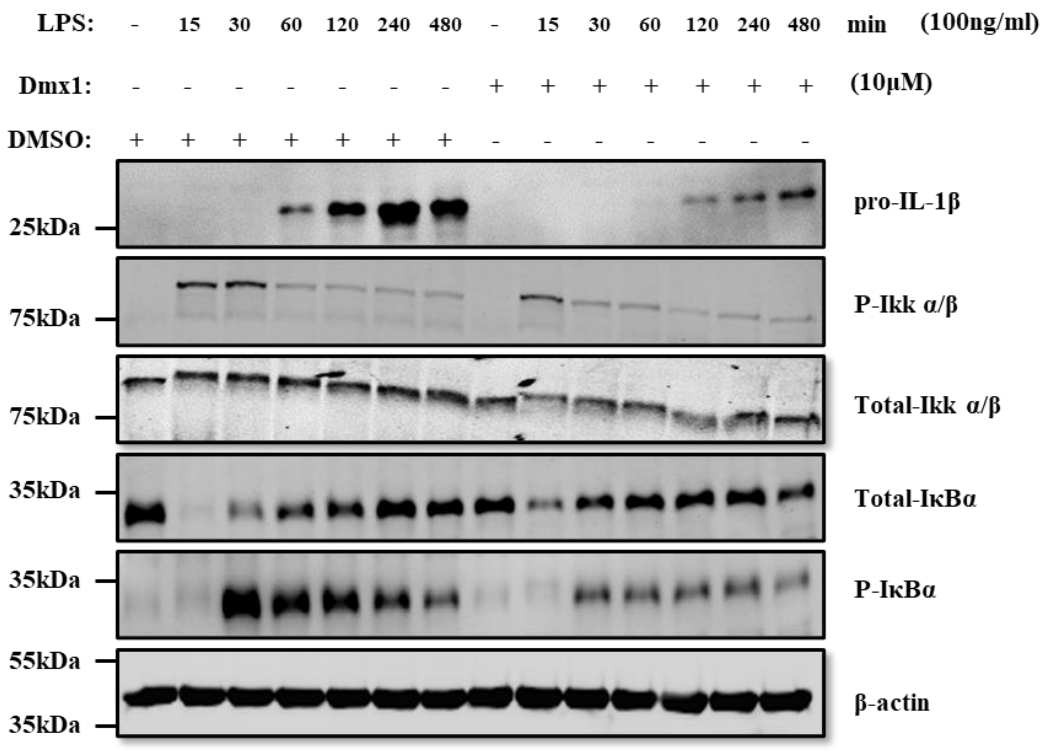

**(b)**

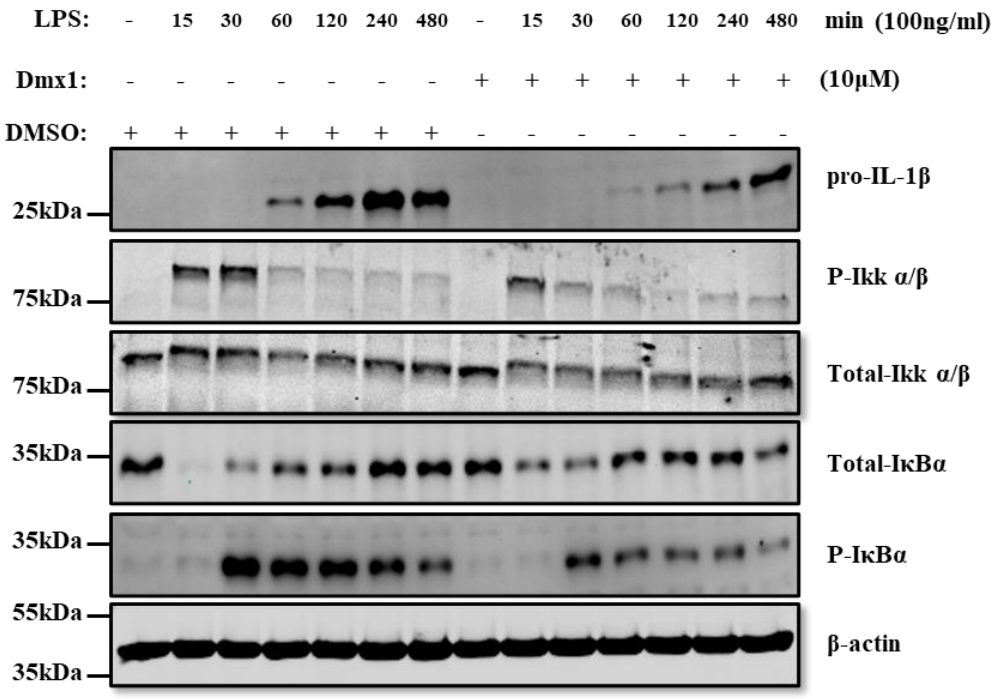


**Fig3.10 Dmx1 and Dmx10 target LPS-induced activation of NF-κB signaling pathway**

WT BMDMs (1 x$10^6$) were plated in 6-well plates. Cells were pre-treated with (a) Dmx1 or (b) Dmx10 (10μM) for 1h. Control cells were treated with DMSO vehicle. Cells were stimulated with LPS (100ng/ml ) for the indicated times. Cell lysates were harvested in 2x loading buffer and subjected to Western Blotting. The resulting membranes were probed with antibodies against pro-IL-1β, Total-IκBα, phosphor-IκBα, Total-IKKα/β, phosphor-IKKα/β and β-actin. Data are shown from an experiment that is representative of three independent experiments.

**(a)**

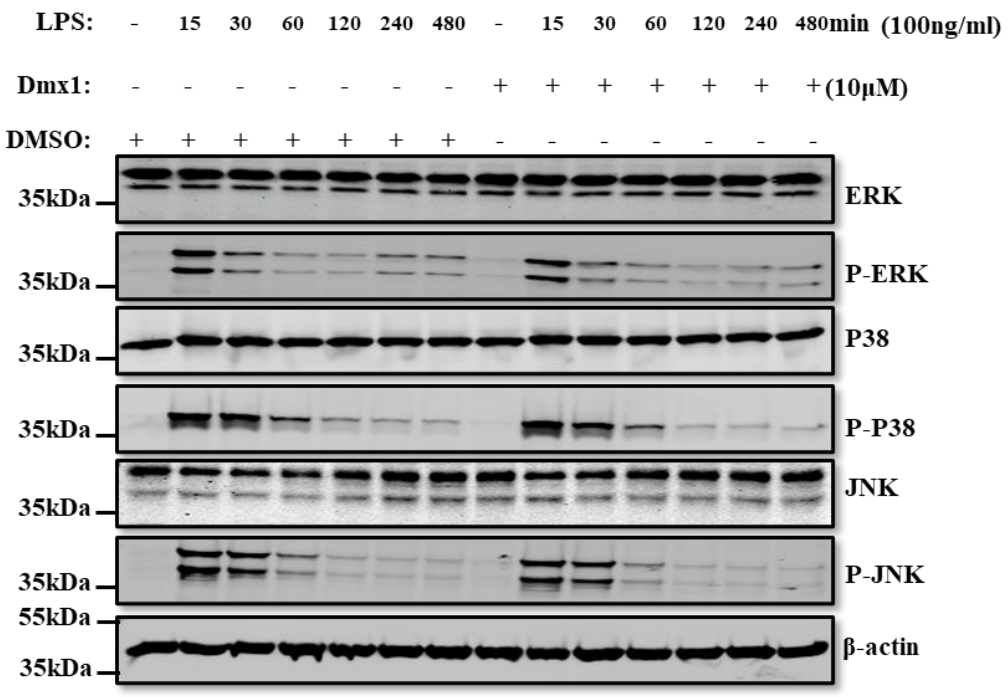
LPS: - 15 30 60 120 240 480 - 15 30 60 120 240 480min (100ng/ml)
Dmx1: - - - - - - - + + + + + + +(10μM)
DMSO: + + + + + + + - - - - - - -
35kDa
ERK
35kDa
P-ERK
35kDa
P38
35kDa
P-P38
35kDa
JNK
35kDa
P-JNK
55kDa
35kDa
β-actin

**(b)**

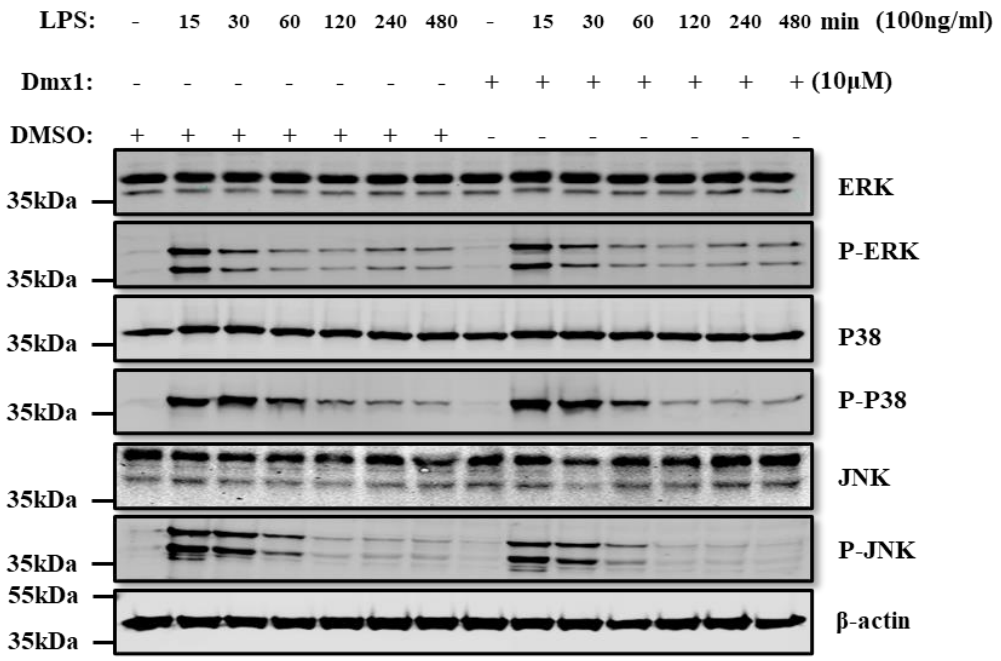


**Fig3.11 Dmx1 and Dmx10 do not affect LPS-induced activation of MAPK signaling pathways**

WT BMDMs (1 x$10^6$) were plated in 6-well plates. Cells were pre-treated with (a) Dmx1 or (b) Dmx10 (10μM) for 1h. Control cells were treated with DMSO vehicle. Cells were stimulated with LPS (100ng/ml ) for the indicated times. Cell lysates were harvested in 2x loading buffer and subjected to Western Blotting. The resulting membranes were probed with antibodies against phosphor-P38, total P38, phosphor-ERK, total ERK, phosphor-JNK, total JNK, and β-actin. Data are shown from an experiment that is representative of three independent experiments.

### 3.2.5 Dmx1 and Dmx10 promote the LPS-induced ubiquitination of IRAK1

Given that the important roles of IRAK1 in the LPS-induced activation of NF-κB signaling pathway and Pellino2 is IRAK-interacting protein (Lin et al. 2008), we next assessed if Dmx1 and Dmx10 could affect the regulation of IRAK by LPS.

We initially characterized the optimum time-point to detect ubiquitination of IRAK1. Given that IRAK degradation is rapid, we focused on very early time-points of 1-10min post LPS stimulation. We found that IRAK1 degradation was apparent after 5min LPS stimulation and almost absent after 10min, We then probed the ubiquitination status of IRAK1 at the various time points and more specifically characterized both Lys48-ubiquitination and Lys63-ubiquitination profiles. We failed to detect any differences in the latter but detected strong Lys48-ubiquitination at 5min post LPS treatment that increased further after 10 min (Fig3.12).

We decided to choose 5min as the suitable time-point to explore any regulatory effects of the Dmx1 and Dmx10 on LPS-induced ubiquitination of IRAK1. To this end, WT BMDMs were pre-treated with Dmx1 or Dmx10 (5μM) for 1h (DMSO as a vehicle control) and then stimulated with LPS (100ng/ml) for 5min. Results showed that Dmx1 and Dmx10 augmented degradation of IRAK1 and its Lys48-ubiquitination status beyond LPS treatment alone (Fig3.13). Interestingly, Dmx1 and Dmx10 also appeared to modestly increase the Lys63-ubiquitination of IRAK1, while Lys63-ubiquitination promote IRAK1's kinase activity (Fig3.13). These results indicated that Dmx1 and 10 promote the ubiquitination and some degradation of IRAK1 and this may underlie their down-regulation effects on the NF-κB signaling pathway.

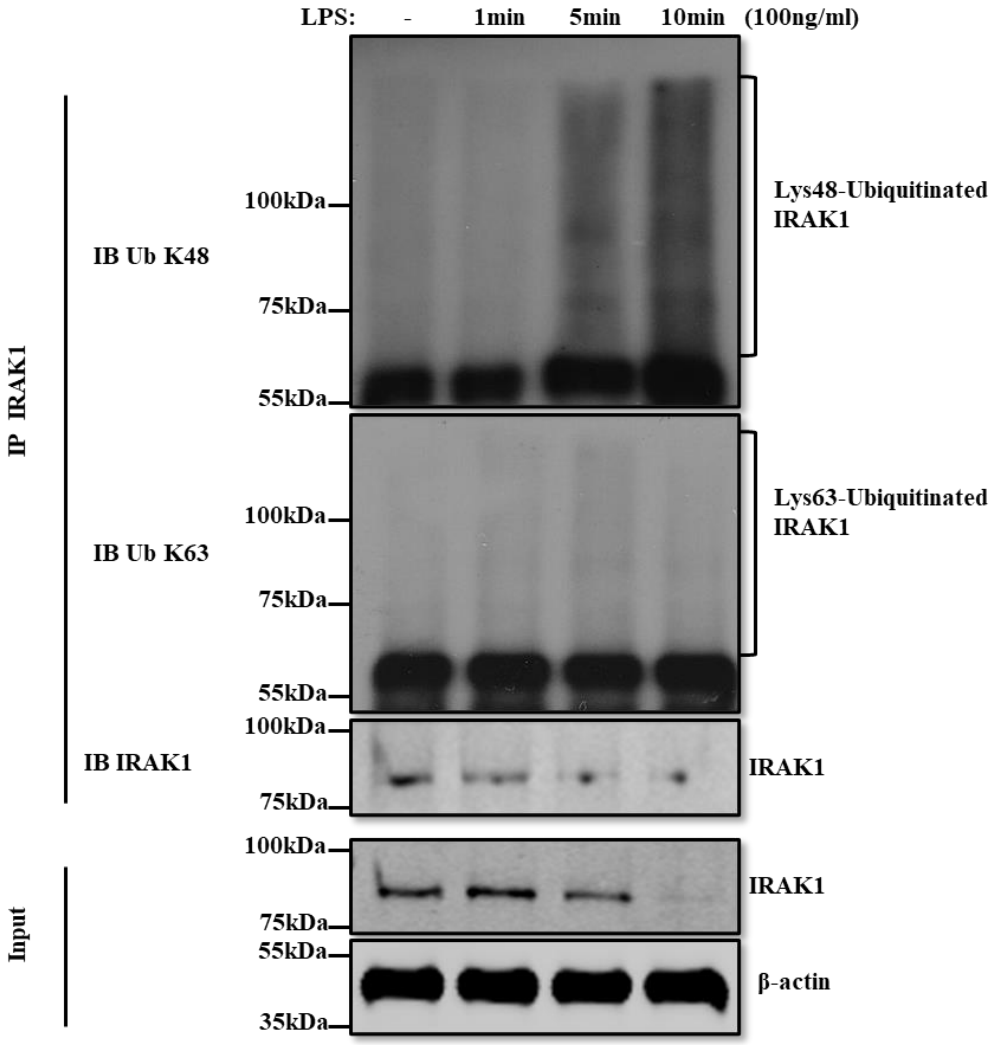


**Fig3.12 LPS-induced ubiquitination of IRAK1 protein**

WT BMDMs (3 x$10^6$) were plated in 6-well plates. Cells were stimulated with LPS (100ng/ml) for the indicated times. Thereafter, cell lysates were extracted in RIPA buffer and immunoprecipitated (IP) using anti-IRAK1 antibody. The resulting membranes with IP samples were probed with antibodies against Lys48-Ubiquitination, Lys63-Ubiquitination and IRKA1. The resulting membranes with lysate samples (input) were probed with antibodies against IRAK1 and β-actin. Data are shown from an experiment that is representative of three independent experiments.

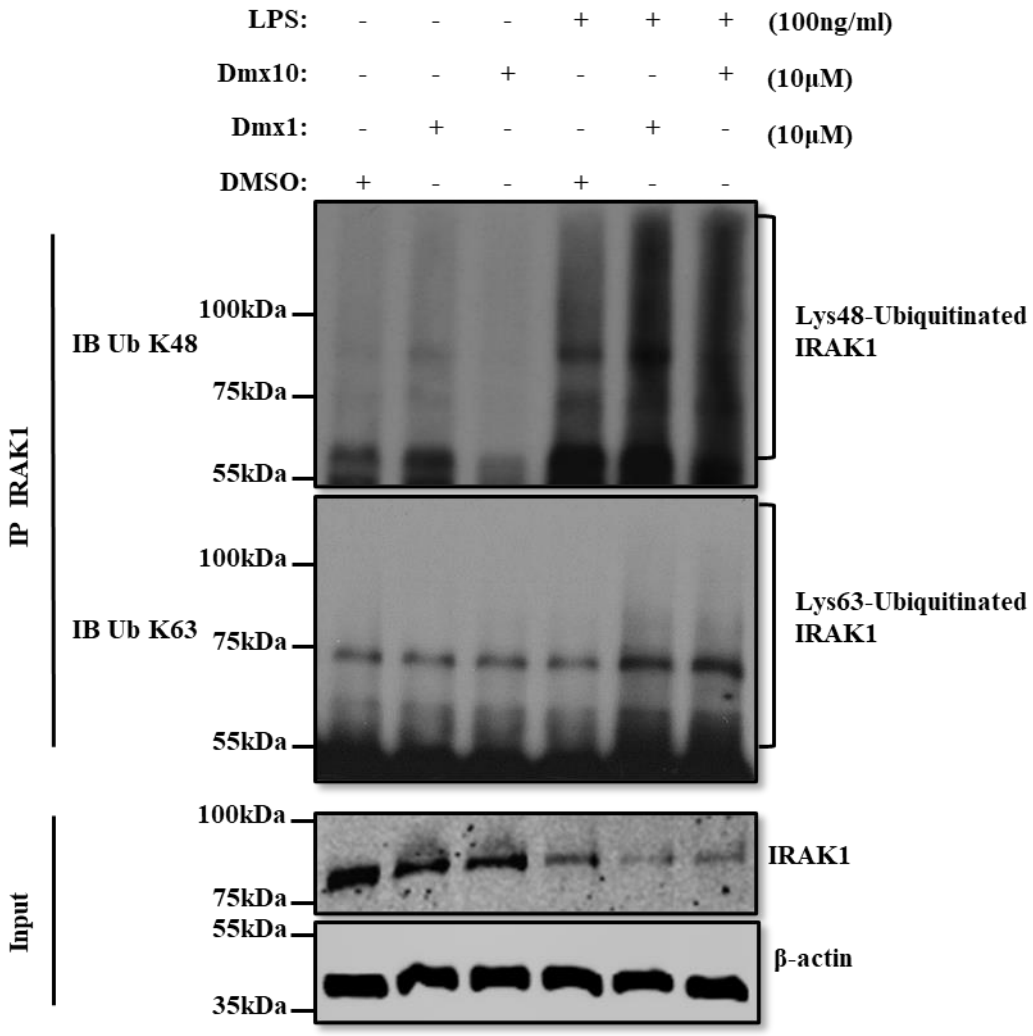


**Fig3.13 Dmx1 and Dmx10 augment LPS-induced ubiquitination of IRAK1 protein**

WT BMDMs (3 x$10^6$) were plated in 6-well plates. Cells were pre-treated with Dmx1 or Dmx10 (10μM) for 1h. Control cells were treated with DMSO vehicle. Cells were stimulated with LPS (100ng/ml) for 5min. Thereafter, cell lysates were extracted in RIPA buffer and immunoprecipitated (IP) using an anti-IRAK1 antibody. The resulting membranes with IP samples were probed with antibodies against Lys48-Ubiquitination, Lys63-Ubiquitination. The resulting membranes with lysate samples (input) were probed with antibodies against IRAK1 and β-actin. Data are shown from an experiment that is representative of three independent experiments.

### 3.2.6 Dmx1 and Dmx10 increase the direct interaction between Pellino2 and IRAK1

Since Pellino2 is a known protein interaction partner and E3 ubiquitin ligase for IRAK1 (Lin et al. 2008) and both compounds can affect IRAK1 ubiquitination, so we were keen to assess if Dmx1 and Dmx10 could affect the interaction between Pellino2 and IRAK1. HEK293T cells were transfected with plasmids encoding Myc-tagged Pellino2 and IRAK1, and then cells were treated with Dmx1 or Dmx10 (5μM) (DMSO as a vehicle control) for 24h. Pellino2 or IRAK1 were immunoprecipitated with anti-Myc antibody or anti-IRAK1 antibody respectively and then analyzed for co-precipitated IRAK1 or Pellino2 respectively by western blotting. As previously reported we could demonstrate that IRAK and Pellino2 co-immunoprecipitated with each other confirming that they are interaction partners (Fig3.14). We also found that after the treatment of Dmx1 and Dmx10, immunoprecipitation protocols demonstrated that Dmx1 and Dmx10 could increase the interaction between Pellino2 and IRAK1 (Fig3.14), These data suggested that the compounds may target the interaction of Pellino2 and IRAK1 so promoting increased ubiquitination and degradation of IRAK and downregulation of downstream NF-κB signaling.

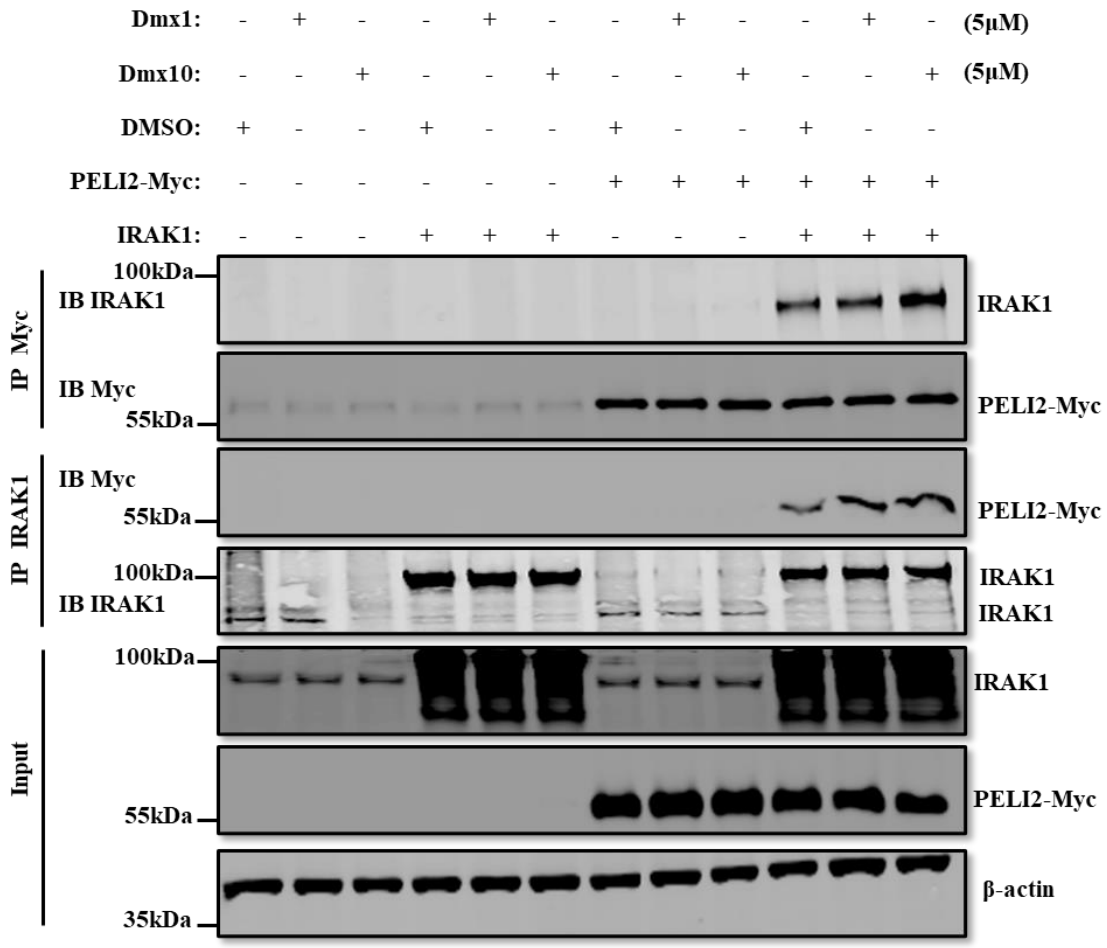


**Fig3.14 Dmx1 and Dmx10 promote the interaction between Pellino2 and IRAK1**

HEK293T (3 x$10^6$) cells were plated in 6-well plates. Cells were transfected with expression constructs encoding PELI2-Myc and IRAK1 plasmid alone or in combination for 24h. Control cells were transfected with empty vector plasmid as vehicle control. Cell lysates were extracted in NP-40 buffer and co-immunoprecipitated (Co-IP) using anti-IRAK1 antibody or anti-Myc-tag antibody. The resulting membranes with IP samples were probed with antibodies against IRAK1 or Myc-tag. The resulting membranes with lysate samples (input) were probed with antibodies against IRAK1, Myc-tag and β-actin. Data are shown from an experiment that is representative of three independent experiments.

### 3.2.7 Dmx1 and Dmx10 do not affect TNFα signaling

While the above data suggests that Dmx1 and Dmx10 target IRAK1 to promote its degradation and ubiquitination to down-regulate the activity of NF-κB signaling pathway in response to LPS, we were keen to examine the effects of the compounds on the TNFα signaling pathway. The latter closely mirrors IL-1β in driving the expression of pro-inflammatory cytokines but their signaling pathways are very different and notably TNF signaling does not employ IRAK (Webster and Vucic 2020). WT BMDMs were pre-treated with Dmx1 or Dmx10 (5μM) (DMSO as a vehicle control) for 1h then stimulated with mTNFα (50ng/ml) for indicated time points. Results showed that Dmx1 (Fig3.15a) and Dmx10 (Fig3.15b) failed to affect the phosphorylation of IκBα at 30, 60 and 120min post mTNFα stimulation, and also did not affect the degradation of IκBα at the same time points. mTNFα also stimulated the MAPKs signaling pathway and again both compounds failed to affect the activation of MAPKs pathway (Fig3.15). Furthermore, neither compounds showed the inhibitory ability of TNFα to up-regulate the transcription of genes encoding pro-inflammatory cytokines IL-1β, IL-6 and TNFα (Fig3.16). These results were consistent with Dmx1 and Dmx10 targeting IRAK1 to down-regulation the activation of NF-κB signaling pathway that is triggered by LPS.

**(a)**

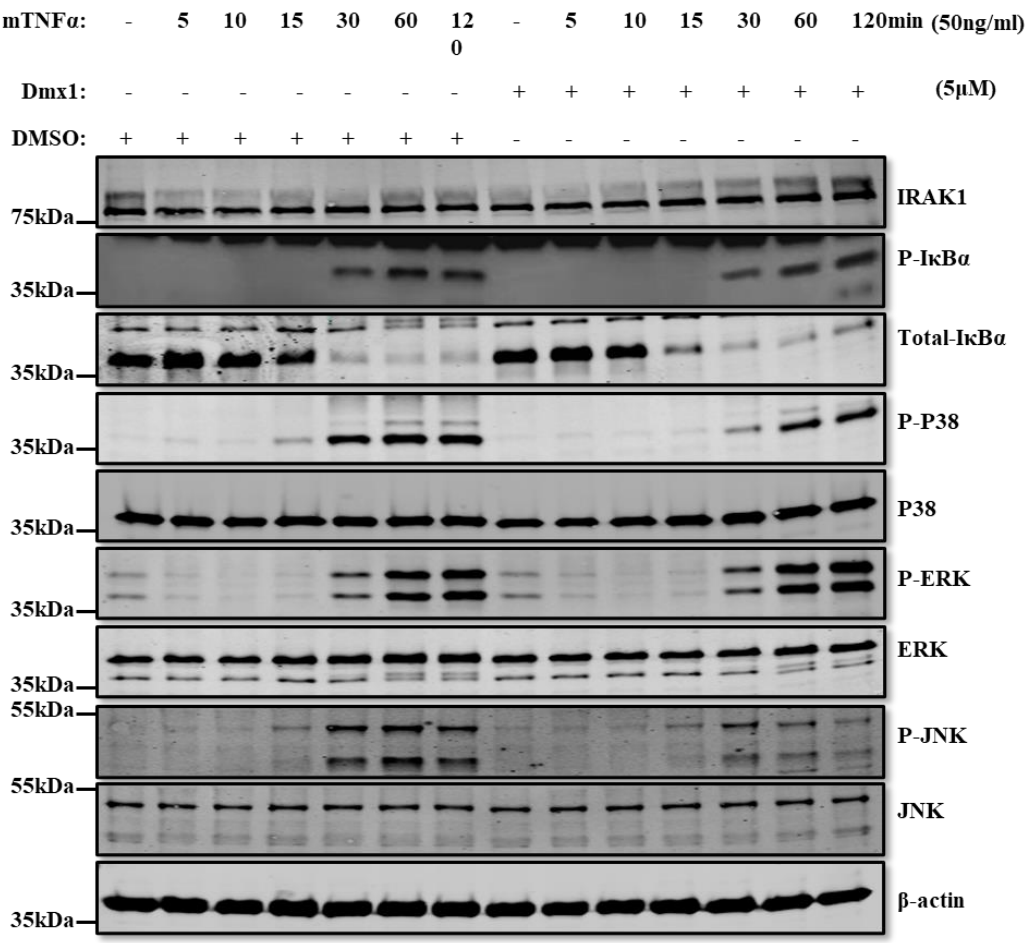
mTNFα: - 5 10 15 30 60 120 - 5 10 15 30 60 120min (50ng/ml)
Dmx1: - - - - - - - + + + + + + + (5μM)
DMSO: + + + + + + + - - - - - - -
75kDa
IRAK1
35kDa
P-IκBα
35kDa
Total-IκBα
35kDa
P-P38
35kDa
P38
35kDa
P-ERK
35kDa
ERK
35kDa
55kDa
P-JNK
55kDa
JNK
35kDa
β-actin

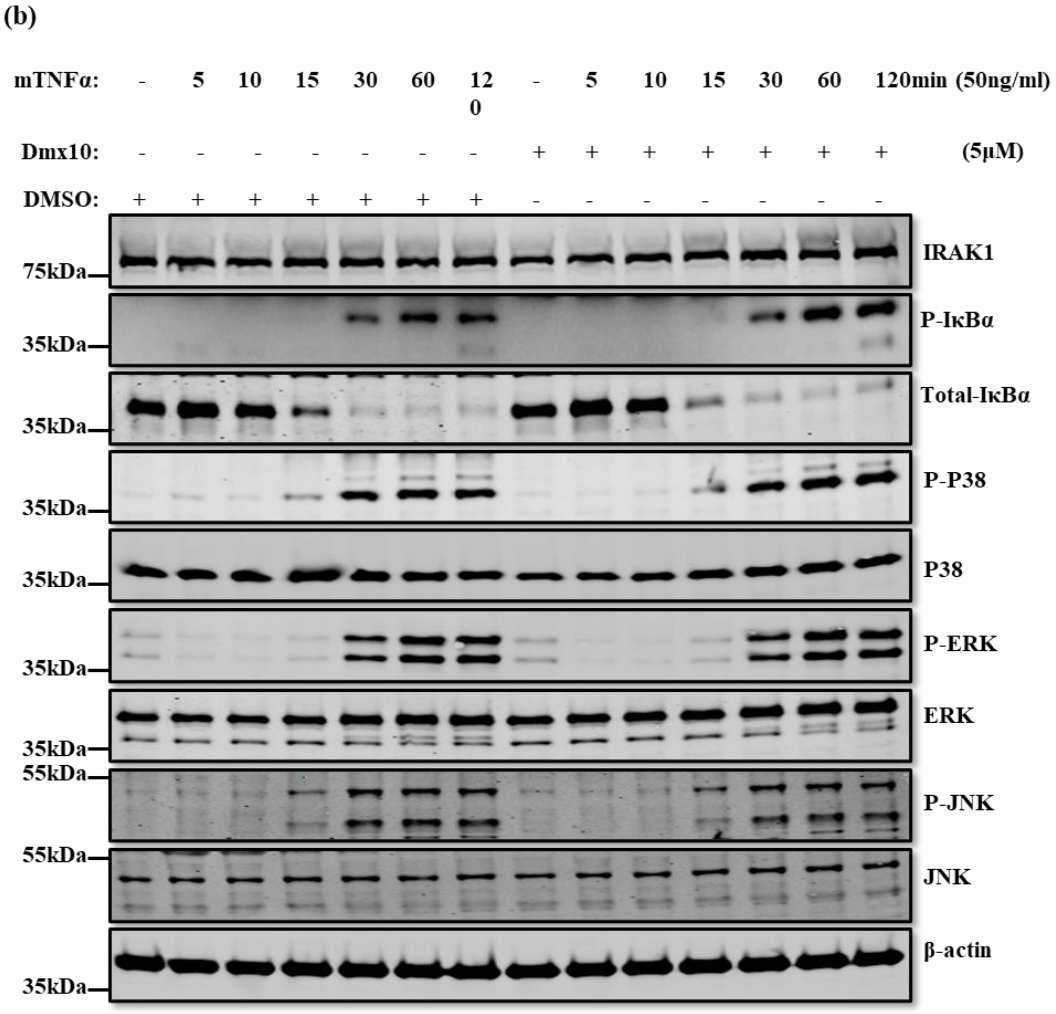


**Fig3.15 Dmx1 and Dmx10 do not impact the TNFα-induced activation of NF-κB signaling pathway**

WT BMDMs (1 x$10^6$) were plated in 6-well plates. Cells were pre-treated with (a) Dmx1 or (b) Dmx10 (10μM) for 1h. Control cells were treated with DMSO vehicle. Cells were stimulated with mTNFα (50ng/ml ) for the indicated times. Cell lysates were harvested in 2x loading buffer and subjected to Western Blotting. The resulting membranes were probed with antibodies against IRAK1, Total-IκBα, phosphor-IκBα, phosphor-P38, total P38, phosphor-ERK, total ERK, phosphor-JNK, total JNK and β-actin. Data are shown from an experiment that is representative of three independent experiments.

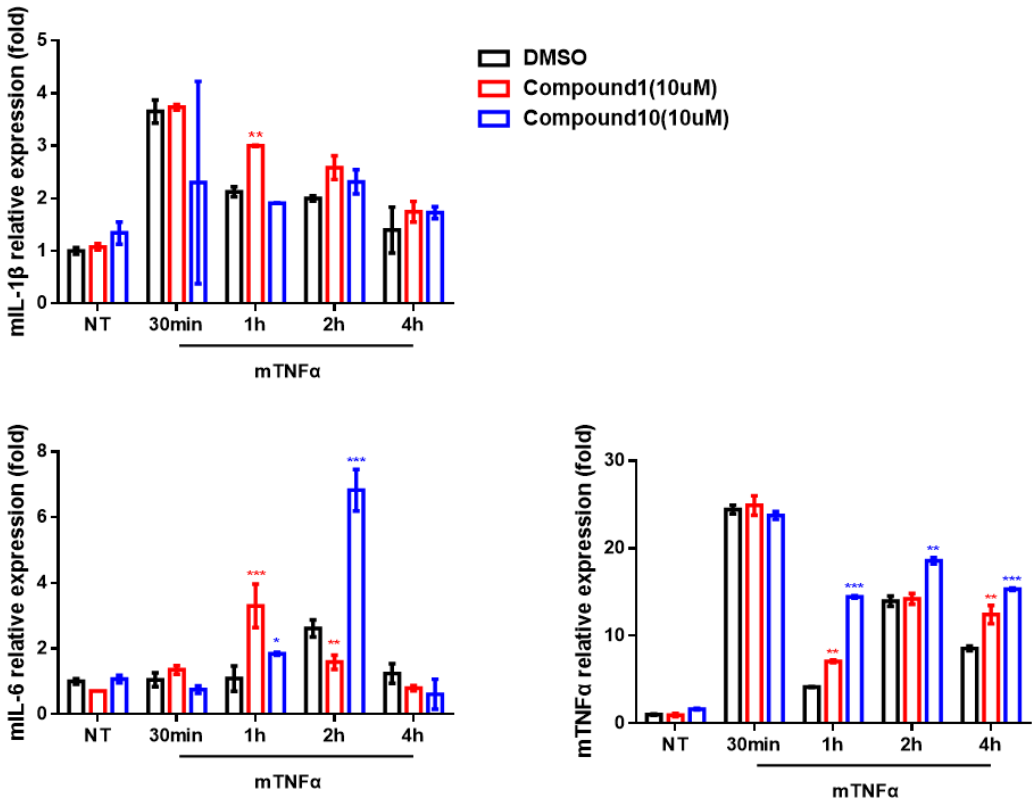


**Fig3.16 Dmx1 and Dmx10 do not inhibit TNFα-induced transcription of *IL-1β*, *IL-6* and *TNFα* mRNA**

WT BMDMs (1 x$10^6$) were plated in 12-well plates. Cells were pre-treated with Dmx1 or Dmx10 (10μM ) for 1h, control cells were treated with DMSO vehicle. Cells were stimulated with LPS (100ng/ml) for indicated time points. Cells were harvested in TriZol and RNA was isolated and subsequently subjected to reverse transcription. *IL-1β*, *IL-6* and *TNFα* mRNA was measured by quantitative real-time PCR and normalized against *HPRT* mRNA. Data are shown from an experiment with duplicate samples that is representative of three independent experiments. Statistical analysis was performed by using the paired Student t-test. Statistically significant differences are indicated by the asterisks: *, P<0.05; **, P<0.01; ***, P<0.001.

### 3.2.8 The presence of Pellino2 is necessary for the anti-inflammatory effect of Dmx1 and Dmx10

As mentioned above, Dmx1 and Dmx10 were designed based on a region of the Pellino2 protein and we next examined if their effects are dependent on the presence of Pellino2 protein. To address this question, we generated WT and Pellino2 knockout (Peli2$^{-/-}$) BMDMs. Cells were pre-treated with Dmx1 or Dmx10 (5μM) (DMSO as a vehicle control) for 1h and then stimulated with LPS (100ng/ml) for 24h. Supernatants were harvested to assay for various cytokines. In parallel, cells were also pre-treated with Dmx1 or Dmx10 (5μM) (DMSO as a vehicle control) for 1h then stimulated with LPS (100ng/ml) for 4h and ATP (20ng/ml) for 30min, cell lysates were harvested by RIPA buffer and supernatants were harvested by 2X loading buffer for Western Blotting.

ELISA results revealed that loss of Pellino2 abrogated the inhibitory effects of the compounds on the induction of processed mature IL-1β (Fig3.17a) released into the supernatants, as well as the production of IL-6 (Fig3.17b) and TNFα (Fig3.17c). These findings suggested that compounds mediate their inhibitory effects in a Pellino2-dependent manner. Consistent results were obtained from Western Blotting. Blocking results further showed that loss of Pellino2 negates the down-regulatory effects of Dmx1 (Fig3.18a) and Dmx10 (Fig3.18b) on the expression of both pro-IL-1β and mature IL-1β.

To further investigate the requirement of Pellino2 to manifest the effects of Dmx1 and Dmx10, we next characterized the LPS-induced ubiquitination change of IRAK1 in WT and Peli2$^{-/-}$ BMDMs with Dmx1 and Dmx10. LPS-induced Lys48-linked ubiquitination of IRAK was severely compromised in Peli2$^{-/-}$ BMDM cells and both compounds lost their ability to augment ubiquitination and degradation of IRAK in the absence of Pellino2 protein (Fig3.19). All these results indicated that the anti-inflammatory effect of Dmx1 and Dmx10 are critically dependent on Pellino2.

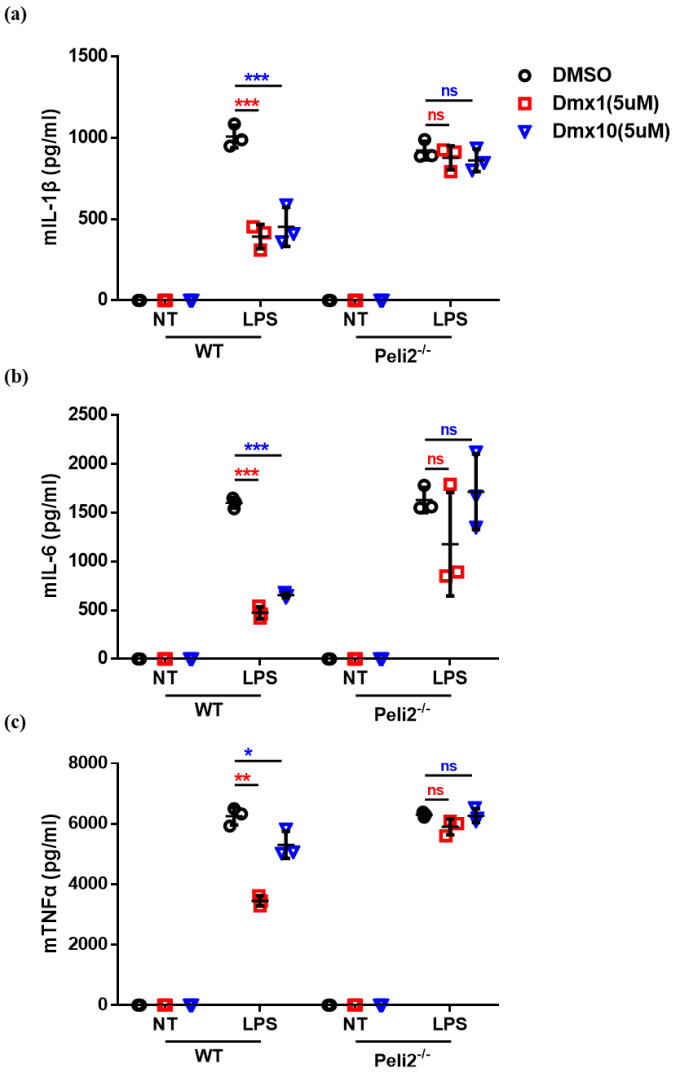


**Fig3.17 Dmx 1 and Dmx 10 suppress pro-inflammatory cytokines production in a Pellino2-dependent manner**

WT BMDMs and Peli2$^{-/-}$ BMDMs (2 x10$^5$) were plated in 96-well plate. Cells were pre-treated with Dmx1 or Dmx10 (5μM) for 1h. Control cells were treated with DMSO vehicle. Cells were then stimulated with LPS (100ng/ml) for 24h. Supernatants were assayed by ELISA for levels of (a) IL-1β, (b) IL-6 and (c) TNFα. Data are shown from an experiment that is representative of three independent experiments. Statistical analysis was performed by using the paired Student t-test. Statistically significant differences are indicated by the asterisks: ns, P>0.05; *, P<0.05; **, P<0.01; ***, P<0.001.

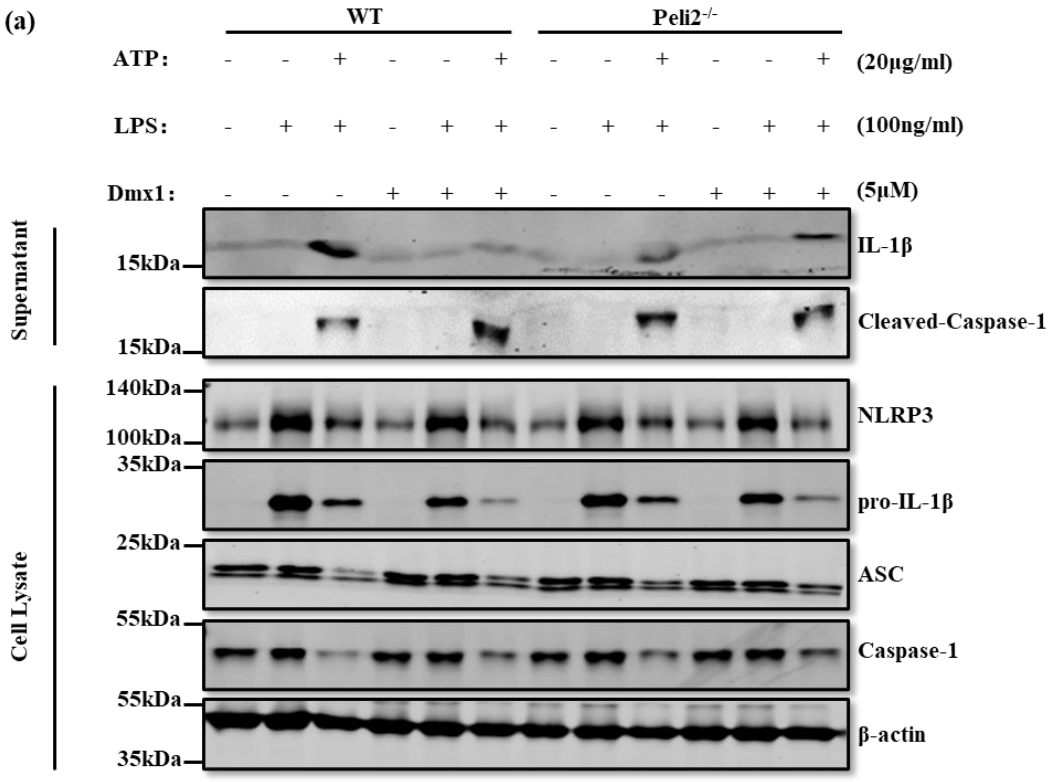
(a)
WT
Peli2-/-
ATP: - - + - - + - - + - - + (20μg/ml)
LPS: - + + - + + - + + - + + (100ng/ml)
Dmx1: - - - + + + - - - + + + (5μM)
Supernatant
Cell Lysate
15kDa
15kDa
140kDa
100kDa
35kDa
25kDa
55kDa
55kDa
35kDa
IL-1β
Cleaved-Caspase-1
NLRP3
pro-IL-1β
ASC
Caspase-1
β-actin

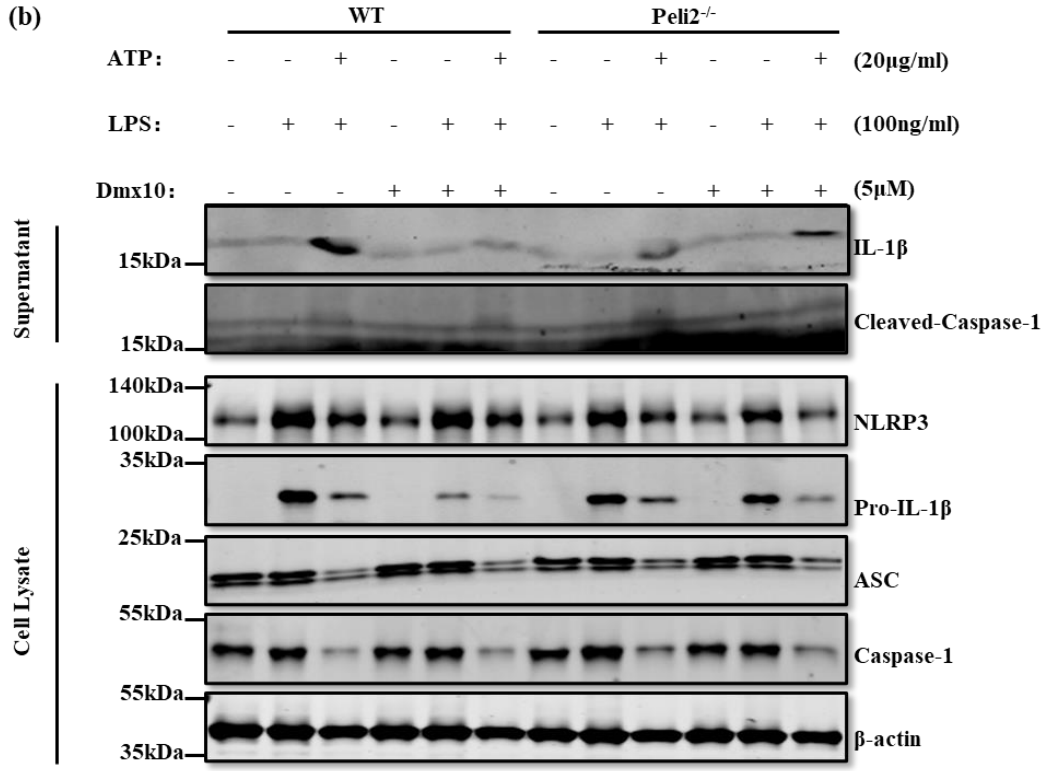


**Fig3.18 Dmx 1 and Dmx 10 suppress induction of IL-1β in a Pellino2-dependent manner**

WT BMDMs and Peli2$^{-/-}$ BMDMs (1 x10$^6$) were plated in 12-well plates. Cells were pre-treated with (a) Dmx1 or (b) Dmx10 (5μM) for 1h. Control cells were treated with DMSO vehicle. Cells were stimulated with LPS (100ng/ml) for 4h and ATP (20μg/ml ) for 30min. Supernatants and Cell lysate were harvested in 2x loading buffer and subjected to Western Blotting. Supernatant samples were probed with antibodies against cleaved-IL-1β and cleaved-Caspase-1 p10, and cell lysate samples were probed with antibodies against pro-IL-1β, NLRP3, Caspase-1, ASC and β-actin. Data are shown from an experiment that is representative of three independent experiments.

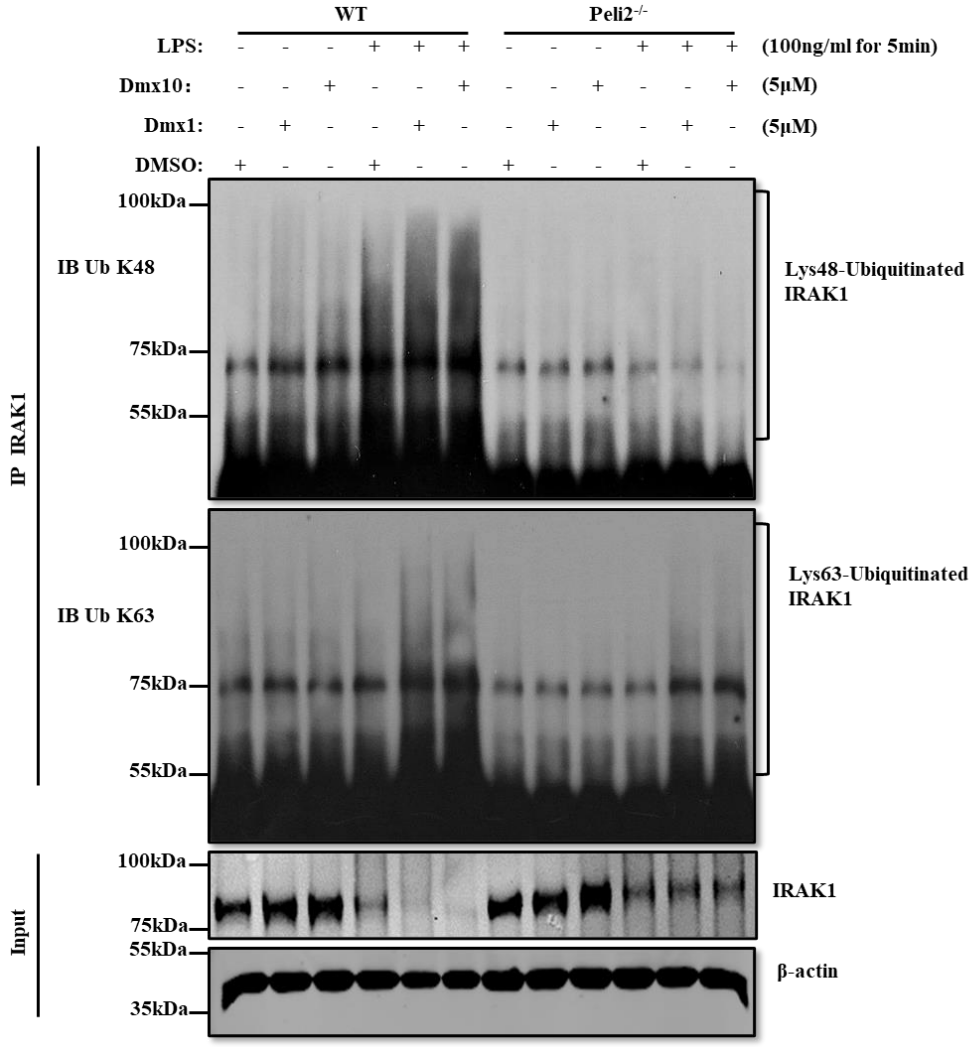


**Fig3.19 Dmx1 and Dmx10 augment the ubiquitination of IRAK1 in a Pellino2-dependent manner**

WT BMDMs and Peli2$^{-/-}$ BMDMs (3 x10$^6$) were plated in 6-well plates. Cells were pre-treated with Dmx1 or Dmx10 (10μM) for 1h. Control cells were treated with DMSO vehicle. Cells were stimulated with LPS (100ng/ml ) for 5min. Thereafter, cell lysates were extracted in RIPA buffer and immunoprecipitated (IP) using anti-IRAK1 antibody. The resulting membranes with IP samples were probed with antibodies against Lys48-Ubiquitination, Lys63-Ubiquitination. The resulting membranes with lysate samples (input) were probed with antibodies against IRAK1 and β-actin. Data are shown from an experiment that is representative of three independent experiments.

### 3.2.9 Dmx10 shows anti-inflammatory effects *in vivo*

Results above demonstrated the anti-inflammatory effects of Dmx1 and Dmx10 on the expression of IL-1β, IL-6 and TNFα *in vitro*. We next explored if these effects could be replicated in an *in vivo* setting. For these studies, we focused our efforts on Dmx10. 8-weeks old WT and Peli2$^{-/-}$ mice were treated with 10mg/kg or 20mg/kg Dmx10 by intraperitoneal injection (i.p injection) for 3h. Mice were monitored every 1h for responsiveness. Subsequently, mice were challenged with 20mg/kg LPS and were monitored every 8h for responsiveness and weight loss assessment (Please refer to Chapter2.6.1 for a comprehensive description of the procedures involved in the preparation of Dmx10 and LPS).

After 18h, mice were sacrificed and serum samples were collected. ELISA assays were carried out to measure serum levels of pro-inflammatory cytokines, including IL-1β (Fig3.20a), IL-6 (Fig3.20b), and TNFα (Fig3.20c). Increased serum cytokines were detected in all mice that were treated with LPS. The LPS-induced expression levels of IL-1β, IL-6 and TNFα showed a significant decrease with the Dmx10 treatment compared with the vehicle control. Notably, the absence of Peli2 reversed the down-regulation effect of Dmx10 on the expression levels IL-1β and TNFα and partially reversing the effect on the IL-6. This anti-inflammatory effect of Dmx10 *in vivo* is consistent with the results shown *in vitro*.

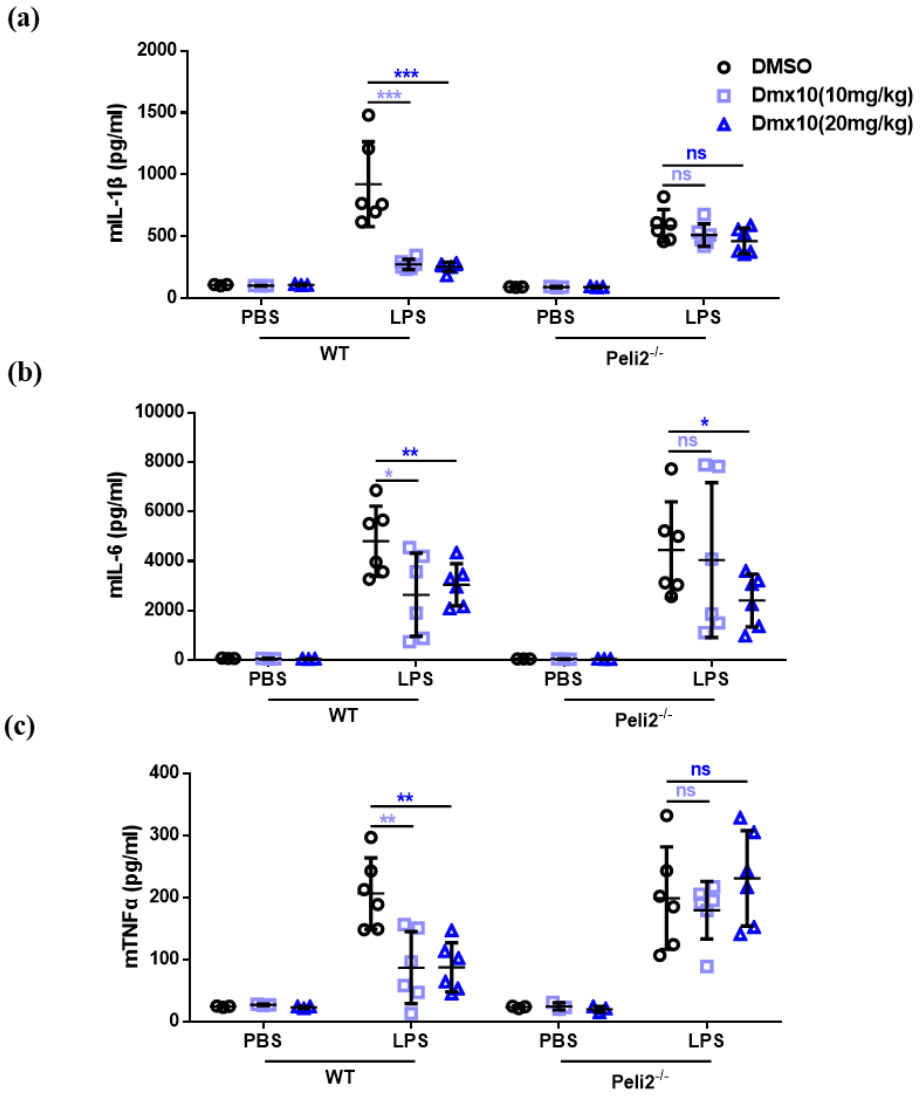


**Fig3.20 Dmx10 shows anti-inflammatory effects *in vivo***

WT and Peli2$^{-/-}$ mice were pre-treated with 10mg/kg or 20mg/kg Dmx10 by intraperitoneal injection (IP injection) for 4h. Control group mice were IP injected with the same volume of PBS (including 1:1000 DMSO) vehicle. Mice were then challenged with 20mg/kg LPS (n=6) for 18h. Control group mice were IP injected with the same volume of PBS (n=3). Mice were sacrificed and serum samples were collected and assayed by ELISA for levels of (a) IL-1β, (b) IL-6 and (c) TNFα. The results shown are the mean (±SD) and Statistical analysis was performed by using the paired Student t-test. Statistically significant differences are indicated by the asterisks: ns, P>0.05; *, P<0.05; **, P<0.01; ***, P<0.001.

## 3.3 Discussion

Inflammation is a hallmark feature of many complex diseases. Numerous human diseases, including atherosclerosis, diabetes, and ageing-related neurological disorders, have been linked to an inflammatory state. Endotoxins have been identified as key players in the pathogenesis of inflammation, particularly in endotoxemia in patients (Pussinen et al. 2011). Accumulating evidence suggests that chronic infection, obesity, alcohol consumption, and ageing may contribute to increased levels of circulating endotoxins, leading to low-grade chronic endotoxemia. If not properly regulated, this low-grade endotoxemia may further push the internal immune environment into a pro-inflammatory state, ultimately triggering the development of inflammatory diseases (Glaros et al. 2013).

LPS is a molecule found on the outer membrane of gram-negative bacteria, comprising a core polysaccharide chain, an O-specific polysaccharide chain (O-antigen), and lipid A. Lipid A as endotoxin, is the major part of the LPS-induced immune response. As a pathogen-associated molecular pattern, LPS is recognized by the pattern recognition receptor TLR4, which triggers downstream biological effects by activating transcription factors such as NF-κB and MAPKs, thereby driving the expression of pro-inflammatory cytokines like IL-1β, IL-6, and TNFα. these cytokines drive inflammation through various mechanisms [46]. However, overproduction of these cytokines can cause tissue and organ damage, leading to a wide range of inflammatory and autoimmune disorders (Schuerwegh et al. 2003; Umare et al. 2014). Furthermore, chronic inflammation and the associated overproduction of pro-inflammatory cytokines have been linked to the development of several chronic diseases, including cardiovascular disease, diabetes, and cancer. Thus, effective management of endotoxemia and the production of pro-inflammatory cytokines in the early stages could prevent or delay the onset of inflammatory diseases.

Pellino proteins constitute a three-membered family of E3 ubiquitin ligases that play an important role in innate immune response. Pellino1 is essential for the pathogenesis of neuropathic pain by affecting the activation of MAPK/NF-κB signaling and the production of pro-inflammation cytokines (Wang et al. 2020), Pellino2 knockout leads to the down-regulation of LPS-induced IL-1β expression through suppressing the activation of NLRP3 inflammasome (Humphries et al. 2018). We were keen to explore whether we could develop small molecules that could target Pellino proteins and serve as novel anti-inflammatory approaches. Here we report on two Pellino2 targeting synthetic small molecules Dmx1 and Dmx10 that suppress the production of pro-inflammatory cytokines in both *in vitro* and *in vivo* settings.

Using the binding region of the Pellino protein FHA domain, we performed a virtual screen of a small molecule drug database and identified an original compound, Dmx22. Subsequently, we used the structure of Dmx22 to identify 10 chemically related compounds (Dmx1 to Dmx10). We evaluated the anti-inflammatory effect of these compounds on LPS-induced IL-1β, IL-6, and TNFα expression *in vitro*, and observed that Dmx1 and Dmx10 showed significant dose-dependent suppression of these pro-inflammatory cytokines without cytotoxicity to BMDMs. Mechanistically, we found that Dmx1 and Dmx10 target and promote the degradation of IRKA1, which leads to the down-regulation of the NF-κB signaling pathway and ultimately results in the suppression of pro-inflammatory gene transcription. Notably, the functional Lys63-linked ubiquitin of IRAK1 was increased. We also investigated the dependence of Dmx1 and Dmx10's anti-inflammatory effects on the Pellino proteins, and found that Pellino2 silencing completely precluded their effects. Finally, we evaluated the anti-inflammatory effect of Dmx10 in an LPS-induced sepsis model *in vivo* and observed that Dmx10 also exhibited significant anti-inflammatory effects on the expressions of several cytokines, raising the exciting possibility that these compounds may have therapeutic anti-inflammatory potential.

The effects of the compounds appear to be mechanistically dependent on Pellino2 and

the ubiquitination and degradation of IRAK1. Interestingly Pellino proteins were initially identified as interacting proteins of IRAK1 and could ubiquitinate it via Lys63-linked poly-ubiquitination chains, without affecting Lys48-ubiquitination of IRAK1 (Moynagh 2014; Gottipati, Rao, and Fung-Leung 2008). However, our studies revealed that Dmx1 and Dmx10 enhance the interaction between IRAK1 and Pellino2 proteins, leading to increased Lys48-ubiquitination of IRAK1. This suggests that the effects of Pellino2 may be indirect and other E3 ligases may be responsible for augmenting levels of Lys48-ubiquitination. Therefore, further investigations are warranted to elucidate this mechanism in more detail.

Additionally, the scope of our *in vivo* experiments was limited to testing the anti-inflammatory effects of Dmx10 in an LPS-induced sepsis model. Pro-inflammatory cytokines such as IL-1β, IL-6, and TNFα have been implicated in the pathogenesis of several diseases. For instance, IL-1β can activate the NF-κB and MAPK signaling pathways by binding to the IL-1R receptor, contributing to positive feedback regulation of the transcription of inflammatory genes (Dinarello 2018). IL-1β expression levels are increased in high-fat diet-induced obesity mice model and are associated with insulin resistance (Bing 2015). In multiple chemical agent-induced cancer models, IL-1β expression levels are significantly elevated, leading to chronic inflammation and the promotion of tumorigenesis (Gelfo et al. 2020; Rebe and Ghiringhelli 2020). IL-6 is also involved in chronic inflammation in various inflammation-related diseases and also plays important role in the hyperimmune response and cytokine storm to coronavirus (Hirano 2021; Neurath and Finotto 2011). Therefore, it would be of interest for future research to focus on determining whether these compounds can also demonstrate efficacy in disease models that are more specific and precise, such as DSS-induced colitis, high-fat diet-induced obesity, and chronic inflammation.

While Dmx1 and Dmx10 have the same effects they also show some differences. Dmx1 appears to regulate multiple TLRs whereas Dmx10 is more selective for TLR4. The same original design protocol was used to develop both compounds and while they may

target the same proteins their small differences in structure may confer some differential effects. It will be of interest for future studies to further explore these compounds in more complex pre-clinical models of inflammatory diseases.

Given that both compounds were based around Pellino2 it is reassuring that their effects are dependent on the presence of Pellino2 and possibly promoting its interaction with IRAK1. However the compounds appear to cause switch of the type of ubiquitination of IRAK1 from K63-linked ubiquitination to K-48 linked ubiquitination. The latter appears to be mediated in an indirect manner by other E3 ubiquitin ligases. One possible mechanism is that the compounds allow for other E3 ligases to interact with IRAK and catalyze its K48-linked ubiquitination. Future studies in my laboratory will further probe the exact molecular mechanism. Irrespective of this detail the proposed targeting of IRAK is a plausible mechanism since the TNF signaling pathway that does not employ IRAK is refractory to the effect of Dmx1 and Dmx10.

The studies also shown that Dmx10 can manifest anti-inflammatory effects in a pre-clinical and simple model of sepsis. This suggests some therapeutic potential for the compounds from an anti-inflammatory context. Our laboratory will expand the present studies to assess their potential to regulate pathology in more complex models of disease. It will also be of value to evaluate their efficacy in human systems by using cells derived from patients and/or organoid systems.

In summary, the synthetic small molecule compounds Dmx1 and Dmx10, based on the FHA domain of Pellino proteins, demonstrate significant anti-inflammatory effects by promoting the degradation of IRAK1 and inhibiting the activation of the NF-κB signaling pathway. Our study represents an extension of the application of Pellino proteins in the field of anti-inflammation and serves as a foundation for future investigations on the design of anti-inflammatory drugs targeting Pellino proteins. Future research will focus on the development of enhanced compounds with greater precision and potency in their anti-inflammatory effects.

# Chapter 4: Exploring the roles of Pellino2 and characterizing the effects of Pellino2-targeted molecules in colorectal cancer

## 4.1 Introduction

Colorectal cancer (CRC) is the second leading cause of cancer-related deaths worldwide (Sawicki et al. 2021). The incidence and mortality rates of CRC have been continuously increasing in adults under 50 over the past decade. It is projected that by 2035, the overall death toll due to CRC will rise by 60% (Hossain et al. 2022). In Ireland, CRC is the second most common cancer in both men and women, with more than 2,500 cases diagnosed each year. Between 1994 and 2017, the incidence rate of CRC remained stable at 7 cases per 10,000 individuals. CRC is a heterogeneous disease, and its development is strongly associated with genetic and epigenetic changes as well as modifiable lifestyle risk factors such as smoking, unhealthy diet, excessive alcohol consumption, physical inactivity, and obesity (Hossain et al. 2022). Conventional treatment of CRC involves a combination of surgery and chemotherapy (Hossain et al. 2022; Xie, Chen, and Fang 2020). Surgical excision of colorectal carcinomas is effective in over 80% of cases. However, approximately 50% of patients experience relapse with metastasis post-surgery. Therefore, adjuvant treatment following surgical excision is imperative. Continuous radio-chemotherapy is widely employed to eradicate residual tumor cells post-surgery, extend disease-free intervals, and improve overall survival rates. Despite its effectiveness, the development of radio-chemotherapeutic resistance and the inevitable toxicity to normal cells have limited its efficacy (Hossain

et al. 2022; Xie, Chen, and Fang 2020). Consequently, it is crucial to explore alternative therapeutic strategies that can overcome these limitations and enhance the clinical outcomes of CRC cancer patients.

Cisplatin is a widely used chemotherapy drug for the treatment of various types of cancer. This platinum-containing compound exerts its anti-tumor activity by forming covalent bonds with the DNA of cancer cells, thereby inducing DNA damage and initiating cell death (Dasari and Tchounwou 2014; Ghosh 2019). It is also one of the most frequently utilized chemotherapeutic agents for clinical treatment of CRC, along with 5-Fluorouracil. However, the widespread development of resistance to Cisplatin has diminished its effectiveness in inducing antiproliferative and cytotoxic effects on malignant cells (Galluzzi et al. 2014). The limited success rate of Cisplatin treatment frequently results in tumor recurrence and therapeutic failure among patients (Galluzzi et al. 2014; Koberle and Schoch 2021). Furthermore, the adverse effects of Cisplatin have posed challenges to its clinical application. To overcome these limitations, researchers have focused on the utilization of adjuvant drugs that can be combined with Cisplatin to enhance its antineoplastic effects and mitigate its toxicity and side effects.

The Pellino family is a group of three members (Pellino1/2/3), which have been evolutionarily conserved (Moynagh 2014). These proteins are characterized by the presence of Ring-like motifs, which are a distinctive feature of the RING class of E3 ubiquitin ligases (Zhang and Li 2022). Pellino proteins interact with various target proteins to form Lys-11, Lys-48 and Lys-63-linked polyubiquitin chains *in vitro* and *in vivo* (Jensen and Whitehead 2003b, 2003a; Jiang et al. 2003; Liu et al. 2004). Recent research has highlighted the crucial role of Pellino proteins in the development of various cancers. Pellino1, for instance, is highly expressed in human lung cancer cell lines and can enhance their chemo-resistance by upregulating the expression of cIAP2 through Lys-63-mediated polyubiquitination (Jeon et al. 2016). Moreover, Pellino1 can target Bcl-6 to form Lys-63 specific polyubiquitination, thus inhibiting cancer development (Park et al. 2014). Similarly, human Pellino2 (PELI2) has been identified

as a predictor of multiple myeloma's response to clinical proteasome inhibitor treatment (Masuda et al. 2022). However, the functional involvement and the underlying molecular mechanisms of Pellino proteins in CRC have not yet been reported and require further investigation.

In this chapter, we present studies from our laboratory showing that deletion of *Peli2* gene in mice results in increased tumor burden in mouse models of colorectal cancer. Given that inflammation can frequently be a contributing factor to colorectal cancer coupled to our development in the previous chapter of two novel Pellino2-targeting molecules that manifest anti-inflammatory effects, we were keen to extend our functional characterization of these compounds and evaluate their potential to regulate pro-tumorigenic pathways.

We investigated the expression of human *PELI2* (h*PELI2*) mRNA in CRC patients and cell lines. Our results indicated a frequent down-regulation of h*PELI2* mRNA in both CRC patients and cell lines. Furthermore, we demonstrated that over-expression of human PELI2 protein (hPELI2) has a significant inhibitory effect on the growth of CRC cell lines by promoting cell apoptosis via Bcl-XL polyubiquitination. Conversely, silencing the expression of hPELI2 protein resulted in the opposite effect. These findings suggest that PELI2 may have a potential therapeutic application in the treatment of CRC.

Additionally, we employed the Pellino2-targeted compounds Dmx1 and Dmx10 to pharmacologically exploit the role of hPELI2 in controlling cell growth and death in colorectal cancer cell lines. Our study has demonstrated that the combination of Dmx1 or Dmx10 with Cisplatin enhances the sensitivity of CRC cell lines to Cisplatin treatment. Additionally, the combined therapy exhibits a significant inhibitory effect on the viability and colony formation ability of CRC cell lines. Furthermore, the combination treatment also promotes Cisplatin-induced apoptosis, suggesting its potential therapeutic benefits for CRC treatment.

## 4.2 Results

### 4.2.1 *Peli2* knockout suppresses tumorigenesis in AOM/DSS-induced CRC model.

To initially investigate the potential function of Peli2 in CRC, we employed an Azoxymethane (AOM)/ Dextran sodium sulfate (DSS)-induced CRC tumor model in Wild-type (WT) and Peli2 knock out (Peli2$^{-/-}$) mice. The AOM/DSS model is a robust and cost-effective initiation-promotion model that involves the induction of DNA damage-induced colitis through chemical induction, followed by repeated cycles to induce colon tumorigenesis (Arnesen et al. 2021; Parang, Barrett, and Williams 2016). Mice (6–8 weeks old) were intraperitoneally injected with a single dose AOM (10mg/kg). After one week, 2% DSS was administered in the drinking water for one week, followed by regular water for two weeks, repeated for three cycles. Throughout the study, body weight, stool consistency and presence of hematochezia were continuously monitored until the mice were sacrificed at the 9$^{th}$ week. Visible tumors on the colorectal mucous were counted, and tumor loads were measured. Additionally, colorectums were photographed and fixed in 4% formalin for histological analysis.

Our results revealed no significant difference in weight loss between AOM/DSS-treated WT mice and Peli2$^{-/-}$ mice (Fig4.1a). Notably, Peli2$^{-/-}$ mice treated with AOM/DSS exhibited higher disease activity index (DAI) scores, indicating more severe stool consistency and hematochezia (Fig4.1b). Furthermore, a higher number of tumors were observed in Peli2$^{-/-}$ mice compared to WT mice (tumor number, 6.54 ± 4.03 (WT) vs. 11.36 ± 4.68 (PELI2$^{-/-}$)) (Fig4.1c), and the tumor loads (tumor bunder) were also increased in Peli2$^{-/-}$ mice (tumor loads, 12.27 ± 7.79 (WT) vs. 20.92 ± 8.69 (PELI2$^{-/-}$)) (Fig4.1c). Moreover, the expression level of Ki-67, a common marker of cell proliferation, was significantly elevated in Peli2$^{-/-}$ mice compared to WT mice (Fig4.1d), which is consistent with the colorectal tumor burden findings. These data demonstrated

that Peli2 exerts a potent suppressive effect on colorectal tumorigenesis and greatly inhibits the tumor development induced by AOM/DSS.

**Dr. Bingwei Wang generated the data shown in Fig4.1.**

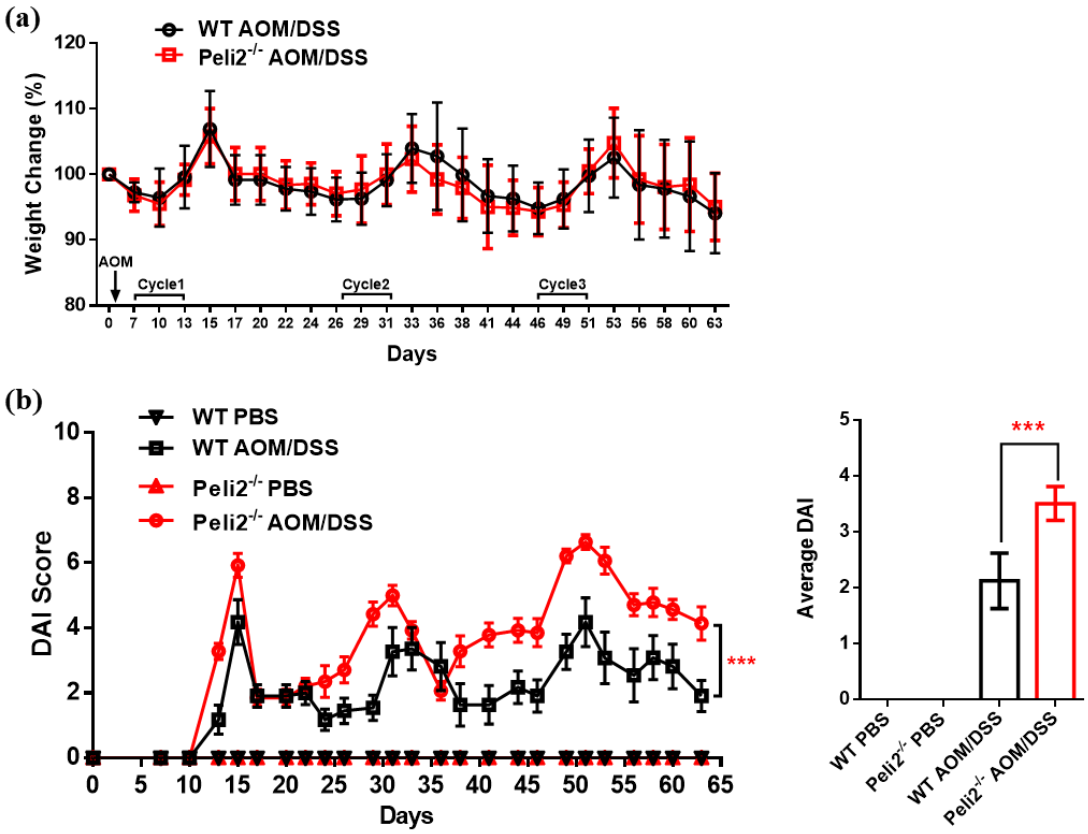
(a)
WT AOM/DSS
Peli2-/- AOM/DSS
Weight Change (%)
AOM
Cycle1
Cycle2
Cycle3
Days
(b)
WT PBS
WT AOM/DSS
Peli2-/- PBS
Peli2-/- AOM/DSS
DAI Score
***
Days
Average DAI
***
WT PBS
Peli2-/- PBS
WT AOM/DSS
Peli2-/- AOM/DSS

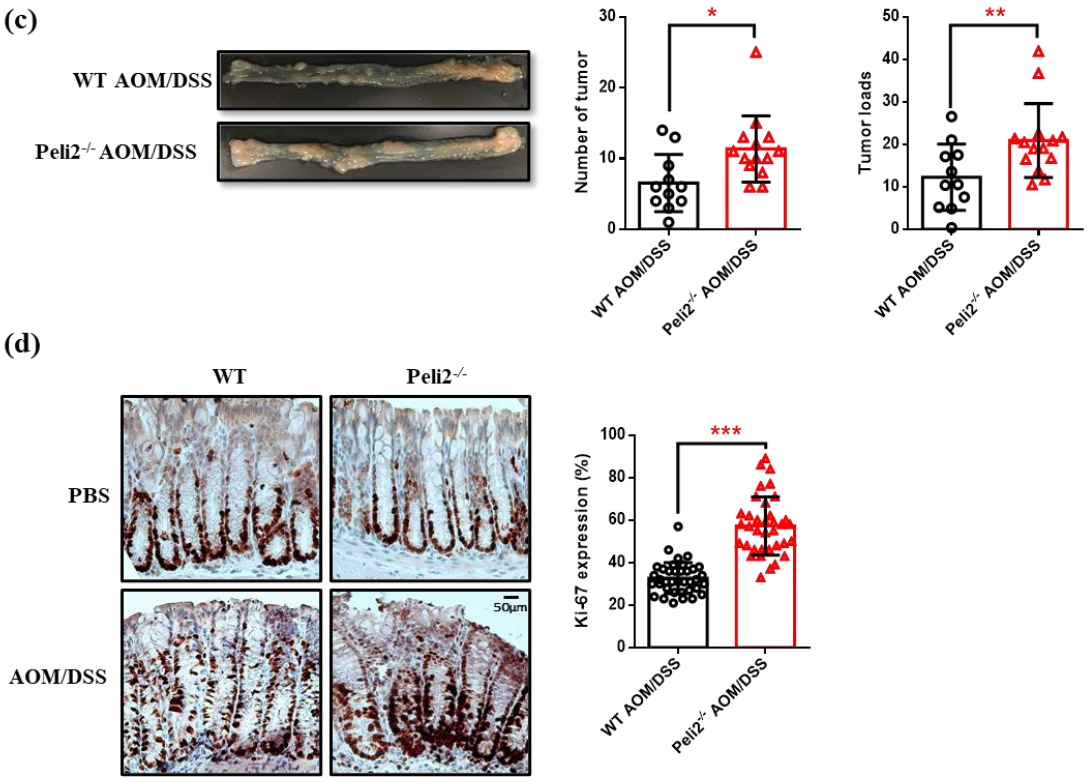


**Fig4.1 Peli2 knockout augments tumorigenesis in AOM/DSS-induced mice model**

WT and Peli2$^{-/-}$ mice were treated with AOM (10mg/kg) via intraperitoneal injection (IP injection). Control group mice were given an IP injection of the same volume of PBS vehicle. One week later, DSS (2%) was administered in the drinking water for a week, followed by two weeks of regular water. This DSS treatment cycle was repeated thrice. (a) Throughout the study, we continuously monitored and scored body weight, stool consistency, and the presence of hematochezia until the mice were euthanized in the 9$^{th}$ week. The mice were weighed every three days for a total period of nine weeks. (b) The Disease Activity Index (DAI) scores is a composite score of body weight, stool consistency, and hematochezia and these were recorded every five days over the total nine-week period. (c) Mice were sacrificed, visible tumors on the colorectal mucous were counted, and tumor loads was measured. (d) Colons were photographed and fixed in 4% formalin for Ki-67 histological analysis (100X, scale bar: 50μm). Statistical analysis was performed by using the paired Student t-test. Statistically significant differences are indicated by the asterisks: *, P<0.05; **, P<0.01; ***, P<0.001.

### 4.2.2 h*PELI2* mRNA shows lower expression levels in colorectal cancer tissues and cell lines.

The outcomes obtained from the AOM/DSS-induced CRC in Peli2$^{-/-}$ mice promoted an investigation of the potential functional significance of hPELI2 in CRC in human. To initially investigate this, we retrieved the expression levels of h*PELI2* mRNA in colorectal cancer were retrieved from the Oncomine database. The analysis demonstrates that h*PELI2* mRNA shows a lower expression level in colorectal cancer tissue compared with the normal tissue (Fig4.2a). Various colorectal cancer cell lines were also measured for h*PELI2* mRNA and compared with NCM460D cell line, a normal human colon mucosal epithelial cell line. Apart from the colorectal cancer cell line HCT116, h*PELI2* mRNA is significantly downregulated in other colorectal cancer cell lines, compared to NCM460D (Fig4.2b). Such association suggested that hPELI2 may act as a tumor suppressor and act to prevent colorectal cancer tumorigenesis. This is also consistent with the increased tumor burden in Peli2$^{-/-}$mice and suggests causality between loss or reduced expression of Pellino2 and tumorigenesis.

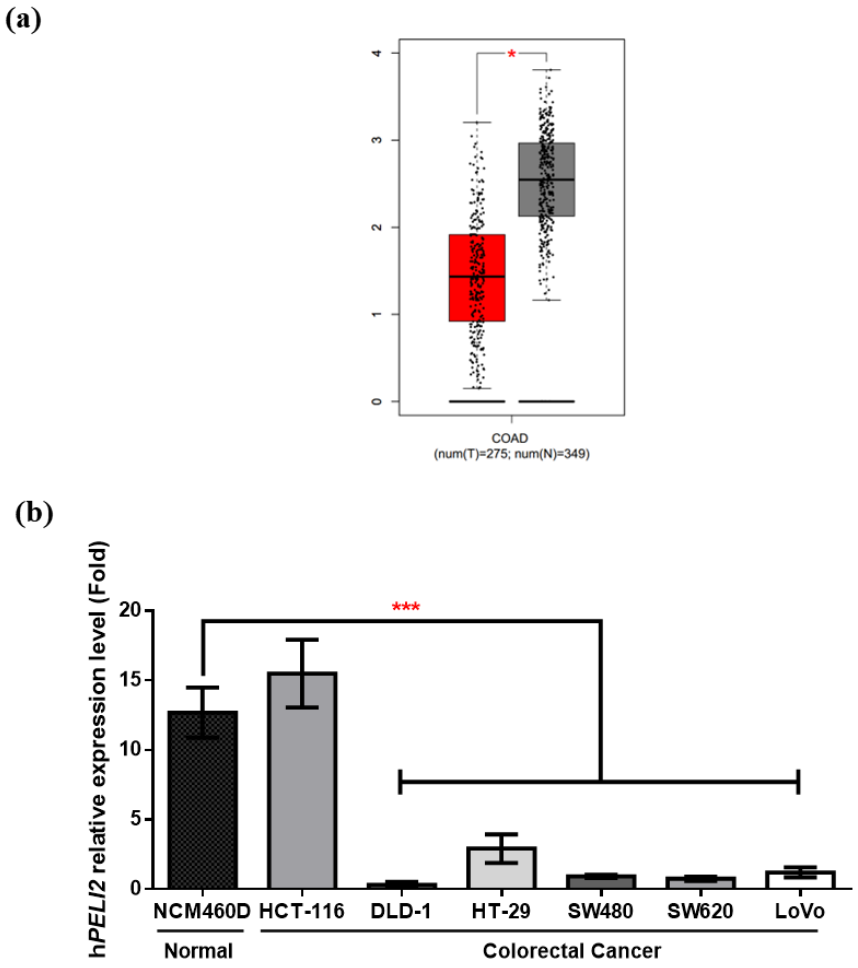


**Fig4.2 Downregulation of h*PELI2* mRNA in colorectal cancer tissues and cell lines**

(a) h*PELI2* mRNA expression levels in colorectal cancer tissues(n=275) and normal tissues (n=349) were obtained from Oncomine based on the TCGA database.

(b) Cells (1 x$10^5$) were harvested in TriZol and RNA was isolated and subsequently subjected to reverse transcription. h*PELI2* mRNA was measured by quantitative real-time PCR and normalized against *β-actin* mRNA. Data are shown from an experiment with duplicate samples and that is representative of three independent experiments.

### 4.2.3 hPELI2 inhibits colorectal cancer cell line growth *in vitro*

Given that there was an increased expression level of Ki-67, a common marker of cell proliferation, in the epithelium of colons from AOM/DSS Peli2$^{-/-}$ mice my studies next probed the epithelial-intrinsic role of hPELI2 in several colorectal cancer cell lines. Three different colorectal cancer cell lines (SW480, SW620, and DLD1) that all show low h*PELI2* mRNA expression levels were modified to stably over-expression hPELI2 by using lentivirus containing expression constructs. Cells were infected with lentivirus and selected for stable expression by puromycin. Selected cells were harvested using TriZol for whole mRNA analysis or with RIPA buffer for whole cell lysate isolation. Subsequently, the hPELI2 mRNA and protein expression levels were detected by Real-time PCR (Fig4.3a) and Western blot, respectively (Fig4.3b). These data confirmed that hPELI2 was over-expressed in all three cell lines at both mRNA and protein levels.

Next, we performed the MTT assay on each of cell lines over a period of 72h. The MTT assay is a measure of cellular metabolic activity and can be used as a measure of cell viability, proliferation and cytotoxicity (Buranaamnuay 2021). hPELI2 over-expressing cell lines and parental control cell lines were plated in 96-well plates and the MTT assay was performed at various times after 12-72h. The results showed that over-expression of hPELI2 reduced cell growth of SW480 and DLD-1 cell lines, but had no impact on the growth of SW620 cell line (Fig4.4). We next addressed whether hPELI2 over-expression would impact the colony-forming ability of each of these cell lines. Cells were plated in 6-well plates to generate single cell-derived colonies, and the colony number was counted after 7days of culture. hPELI2 over-expression impaired the colony formation properties of SW480 and DLD-1 cell lines, reducing the number of colonies from approximately 130 to 60 and from 200 to 120, respectively (Fig4.5). However, hPELI2 over-expression did not impact the colony formation ability of SW620 cell line and this is consistent with its lack of effect on the cell growth characteristics of this cell line (Fig4.5).

Moreover, to build on these findings, we wanted to address whether the results from these cellular assays would translate to a 3D *in vitro* growth assay. Cells were plated into ultra-low attachment U-bottom 96-well plates to generate cell spheroids, and the diameters of cell spheroids were determined after 1d and 5d of culture. Again, hPELI2 over-expression disrupted the cell growth ability of SW480 and DLD-1 cell lines in the 3D spheroid formation model, with smaller-sized spheroids being observed with hPELI2 over-expression (Fig4.6). Meanwhile, hPELI2 over-expression had no effect on spheroid formation or size in SW620 cells (Fig4.6).

Subsequently, to understand whether elevated levels of hPELI2 protein inhibits cell growth in SW480 and DLD-1 cell liens by suppressing cell proliferation or promoting cell death, we performed the Annexin V/propidium iodide (PI) staining flow cytometry assay to assess the rate of cell apoptosis. Annexin V is a cellular protein widely employed for the detection of apoptotic cells due to its ability to bind to phosphatidylserine, a recognized marker of apoptosis. Normally, phosphatidylserine is located on the inner surface of the plasma membrane. However, during the progression of apoptosis, phosphatidylserine becomes exposed on the outer leaflet, facilitating the binding of Annexin V to these cells. PI is a fluorescent intercalating agent and it can intercalate between the bases of DNA double strands. During the initial phases of apoptosis, when the nucleus remains intact, PI cannot bind to DNA due to the presence of the nuclear membrane. Conversely, during the advanced stages of apoptosis, characterized by nuclear fragmentation, PI binds to the released DNA fragments. By setting Annexin V staining as the X-axis and PI as the Y-axis, cells are classified into four distinct quadrants, namely LL, LR, UL, and UR. In the LL quadrant, both stains exhibit a negative signal, showing that the cells are in a normal state. On the other hand, cells in the LR quadrant display a positive Annexin V staining, suggesting their involvement in the early stages of apoptosis. In the UR quadrant, both Annexin V and PI staining show positive results, indicating that the cells were during the advanced stages of apoptosis. Cells were harvested and separated by trypsin, stained with Annexin V and PI and analyzed by cell flow cytometer (Rieger et al. 2011). Results

showed that hPELI2 over-expression led to an increased population of apoptotic cells in SW480 and DLD-1 cell lines. Specifically, the apoptotic cell population increased from 12.4% to 18.9% in SW480 cells and from 13.8% to 21.3% in DLD-1 cells(Fig4.7). These results highlight that elevated level of hPELI2 promotes cell apoptosis and this may contribute to suppression of growth and spheroid formation in CRC cell lines.

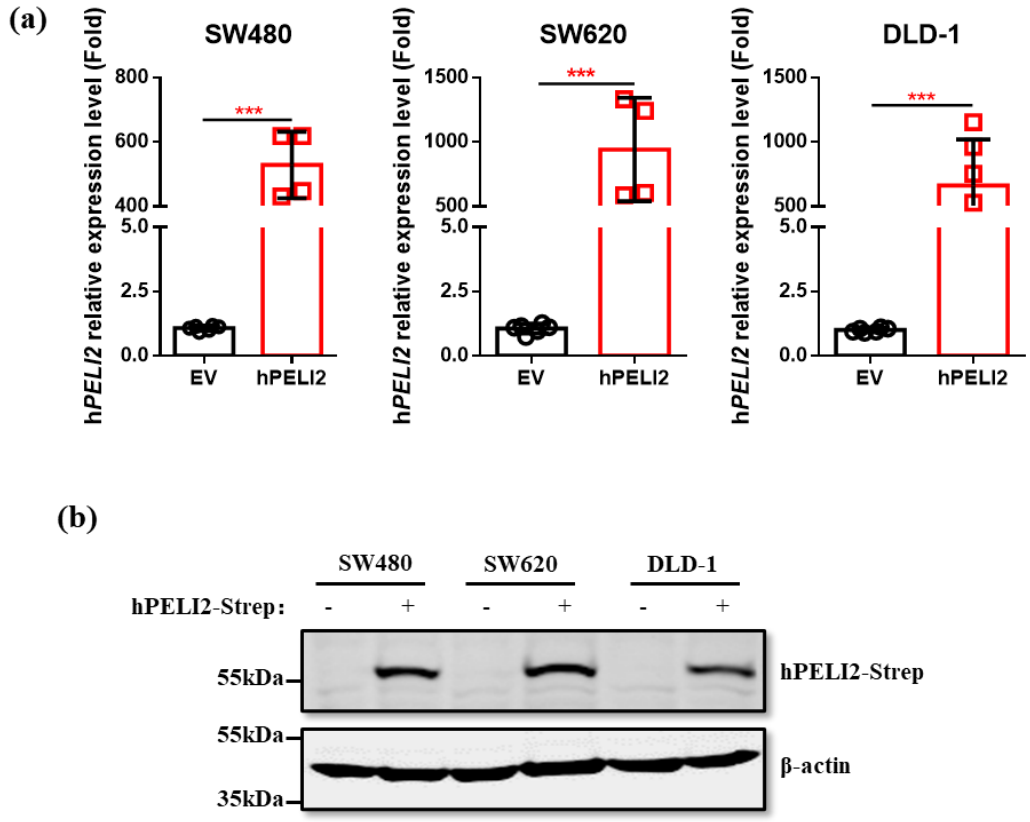


**Fig4.3 Lentivirus mediated hPELI2 over-expression in SW480, SW620 and DLD-1 cells**

HEK293T (1 x$10^6$) were plated in 6-well plates for next-day transfection. hPELI2-pLV encodes for a Strep-tagged form for hPELI2 (Empty pLV vector was used as control ) was co-transfected with psPAX2 and pMD2.G at a 1:1:1 mass ratio into HEK293T cells by using Lipofectamine 2000 transfection regent. The lentivirus supernatant was collected after 48h incubation and filtered through a 0.45μm filter. Empty vector control cells (EV) and hPELI2 over-expression cells (hPELI2) of SW480, SW620 and DLD-1 cell lines (1 x$10^6$) were plated in 6-well plates with 3ml medium overnight. Cells were infected with 1ml of virus suspension and 1ml of normal medium mixture and then selected with puromycin (5μg/ml) for 3 days.

(a) Cells (1 x$10^5$) were harvested in TriZol and RNA was isolated and subsequently subjected to reverse transcription. h*PELI2* mRNA was measured by quantitative real-time PCR and normalized against *β-actin* mRNA. Data are shown from an experiment with duplicate samples and that is representative of three independent experiments. Statistical analysis was performed by using the paired Student t-test. Statistically significant differences are indicated by the asterisks: ***, P<0.001.

(b) Cell lysates were harvested in RIPA buffer and subjected to Western Blotting. The resulting membranes were probed with Strep-tag and β-actin. Data are shown from an experiment that is representative of three independent experiments.

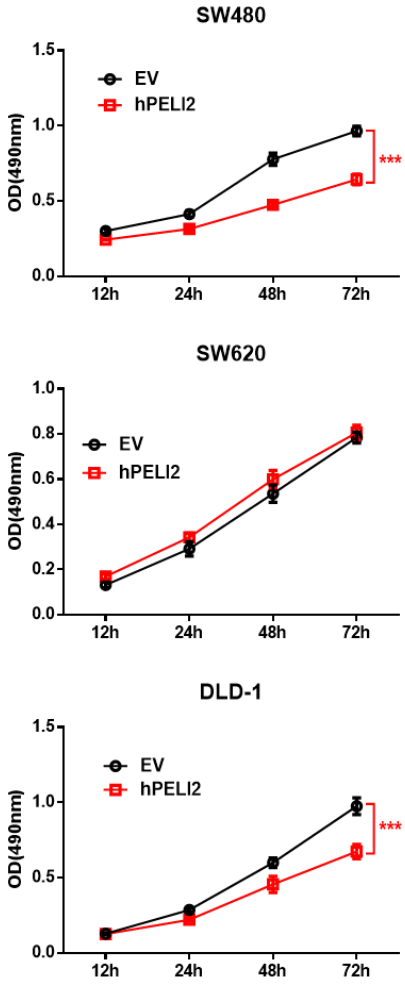


**Fig4.4 hPELI2 over-expression reduces proliferation of SW480 and DLD-1 cells**

SW480, SW620 and DLD-1 cell lines were infected with lentivirus containing an expression vector expressing hPELI2 (hPELI2) or an empty expression vector (EV). Infected cells (4 x$10^3$) were plated in 96-well plates with 200µl medium. After 12, 24, 48, and 72h, MTT solution (50µg) was added into wells and incubated at 37℃ for 4h. The medium was removed and DMSO (150µl) was added into wells to dissolve the crystals. Absorbance was measured at a wavelength of 490nm by using a microplate reader. Data are shown from an experiment with quadruplicates that is representative of three independent experiments. Statistical analysis was performed by using the paired Student t-test. Statistically significant differences are indicated by the asterisks: ***, P<0.001.

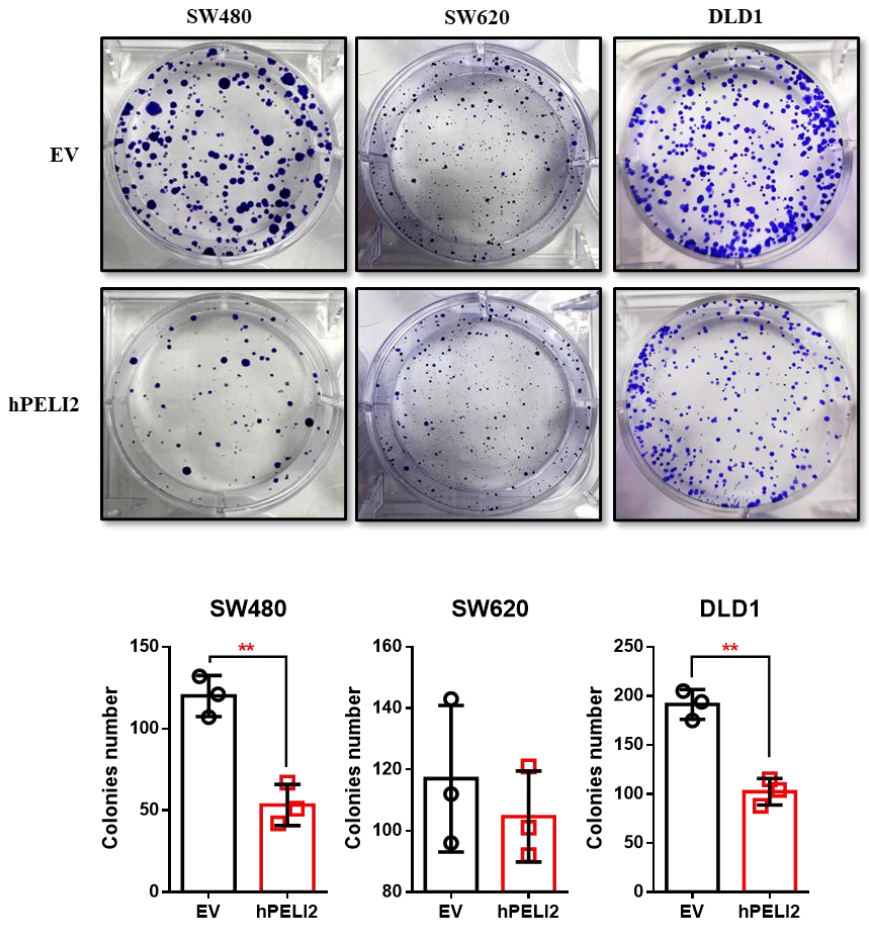


**Fig4.5 hPELI2 over-expression reduces colony-formation in SW480 and DLD-1 cells**

SW480, SW620 and DLD-1 cell lines were infected with lentivirus containing an expression vector expressing hPELI2 (hPELI2) or an empty expression vector (EV). Infected cells (600cells/well) were plated in 6-well plates with 3ml medium to generate single-cell derived colonies. Cell growth was terminated at day7 and colonies were observed under the inverted microscope. Thereafter, medium was removed and the colonies were fixed in 2ml methanol and stained with 0.5% crystal violet. Colony number in each wells was counted by using the OpenCFU software tool. Data are shown from an experiment that is representative of three independent experiments. Statistical analysis was performed by using the paired Student t-test. Statistically significant differences are indicated by the asterisks: **, $P<0.01$.

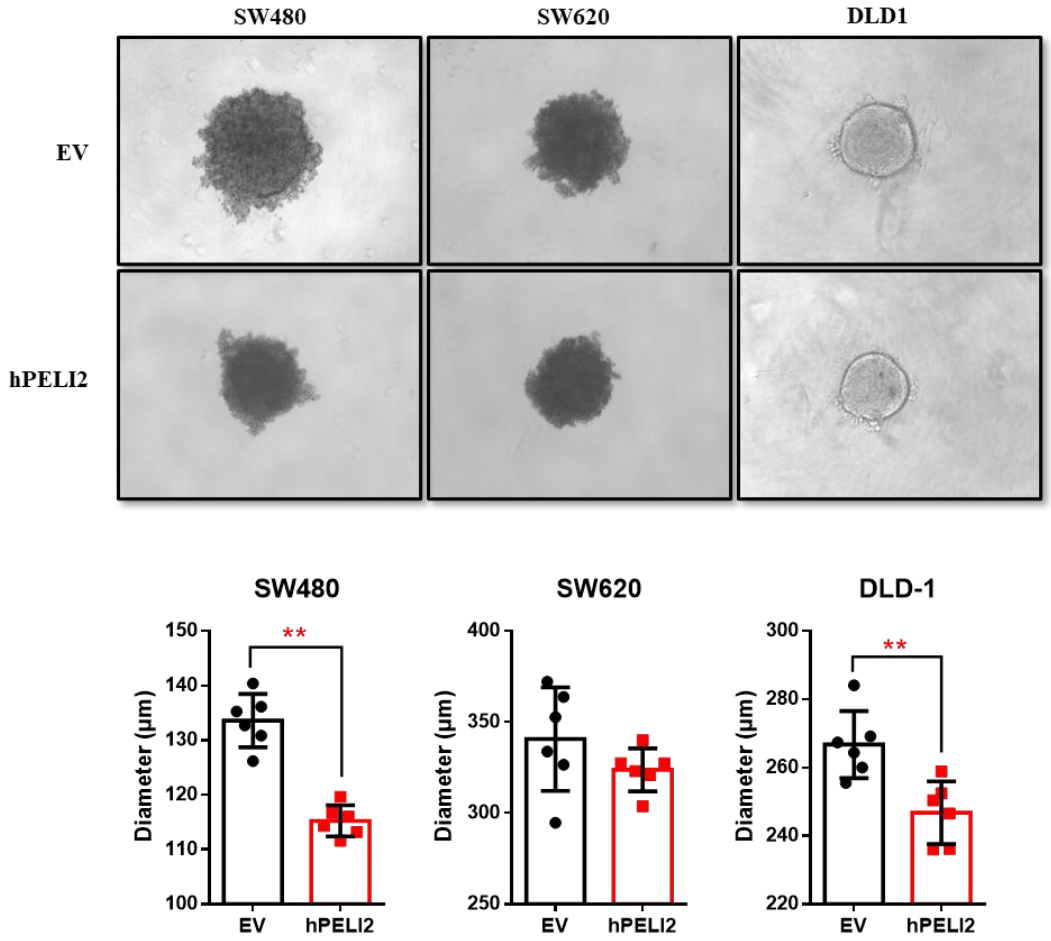


**Fig4.6 hPELI2 over-expression inhibits the growth of SW480 and DLD-1 cells in a 3D spheroid formation model**

SW480, SW620 and DLD-1 cell lines were infected with lentivirus containing an expression vector expressing hPELI2 (hPELI2) or an empty expression vector (EV). Infected cells (500cells/well) were plated in ultra-low attachment U-bottom 96-well plates with 200μl medium. Subsequently, the diameters of the generated spheroids were assessed on day1, day3, and day5, utilizing an Olympus EP50 camera. Additionally, the spheroids were visualized at 4X magnification using an Optika Vision Pro camera. Data are shown from an experiment that is representative of three independent experiments. Statistical analysis was performed by using the paired Student t-test. Statistically significant differences are indicated by the asterisks: **, $P<0.01$.

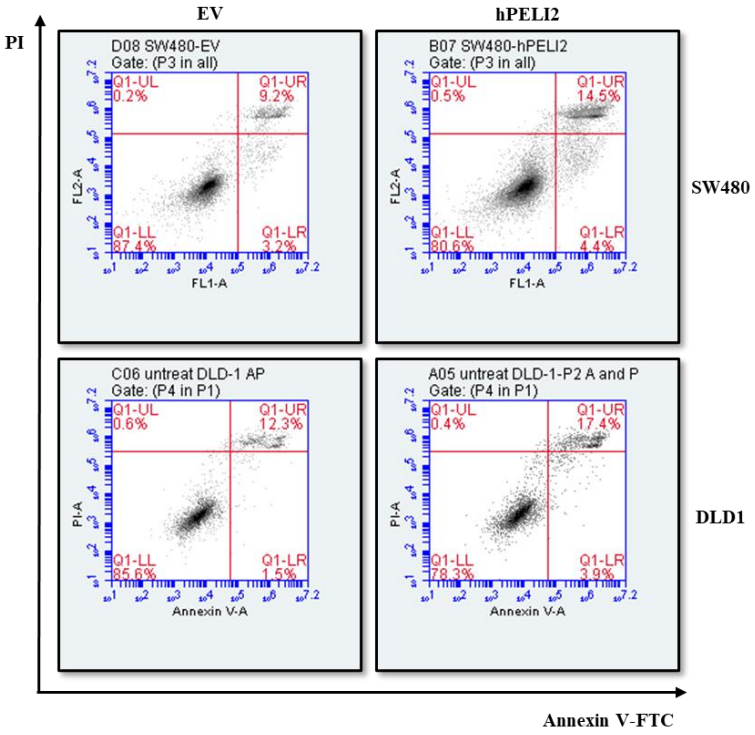


**Fig4.7 hPELI2 over-expression promotes apoptosis in SW480 and DLD-1 cells**

SW480 and DLD-1 cell lines were infected with lentivirus containing an expression vector expressing hPELI2 (hPELI2) or an empty expression vector (EV). Infected cells (1 x$10^4$) were harvested by trypsin treatment. Cells were harvested by trypsin treatment and then cells were twice washed with pre-cold PBS and once with Annexin binding buffer. Cells were resuspension in 1000µl Annexin binding buffer and aliquots cell suspensions (100µl) were transferred into a new Eppendorf tube and 1x Annexin binding buffer (400µl), Annexin V-FITC (5µl, 90µg/ml) and PI (10µl, 1mg/ml) were added into the tube. The components were mixed by pipetting multiple times and incubated at room temperature for 15min. The cells were evaluated by flow cytometry (BD AccuriTM C6). At least 10,000 cells were counted, single live cells were selected and the apoptosis rate and apoptosis stage were determined by using Annexin V-FITC as the X-axis coordinate and PI as the Y-axis coordinate. The unstained sample, Annexin V-FITC alone stain sample and PI alone stain sample were used as controls to delineate the different intervals. Data are shown from an experiment that is representative of three independent experiments.

### 4.2.4 hPELI2 enhances the sensitivity of SW480 and DLD-1 cell lines to Cisplatin induced apoptosis

The increased levels of apoptosis in SW480 and DLD-1 cell lines' response to elevated levels of hPELI2 were quite modest and so we next assessed if hPELI2 could further augment pro-apoptotic signaling pathways. Cisplatin is one of the most potent chemotherapeutic agents for the treatment of colon cancer. It induces a DNA damage response, leading to cancer cell apoptosis (Dasari and Tchounwou 2014; Ghosh 2019). Therefore, we aimed to use Cisplatin to induce cell apoptosis in the above CRC cell lines and investigate the potential of over-expressed hPELI2 to enhance these pro-apoptotic effects and so increase the sensitivity of these cells to Cisplatin. To test our hypothesis, SW480 and DLD-1 cell lines were treated with specific concentrations of Cisplatin for 24h or 48h. Afterwards, cells were harvested, separated by trypsin, stained with Annexin V and PI, and analyzed by a flow cytometer. Compare to the control cells, we found that hPELI2 over-expression augmented Cisplatin-induced apoptosis in SW480. Specifically, the apoptotic cell population increased from 21.9% to 30.8% with 40μg/ml Cisplatin treatment, from 29% to 31% with 80μg/ml Cisplatin treatment, and from 31.3% to 44% with 120μg/ml Cisplatin treatment (Fig4.8a). Similar results were shown in DLD-1 cell lines. The apoptotic cell population enhanced from 14.9% to 20.6% with 5μg/ml Cisplatin treatment, from 17.2% to 26.4% with 20μg/ml Cisplatin treatment, and from 28.3% to 37.2% with 40μg/ml Cisplatin treatment (Fig4.8b). This suggests that over-expression of hPELI2 makes colorectal cell lines more sensitive to Cisplatin.

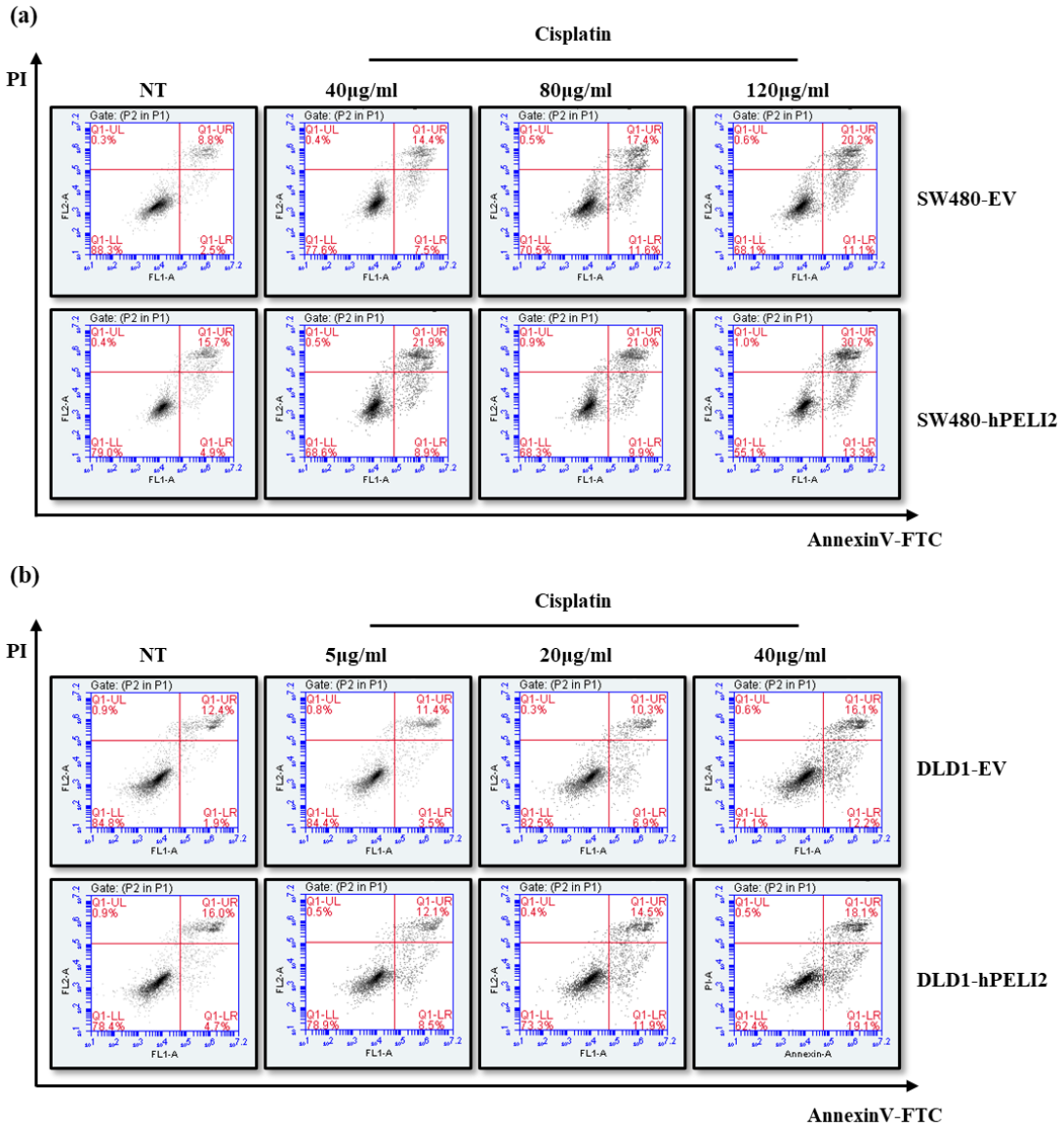


**Fig4.8 hPELI2 over-expression augments Cisplatin-induced apoptosis in SW480 and DLD-1 cells**

SW480 and DLD-1 cell lines were infected with lentivirus containing an expression vector expressing hPELI2 (hPELI2) or an empty expression vector (EV). Infected SW480(a) and DLD-1(b) cells (4 x$10^3$) were plated in 6-well plates with 3ml medium and incubated overnight. Cells were treated with the indicated concentrations of Cisplatin for 24h. Control cells were treated with PBS vehicle. Cells were harvested by trypsin treatment and then cells were twice washed with pre-cold PBS and once with Annexin binding buffer. Cells were resuspension in 1000μl Annexin binding buffer and aliquots cell suspensions (100μl) were transferred into a new Eppendorf tube and 1x

Annexin binding buffer (400µl), Annexin V-FITC (5µl, 90µg/ml) and PI (10µl, 1mg/ml) were added into the tube. The components were mixed by pipetting multiple times and incubated at room temperature for 15min. The cells were evaluated by flow cytometry (BD AccuriTM C6). At least 10,000 cells were counted, single live cells were selected and the apoptosis rate and apoptosis stage were determined by using Annexin V-FITC as the X-axis coordinate and PI as the Y-axis coordinate. The unstained sample, Annexin V-FITC alone stain sample and PI alone stain sample were used as controls to delineate the different intervals. Data are shown from an experiment that is representative of three independent experiments.

We next assessed the potential mechanism by which hPELI2 could be promoting such pro-apoptotic effects. PELI2 is known to regulate NF-κB (Humphries et al. 2018) and the activation of NF-κB signaling is also involved in Cisplatin resistant therapy of head and neck squamous cell carcinoma (Yang et al. 2020). Given the regulatory role of PELI2 in the NF-κB pathway coupled with the role of the latter in mediating the apoptotic effects of Cisplatin we investigated the effect of hPELI2 over-expression on the activation of the NF-κB pathway in DLD-1 cells in the absence and presence of Cisplatin. The activation of the NF-κB pathway was monitored by measuring the time-dependent phosphorylation of IKKα/β, IκBα and the NF-κB subunit p65. Cisplatin-induced strong phosphorylation of each of these proteins and over-expression of hPELI2 failed to affect these phosphorylation patterns (Fig4.9a) suggesting that hPELI2 does not mediate its pro-apoptotic effects by targeting the NF-κB pathway. The PELI2-interaction partner IRAK1, which is an upstream regulator of the NF-κB pathway, was also measured but its levels were not affected by Cisplatin or elevated level of hPELI2 (Fig4.9a).

PELI2 has also been shown to regulate the MAPK signaling pathways (Humphries et al. 2018). Different members of the MAPK signaling pathway have also been identified to either prevent or contribute to Cisplatin-induced apoptotic effects in several forms of cancer (Achkar et al. 2018). Given the regulatory role of PELI2 in MAPK pathways coupled with their role in controlling the apoptotic effects of Cisplatin, we investigated the effect of hPELI2 over-expression on these pathways in the absence and presence of Cisplatin. Cisplatin-induced strong phosphorylation of p38, ERK and JNK MAP kinases in a time-dependent manner but expression of exogenous hPELI2 failed to affect Cisplatin-induced activation of these pathways (Fig4.9b) suggesting that hPELI2 does not mediate its pro-apoptotic effects by regulating MAPK pathways.

Pellino proteins have also been associated with increased activation of the PI3K/Akt signaling pathway and the latter is positively correlated with Cisplatin treatment in colorectal cancer and activation of apoptosis-associated signaling pathways (Jeon et al.

2017; Zheng et al. 2022; Franke et al. 2003). Using phosphorylation of AKT as an indicator of PI3K/Akt activation we demonstrated that Cisplatin can induce activation of the PI3K/Akt signaling pathway but this is unaltered by expression of exogenous hPELI2 (Fig4.10) again suggesting that this pathway is not targeted by hPELI2 in promoting its cellular apoptotic effects.

Having failed to show any effects of hPELI2 on the above pathways that regulate apoptotic cell killing we next characterized the direct effects of hPELI2 on the caspase-mediated pathways that execute cell apoptosis by characterizing the effects of hPELI2 on intracellular markers of apoptosis. Since cleaved-Poly (ADP-ribose) polymerase (cleaved-PARP) is a common marker of cell apoptosis (Chaitanya, Steven, and Babu 2010), we investigated the effect of hPELI2 on Cisplatin-induced PARP cleavage in DLD-1 cell line. As expected, Cisplatin-induced PARP cleavage in a dose-dependent manner and hPELI2 over-expression further sensitized the cells to Cisplatin as evidenced by higher levels of cleaved PARP at the same concentrations of Cisplatin (Fig4.11). Moreover, hPELI2 over-expression greatly enhanced the Cisplatin-induced cleavage of Caspase3 (Fig4.11), one of the executioners of the caspase pathway (Obeng 2021). B-cell lymphoma-extra-large (Bcl-xL) is one of the critically important anti-apoptotic protein and Cisplatin was shown to significantly reduce its levels which is consistent with the pro-apoptotic effects of Cisplatin (Loo et al. 2020; Singh, Letai, and Sarosiek 2019). Over-expression of hPELI2 caused further depletion of Bcl-xL in response to Cisplatin treatment (Fig4.11). Thus, these results suggest that hPELI2 promotes Cisplatin-induced apoptosis of SW480 and DLD-1 cell lines by directly promoting the activation of the Caspase3-dependent apoptosis signaling pathway.

(a)

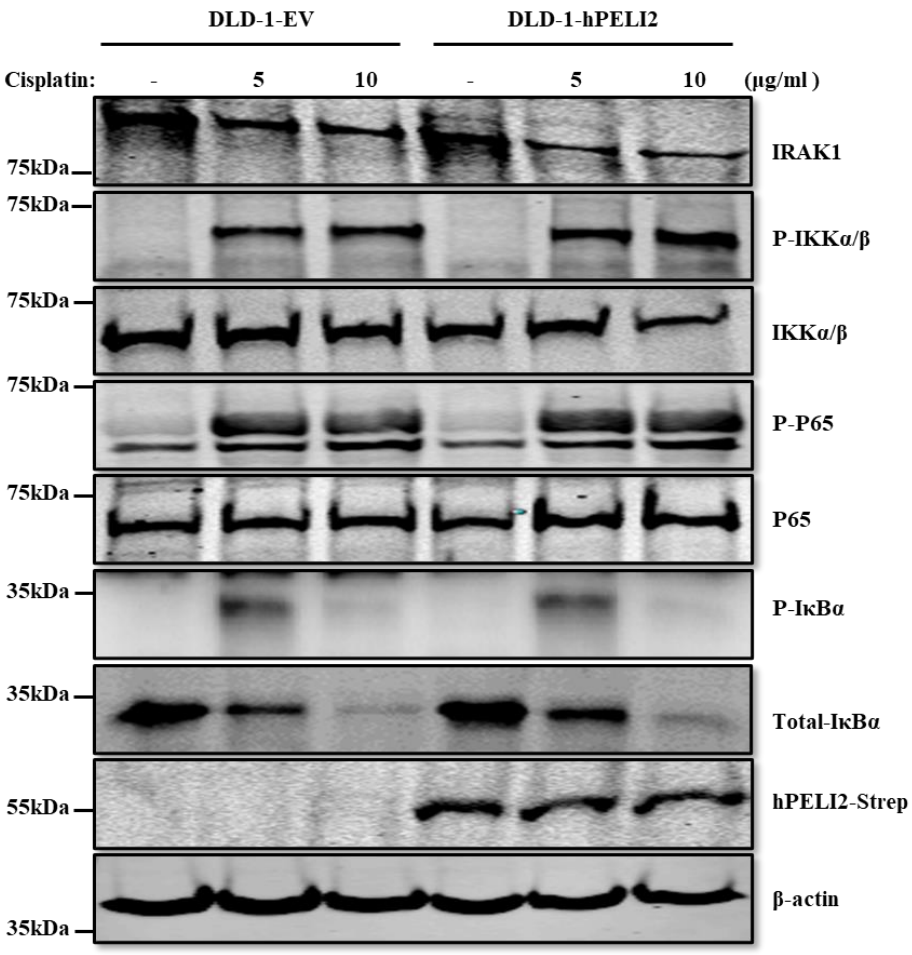
DLD-1-EV
DLD-1-hPELI2
Cisplatin: - 5 10 - 5 10 (μg/ml)
75kDa
IRAK1
75kDa
P-IKKα/β
75kDa
IKKα/β
75kDa
P-P65
75kDa
P65
35kDa
P-IκBα
35kDa
Total-IκBα
55kDa
hPELI2-Strep
35kDa
β-actin

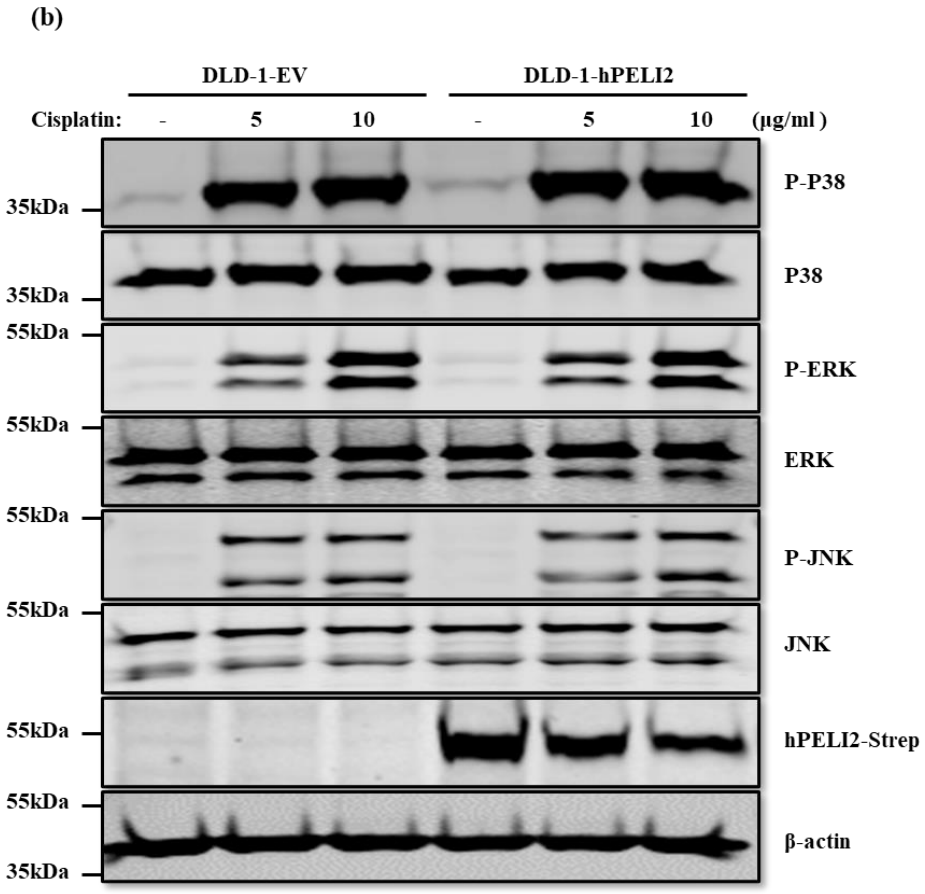


**Fig4.9 hPELI2 does not affect Cisplatin-induced activation of NF-κB and MAPK signaling pathways**

DLD-1 cell line was infected with lentivirus containing an expression vector expressing hPELI2 (hPELI2) or an empty expression vector (EV). Infected cells (5 x$10^5$) were plated in 6-well plates and incubated overnight. Cells were treated with Cisplatin (5μg/ml or 10μg/ml) for 48h. Control cells were treated with DMSO vehicle. Cell lysates were extracted in RIPA buffer and subjected to Western Blotting. The resulting membranes (a) were probed with antibodies against IRAK1, phosphor-IKKα/β, total IKKα/β, phosphor-P65, total P65, phosphor-IκBα, total IκBα, hPELI2-strep and β-actin. The resulting membranes (b) were probed with antibodies against phosphor-P38, total P38, phosphor-ERK, total ERK, phosphor-JNK, total JNK, hPELI2-strep and β-actin. Data are shown from an experiment that is representative of three independent experiments.

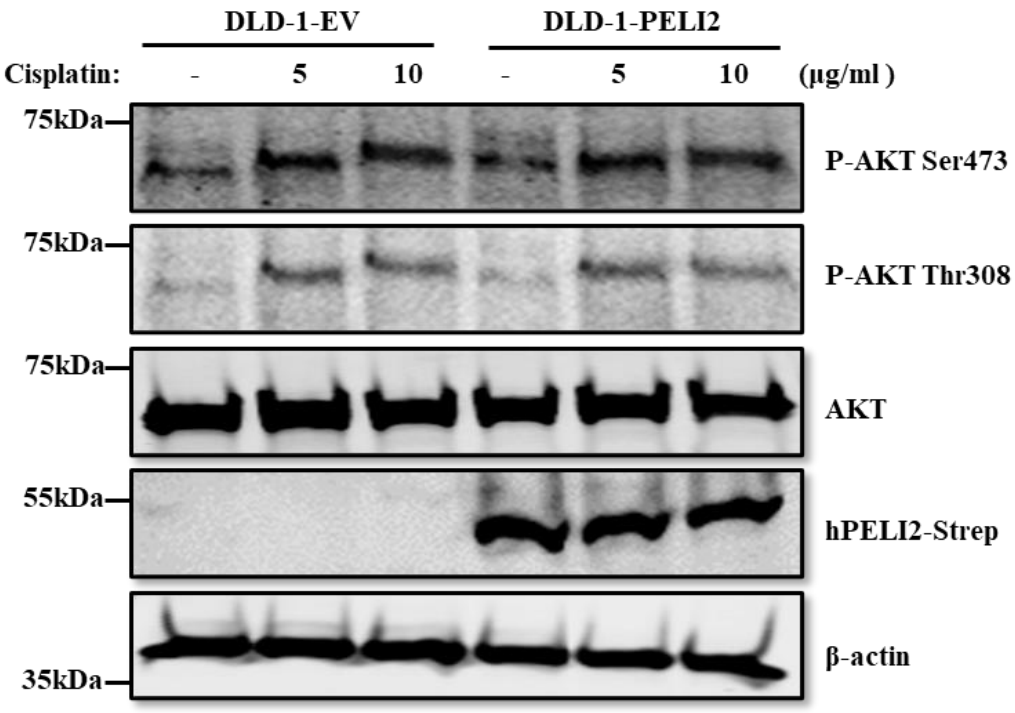


**Fig4.10 hPELI2 does not affect the Cisplatin-induced PI3K-AKT signaling pathway activation**

DLD-1 cell line was infected with lentivirus containing an expression vector expressing hPELI2 (hPELI2) or an empty expression vector (EV). Infected cells (5 x$10^5$) were seeded in 6-well plates and incubated overnight. Cells were treated with Cisplatin (5µg/ml or 10µg/ml) for 48h. Control cells were treated with DMSO vehicle. Following treatment, cell lysates were extracted using RIPA buffer and subjected to Western Blotting. The resulting membranes were probed with antibodies against phospho-AKT Ser473, phospho-AKT Thr308, total AKT, PELI2-strep, and β-actin. Data are shown from an experiment that is representative of three independent experiments.

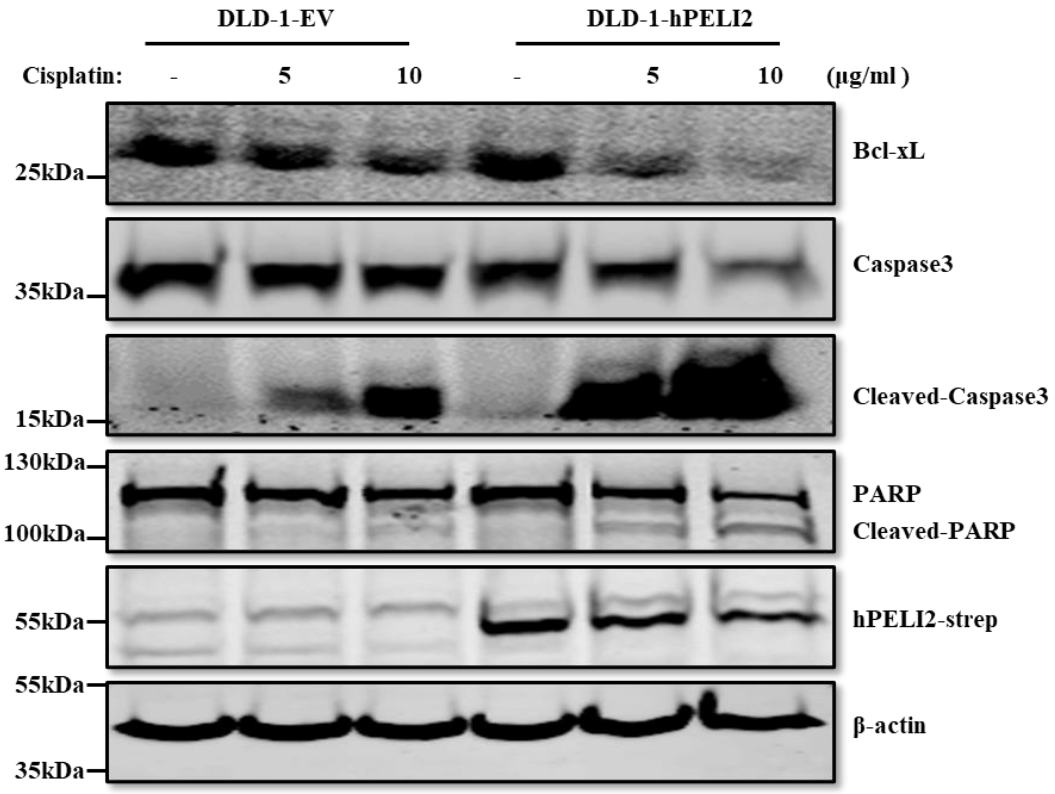


**Fig4.11 Over-expression of hPELI2 promotes Caspase3-dependent apoptosis signaling pathway in DLD-1 cell**

DLD-1 cell line was infected with lentivirus containing an expression vector expressing hPELI2 (hPELI2) or an empty expression vector (EV). Infected cells (5 x$10^5$) were plated in 6-well plates and incubated overnight. Cells were treated with Cisplatin (5μg/ml or 10μg/ml) for 48h. Control cells were treated with DMSO vehicle. Cell lysates were extracted in RIPA buffer and subjected to Western Blotting. The resulting membranes were probed with antibodies against BCL-xL, Full-length Caspase3, Cleaved-Caspase3, hPELI2-Strep, PARP and β-actin. Data are shown from an experiment that is representative of three independent experiments.

### 4.2.5 hPELI2 promotes Cisplatin-induced cell apoptosis and targets the ubiquitination of Bcl-xL

Having discovered that hPELI2 protein promotes Cisplatin-induced apoptosis in colorectal cancer cell lines by enhancing Caspase3 pathway and at the same time reducing the levels of the anti-apoptotic protein and caspase inhibitor Bcl-xL and given that Bcl-6, another member of the Bcl family has been shown to be a target of PELI1, we hypothesized that hPELI2 might target Bcl-xL.

Bcl-xL is encoded by the *BCL2-like 1* gene and is a transmembrane protein located in the mitochondria. It belongs to the Bcl-2 family of proteins and functions as an anti-apoptotic protein by inhibiting the release of mitochondrial contents, such as Cytochrome c, which in turn prevents caspase activation and cell apoptosis (Loo et al. 2020; Singh, Letai, and Sarosiek 2019; Dou et al. 2021). Cisplatin treatment induces ubiquitination and degradation of the Bcl-xL protein via the proteasome. Therefore, we hypothesized that hPELI2 protein may regulate the ubiquitination and degradation of Bcl-xL protein, ultimately promoting cell apoptosis in colorectal cancer cell lines.

To challenge our hypotheses, we treated the DLD-1 cell lines with 0-2.5-5-10-15-20 µg/ml Cisplatin for 24h and performed immunoprecipitation of the Bcl-xL protein after denaturation of cell extracts to dissociate any Bcl-xL-interacting proteins. Immunoprecipitants were then subjected to western immunoblotting using anti-ubiquitin antibody. The results demonstrated that Bcl-xL protein exhibited substantial ubiquitination in a time-dependent manner with Cisplatin treatment at 5µg/ml or higher concentrations (Fig4.12). This was also associated with depletion of levels of Bcl-xL protein in cell extracts. Subsequently, we treated the hPELI2 over-expression DLD-1 cell line and its control cell line with 5µg/ml and 10µg/ml Cisplatin for 24h and performed immunoprecipitation of the Bcl-xL protein to assess its ubiquitination. Interestingly, the hPELI2 over-expression cell lines exhibited augmented Bcl-xL ubiquitination response to Cisplatin treatment(Fig4.13). These findings are consistent

with hPELI2 enhancing the ubiquitination and degradation of Bcl-xL, thereby promoting Cisplatin-induced apoptosis in colorectal cancer cell line

Additionally, we were keen to assess if hPELI2 protein can directly interact with Bcl-xL protein. HEK293T cells were transfected with plasmids encoding Strep-tagged hPELI2 and Bcl-xL for 24h. Bcl-xL was immunoprecipitated with anti-Bcl-xL antibody and then analyzed for co-precipitated Strep-tagged hPELI2 protein by western blotting. Results showed that Strep-tagged hPELI2 protein could not be detected in Bcl-xL immunoprecipitants, suggesting that hPELI2 protein and Bcl-xL protein do not interact with each other (Fig4.14).

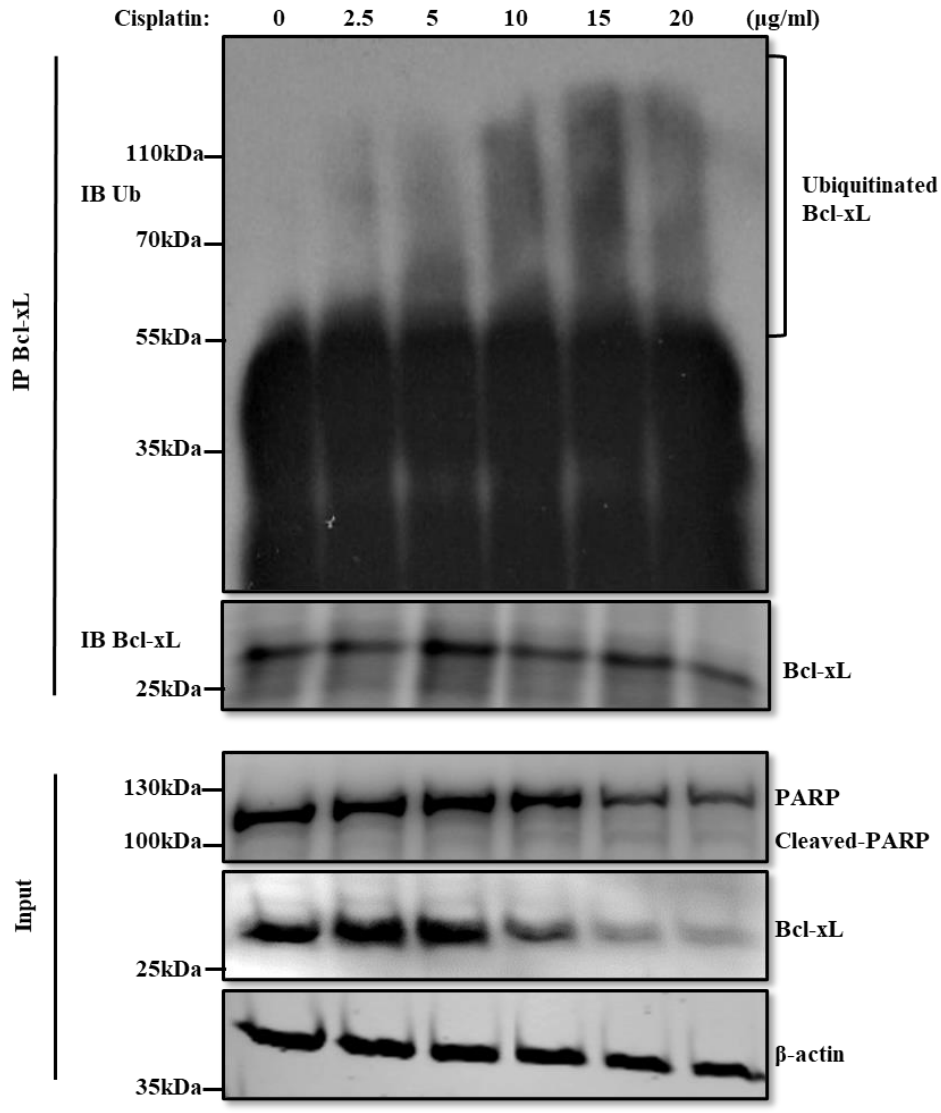


**Fig4.12 Cisplatin-induced ubiquitination of Bcl-xL protein**

DLD-1 cells (5 x$10^5$) were plated in 6-well plates and incubated overnight. Cells were treated with indicated concentrations of Cisplatin for 48h. Control cells were treated with DMSO vehicle. Thereafter, cell lysates were extracted in RIPA buffer and immunoprecipitated (IP) using an anti-Bcl-xL antibody. The resulting membranes with IP samples were probed with antibodies against Ubiquitin (Ub) and Bcl-xL. The resulting membranes with lysate samples (Input) were probed with antibodies against PARP, Bcl-xL and β-actin. Data are shown from an experiment that is representative of three independent experiments.

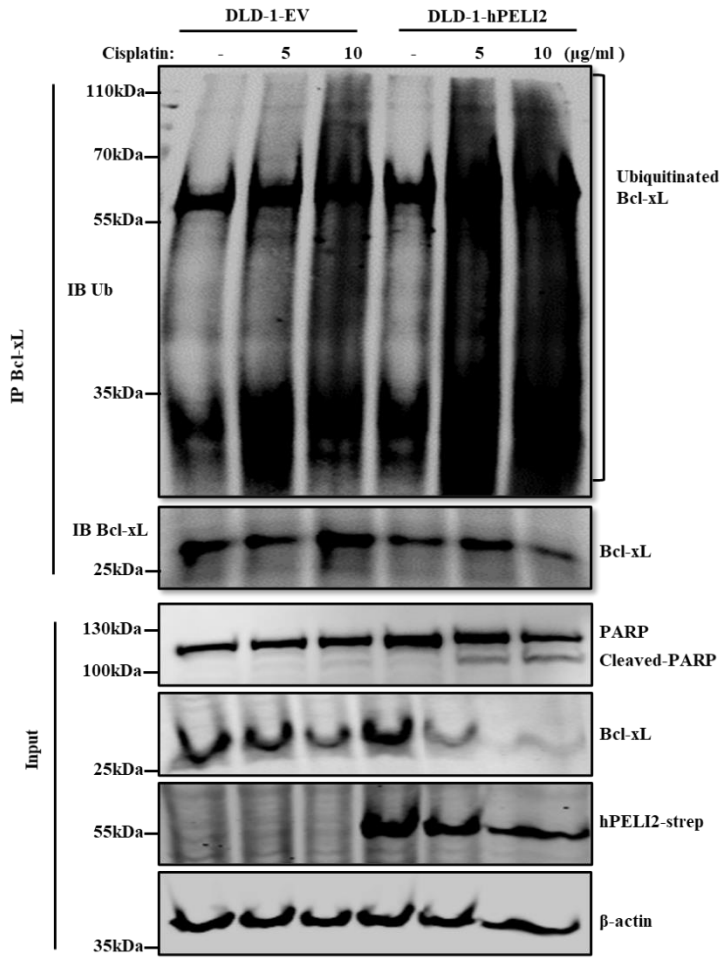


**Fig4.13 hPELI2 over-expression augment the Cisplatin-induced ubiquitination of Bcl-xL**

DLD-1 cell line was infected with lentivirus containing an expression vector expressing hPELI2 (hPELI2) or an empty expression vector (EV). Infected cells (5 x$10^5$) were plated in 6-well plates overnight. Cells were treated with Cisplatin (5μg/ml or 10μg/ml) for 48h. Control cells were treated with DMSO vehicle. Whole cell lysates were extracted in RIPA buffer and immunoprecipitated (IP) using an anti-Bcl-xL antibody. The resulting membranes with IP samples were probed with antibodies against Ubiquitin (Ub) and Bcl-xL. The resulting membranes with lysate samples (Input) were probed with antibodies against PARP, Bcl-xL, hPELI2-strep and β-actin. Data are shown from an experiment that is representative of three independent experiments.

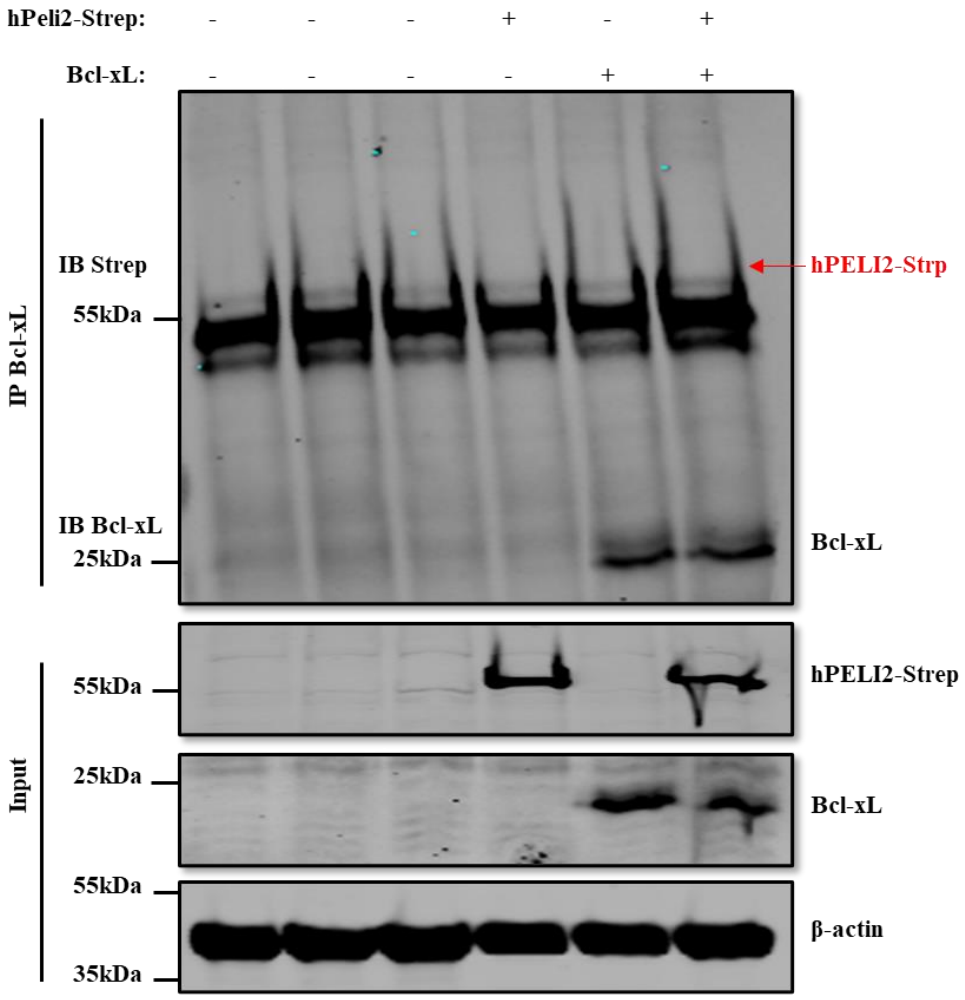


**Fig4.14 hPELI2 does not directly interaction with Bcl-xL**

HEK293T (3 x$10^6$) cells were plated in 6-well plates. Cells were transfected with expression constructs encoding Strep-tagged hPELI2 and Bcl-xL plasmid alone or combination for 48h. Control cells were transferred with empty vector plasmid as vehicle control. Cell lysates were extracted in NP-40 buffer and Co-immunoprecipitated (Co-IP) using anti-Bcl-xL antibody. The resulting membranes with IP samples were probed with antibodies against Strep-tag and Bcl-xL. The resulting membranes with lysate samples (Input) were probed with antibodies against Strep-tag, Bcl-xL and β-actin. Data are shown from an experiment that is representative of three independent experiments.

### 4.2.6 Loss of hPELI2 promotes colorectal cancer cell line growth *in vitro*

Since the above data show that elevated levels of hPELI2 can suppress the growth of colorectal cancer cell lines and this is associated with ubiquitination of Bcl-xL and cell apoptosis, we also wanted to perform the complementary approach of suppressing the expression of hPELI2 and assessing the effects on the growth of colorectal cancer cell lines. Initially, we selected HCT116 and HT29 cell lines, which exhibited higher h*PELI2* mRNA expression levels (Fig4.2b), to establish a stable knockdown model of hPELI2 using two independent hPELI2-shRNA-A3 and B7 constructs, employing a lentiviral approach. After the infection and puromycin selection for 2 weeks, the h*PELI2* mRNA expression level was detected by Real-time PCR. The results showed that both independent shRNAs downregulated the expression of h*PELI2* mRNA in HCT116 and HT29 cell lines(Fig4.15).

Subsequently, we conducted the MTT assay as before and observed that hPELI2 knockdown significantly enhanced the growth of the HCT116 cell line but had no effect on the growth of the HT29 cell line (Fig4.16). Furthermore, we investigated the effect of hPELI2 knockdown on the colony formation ability of these two cell lines. The results were consistent with the MTT assay, showing that hPELI2 loss increased the colony formation ability of the HCT116 cell line, enhancing the number of colonies from approximately 80 to 200, exhibiting significant differences compared to the parental HCT116 cell line (Fig4.17). Conversely, no differences were observed in the HT29 cell line (Fig4.17). Similar results were obtained from the 3D *in vitro* growth assay, where hPELI2 knockdown augmented the size of the 3D spheroid formation model in the HCT116 cell line, while it did not affect the spheroid formation or size in HT29 cell line (Fig4.18). Overall, the results from the 2D and 3D assays collectively indicate that the loss of hPELI2 accelerates the growth of the HCT116 cell line, which is wholly consistent with the pro-apoptotic effects of hPELI2 protein over-expression in the SW480 and DLD-1 cell lines.

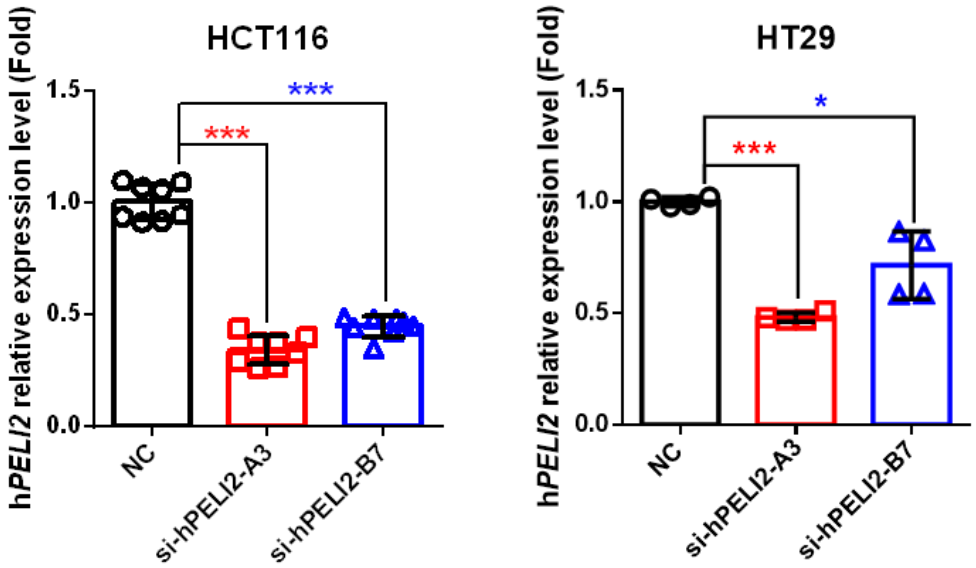


**Fig4.15 Lentivirus-mediated hPELI2 knockdown in HCT116 and HT29 cells**

HEK293T ($1x10^6$) cells were plated into 6-well plates with 3ml medium to reach a confluency of 70-80% for next-day transfection. PELI2-shRNA-A3 pGIPZ or PELI2-shRNA-B7 pGIPZ encode for two different shRNA of hPELI2 (A3 and B7) (non-silencing pGIPZ vector (NC) was used as control) were co-transfected with psPAX2 and pMD2.G at a 1:1:1 mass ratio into HEK293T cells by using Lipofectamine 2000 transfection regent. The lentivirus supernatant was collected after 48h incubation and filtered through a 0.45μm filter. HCT-116 and HT29 cells ($1 x10^6$) were plated in 6-well plates with 3ml medium and incubated overnight. Cells were infected with 1ml of virus suspension and 1ml of normal medium mixture and then selected with 5μg/ml of puromycin for 7days. After puromycin selection, cells ($1 x10^5$) were harvested in TriZol and RNA was isolated and subsequently subjected to reverse transcription. h*PELI2* mRNA was measured by quantitative real-time PCR and normalized against *β-actin* mRNA. Data are shown from an experiment with duplicate samples and that is representative of three independent experiments. Statistical analysis was performed by using the paired Student t-test. Statistically significant differences are indicated by the asterisks: *, $P<0.05$; ***, $P<0.001$.

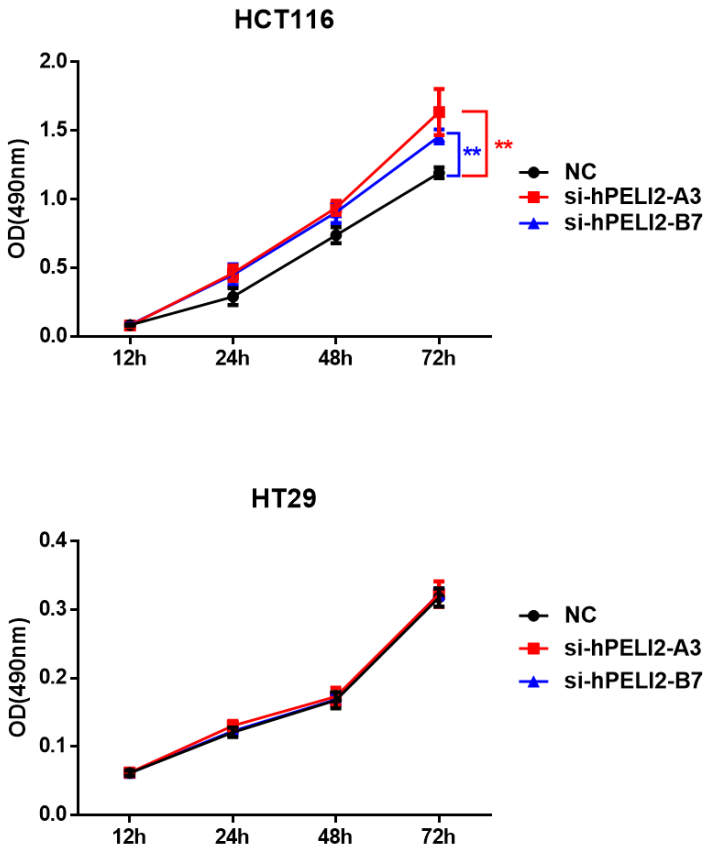


**Fig4.16 hPELI2 knockdown increases proliferation in HCT116 cell**

HCT116 and HT29 cell lines were infected with lentivirus containing an expression vector expressing shRNA of hPELI2 (A3 or B7) or a non-silencing vector (NC). Infected cells (4 x$10^3$) were plated in 96-well plates with 200µl medium. After 12, 24, 48, and 72h, MTT solution (50µg) was added into wells and incubated at 37℃ for 4h. The medium was removed and DMSO (150µl) was added into wells to dissolve the crystals. Absorbance was measured at a wavelength of 490nm by using a microplate reader. Data are shown from an experiment with quadruplicates that is representative of three independent experiments. Statistical analysis was performed by using the paired Student t-test. Statistically significant differences are indicated by the asterisks: **, P<0.01.

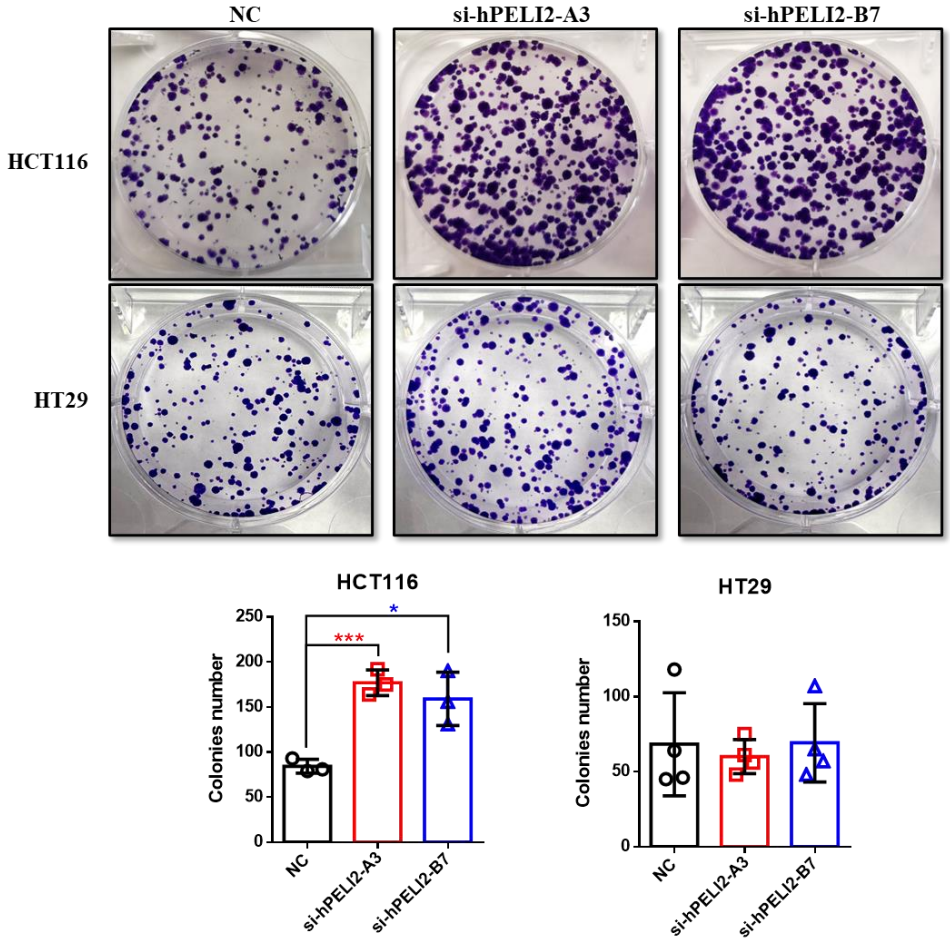


**Fig4.17 hPELI2 knockdown promotes colony-formation in HCT116 cell**

HCT116 and HT29 cell lines were infected with lentivirus containing an expression vector expressing shRNA of hPELI2 (A3 or B7) or a non-silencing vector (NC). Infected cells (600cells/well) were plated in 6-well plates with 3ml medium to generate single-cell derived colonies. Cell growth was terminated at day7 and colonies were observed under the inverted microscope. Thereafter, medium was removed and the colonies were fixed in 2ml methanol and stained with 0.5% crystal violet. colony number in each wells was counted by using the OpenCFU software tool. Data are shown from an experiment that is representative of three independent experiments. Statistical analysis was performed by using the paired Student t-test. Statistically significant differences are indicated by the asterisks: *, $P<0.05$; ***, $P<0.001$.

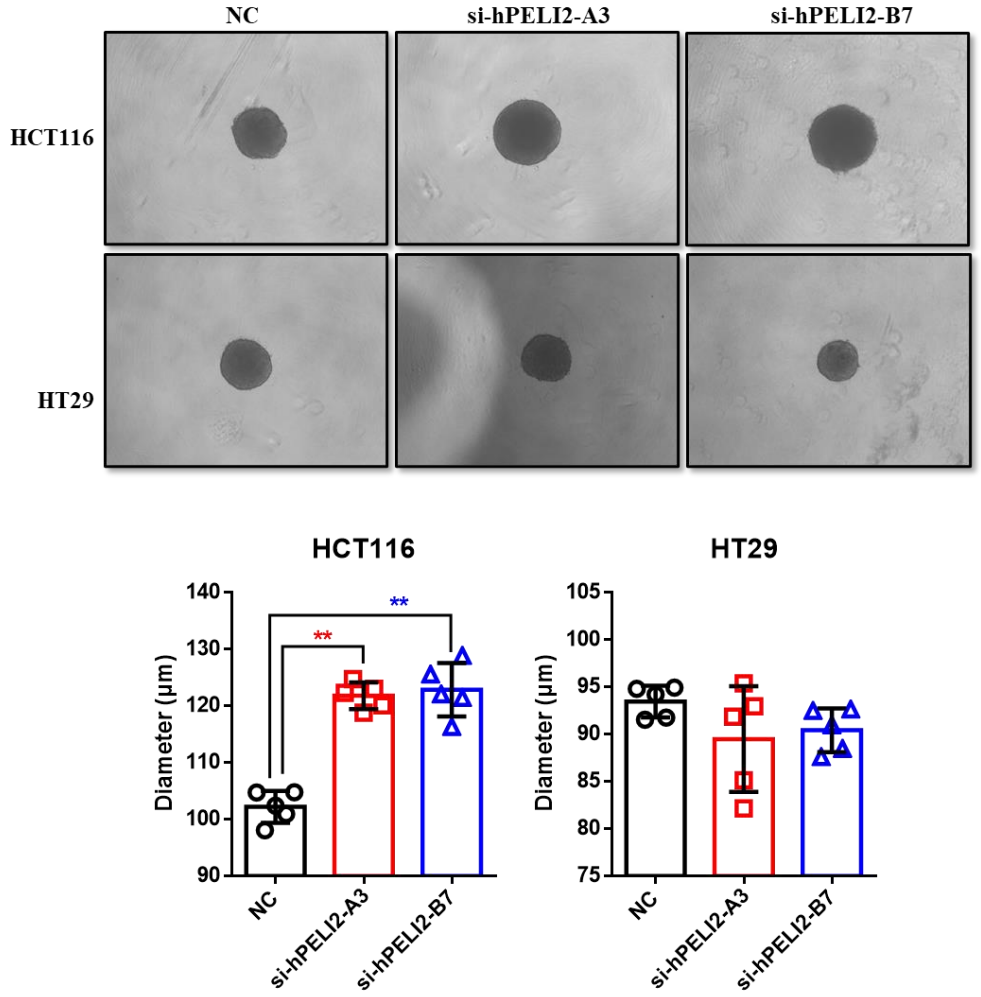


**Fig4.18 hPELI2 knockdown enhances the growth of HCT116 cell in a 3D spheroid formation model**

HCT116 and HT29 cell lines were infected with lentivirus containing an expression vector expressing shRNA of hPELI2 (A3 or B7) or a non-silencing vector (NC). Infected cells (500cells/well) were plated in ultra-low attachment U-bottom 96-well plates with 200μl medium. Subsequently, the diameters of the generated spheroids were assessed on day1, day3, and day5, utilizing an Olympus EP50 camera. Additionally, the spheroids were visualized at 4X magnification using an Optika Vision Pro camera. Data are shown from an experiment that is representative of three independent experiments. Statistical analysis was performed by using the paired Student t-test. Statistically significant differences are indicated by the asterisks: **, $P<0.01$.

### 4.2.7 hPELI2 knockdown suppresses cell apoptosis and the ubiquitination of Bcl-xL

Considering the observed correlation between hPELI2 knockdown and the suppression of cell growth in the HCT116 cell line, we aimed to determine whether the knockdown of hPELI2 protein would inhibit apoptosis and reduce the cell's responsiveness to Cisplatin. The Annexin V/PI staining flow cytometry assay revealed that both hPELI2-shRNA-A3 and B7 can downregulate the expression of hPELI2 while reducing the proportion of apoptotic cells from 14.5% to 9% and 10.4% in the HCT116 cell line compared to the control cells, respectively (Fig4.19). Additionally, HCT116 cell lines with hPELI2 knockdown exhibited increased resistance to Cisplatin treatment at concentrations of 5μg/ml and 10μg/ml. Specifically, both hPELI2-shRNA-A3 and B7 decreased the apoptotic cell population from 22.9% to 12% and 11.7% with 5μg/ml Cisplatin treatment, from 30.5% to 21.9% and 20.3% with 10μg/ml Cisplatin treatment compared to the control cells, respectively (Fig4.20).

We also confirmed the inhibitory effects of hPELI2 knockdown on apoptosis by demonstrating modest suppressive effects on Cisplatin-induced cleavage of Caspase3 and PARP in hPELI2 knockdown HCT116 cells (Fig4.21). This is also consistent with hPELI2 knockdown resulting in reduced degradation of Bcl-xL in response to Cisplatin treatment (Fig4.21). Interestingly, the basal expression level of Bcl-xL protein in the absence of Cisplatin treatment was also higher in the hPELI2 knockdown HCT116 cell lines compared to the control cell line (Fig4.21). This result suggests that reduced hPELI2 expression may affect the balance between synthesis and degradation of the Bcl-xL protein in the HCT116 cell line (Fig4.21).

Finally, we performed immunoprecipitation of the Bcl-xL protein to detect its ubiquitination after 24h of treatment with 5μg/ml and 10μg/ml of Cisplatin. Results showed that hPELI2 knockdown suppresses the Cisplatin-induced ubiquitination of Bcl-xL protein and this is coincident with its reduced degradation and attenuation of

downstream Caspase3 cleavage (Fig4.22).

All of these aforementioned results suggest that hPELI2 promotes ubiquitination and degradation of Bcl-xL resulting in enhanced downstream activation of the caspase pathway in response to Cisplatin culminating in augmentation of cell apoptosis. This provides a credible mechanism underlying the suppressive effects of hPELI2 on epithelial cancer cell lines and promotes itself as an anti-cancer gene.

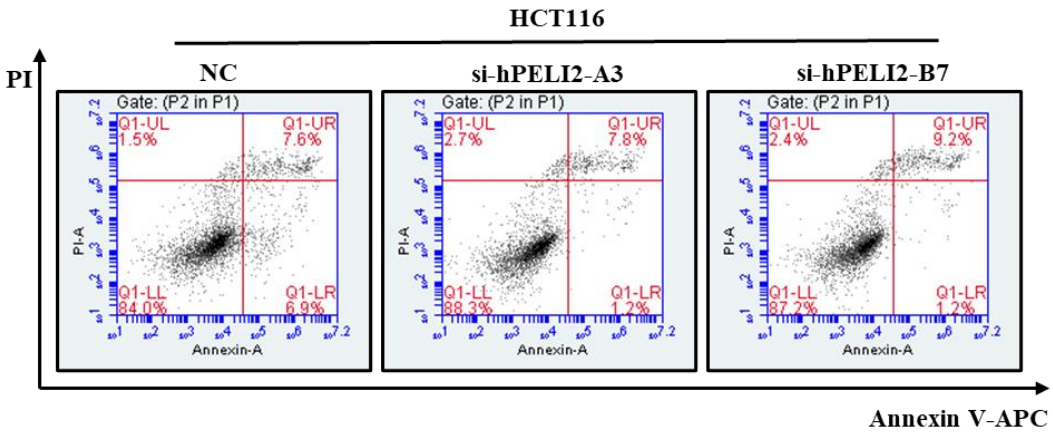


**Fig4.19 hPELI2 knockdown suppresses apoptosis in HCT116 cell**

HCT116 cell line was infected with lentivirus containing an expression vector expressing shRNA of hPELI2 (A3 or B7) or a non-silencing vector (NC). Infected cells ($1 \times 10^4$) were harvested by trypsin treatment and then cells were twice washed with pre-cold PBS and once with Annexin binding buffer. Cells were resuspension in 1000µl Annexin binding buffer and aliquots cell suspensions (100µl) were transferred into a new Eppendorf tube and 1x Annexin binding buffer (400µl), Annexin V-APC (5µl, 90µg/ml) and PI (10µl, 1mg/ml) were added into the tube. The components were mixed by pipetting multiple times and incubated at room temperature for 15min. The cells were evaluated by flow cytometry (BD AccuriTM C6). At least 10,000 cells were counted, single live cells were selected and the apoptosis rate and apoptosis stage were determined by using Annexin V-APC as the X-axis coordinate and PI as the Y-axis coordinate. The unstained sample, Annexin V-APC alone stain sample and PI alone stain sample were used as controls to delineate the different intervals. Data are shown from an experiment that is representative of three independent experiments.

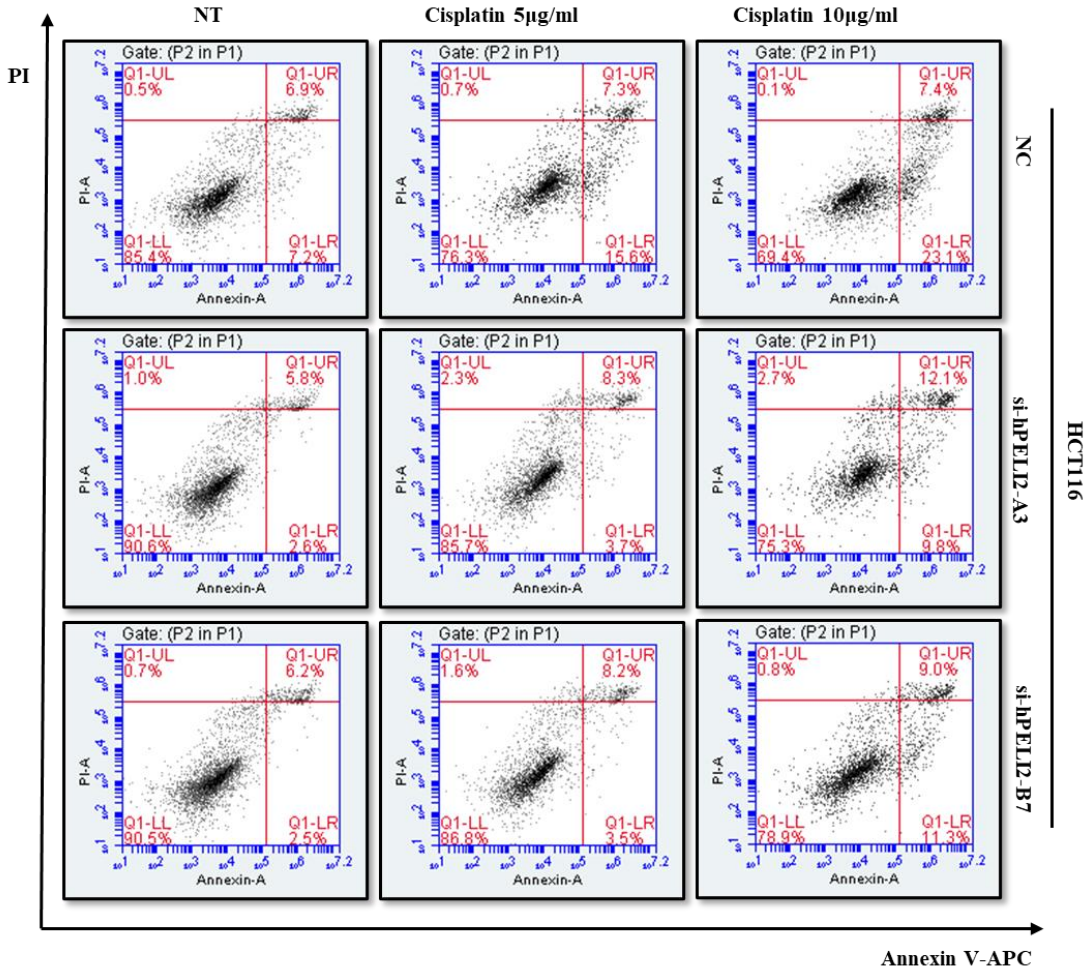


**Fig4.20 hPELI2 knockdown inhibits the Cisplatin-induced apoptosis in HCT116 cell**

HCT116 cell line was infected with lentivirus containing an expression vector expressing shRNA of hPELI2 (A3 or B7) or a non-silencing vector (NC). Infected cells (4 x$10^3$) were plated in 6-well plates with 3ml medium and incubated overnight. Cells were treated with Cisplatin (5μg/ml or 10μg/ml ) for 24h. Control cells were treated with PBS vehicle. Cells were harvested by trypsin treatment and then cells were twice washed with pre-cold PBS and once with Annexin binding buffer. Cells were resuspension in 1000μl Annexin binding buffer and aliquots cell suspensions (100μl) were transferred into a new Eppendorf tube and 1x Annexin binding buffer (400μl), Annexin V-APC (5μl, 90μg/ml) and PI (10μl, 1mg/ml) were added into the tube. The components were mixed by pipetting multiple times and incubated at room

temperature for 15min. The cells were evaluated by flow cytometry (BD AccuriTM C6). At least 10,000 cells were counted, single live cells were selected and the apoptosis rate and apoptosis stage were determined by using Annexin V-APC as the X-axis coordinate and PI as the Y-axis coordinate. The unstained sample, Annexin V-APC alone stain sample and PI alone stain sample were used as controls to delineate the different intervals. Data are shown from an experiment that is representative of three independent experiments.

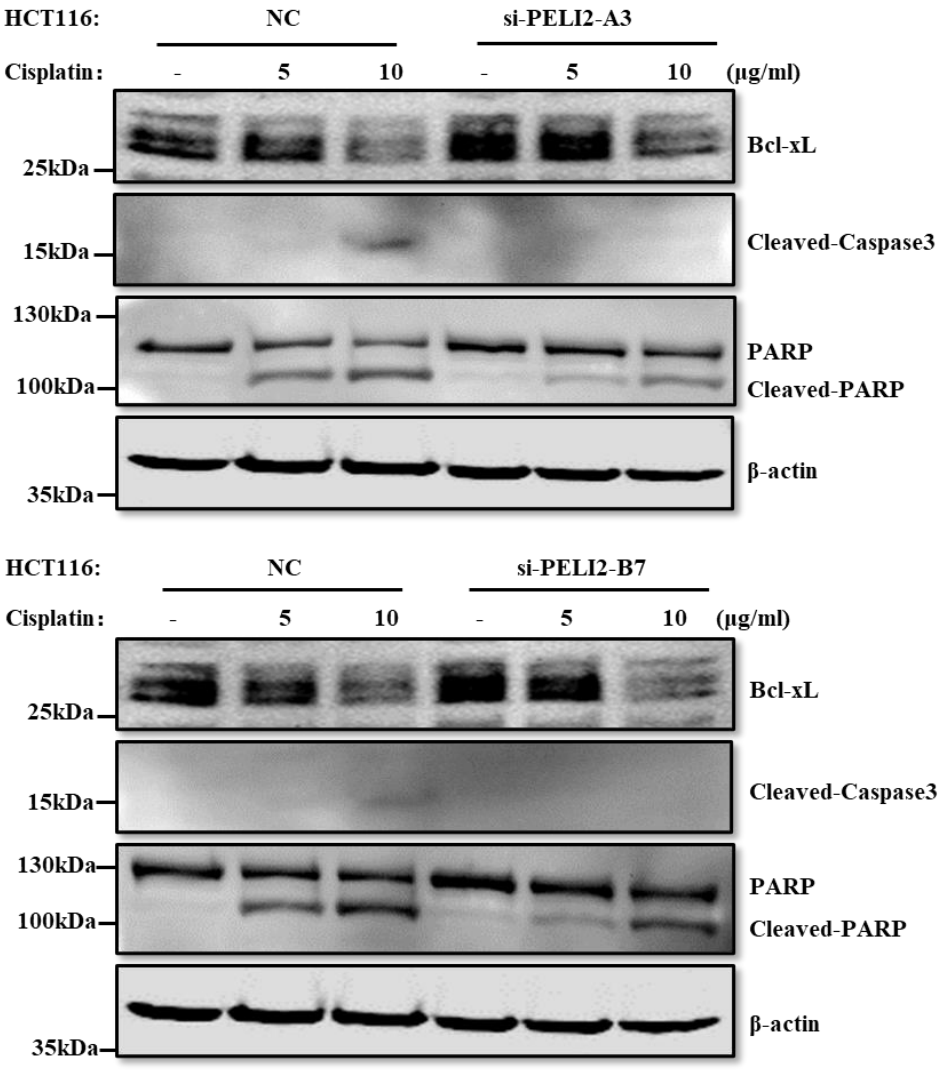


**Fig4.21 hPELI2 knockdown inhibits Caspase3-dependent apoptosis signaling pathway in HCT116 cell line**

HCT116 cell line was infected with lentivirus containing an expression vector expressing shRNA of hPELI2 (A3 or B7) or a non-silencing vector (NC). Infected cells (5 x$10^5$) were plated in 6-well plates and incubated overnight. Cells were treated with Cisplatin (5μg/ml or 10μg/ml) for 48h. Control cells were treated with DMSO vehicle. Cell lysates were extracted in RIPA buffer and subjected to Western Blotting. The resulting membranes were probed with antibodies against BCL-xL, Cleaved-Caspase3, hPELI2-Strep, PARP and β-actin. Data are shown from an experiment that is representative of three independent experiments.

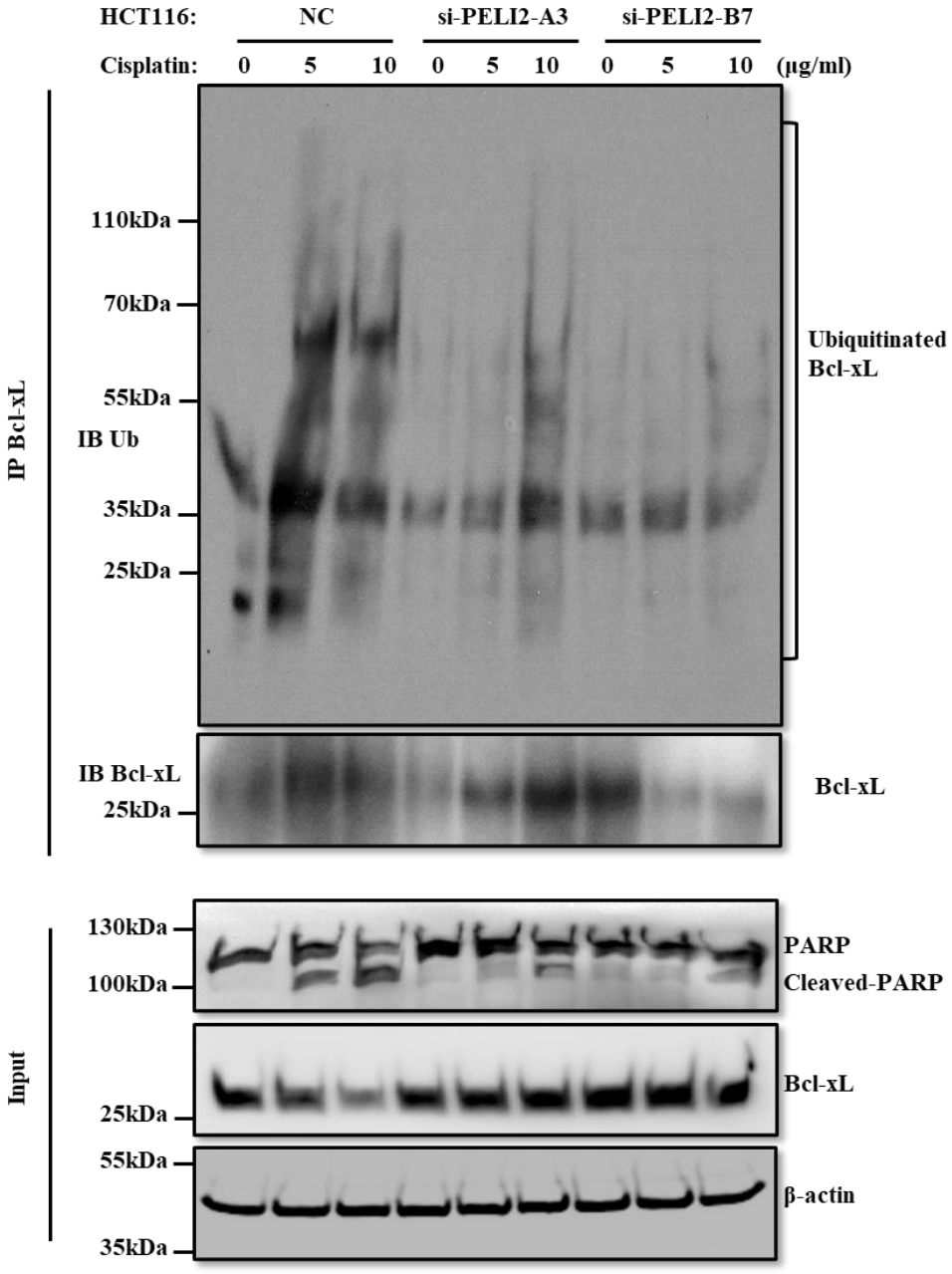


**Fig4.22 hPELI2 knockdown suppresses Cisplatin-induced ubiquitination of Bcl-xL**

HCT116 cell line was infected with lentivirus containing an expression vector expressing shRNA of hPELI2 (A3 or B7) or a non-silencing vector (NC). Infected cells (5 x$10^5$) were plated in 6-well plates and incubated overnight. Cells were treated with Cisplatin (5μg/ml or 10μg/ml) for 48h. Control cells were treated with DMSO

vehicle. Thereafter, whole cell lysates were extracted in RIPA buffer and immunoprecipitated (IP) using an anti-Bcl-xL antibody. The resulting membranes with IP samples were probed with antibodies against Ubiquitin (Ub) and Bcl-xL. The resulting membranes with lysate samples (Input) were probed with antibodies against PARP, Bcl-xL, hPELI2-strep and β-actin. Data are shown from an experiment that is representative of three independent experiments.

### 4.2.8 Dmx1 and Dmx10 augment the suppressive effects of Cisplatin on colorectal cancer cell viability

Having used hPELI2 knockdown approaches to demonstrated a role for hPELI2 in controlling colorectal cancer cell lines growth, our subsequent aim was to explore the pharmacological modulation of this hPELI2-controlled process using PELI2-targeted compounds Dmx1 and Dmx10. We sought to investigate whether the combined administration of Dmx1 and Dmx10 with Cisplatin could effectively modulate the growth and induce cell death in colorectal cancer cell lines. To this end we probed the combinatorial effects of Dmx1 and Dmx10 with Cisplatin on colorectal cancer cell lines growth and death.

The various colorectal cancer cell lines were treated with indicated concentrations of either Dmx1 or Dmx10 (DMSO as a vehicle control) for 48h. The cell viabilities of these colorectal cancer cell lines were determined using the MTT assay. The results demonstrated that Dmx1 and Dmx10 significantly inhibited cell viability in a dose-dependent manner in DLD-1, HCT116, and HT29 cell lines (Fig4.23). The IC50 values of Dmx1 and Dmx10 for reducing cell viability were calculated with the IC50 value of Dmx1 ranging from 18.89 to 36.33μM and of Dmx10 ranging from 13.48 to 12.96μM (Fig4.23).

The potential effects of Dmx1 and Dmx10 on regulating sensitivity of these cell lines to the killing action of Cisplatin were next explored. The three colorectal cancer cell lines were pre-treated with Dmx1 or Dmx10 (5μM) (DMSO as a vehicle control) for 1h. Subsequently, the cells were stimulated with the indicated concentrations of Cisplatin for 48h. The MTT assay was performed to measure cell viability and determine the IC50 values of Cisplatin in these colorectal cancer cell lines. The results showed that Dmx1 and Dmx10 increased the sensitivity of DLD-1 and HCT116 cell lines to the suppressive effects of Cisplatin on cell viability, while they had no effect on the HT29 cell line (Fig4.24a).

More specifically, the combined treatment of Dmx1 or Dmx10 with Cisplatin resulted in a significant reduction in the IC50 value of Cisplatin in DLD-1 cell line from 14.83µg/ml to 3.599µg/ml or 4.101µg/ml, respectively. Similar results were observed in the HCT116 cell line, where the IC50 values of Cisplatin decreased from 15.19µg/ml to 9.943µg/ml or 8.538µg/ml when co-treated with Dmx1 or Dmx10. However, neither Dmx1 nor Dmx10 had an effect on the HT29 cell line (Fig4.24b). These findings demonstrate that Dmx1 and Dmx10 increase the sensitivity of colorectal cancer cell lines to Cisplatin its effects on cell viability.

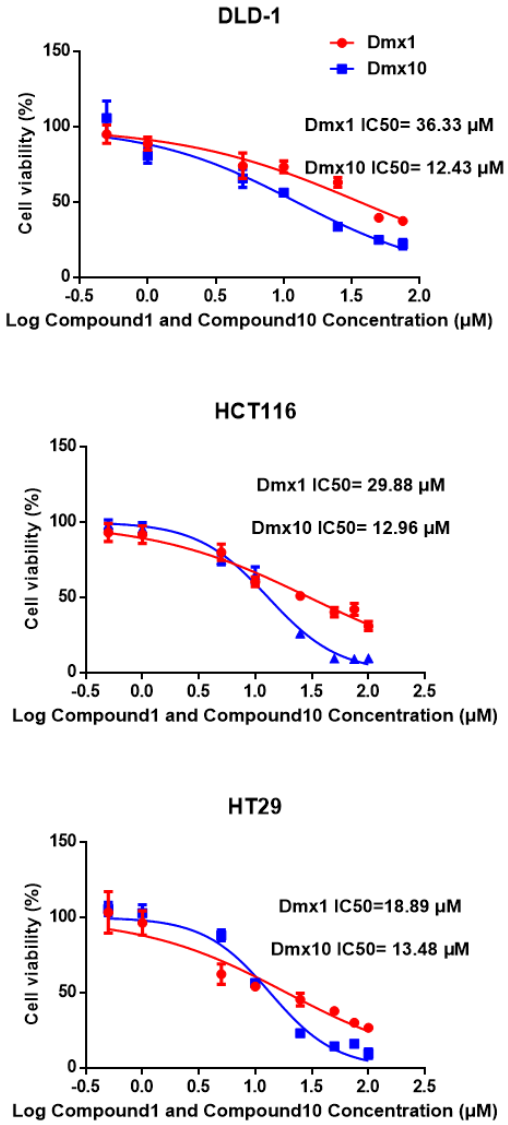


**Fig4.23 Inhibitory effects of Dmx1 and Dmx10 on cell viability of DLD-1, HCT116 and HT29 cell lines.**

DLD-1, HCT116 and HT29 cells (8000cells/well) were plated in 96-well plates and incubated overnight. Cells were treated with indicated concentrations of Dmx1 or Dmx10 for 48h. Control cells were treated with DMSO vehicle. 3-(4,5-dimethylthiazol-2-yl)-2,5-diphenyltetrazolium bromide (MTT) (50µg) was added into wells and incubate at 37℃ for 4h. The medium was removed and DMSO (150µl) was added into wells to dissolve the crystals. Absorbance was measured at a wavelength of 490nm by using a microplate reader. Cell viabilities were normalized against DMSO vehicle control samples and the half maximal inhibitory concentration (IC50) of cell viabilities were calculated by Prism Graphpad. Data are shown from an experiment that is representative of three independent experiments.

**(a)**

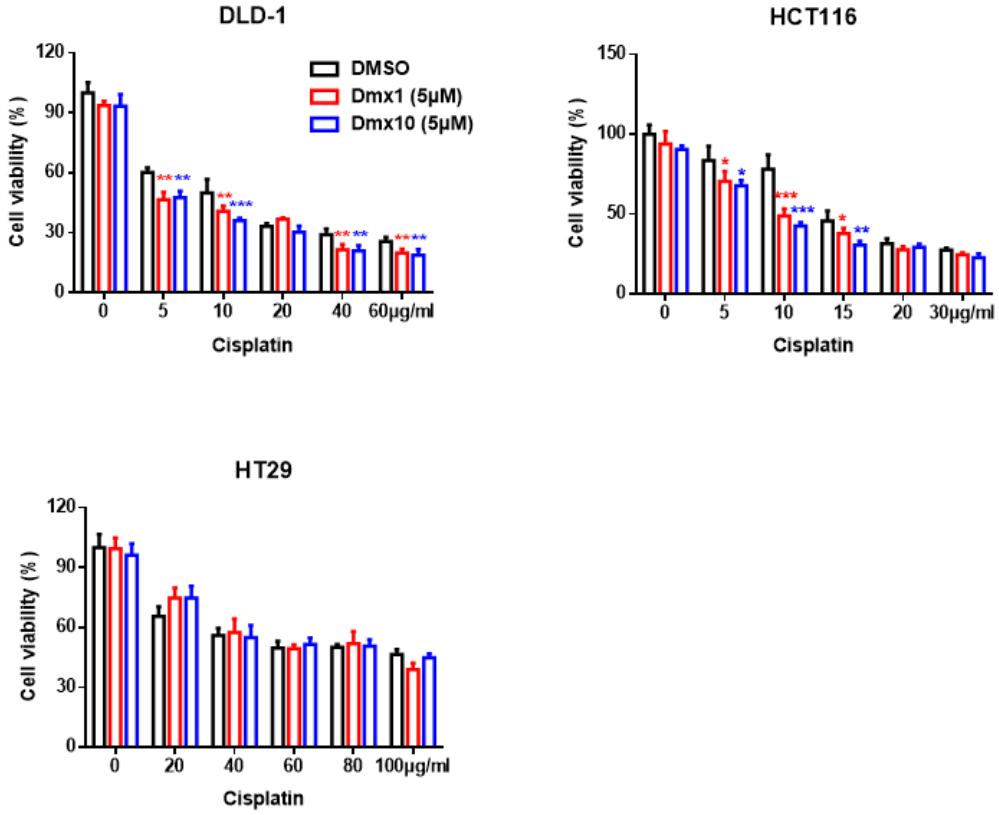
DLD-1
DMSO
Dmx1 (5μM)
Dmx10 (5μM)
Cell viability (%)
120
90
60
30
0
0
5
10
20
40
60μg/ml
Cisplatin
HCT116
150
100
50
0
0
5
10
15
20
30μg/ml
Cisplatin
HT29
120
90
60
30
0
0
20
40
60
80
100μg/ml
Cisplatin

**(b)**

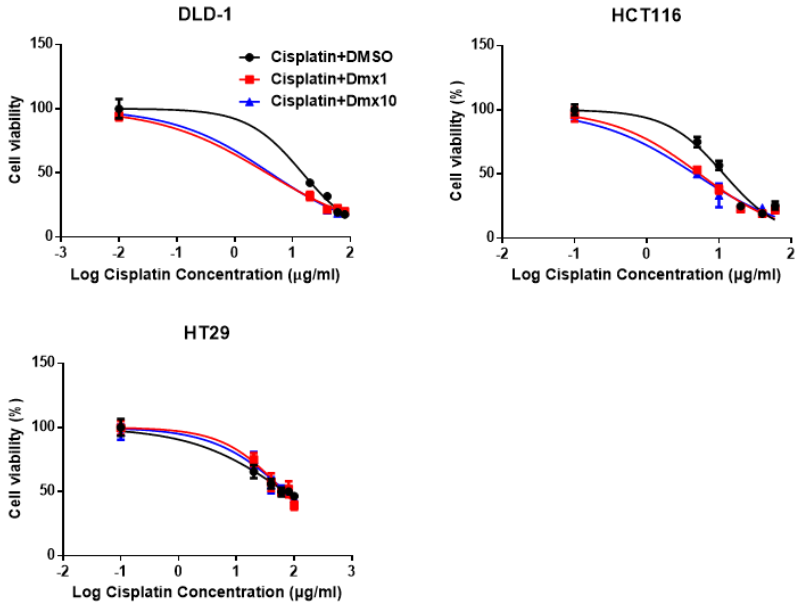


| Cells | IC50 | | |
|---|---|---|---|
| | Cis+DMSO | Cis+Dmx1 | Cis+Dmx10 |
| DLD-1 | 14.83μg/ml | 3.599μg/ml | 4.101μg/ml |
| HCT116 | 15.19μg/ml | 9.943μg/ml | 8.538μg/ml |
| HT29 | 69.20μg/ml | 65.73μg/ml | 72.05μg/ml |

**Fig4.24 Dmx1 and Dmx10 increase the sensitivity of DLD-1 and HCT116 cell lines to the suppressive effects of Cisplatin on cell viability.**

DLD-1, HCT116 and HT29 cells (8000cells/well) were plated in 96-well plates with 200μl medium and incubated overnight. Cells were pre-treated with Dmx1 or Dmx10 (5μM) for 1h. Control cells were treated with DMSO vehicle. Cells were stimulated with indicated concentrations of Cisplatin for 48h. Control cells were treated with PBS vehicle. Thereafter, MTT solution (50μg) was added into wells and incubated at 37℃ for 4h. After the incubation, the medium was removed and DMSO (150μl) was added to dissolve the crystals. Absorbance was measured at a wavelength of 490nm by using a microplate reader. Cell viabilities (a) were normalized against DMSO vehicle control samples and the half maximal inhibitory concentration (IC50) of cell viabilities (b) were calculated by Prism Graphpad. Data are shown from an experiment that is representative of three independent experiments. Statistical analysis was performed by using the paired Student t-test. Statistically significant differences are indicated by the asterisks: *, $P<0.05$; **, $P<0.01$; ***, $P<0.001$.

### 4.2.9 Dmx1 and Dmx10 augment the inhibitory effects of Cisplatin on cell colony-formation with DLD-1 and HCT116 cells

After observing the promotion of the inhibitory effects of Cisplatin on cell viability by Dmx1 and Dmx10, we employed a colony formation assay to evaluate the influence of the combined treatments on clonogenic capacities. For this assay, cells were plated in 6-well plate to generate single-cell-derived colonies. On day5, cells were pre-treated with Dmx1 or Dmx10 (5µM) (DMSO as a vehicle control) for 1h. Cells were stimulated with Cisplatin (10µg/ml) for 48h. Cell cultivation was terminated on day7. As before, the results demonstrated that Cisplatin treatment decreased the number and size of colonies and the treatment of cells with Dmx1 or Dmx10 alone had no effect on colony formation. However, both Dmx1 and Dmx10 further augmented the inhibitory effects of Cisplatin on colony formation with DLD-1 and HCT116 colorectal cancer cell lines (Fig4.25).

### 4.2.10 Dmx1 and Dmx10 augment the inhibitory effect of Cisplatin on 3D spheroid formation in DLD-1 and HCT116 cells

To further expand on the findings mentioned above, we aimed to investigate whether the enhanced inhibitory effect of the combination treatment with Dmx1 or Dmx10 and Cisplatin observed in the MTT assay and colony formation assay would translate to a 3D *in vitro* growth model. For this purpose, cells were plated in ultra-low attachment U-bottom 96-well plate. On day3, cells were pre-treated with Dmx1 or Dmx10 (5µM) (DMSO as a vehicle control) for 1h. Then cells were stimulated with the indicated concentrations of Cisplatin. The diameters of the resulting spheroids were measured on day1 and day5 using an Olympus EP50 camera. While treatment of cells with Dmx1 and Dmx 10 alone had no effect on spheroid formation and treatment with Cisplatin decreased the size of spheroids, we discovered that Dmx1 and Dmx10 augmented the inhibitory effect of Cisplatin on the growth of DLD-1 and HCT116 cell lines in the 3D spheroid formation model. The spheroids formed with the combination treatment of

Dmx1 or Dmx10 and Cisplatin exhibited smaller sizes compared to those treated with Cisplatin alone (Fig4.26). These results collectively demonstrated that Dmx1 and Dmx10 can enhance the inhibitory effect of Cisplatin on the growth of colorectal cancer cell lines in an *in vitro* setting.

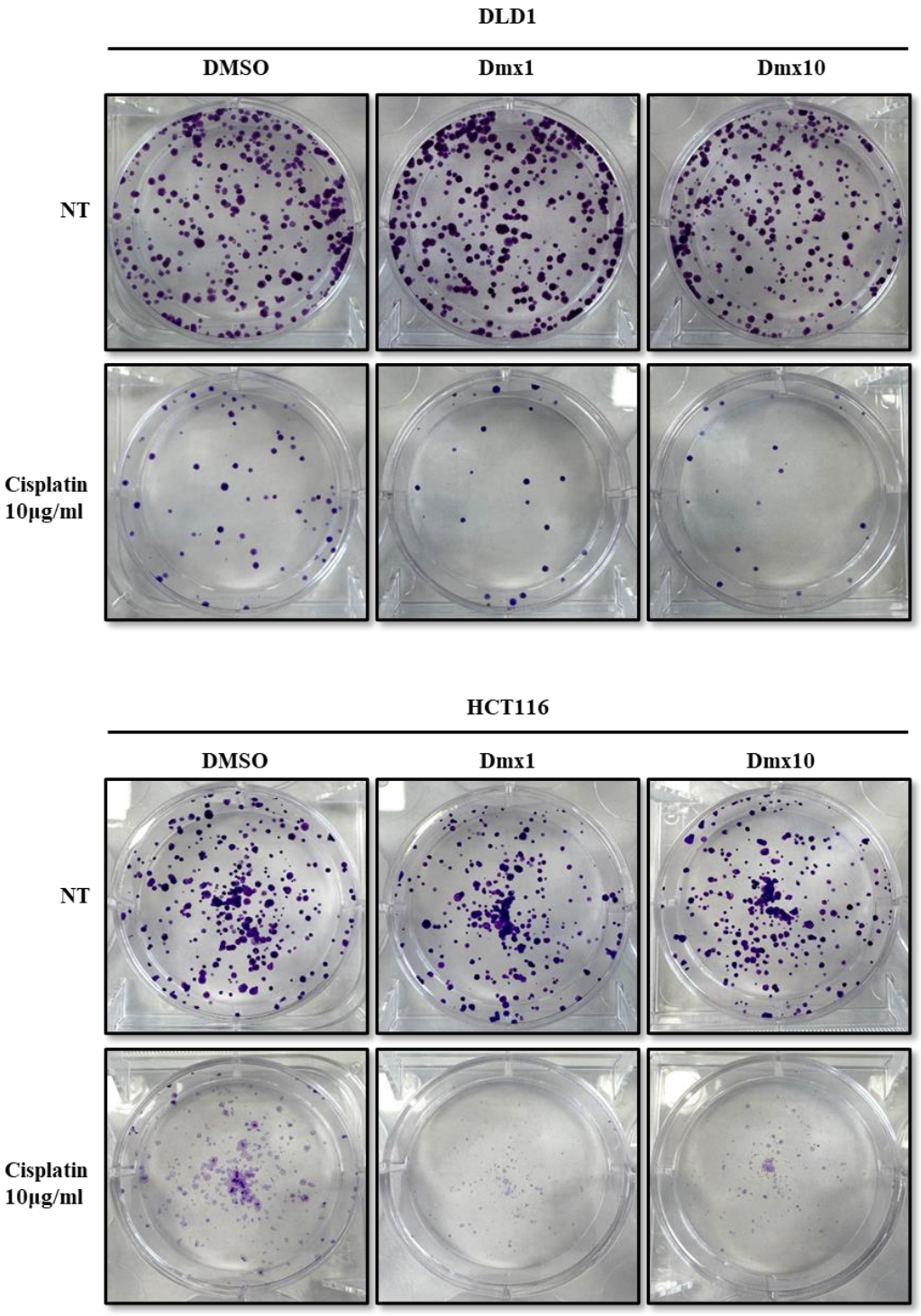
DLD1
DMSO
Dmx1
Dmx10
NT
Cisplatin
10µg/ml
HCT116
DMSO
Dmx1
Dmx10
NT
Cisplatin
10µg/ml

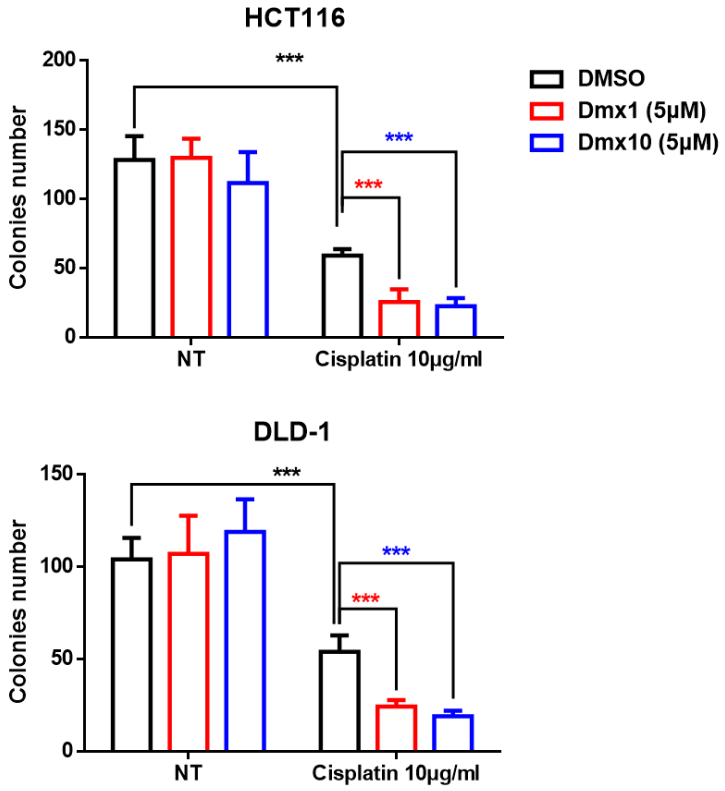


**Fig4.25 Dmx1 and Dmx10 augment the inhibitory effect of Cisplatin on cell colony formation in DLD-1 and HCT116 cell lines.**

DLD-1 and HCT116 cells (600cells/well) were plated in 6-well plates with 3ml medium to generate single-cell derived colonies. On day5, cells were pre-treated with Dmx1 or Dmx10 (5µM) for 1h. Control cells were treated with DMSO vehicle. Cells were stimulated with Cisplatin (10µg/ml) for 48h. Control cells were treated with PBS vehicle. Cell cultivation was terminated on day 7 and colonies could be observed under the inverted microscope. Thereafter, medium was removed and the colonies were fixed in 2ml methanol and stained with 0.5% crystal violet. Eventually, the colonies number in each wells were counted by using the OpenCFU software tool. Data are shown from an experiment that is representative of three independent experiments. Statistical analysis was performed by using the paired Student t-test. Statistically significant differences are indicated by the asterisks: ***, P<0.001.

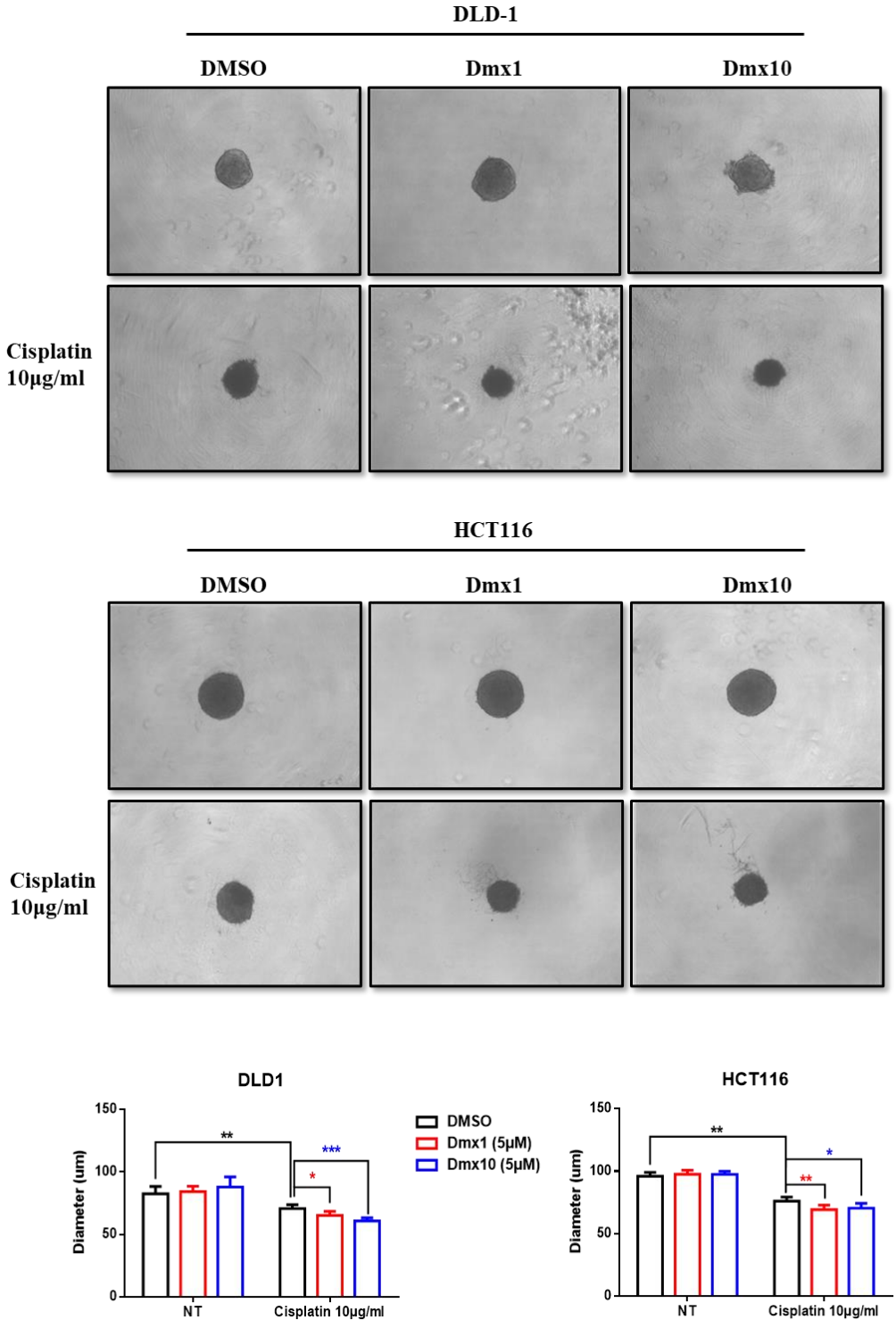


**Fig4.26 Dmx1 and Dmx10 augment the inhibitory effects of Cisplatin on 3D spheroid formation in DLD-1 and HCT116 cell lines.**

DLD-1 and HCT116 cells (500cells/well) were plated in ultra-low attachment U-

bottom 96-well plate with 200µl medium. On day3, cells were pre-treated with Dmx1 or Dmx10 (5µM) for 1h. Control cells were treated with DMSO vehicle. Then cells were stimulated with Cisplatin (10µg/ml) for 48h. Control cells were treated with PBS vehicle. Subsequently, the diameters of the generated spheroids were assessed on day 1, day 3, and day 5, utilizing an Olympus EP50 camera. Additionally, the spheroids were visualized at 4X magnification using an Optika Vision Pro camera. Data are shown from an experiment that is representative of three independent experiments. Statistical analysis was performed by using the paired Student t-test. Statistically significant differences are indicated by the asterisks: *, $P<0.05$; **, $P<0.01$; ***, $P<0.001$.

### 4.2.11 Dmx1 and Dmx10 enhance the Cisplatin-induced apoptosis of DLD-1 and HCT116 cell lines

Subsequently, we conducted further investigations to explore the influence of Dmx1 and Dmx10 on Cisplatin-induced apoptosis. DLD-1 and HCT116 cell lines were pre-treated with Dmx1 or Dmx10 (5μM) (DMSO as a vehicle control) for 1h and stimulated with Cisplatin (20μg/ml) for 24h. Afterwards, cells were harvested, separated by trypsin, stained with Annexin V and PI, and analyzed by a flow cytometer. Our findings revealed that the addition of Dmx1 and Dmx10 significantly augmented Cisplatin-induced apoptosis from 22.5% increase to 48% and 33.7% in DLD-1 cell line. And in HCT116 cell line, Cisplatin-induced apoptosis increased from 24.1% to 32.5% and 33.5% with the combination of Dmx1 and Dmx10. However, treatment with Dmx1 or Dmx10 alone did not affect apoptosis compared with the DMSO control (Fig4.27).

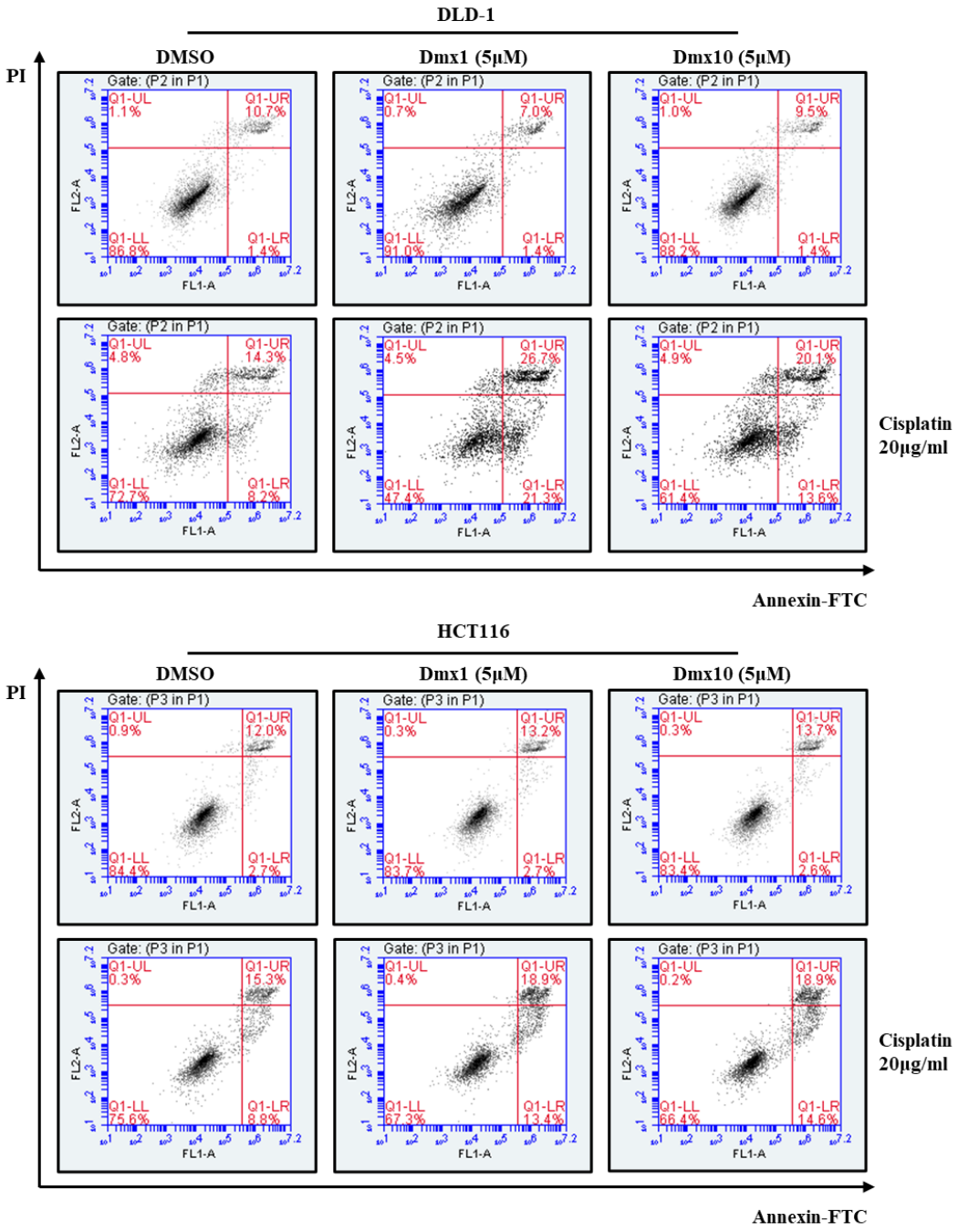


**Fig4.27 Dmx1 and Dmx10 enhance the Cisplatin-induced apoptosis in DLD-1 and HCT116 cells**

DLD-1 and HCT116 cells (4 x$10^3$) were plated in 6-well plates with 3ml medium and incubated overnight. Cells were pre-treated with Dmx1 or Dmx10 (5μM) for 1h. Control cells were treated with DMSO vehicle. And then cells were treated with Cisplatin (10μg/ml) for 24h. Control cells were treated with PBS vehicle. Cells were harvested by trypsin treatment and then cells were twice washed with pre-cold PBS

and once with Annexin binding buffer. Cells were resuspension with 1000µl Annexin binding buffer and aliquots cell suspensions (100µl) were transferred into a new Eppendorf tube and 1x Annexin binding buffer (400µl), Annexin V-FITC (5µl, 90µg/ml) and PI (10µl, 1mg/ml) were added into the tube. The components were mixed by pipetting multiple times and incubated at room temperature for 15min. Then the cells were evaluated by flow cytometry (BD AccuriTM C6). At least 10,000 cells were counted, single live cells were selected and the apoptosis rate and apoptosis stage were determined by using Annexin V-FITC as the X-axis coordinate and PI as the Y-axis coordinate. The unstained sample, Annexin V-FITC alone stain sample and PI alone stain sample were used as controls to delineate the different intervals. Data are shown from an experiment that is representative of three independent experiments.

### 4.2.12 Dmx1 and Dmx10 augment the effect with Cisplatin on cell viability in a PELI2 protein-dependent manner

Based on our intentional design of Dmx1 and Dmx10 to target Pellino protein, we were keen to assess if their enhancement of the inhibitory effects of Cisplatin on cell viability were dependent on the presence of PELI2 protein. To test this hypothesis, we utilized two HCT116 cell lines with PELI2 knockdown, namely si-PELI2-A3 and si-PELI2-B3 that were constructed by lentivirus with distinct shRNA sequences targeting *PELI2*. Parental and PELI2 knockdown cells were pre-treated with Dmx1 or Dmx10 (5μM) (DMSO as a vehicle control) for 1h and then stimulated with indicated concentrations of Cisplatin for 48h. MTT assay was performed to measure the cell viability. Our results demonstrated that Dmx1 and Dmx10 significantly promoted the inhibitory effect of Cisplatin on cell viability in the HCT116 cells infected with the control non-targeting (NC) shRNA. However, this augmented effect of Dmx1 and Dmx10 was partially attenuated in the si-PELI2-A3 and si-PELI2-B7 cell lines(Fig4.28). These findings provide some evidences that the enhancement effects of Dmx1 and Dmx10 on Cisplatin-induced cell viability is dependent on the presence of the PELI2 protein.

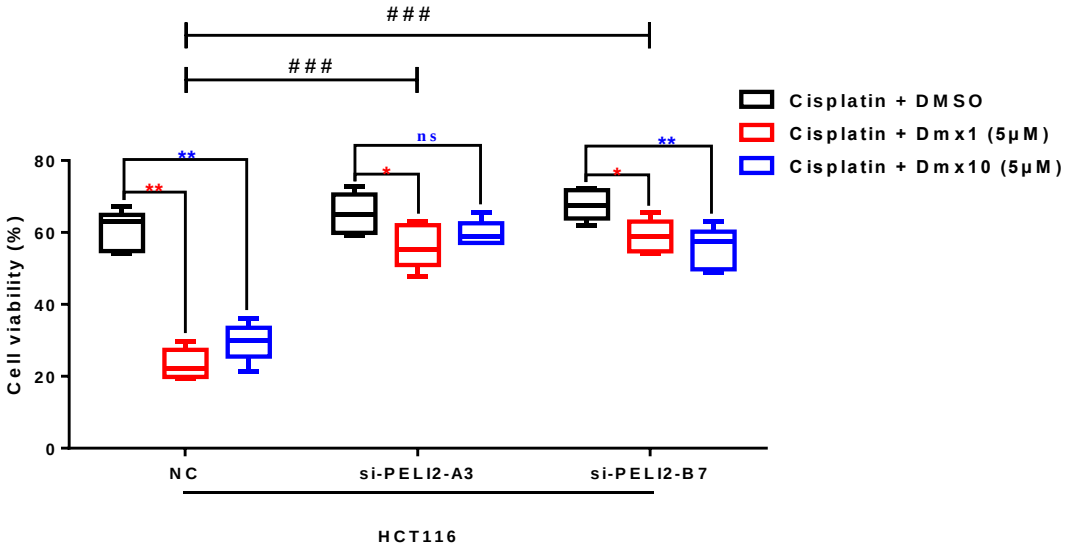


**Fig4.27 Dmx1 and Dmx10 augment the effects of Cisplatin on cell viability in a PELI2-dependent manner.**

Non-silencing control cells (NC) and hPELI2 knockdown cells (A3 and B7) of HCT116 cell line (8000cells/well) were plated in 6-well plates with 3ml medium and incubated overnight. Cells were pre-treated with Dmx1 or Dmx10 (5µM) for 1h. Control cells were treated with DMSO vehicle. And then cells were treated with Cisplatin (10µg/ml) for 48h. Control cells were treated with PBS vehicle. Thereafter, MTT solution (50µg) was added into wells and incubated at 37°C for 4h. After the incubation, medium was removed and DMSO (150µl) was added into wells to dissolve the crystals. Absorbance was measured at a wavelength of 490nm by using microplate reader. Cell viabilities were normalized against DMSO vehicle control samples and the half maximal inhibitory concentration (IC50) of cell viabilities were performed by Prism Graphpad. Data are shown from an experiment with quadruplicates that is representative of three independent experiments. Statistical analysis was performed by using the paired Student t-test and joint hypotheses test (F-test). Statistically significant differences of t-test are indicated by the asterisks: ns, $P>0.05$; *, $P<0.05$; **, $P<0.01$. And Statistically significant differences in F-test are indicated by the asterisks: ###, $P<0.001$.

## 4.3 Discussion

CRC is a prevalent malignancy with a considerable risk of recurrence and metastasis in humans. Although surgical intervention is the primary therapy for colon cancer, a significant proportion of patients eventually relapse and die due to metastatic disease. Therefore, adjuvant therapies such as chemotherapy, radiotherapy, targeted therapy, and immunotherapy have emerged as promising approaches to decrease recurrence and improve survival rates. However, the development of resistance to these treatments and their adverse effects on normal cells have limited their therapeutic efficacy and ultimately leads to a poor prognosis (Wang et al. 2022). In particular, resistance to Cisplatin, a highly effective chemotherapeutic drug with broad-spectrum antitumor activity, has become a significant clinical challenge, especially in the treatment of colon cancer. Despite its benefits, Cisplatin treatment also has limitations, largely due to its adverse effects on normal cells. Therefore, there is an urgent need to identify novel and effective molecular targets for the diagnosis and treatment of CRC.

Pellino family proteins (PELI1 and PELI2) have been reported to be closely associated with oncogenesis and cancer development. However, there is no understanding of the expression and functions of Pellino proteins in CRC.

In this study, we focused on hPELI2 protein, which has been verified as a positive marker correlated with better prognosis in myeloma patients (Masuda et al. 2022). PELI2$^{-/-}$ mice exhibited increased tumor size and tumor loads in the AOM/DSS-induced CRC model. We also demonstrated that h*PELI2* mRNA expression level is down-regulated in CRC tissues and cell lines. Further functional results suggested that hPELI2 inhibits cell growth by promoting cell apoptosis, which is achieved through the regulation of the ubiquitination and degradation of Bcl-xL in CRC cell lines. This represents a novel mechanism by which hPELI2 contributes to CRC development.

Based on RNAseq data from the TCGA database, we observed significantly lower expression levels of hPELI2 mRNA in CRC tissue. To further validate this finding, we examined its expression in 6 types of CRC cell lines. The results showed that compared with normal colon epithelial cell lines, 5 types of CRC cell lines showed more than an 80% lower expression level of h*PELI2* mRNA, except for the HCT116 cell line, which showed a higher expression level. Subsequently, we found that overexpressing hPELI2 proteins in SW480 and DLD-1 cell lines led to inhibitory effects on cell growth in both 2D and 3D culture, while the opposite results were found in the HCT116 cell line with silenced hPELI2 protein expression. Furthermore, we found that hPELI2 protein inhibits the growth of CRC cell lines by promoting cell apoptosis. Additionally, hPELI2 protein expression level is positively correlated with the Cisplatin sensitivity of DLD-1 and HCT116 cell lines. Mechanistically, we found that hPELI2 promotes the degradation of Bcl-xL by increasing its ubiquitination, leading to upregulation of Caspase3 activation and ultimately resulting in higher sensitivity to Cisplatin-induced cell apoptosis.

This study does have some limitations, as we observed no response in the SW620 and HT29 cell lines following alterations in hPELI2 expression levels. This lack of response may be due to genetic and epigenetic variations between CRC cell lines. Therefore, it is necessary to further investigate the differences in expression levels and mutation statuses of apoptosis-related proteins or markers in these CRC cell lines to gain a more comprehensive understanding of the role of hPELI2 in cell apoptosis. Additionally, more research is needed to fully explore the underlying mechanisms through which hPELI2 promotes apoptosis.

Our study also used a Cisplatin-induced apoptosis model to explore the potential mechanisms underlying hPELI2's pro-apoptotic effects. Therefore, it would be of value for future studies to expand our research to include other chemotherapeutic drugs or compounds with different mechanisms to induce apoptosis to further corroborate our findings.

Cisplatin has been a prominent chemotherapy drug played a critical role in the treatment of various cancer types for decades (Dasari and Tchounwou 2014). However, the development of resistance to Cisplatin poses a significant challenge in clinical practice. Therefore, maintaining or enhancing the sensitivity of cancer cells to Cisplatin is of utmost importance to optimize its efficacy in chemotherapy. In our study, we present novel findings that establish a positive correlation between the expression of hPELI2 protein and the sensitivity of colon cancer cells to Cisplatin. These results shed light on potential avenues for future research aiming to elucidate the mechanisms underlying the inhibition of Cisplatin resistance formation in colon cancer.

Moreover, while our findings confirm that hPELI2 enhances the Cisplatin-induced ubiquitination and degradation of Bcl-xL, we also discovered that hPELI2 does not directly interact with Bcl-xL. Hence, any effects of hPELI2 on Bcl-xL appears to be indirect in nature and the exact mechanism by which hPELI2 promotes Bcl-xL ubiquitination and subsequent degradation requires further investigation in future studies. For instance, *in vitro* ubiquitination assays could be performed to determine whether hPELI2 directly promotes Bcl-xL ubiquitination. Furthermore, we have only examined the total ubiquitination of Bcl-xL and have not assessed the differential ubiquitination at distinct loci, The literature suggests that Bcl-xL may undergo Lys48-ubiquitination as well as other specific types of ubiquitination, such as Lys20- and Lys87-specific ubiquitination(Lv et al. 2021; Wu et al. 2018). Therefore, it is necessary to conduct further investigations to determine the specific type of Bcl-xL protein ubiquitination that is altered by the presence of the PELI2 protein.

PELI2 has been identified as an E3 ligase that plays a critical role in the TLR signaling pathway. For instance, PELI2 has been shown to mediate the TLR9 signaling pathway in DC cells and is also a crucial factor for TLR/IL-1R-mediated post-transcriptional control (Oleszycka et al. 2021). PELI2 can directly interact with IRAK1 to influence its Lys63-ubiquitination (Kim et al. 2012). On the other hand, accumulating evidence suggests that TLR signaling may be involved in oncogenesis and development of CRC.

Specifically, colon carcinogenesis is associated with increased expression levels of TLR2 and TLR4 (Li, Ogino, and Qian 2014). Moreover, functional TLR2 and TLR4 polymorphisms can significantly alter the risk of developing CRC, while factors such as smoking and obesity may also influence this risk in conjunction with genetic profiles (Li, Ogino, and Qian 2014). TLR4 is expressed in human CRC cells and is functionally active, playing a crucial role in promoting the immune escape of CRC cells by inducing immunosuppressive factors and apoptosis resistance. High expression levels of TLR4 are associated with liver metastasis of CRC (Yesudhas et al. 2014). Additionally, it has been reported that oligodeoxynucleotides targeting TLR9 have opposite effects in modulating DNA repair genes in tumour cells compared to immune cells and enhance the biological effects of chemotherapy (Sommariva et al. 2011). TLR9 expression was decreased in hyperplastic and villous polyps from patients who developed CRC, suggesting a possible protective role of TLR9 expression against malignant transformation in the colorectal mucosa (Gao et al. 2018; Luo et al. 2020). Given this evidence, it is possible that the expression and function of TLR proteins may be involved in the inhibitory effects of PELI2 on CRC. Therefore, future studies that further investigate this potential relationship would be of significant value.

In this study, we further investigated whether the small molecule compounds Dmx1 and Dmx10, designed to mimic a region of the FHA-domain of PELI2 protein, could enhance the anti-tumor effect of Cisplatin in colorectal cancer cell lines. We found that the co-treatment of Cisplatin with Dmx1 or Dmx10 resulted in the ability of Cisplatin to promote apoptosis in colorectal cancer cell lines and so reduce cell viability and cell colony and 3D spheroid formation. It will be interesting for future studies to explore the anti-tumorigenic potential of these novel molecules.

Our results showed that Dmx1 did not affect the cell viability of CRC cell lines at 5μM and 10μM which are the concentrations that could effectively inhibit the activation of the NF-κB signaling pathway in BMDMs. However, treatment with 10μM Dmx10 resulted in a significant decrease in cell viability in all three CRC cell lines. Next, we

examined whether co-treatment with Dmx1 or Dmx10 could enhance the sensitivity of CRC cell lines to Cisplatin. Our data showed that both Dmx1 and Dmx10 significantly increased the sensitivity of DLD-1 and HCT116 cell lines to Cisplatin with Cisplatin being more potent and efficacious in the presence of Dmx1 and Dmx10. However, there was no effect on the Cisplatin-resistant HT29 cell line. Additionally, we observed that the combination of Dmx1 or Dmx10 with Cisplatin led to an increase in the inhibitory effect of Cisplatin on colony formation ability and cell growth in 3D culture of CRC cell lines, as well as an increase in Cisplatin-induced cell apoptosis. Furthermore, we investigated whether the impact of Dmx1 and Dmx10 on Cisplatin sensitivity was dependent on the presence of PELI2 protein. We found that the sensitization effect of Dmx1 and Dmx10 on CRC cells to Cisplatin was PELI2-dependent, as demonstrated by using PELI2 knockdown HCT116 cell lines.

At present, this topic is in its early stages and further studies are required to characterize the potential therapeutic effects of these compounds. In the present study, we only tested the impact of the Dmx1 and Dmx10 combination with Cisplatin in *in vitro* models. It will be of interest for future studies to use pre-clinical models of CRC to characterize the interplay of Dmx1 and Dmx10 with the anti-tumor effects of Cisplatin. More specifically, this could be assessed by exploring the ability of Dmx1 and Dmx10 to enhance the therapeutic efficacy of Cisplatin in a CRC cell line-derived xenograft model, or an AOM/DSS-induced colon cancer model.

We also demonstrated that Dmx1 and Dmx10 enhance Cisplatin-induced apoptosis; however, the underlying mechanisms remain to be investigated further. It is well established that Cisplatin-induced apoptosis is mainly mediated through the activation of the endogenous mitochondrial pathway. Therefore, the next step in any investigation would be to determine the expression levels of various key anti-apoptotic and pro-apoptotic proteins that play a critical role in this pathway. Future studies can also explore the activation of other signaling pathways that regulate apoptosis to provide further insight into how Dmx1 and Dmx10 promote Cisplatin-induced apoptosis. In

addition, it is worth noting that apoptosis is not the sole mode of cell death induced by Cisplatin. Necroptosis and autophagy have also been reported to be triggered by Cisplatin (Alassaf and Attia 2023; Xu et al. 2015; Xu et al. 2017). Therefore, in addition to investigating the impact of Dmx1 and Dmx10 on Cisplatin-induced apoptosis, future studies should determine if the combination of Dmx1 or Dmx10 and Cisplatin can promote other forms of cell death caused by Cisplatin, including necroptosis and autophagy.

Furthermore, our findings demonstrated that Dmx1 and Dmx10 synergistically enhanced the inhibitory effect of Cisplatin on the colony forming ability and 3D growth of CRC cell lines. However, it is important to note that the NF-kB and MAPK signaling pathways, which are pivotal in colon cancer cell growth and resistance to chemotherapy drugs, are activated by Cisplatin (Achkar et al. 2018; Yang et al. 2020). Hence, it would be important to investigate whether the combination of Dmx1 or Dmx10 with Cisplatin can influence the activation status of these signaling pathways. Further studies are warranted to comprehensively elucidate the mechanisms underlying the synergistic effect of these compounds and Cisplatin in suppressing CRC cell lines growth.

In conclusion, our study suggests that hPELI2 could be a novel biomarker and potential therapeutic target for CRC treatment. We propose an underling mechanism in which hPELI2 enhances the ubiquitination and degradation of the Bcl-xL protein. On the basis of this, we also demonstrated that PELI2-targetting compounds Dmx1 and Dmx10 can modestly enhance the inhibitory effects of Cisplatin on CRC cell lines by further promoting cell apoptosis.

Our study sheds light on the potential application of these novel small molecule drugs as sensitizers in combination with chemotherapy for CRC. By showing that Dmx1 and Dmx10 can sensitize CRC cells to Cisplatin, our study provides a basis for further exploring the potential of these drugs in clinical settings. Future studies can focus on further elucidating the underlying molecular mechanisms by which Dmx1 and Dmx10

promote Cisplatin-induced apoptosis, as well as investigating the potential of these drugs *in vivo* models. Additionally, exploring the effect of the combination therapy on other forms of cell death caused by Cisplatin, such as necroptosis and autophagy, may provide a more comprehensive understanding of the potential benefits of this approach.

# Chapter 5: Concluding remarks

Ubiquitination is a post-translational modification process that involves the attachment of a small protein called ubiquitin to target proteins. This process serves as a molecular tag, directing the target proteins towards diverse cellular processes such as degradation, signaling, protein transport, and DNA repair.

Pellino proteins are a family of E3 ubiquitin ligases consisting of Pellino1, Pellino2 and Pellino3. Many studies have demonstrated that Pellino proteins play diverse regulatory roles in immunity and cancer. Our present study focused on the role of Pellino2 in inflammation and cancer models. Studies to date have used over-expression approaches and knockdown approaches in cells, as well as Pellino-deficient mice to interrogate Pellino function. Our research explores a pharmacological approach to target Pellino proteins, especially Pellino2, for the first time.

Small molecule drugs are a class of therapeutic agents widely used in medicine, characterized by their relatively low molecular weight and organic composition. These drugs are specifically designed to interact with and modulate the activity of target proteins, enzymes, receptors, or other biomolecules involved in disease pathways. By binding to these specific targets, small molecule drugs can exert their effects by enhancing or inhibiting their function, thereby influence the underlying processes associated with the disease. Over the past few decades, small molecule drugs have made significant contributions to the field of medicine by offering effective treatments for a wide range of diseases. These diseases include infections caused by bacteria, viruses,

fungi, various forms of cancer, cardiovascular disorders, neurological conditions, and autoimmune diseases.

In this research, we utilized a ligand-based pharmacophore strategy to design drugs aimed at Pellino proteins. The x-ray crystal structure of Pellino2 provided the necessary protein structure information for our research. We developed a pharmacophore model based on a specific peptide sequence derived from Pellino proteins. This model was used to perform a virtual screening of a chemical compound library. Subsequently, we identified potential lead compounds informed by the identified virtual hits from the virtual screen and use these as parent molecules for further modification by medicinal chemistry. As a result, we were able to highlight two small molecule compounds, Dmx1 and Dmx10 with novel composition of matter. These two compounds significantly inhibit inflammatory responses by targeting and facilitating the degradation of IRAK1, thereby down-regulating the NF-κB signaling pathway and suppressing the expression of pro-inflammatory cytokines IL-1β, IL-6 and TNFα. The notable anti-inflammatory effects of Dmx1 and Dmx10, which have been demonstrated in a dose-dependent manner without inducing cytotoxicity, are also mediated in a Pellino2-dependent manner. Our study represents an extension of the application of Pellino proteins in the field of anti-inflammatory targets and serves as a foundation for future investigations on the design of anti-inflammatory drugs targeting Pellino proteins.

This thesis forms the solid foundation for future research and development of these compounds. At this stage, our laboratory will continue to undertake comprehensive investigations on these compounds. Our current findings indicate that Dmx1 and Dmx10 are both effective at micromolar concentrations considerably below the dose that can effect cytotoxicity. However, we expect to be able to apply further medicinal chemistry approaches to enhance their performance and ensure effectiveness at lower concentrations and is so doing enhance their potency. Future studies will also investigate their pharmacokinetic properties and characterize their Absorption, Distribution, Metabolism and Excretion (ADME) features. My research has so far

examined the inhibitory effect of Dmx10 in LPS-induced sepsis via intraperitoneal injection in a mice model. Future studies will aim to investigate if these compounds can exhibit similar anti-inflammatory effects when administered orally. Additionally, LPS is only a single molecule derived from Gram-negative bacteria. It would be interesting to extend our studies to assess whether these compounds can also manifest similar anti-inflammatory effects in sepsis triggered by live bacteria. This investigation would contribute to determining their clinical potential as therapeutic agents for sepsis. Moreover, subsequent research could benefit from examining whether these compounds can also demonstrate efficacy against complex inflammatory diseases such as colitis. This is particularly relevant given that pro-inflammatory cytokines, such as IL-1β, IL-6, and TNFα, have been implicated in the pathogenesis of colitis, potentially providing further avenues for the therapeutic application of these compounds.

Furthermore, our investigation shows that Pellino2 exhibits anti-tumor effects in CRC. Our results indicated a frequent down-regulation of human *Pellino2* mRNA in both CRC patients and cell lines. Furthermore, we demonstrated that over-expression of human Pellino2 protein has a significant inhibitory effect on the growth of CRC cell lines by promoting cell apoptosis via targeting the ubiquitination and degradation of Bcl-xL. Conversely, silencing the expression of human Pellino2 protein resulted in the opposite effect. Similar results were also observed *in vivo*. Pellino2 -deficient mice demonstrate a higher tumor load and burden in the AOM/DSS-induced CRC model. These findings suggest that Pellino2 may have value as a potential therapeutic target in the treatment of CRC. By extension, we also investigated the potential role of Dmx1 and Dmx10 in CRC. Although Dmx1 and Dmx10 alone did not consistently inhibit CRC cell growth, we found that combining Dmx1 or Dmx10 with Cisplatin significantly enhanced the sensitivity of CRC to Cisplatin. These effects are dependent on the presence of Pellino2, indicating the potential of Dmx1 and Dmx10 as adjuvants in CRC chemotherapy, opening new possibilities for improving the effectiveness of established chemotherapeutic regimens.

In conclusion, this study suggests that Pellino2 may have dualist roles, contributing both to inflammation and maintenance of intestinal homeostasis. The development of small molecules targeting Pellino2, such as Dmx1 and Dmx10, presents promising potential in the treatment of inflammatory diseases and cancer. Our investigation offers evidence for the therapeutic potential of Dmx1 and Dmx10 on managing inflammatory conditions as well as sensitizing colorectal cancer to chemotherapy. Our results offer the initial steps toward innovation of anti-inflammatory and anticancer therapeutics targeting Pellino proteins. Future research, driven by the findings of this study, will be instrumental in exploring the broad therapeutic landscape that these compounds open up.

# Chapter 6: Bibliography


Abel, A. M., C. Yang, M. S. Thakar, and S. Malarkannan. 2018. 'Natural Killer Cells: Development, Maturation, and Clinical Utilization', *Front Immunol*, 9: 1869.

Achkar, I. W., N. Abdulrahman, H. Al-Sulaiti, J. M. Joseph, S. Uddin, and F. Mraiche. 2018. 'Cisplatin based therapy: the role of the mitogen activated protein kinase signaling pathway', *J Transl Med*, 16: 96.

Akira, S., K. Takeda, and T. Kaisho. 2001. 'Toll-like receptors: critical proteins linking innate and acquired immunity', *Nat Immunol*, 2: 675-80.

Akkaya, M., K. Kwak, and S. K. Pierce. 2020. 'B cell memory: building two walls of protection against pathogens', *Nat Rev Immunol*, 20: 229-38.

Alassaf, N., and H. Attia. 2023. 'Autophagy and necroptosis in cisplatin-induced acute kidney injury: Recent advances regarding their role and therapeutic potential', *Front Pharmacol*, 14: 1103062.

Alfano, D., I. Iaccarino, and M. P. Stoppelli. 2006. 'Urokinase signaling through its receptor protects against anoikis by increasing BCL-xL expression levels', *J Biol Chem*, 281: 17758-67.

Amarante-Mendes, G. P., S. Adjemian, L. M. Branco, L. C. Zanetti, R. Weinlich, and K. R. Bortoluci. 2018. 'Pattern Recognition Receptors and the Host Cell Death Molecular Machinery', *Front Immunol*, 9: 2379.

Arango Duque, G., and A. Descoteaux. 2014. 'Macrophage cytokines: involvement in immunity and infectious diseases', *Front Immunol*, 5: 491.

Arbibe, L., D. W. Kim, E. Batsche, T. Pedron, B. Mateescu, C. Muchardt, C. Parsot, and P. J. Sansonetti. 2007. 'An injected bacterial effector targets chromatin access for transcription factor NF-kappaB to alter transcription of host genes involved in immune responses', *Nat Immunol*, 8: 47-56.

Ardavin, C., S. Amigorena, and C. Reis e Sousa. 2004. 'Dendritic cells: immunobiology and cancer immunotherapy', *Immunity*, 20: 17-23.

Arkin, M. R., Y. Tang, and J. A. Wells. 2014. 'Small-molecule inhibitors of protein-protein interactions: progressing toward the reality', *Chem Biol*, 21: 1102-14.

Arnesen, H., M. H. B. Muller, M. Aleksandersen, G. C. Ostby, H. Carlsen, J. E. Paulsen, and P. Boysen. 2021. 'Induction of colorectal carcinogenesis in the C57BL/6J and A/J mouse strains with a reduced DSS dose in the AOM/DSS model', *Lab Anim Res*, 37: 19.

Banias, L., I. Jung, R. Chiciudean, and S. Gurzu. 2022. 'From Dukes-MAC Staging System to Molecular Classification: Evolving Concepts in Colorectal Cancer', *Int J Mol Sci*, 23.

Beck, H., M. Harter, B. Hass, C. Schmeck, and L. Baerfacker. 2022. 'Small molecules and their impact

in drug discovery: A perspective on the occasion of the 125th anniversary of the Bayer Chemical Research Laboratory', *Drug Discov Today*, 27: 1560-74.

Bertani, B., and N. Ruiz. 2018. 'Function and Biogenesis of Lipopolysaccharides', *EcoSal Plus*, 8.

Bharatham, N., S. W. Chi, and H. S. Yoon. 2011. 'Molecular basis of Bcl-X(L)-p53 interaction: insights from molecular dynamics simulations', *PLoS One*, 6: e26014.

Bing, C. 2015. 'Is interleukin-1beta a culprit in macrophage-adipocyte crosstalk in obesity?', *Adipocyte*, 4: 149-52.

Blanco, P., A. K. Palucka, V. Pascual, and J. Banchereau. 2008. 'Dendritic cells and cytokines in human inflammatory and autoimmune diseases', *Cytokine Growth Factor Rev*, 19: 41-52.

Bou Malhab, L. J., and W. M. Abdel-Rahman. 2022. 'Obesity and Inflammation: Colorectal Cancer Engines', *Curr Mol Pharmacol*, 15: 620-46.

Braciale, T. J., J. Sun, and T. S. Kim. 2012. 'Regulating the adaptive immune response to respiratory virus infection', *Nat Rev Immunol*, 12: 295-305.

Brebner, K., S. Hayley, R. Zacharko, Z. Merali, and H. Anisman. 2000. 'Synergistic effects of interleukin-1beta, interleukin-6, and tumor necrosis factor-alpha: central monoamine, corticosterone, and behavioral variations', *Neuropsychopharmacology*, 22: 566-80.

Broz, P., and V. M. Dixit. 2016. 'Inflammasomes: mechanism of assembly, regulation and signalling', *Nat Rev Immunol*, 16: 407-20.

Broz, P., and D. M. Monack. 2013. 'Newly described pattern recognition receptors team up against intracellular pathogens', *Nat Rev Immunol*, 13: 551-65.

Buranaamnuay, K. 2021. 'The MTT assay application to measure the viability of spermatozoa: A variety of the assay protocols', *Open Vet J*, 11: 251-69.

Burdette, B. E., A. N. Esparza, H. Zhu, and S. Wang. 2021. 'Gasdermin D in pyroptosis', *Acta Pharm Sin B*, 11: 2768-82.

Burn, G. L., A. Foti, G. Marsman, D. F. Patel, and A. Zychlinsky. 2021. 'The Neutrophil', *Immunity*, 54: 1377-91.

Butler, M. P., J. A. Hanly, and P. N. Moynagh. 2005. 'Pellino3 is a novel upstream regulator of p38 MAPK and activates CREB in a p38-dependent manner', *J Biol Chem*, 280: 27759-68.

— — — . 2007. 'Kinase-active interleukin-1 receptor-associated kinases promote polyubiquitination and degradation of the Pellino family: direct evidence for PELLINO proteins being ubiquitin-protein isopeptide ligases', *J Biol Chem*, 282: 29729-37.

Cai, K. Q., C. Shellhamer, T. Akiyama, and L. E. Jensen. 2023. 'Pellino1 Restricts Herpes Simplex Virus Infections in the Epidermis and Dissemination to Sebaceous Glands', *J Invest Dermatol*, 143: 639-47 e2.

Cerretti, D. P., C. J. Kozlosky, B. Mosley, N. Nelson, K. Van Ness, T. A. Greenstreet, C. J. March, S. R. Kronheim, T. Druck, L. A. Cannizzaro, and et al. 1992. 'Molecular cloning of the interleukin-1 beta converting enzyme', *Science*, 256: 97-100.

Chaitanya, G. V., A. J. Steven, and P. P. Babu. 2010. 'PARP-1 cleavage fragments: signatures of cell-death proteases in neurodegeneration', *Cell Commun Signal*, 8: 31.

Chakrabarti, S., C. Y. Peterson, D. Sriram, and A. Mahipal. 2020. 'Early stage colon cancer: Current treatment standards, evolving paradigms, and future directions', *World J Gastrointest Oncol*, 12: 808-32.

Chan, F. K., K. Moriwaki, and M. J. De Rosa. 2013. 'Detection of necrosis by release of lactate dehydrogenase activity', *Methods Mol Biol*, 979: 65-70.

Chang, M., W. Jin, and S. C. Sun. 2009. 'Peli1 facilitates TRIF-dependent Toll-like receptor signaling and proinflammatory cytokine production', *Nat Immunol*, 10: 1089-95.

Chaplin, D. D. 2010. 'Overview of the immune response', *J Allergy Clin Immunol*, 125: S3-23.

Chen, Z. J. 2012. 'Ubiquitination in signaling to and activation of IKK', *Immunol Rev*, 246: 95-106.

Childs-Disney, J. L., X. Yang, Q. M. R. Gibaut, Y. Tong, R. T. Batey, and M. D. Disney. 2022. 'Targeting RNA structures with small molecules', *Nat Rev Drug Discov*, 21: 736-62.

Choi, K. C., Y. S. Lee, S. Lim, H. K. Choi, C. H. Lee, E. K. Lee, S. Hong, I. H. Kim, S. J. Kim, and S. H. Park. 2006. 'Smad6 negatively regulates interleukin 1-receptor-Toll-like receptor signaling through direct interaction with the adaptor Pellino-1', *Nat Immunol*, 7: 1057-65.

Cicchese, J. M., S. Evans, C. Hult, L. R. Joslyn, T. Wessler, J. A. Millar, S. Marino, N. A. Cilfone, J. T. Mattila, J. J. Linderman, and D. E. Kirschner. 2018. 'Dynamic balance of pro- and anti-inflammatory signals controls disease and limits pathology', *Immunol Rev*, 285: 147-67.

Coates, M., S. Blanchard, and A. S. MacLeod. 2018. 'Innate antimicrobial immunity in the skin: A protective barrier against bacteria, viruses, and fungi', *PLoS Pathog*, 14: e1007353.

Cyster, J. G., and C. D. C. Allen. 2019. 'B Cell Responses: Cell Interaction Dynamics and Decisions', *Cell*, 177: 524-40.

Danial, N. N., and S. J. Korsmeyer. 2004. 'Cell death: critical control points', *Cell*, 116: 205-19.

Dasari, S., and P. B. Tchounwou. 2014. 'Cisplatin in cancer therapy: molecular mechanisms of action', *Eur J Pharmacol*, 740: 364-78.

Delves, P. J., and I. M. Roitt. 2000. 'The immune system. First of two parts', *N Engl J Med*, 343: 37-49.

Demarchi, F., C. Bertoli, P. Sandy, and C. Schneider. 2003. 'Glycogen synthase kinase-3 beta regulates NF-kappa B1/p105 stability', *J Biol Chem*, 278: 39583-90.

Dinarello, C. A. 2018. 'Overview of the IL-1 family in innate inflammation and acquired immunity', *Immunol Rev*, 281: 8-27.

Dodoo, D., F. M. Omer, J. Todd, B. D. Akanmori, K. A. Koram, and E. M. Riley. 2002. 'Absolute levels and ratios of proinflammatory and anti-inflammatory cytokine production in vitro predict clinical immunity to Plasmodium falciparum malaria', *J Infect Dis*, 185: 971-9.

Doescher, J., J. A. Veit, and T. K. Hoffmann. 2017. '[The 8th edition of the AJCC Cancer Staging Manual : Updates in otorhinolaryngology, head and neck surgery]', *HNO*, 65: 956-61.

Dong, W., Y. Liu, J. Peng, L. Chen, T. Zou, H. Xiao, Z. Liu, W. Li, Y. Bu, and Y. Qi. 2006. 'The IRAK-1-BCL10-MALT1-TRAF6-TAK1 cascade mediates signaling to NF-kappaB from Toll-like receptor 4', *J Biol Chem*, 281: 26029-40.

Dou, Z., D. Zhao, X. Chen, C. Xu, X. Jin, X. Zhang, Y. Wang, X. Xie, Q. Li, C. Di, and H. Zhang. 2021. 'Aberrant Bcl-x splicing in cancer: from molecular mechanism to therapeutic modulation', *J Exp Clin Cancer Res*, 40: 194.

Douaiher, J., A. Ravipati, B. Grams, S. Chowdhury, O. Alatise, and C. Are. 2017. 'Colorectal cancer-global burden, trends, and geographical variations', *J Surg Oncol*, 115: 619-30.

Dunkelberger, J. R., and W. C. Song. 2010. 'Complement and its role in innate and adaptive immune responses', *Cell Res*, 20: 34-50.

Ebner, P., G. A. Versteeg, and F. Ikeda. 2017. 'Ubiquitin enzymes in the regulation of immune responses', *Crit Rev Biochem Mol Biol*, 52: 425-60.

Elmore, S. 2007. 'Apoptosis: a review of programmed cell death', *Toxicol Pathol*, 35: 495-516.

Emmerich, C. H., A. Ordureau, S. Strickson, J. S. Arthur, P. G. Pedrioli, D. Komander, and P. Cohen.

2013. 'Activation of the canonical IKK complex by K63/M1-linked hybrid ubiquitin chains', *Proc Natl Acad Sci U S A*, 110: 15247-52.

Fajgenbaum, D. C., and C. H. June. 2020. 'Cytokine Storm', *N Engl J Med*, 383: 2255-73.

Fiebig, A. A., W. Zhu, C. Hollerbach, B. Leber, and D. W. Andrews. 2006. 'Bcl-XL is qualitatively different from and ten times more effective than Bcl-2 when expressed in a breast cancer cell line', *BMC Cancer*, 6: 213.

Franke, T. F., C. P. Hornik, L. Segev, G. A. Shostak, and C. Sugimoto. 2003. 'PI3K/Akt and apoptosis: size matters', *Oncogene*, 22: 8983-98.

Frigo, D. E., Y. Tang, B. S. Beckman, A. B. Scandurro, J. Alam, M. E. Burow, and J. A. McLachlan. 2004. 'Mechanism of AP-1-mediated gene expression by select organochlorines through the p38 MAPK pathway', *Carcinogenesis*, 25: 249-61.

Fujiyoshi, K., Y. Chen, K. Haruki, T. Ugai, J. Kishikawa, T. Hamada, L. Liu, K. Arima, J. Borowsky, J. P. Vayrynen, M. Zhao, M. C. Lau, S. Gu, S. Shi, N. Akimoto, T. S. Twombly, D. A. Drew, M. Song, A. T. Chan, E. L. Giovannucci, J. A. Meyerhardt, C. S. Fuchs, R. Nishihara, J. K. Lennerz, M. Giannakis, J. A. Nowak, X. Zhang, K. Wu, and S. Ogino. 2020. 'Smoking Status at Diagnosis and Colorectal Cancer Prognosis According to Tumor Lymphocytic Reaction', *JNCI Cancer Spectr*, 4: pkaa040.

Fujiyoshi, K., T. Sudo, F. Fujita, A. Chino, K. Akagi, A. Takao, M. Yamada, K. Tanakaya, H. Ishida, K. Komori, S. Ishihara, M. Miguchi, K. Hirata, Y. Miyakura, T. Ishikawa, T. Yamaguchi, N. Tomita, Y. Ajioka, and K. Sugihara. 2022. 'Risk of first onset of colorectal cancer associated with alcohol consumption in Lynch syndrome: a multicenter cohort study', *Int J Clin Oncol*, 27: 1051-59.

Galamb, O., B. Molnar, and Z. Tulassay. 2003. '[Immunobiology of dendritic cells and their application in clinical practice]', *Orv Hetil*, 144: 1873-9.

Gallo, G., G. Sena, G. Vescio, M. Papandrea, R. Sacco, M. Trompetto, and G. Sammarco. 2019. 'The prognostic value of KRAS and BRAF in stage I-III colorectal cancer. A systematic review', *Ann Ital Chir*, 90: 127-37.

Galluzzi, L., I. Vitale, J. Michels, C. Brenner, G. Szabadkai, A. Harel-Bellan, M. Castedo, and G. Kroemer. 2014. 'Systems biology of cisplatin resistance: past, present and future', *Cell Death Dis*, 5: e1257.

Gao, C. X., T. K. Qiao, B. Zhang, S. J. Yuan, X. B. Zhuang, and Y. J. Luo. 2018. 'TLR9 signaling activation at different stages in colorectal cancer and NF-kappaB expression', *Oncotargets and Therapy*, 11: 5963-71.

Gasteiger, G., A. D'Osualdo, D. A. Schubert, A. Weber, E. M. Bruscia, and D. Hartl. 2017. 'Cellular Innate Immunity: An Old Game with New Players', *J Innate Immun*, 9: 111-25.

Gelfo, V., D. Romaniello, M. Mazzeschi, M. Sgarzi, G. Grilli, A. Morselli, B. Manzan, K. Rihawi, and M. Lauriola. 2020. 'Roles of IL-1 in Cancer: From Tumor Progression to Resistance to Targeted Therapies', *Int J Mol Sci*, 21.

Ghayur, T., S. Banerjee, M. Hugunin, D. Butler, L. Herzog, A. Carter, L. Quintal, L. Sekut, R. Talanian, M. Paskind, W. Wong, R. Kamen, D. Tracey, and H. Allen. 1997. 'Caspase-1 processes IFN-gamma-inducing factor and regulates LPS-induced IFN-gamma production', *Nature*, 386: 619-23.

Ghobrial, I. M., T. E. Witzig, and A. A. Adjei. 2005. 'Targeting apoptosis pathways in cancer therapy', *CA Cancer J Clin*, 55: 178-94.

Ghosh, S. 2019. 'Cisplatin: The first metal based anticancer drug', *Bioorg Chem*, 88: 102925.

Giridharan, S., and M. Srinivasan. 2018. 'Mechanisms of NF-kappaB p65 and strategies for therapeutic manipulation', *J Inflamm Res*, 11: 407-19.

Glaros, T. G., S. Chang, E. A. Gilliam, U. Maitra, H. Deng, and L. Li. 2013. 'Causes and consequences of low grade endotoxemia and inflammatory diseases', *Front Biosci (Schol Ed)*, 5: 754-65.

Gordon, S. 2016. 'Phagocytosis: An Immunobiologic Process', *Immunity*, 44: 463-75.

Gottipati, S., N. L. Rao, and W. P. Fung-Leung. 2008. 'IRAK1: a critical signaling mediator of innate immunity', *Cell Signal*, 20: 269-76.

Govind, S. 2008. 'Innate immunity in Drosophila: Pathogens and pathways', *Insect Sci*, 15: 29-43.

Griffin, G. K., G. Newton, M. L. Tarrio, D. X. Bu, E. Maganto-Garcia, V. Azcutia, P. Alcaide, N. Grabie, F. W. Luscinskas, K. J. Croce, and A. H. Lichtman. 2012. 'IL-17 and TNF-alpha sustain neutrophil recruitment during inflammation through synergistic effects on endothelial activation', *J Immunol*, 188: 6287-99.

Grosshans, J., F. Schnorrer, and C. Nusslein-Volhard. 1999. 'Oligomerisation of Tube and Pelle leads to nuclear localisation of dorsal', *Mech Dev*, 81: 127-38.

Gu, J., L. Pang, D. Yan, C. Wang, Y. Song, Z. Jin, Z. Xu, Y. Mao, S. Liu, and S. Chen. 2023. 'Ubiquitin-proteasome system-mediated ubiquitination modification patterns and characterization of tumor microenvironment infiltration, stemness and cellular senescence in low-grade glioma', *Aging (Albany NY)*, 15.

Guilliams, M., A. Mildner, and S. Yona. 2018. 'Developmental and Functional Heterogeneity of Monocytes', *Immunity*, 49: 595-613.

Guo, H., K. Zhuang, N. Ding, R. Hua, H. Tang, Y. Wu, Z. Yuan, T. Li, and S. He. 2022. 'High-fat diet induced cyclophilin B enhances STAT3/lncRNA-PVT1 feedforward loop and promotes growth and metastasis in colorectal cancer', *Cell Death Dis*, 13: 883.

Hari, D. M., A. M. Leung, J. H. Lee, M. S. Sim, B. Vuong, C. G. Chiu, and A. J. Bilchik. 2013. 'AJCC Cancer Staging Manual 7th edition criteria for colon cancer: do the complex modifications improve prognostic assessment?', *J Am Coll Surg*, 217: 181-90.

He, W. T., H. Wan, L. Hu, P. Chen, X. Wang, Z. Huang, Z. H. Yang, C. Q. Zhong, and J. Han. 2015. 'Gasdermin D is an executor of pyroptosis and required for interleukin-1beta secretion', *Cell Res*, 25: 1285-98.

Heine, Holger, Carsten J. Kirschning, Egil Lien, Brian G. Monks, Mike Rothe, and Douglas T. Golenbock. 1999. 'Cutting Edge: Cells That Carry A Null Allele for Toll-Like Receptor 2 Are Capable of Responding to Endotoxin', *The Journal of Immunology*, 162: 6971-75.

Hengartner, M. O. 2001. 'Apoptosis: corralling the corpses', *Cell*, 104: 325-8.

Hilhorst, M., T. Shirai, G. Berry, J. J. Goronzy, and C. M. Weyand. 2014. 'T cell-macrophage interactions and granuloma formation in vasculitis', *Front Immunol*, 5: 432.

Hirano, T. 2021. 'IL-6 in inflammation, autoimmunity and cancer', *Int Immunol*, 33: 127-48.

Hoffman, W., F. G. Lakkis, and G. Chalasani. 2016. 'B Cells, Antibodies, and More', *Clin J Am Soc Nephrol*, 11: 137-54.

Hossain, M. S., H. Karuniawati, A. A. Jairoun, Z. Urbi, J. Ooi, A. John, Y. C. Lim, K. M. K. Kibria, A. K. M. Mohiuddin, L. C. Ming, K. W. Goh, and M. A. Hadi. 2022. 'Colorectal Cancer: A Review of Carcinogenesis, Global Epidemiology, Current Challenges, Risk Factors, Preventive and Treatment Strategies', *Cancers (Basel)*, 14.

Huang, Q. Q., and R. M. Pope. 2009. 'The role of toll-like receptors in rheumatoid arthritis', *Curr*

*Rheumatol Rep*, 11: 357-64.

Humphries, F., R. Bergin, R. Jackson, N. Delagic, B. Wang, S. Yang, A. V. Dubois, R. J. Ingram, and P. N. Moynagh. 2018. 'The E3 ubiquitin ligase Pellino2 mediates priming of the NLRP3 inflammasome', *Nat Commun*, 9: 1560.

Jacobson, A. D., N. Y. Zhang, P. Xu, K. J. Han, S. Noone, J. Peng, and C. W. Liu. 2009. 'The lysine 48 and lysine 63 ubiquitin conjugates are processed differently by the 26 s proteasome', *J Biol Chem*, 284: 35485-94.

Jahangirian, H., K. Kalantari, Z. Izadiyan, R. Rafiee-Moghaddam, K. Shameli, and T. J. Webster. 2019. 'A review of small molecules and drug delivery applications using gold and iron nanoparticles', *Int J Nanomedicine*, 14: 1633-57.

Jensen, L. E., and A. S. Whitehead. 2003a. 'Pellino2 activates the mitogen activated protein kinase pathway', *FEBS Lett*, 545: 199-202.

———. 2003b. 'Pellino3, a novel member of the Pellino protein family, promotes activation of c-Jun and Elk-1 and may act as a scaffolding protein', *J Immunol*, 171: 1500-6.

Jeon, Y. K., C. K. Kim, K. R. Hwang, H. Y. Park, J. Koh, D. H. Chung, C. W. Lee, and G. H. Ha. 2017. 'Pellino-1 promotes lung carcinogenesis via the stabilization of Slug and Snail through K63-mediated polyubiquitination', *Cell Death and Differentiation*, 24: 469-80.

Jeon, Y. K., C. K. Kim, J. Koh, D. H. Chung, and G. H. Ha. 2016. 'Pellino-1 confers chemoresistance in lung cancer cells by upregulating cIAP2 through Lys63-mediated polyubiquitination', *Oncotarget*, 7: 41811-24.

Jiang, X., Z. Jiang, Q. Cheng, W. Sun, M. Jiang, and Y. Sun. 2022. 'Cholecystectomy promotes the development of colorectal cancer by the alternation of bile acid metabolism and the gut microbiota', *Front Med (Lausanne)*, 9: 1000563.

Jiang, Z., H. J. Johnson, H. Nie, J. Qin, T. A. Bird, and X. Li. 2003. 'Pellino 1 is required for interleukin-1 (IL-1)-mediated signaling through its interaction with the IL-1 receptor-associated kinase 4 (IRAK4)-IRAK-tumor necrosis factor receptor-associated factor 6 (TRAF6) complex', *J Biol Chem*, 278: 10952-6.

Kaech, S. M., E. J. Wherry, and R. Ahmed. 2002. 'Effector and memory T-cell differentiation: implications for vaccine development', *Nat Rev Immunol*, 2: 251-62.

Kapahi, P., T. Takahashi, G. Natoli, S. R. Adams, Y. Chen, R. Y. Tsien, and M. Karin. 2000. 'Inhibition of NF-kappa B activation by arsenite through reaction with a critical cysteine in the activation loop of Ikappa B kinase', *J Biol Chem*, 275: 36062-6.

Kapellos, T. S., L. Bonaguro, I. Gemund, N. Reusch, A. Saglam, E. R. Hinkley, and J. L. Schultze. 2019. 'Human Monocyte Subsets and Phenotypes in Major Chronic Inflammatory Diseases', *Front Immunol*, 10: 2035.

Karin, M. 1996. 'The regulation of AP-1 activity by mitogen-activated protein kinases', *Philos Trans R Soc Lond B Biol Sci*, 351: 127-34.

Kawai, T., and S. Akira. 2007. 'Signaling to NF-kappaB by Toll-like receptors', *Trends Mol Med*, 13: 460-9.

Khandia, R., and A. Munjal. 2020. 'Interplay between inflammation and cancer', *Adv Protein Chem Struct Biol*, 119: 199-245.

Kim, D., J. Koh, J. S. Ko, H. Y. Kim, H. Lee, and D. H. Chung. 2019. 'Ubiquitin E3 Ligase Pellino-1 Inhibits IL-10-mediated M2c Polarization of Macrophages, Thereby Suppressing Tumor Growth', *Immune Netw*, 19: e32.

Kim, T. W., M. J. Yu, H. Zhou, W. Cui, J. A. Wang, P. DiCorleto, P. Fox, H. Xiao, and X. X. Li. 2012. 'Pellino 2 Is critical for Toll-like Receptor/Interleukin-1 Receptor (TLR/IL-1R)-mediated Post-transcriptional Control', *Journal of Biological Chemistry*, 287: 25686-95.

Koberle, B., and S. Schoch. 2021. 'Platinum Complexes in Colorectal Cancer and Other Solid Tumors', *Cancers (Basel)*, 13.

Kolligs, F. T. 2016. 'Diagnostics and Epidemiology of Colorectal Cancer', *Visc Med*, 32: 158-64.

Kraus, S., and N. Arber. 2009. 'Inflammation and colorectal cancer', *Curr Opin Pharmacol*, 9: 405-10.

Kroemer, G., L. Galluzzi, and C. Brenner. 2007. 'Mitochondrial membrane permeabilization in cell death', *Physiol Rev*, 87: 99-163.

Kroemer, G., L. Galluzzi, P. Vandenabeele, J. Abrams, E. S. Alnemri, E. H. Baehrecke, M. V. Blagosklonny, W. S. El-Deiry, P. Golstein, D. R. Green, M. Hengartner, R. A. Knight, S. Kumar, S. A. Lipton, W. Malorni, G. Nunez, M. E. Peter, J. Tschopp, J. Yuan, M. Piacentini, B. Zhivotovsky, G. Melino, and Death Nomenclature Committee on Cell. 2009. 'Classification of cell death: recommendations of the Nomenclature Committee on Cell Death 2009', *Cell Death and Differentiation*, 16: 3-11.

Krystel-Whittemore, M., K. N. Dileepan, and J. G. Wood. 2015. 'Mast Cell: A Multi-Functional Master Cell', *Front Immunol*, 6: 620.

Kumar, P., A. Nagarajan, and P. D. Uchil. 2018. 'Analysis of Cell Viability by the Lactate Dehydrogenase Assay', *Cold Spring Harb Protoc*, 2018.

Kumar, V. 2020. 'Toll-like receptors in sepsis-associated cytokine storm and their endogenous negative regulators as future immunomodulatory targets', *Int Immunopharmacol*, 89: 107087.

Kuriakose, S., C. Onyilagha, R. Singh, F. Olayinka-Adefemi, P. Jia, and J. E. Uzonna. 2019. 'TLR-2 and MyD88-Dependent Activation of MAPK and STAT Proteins Regulates Proinflammatory Cytokine Response and Immunity to Experimental Trypanosoma congolense Infection', *Front Immunol*, 10: 2673.

Kwok, B. H., B. Koh, M. I. Ndubuisi, M. Elofsson, and C. M. Crews. 2001. 'The anti-inflammatory natural product parthenolide from the medicinal herb Feverfew directly binds to and inhibits IkappaB kinase', *Chem Biol*, 8: 759-66.

Lacy, P., and J. L. Stow. 2011. 'Cytokine release from innate immune cells: association with diverse membrane trafficking pathways', *Blood*, 118: 9-18.

Lanier, L. L. 2005. 'NK cell recognition', *Annu Rev Immunol*, 23: 225-74.

Lee, T. L., J. Yeh, J. Friedman, B. Yan, X. Yang, N. T. Yeh, C. Van Waes, and Z. Chen. 2008. 'A signal network involving coactivated NF-kappaB and STAT3 and altered p53 modulates BAX/BCL-XL expression and promotes cell survival of head and neck squamous cell carcinomas', *Int J Cancer*, 122: 1987-98.

Lester, S. N., and K. Li. 2014. 'Toll-like receptors in antiviral innate immunity', *J Mol Biol*, 426: 1246-64.

Li, D., and M. Wu. 2021. 'Pattern recognition receptors in health and diseases', *Signal Transduct Target Ther*, 6: 291.

Li, H., X. Chen, M. Hoffmeister, and H. Brenner. 2023. 'Associations of smoking with early- and late-onset colorectal cancer', *JNCI Cancer Spectr*, 7.

Li, S., A. Strelow, E. J. Fontana, and H. Wesche. 2002. 'IRAK-4: a novel member of the IRAK family

with the properties of an IRAK-kinase', *Proc Natl Acad Sci U S A*, 99: 5567-72.

Li, T. T., S. Ogino, and Z. R. Qian. 2014. 'Toll-like receptor signaling in colorectal cancer: carcinogenesis to cancer therapy', *World J Gastroenterol*, 20: 17699-708.

Lichtenstern, C. R., R. K. Ngu, S. Shalapour, and M. Karin. 2020. 'Immunotherapy, Inflammation and Colorectal Cancer', *Cells*, 9.

Lin, C. C., Y. S. Huoh, K. R. Schmitz, L. E. Jensen, and K. M. Ferguson. 2008. 'Pellino proteins contain a cryptic FHA domain that mediates interaction with phosphorylated IRAK1', *Structure*, 16: 1806-16.

Lin, X. W., W. C. Xu, J. G. Luo, X. J. Guo, T. Sun, X. L. Zhao, and Z. J. Fu. 2013. 'WW domain containing E3 ubiquitin protein ligase 1 (WWP1) negatively regulates TLR4-mediated TNF-alpha and IL-6 production by proteasomal degradation of TNF receptor associated factor 6 (TRAF6)', *PLoS One*, 8: e67633.

Lin, Y. Z., S. Y. Yao, R. A. Veach, T. R. Torgerson, and J. Hawiger. 1995. 'Inhibition of nuclear translocation of transcription factor NF-kappa B by a synthetic peptide containing a cell membrane-permeable motif and nuclear localization sequence', *J Biol Chem*, 270: 14255-8.

Liu, S. S., J. Qi, Z. D. Teng, F. T. Tian, X. X. Lv, K. Li, Y. J. Song, W. D. Xie, Z. W. Hu, and X. Li. 2020. 'Resistomycin attenuates triple-negative breast cancer progression by inhibiting E3 ligase Pellino-1 and inducing SNAIL/SLUG degradation', *Signal Transduct Target Ther*, 5: 133.

Liu, X., Z. Lin, and X. Yin. 2022. 'Pellino2 accelerate inflammation and pyroptosis via the ubiquitination and activation of NLRP3 inflammation in model of pediatric pneumonia', *Int Immunopharmacol*, 110: 108993.

Liu, Y., W. Dong, L. Chen, R. Xiang, H. Xiao, G. De, Z. Wang, and Y. Qi. 2004. 'BCL10 mediates lipopolysaccharide/toll-like receptor-4 signaling through interaction with Pellino2', *J Biol Chem*, 279: 37436-44.

Liu, Z., C. Wang, J. Yang, Y. Chen, B. Zhou, D. W. Abbott, and T. S. Xiao. 2020. 'Caspase-1 Engages Full-Length Gasdermin D through Two Distinct Interfaces That Mediate Caspase Recruitment and Substrate Cleavage', *Immunity*, 53: 106-14 e5.

Lomonosova, E., and G. Chinnadurai. 2008. 'BH3-only proteins in apoptosis and beyond: an overview', *Oncogene*, 27 Suppl 1: S2-19.

Long, A. G., E. T. Lundsmith, and K. E. Hamilton. 2017. 'Inflammation and Colorectal Cancer', *Curr Colorectal Cancer Rep*, 13: 341-51.

Loo, L. S. W., A. A. P. Soetedjo, H. H. Lau, N. H. J. Ng, S. Ghosh, L. Nguyen, V. G. Krishnan, H. Choi, X. Roca, S. Hoon, and A. K. K. Teo. 2020. 'BCL-xL/BCL2L1 is a critical anti-apoptotic protein that promotes the survival of differentiating pancreatic cells from human pluripotent stem cells', *Cell Death & Disease*, 11.

Lopez-Castejon, G., and D. Brough. 2011. 'Understanding the mechanism of IL-1beta secretion', *Cytokine Growth Factor Rev*, 22: 189-95.

Lopez, J., and S. W. Tait. 2015. 'Mitochondrial apoptosis: killing cancer using the enemy within', *Br J Cancer*, 112: 957-62.

Lu, Y. C., W. C. Yeh, and P. S. Ohashi. 2008. 'LPS/TLR4 signal transduction pathway', *Cytokine*, 42: 145-51.

Luckheeram, R. V., R. Zhou, A. D. Verma, and B. Xia. 2012. 'CD4(+)T cells: differentiation and functions', *Clin Dev Immunol*, 2012: 925135.

Luo, Q., L. Zeng, C. Tang, Z. Zhang, Y. Chen, and C. Zeng. 2020. 'TLR9 induces colitis-associated colorectal carcinogenesis by regulating NF-kappaB expression levels', *Oncol Lett*, 20: 110.

Lv, D., P. Pal, X. Liu, Y. Jia, D. Thummuri, P. Zhang, W. Hu, J. Pei, Q. Zhang, S. Zhou, S. Khan, X. Zhang, N. Hua, Q. Yang, S. Arango, W. Zhang, D. Nayak, S. K. Olsen, S. T. Weintraub, R. Hromas, M. Konopleva, Y. Yuan, G. Zheng, and D. Zhou. 2021. 'Development of a BCL-xL and BCL-2 dual degrader with improved anti-leukemic activity', *Nat Commun*, 12: 6896.

Ma, Y., R. Qu, Y. Zhang, C. Jiang, Z. Zhang, and W. Fu. 2022. 'Progress in the Study of Colorectal Cancer Caused by Altered Gut Microbiota After Cholecystectomy', *Front Endocrinol (Lausanne)*, 13: 815999.

Ma, Y., W. Yang, M. Song, S. A. Smith-Warner, J. Yang, Y. Li, W. Ma, Y. Hu, S. Ogino, F. B. Hu, D. Wen, A. T. Chan, E. L. Giovannucci, and X. Zhang. 2018. 'Type 2 diabetes and risk of colorectal cancer in two large U.S. prospective cohorts', *Br J Cancer*, 119: 1436-42.

Maccio, A., and C. Madeddu. 2020. 'Blocking inflammation to improve immunotherapy of advanced cancer', *Immunology*, 159: 357-64.

Mahnke, Y. D., T. M. Brodie, F. Sallusto, M. Roederer, and E. Lugli. 2013. 'The who's who of T-cell differentiation: human memory T-cell subsets', *Eur J Immunol*, 43: 2797-809.

Majno, G., and I. Joris. 1995. 'Apoptosis, oncosis, and necrosis. An overview of cell death', *Am J Pathol*, 146: 3-15.

Mantovani, A., and C. Garlanda. 2023. 'Humoral Innate Immunity and Acute-Phase Proteins', *N Engl J Med*, 388: 439-52.

Marsh, E. K., E. C. Prestwich, L. Williams, A. R. Hart, C. F. Muir, L. C. Parker, M. R. Jonker, I. H. Heijink, W. Timens, M. Fife, T. Hussell, M. B. Hershenson, J. K. Bentley, S. C. Sun, B. S. Barksby, L. A. Borthwick, J. P. Stewart, I. Sabroe, D. H. Dockrell, and H. M. Marriott. 2020. 'Pellino-1 Regulates the Responses of the Airway to Viral Infection', *Front Cell Infect Microbiol*, 10: 456.

Maslinska, D., M. Laure-Kamionowska, and S. Maslinska. 2012. 'Toll-like receptors as an innate immunity bridge to neuroinflammation in medulloblastoma', *Folia Neuropathol*, 50: 375-81.

Masuda, T., S. Haji, Y. Nakashima, M. Tsuda, D. Kimura, A. Takamatsu, N. Iwahashi, H. Umakoshi, M. Shiratsuchi, C. Kikutake, M. Suyama, Y. Ohkawa, and Y. Ogawa. 2022. 'Identification of a drug-response gene in multiple myeloma through longitudinal single-cell transcriptome sequencing', *iScience*, 25: 104781.

McIlwain, D. R., T. Berger, and T. W. Mak. 2015. 'Caspase functions in cell death and disease', *Cold Spring Harb Perspect Biol*, 7.

Medzhitov, R. 2001. 'Toll-like receptors and innate immunity', *Nat Rev Immunol*, 1: 135-45.

Merle, N. S., S. E. Church, V. Fremeaux-Bacchi, and L. T. Roumenina. 2015. 'Complement System Part I - Molecular Mechanisms of Activation and Regulation', *Front Immunol*, 6: 262.

Merle, N. S., R. Noe, L. Halbwachs-Mecarelli, V. Fremeaux-Bacchi, and L. T. Roumenina. 2015. 'Complement System Part II: Role in Immunity', *Front Immunol*, 6: 257.

Miller, A. M., N. Horiguchi, W. I. Jeong, S. Radaeva, and B. Gao. 2011. 'Molecular mechanisms of alcoholic liver disease: innate immunity and cytokines', *Alcohol Clin Exp Res*, 35: 787-93.

Miller, S. I., R. K. Ernst, and M. W. Bader. 2005. 'LPS, TLR4 and infectious disease diversity', *Nat Rev Microbiol*, 3: 36-46.

Mittrucker, H. W., A. Visekruna, and M. Huber. 2014. 'Heterogeneity in the differentiation and

function of CD8(+) T cells', *Arch Immunol Ther Exp (Warsz)*, 62: 449-58.

Mohr, A. M., J. J. Gould, J. L. Kubik, G. A. Talmon, C. A. Casey, P. Thomas, D. J. Tuma, and B. L. McVicker. 2017. 'Enhanced colorectal cancer metastases in the alcohol-injured liver', *Clin Exp Metastasis*, 34: 171-84.

Mohty, M., and B. Gaugler. 2003. 'Dendritic cells: interfaces with immunobiology and medicine. A report from the Keystone Symposia Meeting held in Keystone, 3-8 March 2003', *Leukemia*, 17: 1753-8.

Molteni, M., S. Gemma, and C. Rossetti. 2016. 'The Role of Toll-Like Receptor 4 in Infectious and Noninfectious Inflammation', *Mediators Inflamm*, 2016: 6978936.

Morgan, R. A., J. C. Yang, M. Kitano, M. E. Dudley, C. M. Laurencot, and S. A. Rosenberg. 2010. 'Case report of a serious adverse event following the administration of T cells transduced with a chimeric antigen receptor recognizing ERBB2', *Mol Ther*, 18: 843-51.

Mosser, D. M., and J. P. Edwards. 2008. 'Exploring the full spectrum of macrophage activation', *Nat Rev Immunol*, 8: 958-69.

Motshwene, P. G., M. C. Moncrieffe, J. G. Grossmann, C. Kao, M. Ayaluru, A. M. Sandercock, C. V. Robinson, E. Latz, and N. J. Gay. 2009. 'An oligomeric signaling platform formed by the Toll-like receptor signal transducers MyD88 and IRAK-4', *J Biol Chem*, 284: 25404-11.

Moynagh, P. N. 2005. 'The NF-kappaB pathway', *J Cell Sci*, 118: 4589-92.

———. 2014. 'The roles of Pellino E3 ubiquitin ligases in immunity', *Nat Rev Immunol*, 14: 122-31.

Muchmore, S. W., M. Sattler, H. Liang, R. P. Meadows, J. E. Harlan, H. S. Yoon, D. Nettesheim, B. S. Chang, C. B. Thompson, S. L. Wong, S. L. Ng, and S. W. Fesik. 1996. 'X-ray and NMR structure of human Bcl-xL, an inhibitor of programmed cell death', *Nature*, 381: 335-41.

Mukai, K., M. Tsai, H. Saito, and S. J. Galli. 2018. 'Mast cells as sources of cytokines, chemokines, and growth factors', *Immunol Rev*, 282: 121-50.

Muroi, M., and K. Tanamoto. 2012. 'IRAK-1-mediated negative regulation of Toll-like receptor signaling through proteasome-dependent downregulation of TRAF6', *Biochim Biophys Acta*, 1823: 255-63.

Murray, P. J., and T. A. Wynn. 2011. 'Protective and pathogenic functions of macrophage subsets', *Nat Rev Immunol*, 11: 723-37.

Murray, R. Z., and J. L. Stow. 2014. 'Cytokine Secretion in Macrophages: SNAREs, Rabs, and Membrane Trafficking', *Front Immunol*, 5: 538.

Namasivayam, V., and S. Lim. 2017. 'Recent advances in the link between physical activity, sedentary behavior, physical fitness, and colorectal cancer', *F1000Res*, 6: 199.

Neurath, M. F., and S. Finotto. 2011. 'IL-6 signaling in autoimmunity, chronic inflammation and inflammation-associated cancer', *Cytokine Growth Factor Rev*, 22: 83-9.

Neutzner, M., and A. Neutzner. 2012. 'Enzymes of ubiquitination and deubiquitination', *Essays Biochem*, 52: 37-50.

Nigam, A. K., U. Kumari, S. Mittal, and A. K. Mittal. 2012. 'Comparative analysis of innate immune parameters of the skin mucous secretions from certain freshwater teleosts, inhabiting different ecological niches', *Fish Physiol Biochem*, 38: 1245-56.

O'Brien, Mauria A., and Rebecca Kirby. 2008. 'Apoptosis: A review of pro-apoptotic and anti-apoptotic pathways and dysregulation in disease', *Journal of Veterinary Emergency and Critical Care*, 18: 572-85.

O'Neill, L. A., D. Golenbock, and A. G. Bowie. 2013. 'The history of Toll-like receptors - redefining

innate immunity', *Nat Rev Immunol*, 13: 453-60.

Obeng, E. 2021. 'Apoptosis (programmed cell death) and its signals - A review', *Braz J Biol*, 81: 1133-43.

Ohto, U. 2016. '[Structural studies of Toll-like receptors in innate immunity]', *Seikagaku*, 88: 476-88.

Oleszycka, E., A. M. Rodgers, L. A. Xu, and P. N. Moynagh. 2021. 'Dendritic Cell-Specific Role for Pellino2 as a Mediator of TLR9 Signaling Pathway', *Journal of Immunology*, 207: 2325-36.

P A Baeuerle, and, and T Henkel. 1994. 'Function and Activation of NF-kappaB in the Immune System', *Annual Review of Immunology*, 12: 141-79.

Pande, V., and M. J. Ramos. 2005. 'NF-kappaB in human disease: current inhibitors and prospects for de novo structure based design of inhibitors', *Curr Med Chem*, 12: 357-74.

Pang, Y., C. Kartsonaki, Y. Guo, Y. Chen, L. Yang, Z. Bian, F. Bragg, I. Y. Millwood, L. Shen, S. Zhou, J. Liu, J. Chen, L. Li, M. V. Holmes, and Z. Chen. 2018. 'Diabetes, plasma glucose and incidence of colorectal cancer in Chinese adults: a prospective study of 0.5 million people', *J Epidemiol Community Health*, 72: 919-25.

Parang, B., C. W. Barrett, and C. S. Williams. 2016. 'AOM/DSS Model of Colitis-Associated Cancer', *Methods Mol Biol*, 1422: 297-307.

Park, B. S., and J. O. Lee. 2013. 'Recognition of lipopolysaccharide pattern by TLR4 complexes', *Exp Mol Med*, 45: e66.

Park, H. Y., H. Go, H. R. Song, S. Kim, G. H. Ha, Y. K. Jeon, J. E. Kim, H. Lee, H. Cho, H. C. Kang, H. Y. Chung, C. W. Kim, D. H. Chung, and C. W. Lee. 2014. 'Pellino 1 promotes lymphomagenesis by deregulating BCL6 polyubiquitination', *J Clin Invest*, 124: 4976-88.

Park, J., J. H. Lee, M. La, M. J. Jang, G. W. Chae, S. B. Kim, H. Tak, Y. Jung, B. Byun, J. K. Ahn, and C. O. Joe. 2007. 'Inhibition of NF-kappaB acetylation and its transcriptional activity by Daxx', *J Mol Biol*, 368: 388-97.

Park, J., H. Y. Park, S. Kim, H. S. Kim, J. Y. Park, H. Go, and C. W. Lee. 2017. 'Pellino 1 inactivates mitotic spindle checkpoint by targeting BubR1 for ubiquitinational degradation', *Oncotarget*, 8: 32055-67.

Petros, A. M., A. Medek, D. G. Nettesheim, D. H. Kim, H. S. Yoon, K. Swift, E. D. Matayoshi, T. Oltersdorf, and S. W. Fesik. 2001. 'Solution structure of the antiapoptotic protein bcl-2', *Proc Natl Acad Sci U S A*, 98: 3012-7.

Pu, D., and W. Wang. 2014. 'Toll-like receptor 4 agonist, lipopolysaccharide, increases the expression levels of cytokines and chemokines in human peripheral blood mononuclear cells', *Exp Ther Med*, 8: 1914-18.

Pussinen, P. J., A. S. Havulinna, M. Lehto, J. Sundvall, and V. Salomaa. 2011. 'Endotoxemia is associated with an increased risk of incident diabetes', *Diabetes Care*, 34: 392-7.

Qian, S., O. Golubnitschaja, and X. Zhan. 2019. 'Chronic inflammation: key player and biomarker-set to predict and prevent cancer development and progression based on individualized patient profiles', *EPMA J*, 10: 365-81.

Qin, Q., W. Li, A. Ren, R. Luo, and S. Luo. 2022. 'Benign gallbladder disease is a risk factor for colorectal cancer, but cholecystectomy is not: A propensity score matching analysis', *Front Oncol*, 12: 1008394.

Ramadan, B., H. Dahboul, C. Mouawad, R. Aoun, S. Kassar, E. Kassouf, G. Chakhtoura, R. Noun, and M. Osseis. 2022. 'Obesity: A risk factor for postoperative complications in laparoscopic

surgery for colorectal cancer', *J Minim Access Surg*.

Ravi, R., and A. Bedi. 2004. 'NF-kappaB in cancer--a friend turned foe', *Drug Resist Updat*, 7: 53-67.

Rawla, P., T. Sunkara, and A. Barsouk. 2019. 'Epidemiology of colorectal cancer: incidence, mortality, survival, and risk factors', *Prz Gastroenterol*, 14: 89-103.

Rebe, C., and F. Ghiringhelli. 2020. 'Interleukin-1beta and Cancer', *Cancers (Basel)*, 12.

Rich, T., R. L. Allen, A. M. Lucas, A. Stewart, and J. Trowsdale. 2000. 'Pellino-related sequences from Caenorhabditis elegans and Homo sapiens', *Immunogenetics*, 52: 145-9.

Rieger, A. M., K. L. Nelson, J. D. Konowalchuk, and D. R. Barreda. 2011. 'Modified annexin V/propidium iodide apoptosis assay for accurate assessment of cell death', *J Vis Exp*.

Roberts, C. A., A. K. Dickinson, and L. S. Taams. 2015. 'The Interplay Between Monocytes/Macrophages and CD4(+) T Cell Subsets in Rheumatoid Arthritis', *Front Immunol*, 6: 571.

Rock, F. L., G. Hardiman, J. C. Timans, R. A. Kastelein, and J. F. Bazan. 1998. 'A family of human receptors structurally related to Drosophila Toll', *Proc Natl Acad Sci U S A*, 95: 588-93.

Rosales, C. 2018. 'Neutrophil: A Cell with Many Roles in Inflammation or Several Cell Types?', *Front Physiol*, 9: 113.

Rubin, D. C., A. Shaker, and M. S. Levin. 2012. 'Chronic intestinal inflammation: inflammatory bowel disease and colitis-associated colon cancer', *Front Immunol*, 3: 107.

Sanchez-Duffhues, G., M. A. Calzado, A. G. de Vinuesa, G. Appendino, B. L. Fiebich, U. Loock, A. Lefarth-Risse, K. Krohn, and E. Munoz. 2009. 'Denbinobin inhibits nuclear factor-kappaB and induces apoptosis via reactive oxygen species generation in human leukemic cells', *Biochem Pharmacol*, 77: 1401-9.

Sander, L. E., S. D. Sackett, U. Dierssen, N. Beraza, R. P. Linke, M. Muller, J. M. Blander, F. Tacke, and C. Trautwein. 2010. 'Hepatic acute-phase proteins control innate immune responses during infection by promoting myeloid-derived suppressor cell function', *J Exp Med*, 207: 1453-64.

Sarma, J. V., and P. A. Ward. 2011. 'The complement system', *Cell Tissue Res*, 343: 227-35.

Sawicki, T., M. Ruszkowska, A. Danielewicz, E. Niedzwiedzka, T. Arlukowicz, and K. E. Przybylowicz. 2021. 'A Review of Colorectal Cancer in Terms of Epidemiology, Risk Factors, Development, Symptoms and Diagnosis', *Cancers (Basel)*, 13.

Scheller, J., A. Chalaris, D. Schmidt-Arras, and S. Rose-John. 2011. 'The pro- and anti-inflammatory properties of the cytokine interleukin-6', *Biochim Biophys Acta*, 1813: 878-88.

Schneider, P., and J. Tschopp. 2000. 'Apoptosis induced by death receptors', *Pharm Acta Helv*, 74: 281-6.

Schuerwegh, A. J., E. J. Dombrecht, W. J. Stevens, J. F. Van Offel, C. H. Bridts, and L. S. De Clerck. 2003. 'Influence of pro-inflammatory (IL-1 alpha, IL-6, TNF-alpha, IFN-gamma) and anti-inflammatory (IL-4) cytokines on chondrocyte function', *Osteoarthritis Cartilage*, 11: 681-7.

Schulman, B. A., and J. W. Harper. 2009. 'Ubiquitin-like protein activation by E1 enzymes: the apex for downstream signalling pathways', *Nat Rev Mol Cell Biol*, 10: 319-31.

Schwabe, R. F., and D. A. Brenner. 2002. 'Role of glycogen synthase kinase-3 in TNF-alpha-induced NF-kappaB activation and apoptosis in hepatocytes', *Am J Physiol Gastrointest Liver Physiol*, 283: G204-11.

Sen, R., and D. Baltimore. 1986. 'Multiple nuclear factors interact with the immunoglobulin enhancer sequences', *Cell*, 46: 705-16.

Seol, J. E., J. Kim, B. H. Lee, D. Y. Hwang, J. Jeong, H. J. Lee, Y. O. Ahn, J. E. Lee, and D. H. Kim. 2020. 'Folate, alcohol, ADH1B and ALDH2 and colorectal cancer risk', *Public Health Nutr*: 1-8.

Seyedian, S. S., F. Nokhostin, and M. D. Malamir. 2019. 'A review of the diagnosis, prevention, and treatment methods of inflammatory bowel disease', *J Med Life*, 12: 113-22.

Shembade, N., A. Ma, and E. W. Harhaj. 2010. 'Inhibition of NF-kappaB signaling by A20 through disruption of ubiquitin enzyme complexes', *Science*, 327: 1135-9.

Shussman, N., and S. D. Wexner. 2014. 'Colorectal polyps and polyposis syndromes', *Gastroenterol Rep (Oxf)*, 2: 1-15.

Siegel, Rebecca L., Kimberly D. Miller, Hannah E. Fuchs, and Ahmedin Jemal. 2022. 'Cancer statistics, 2022', *CA: A Cancer Journal for Clinicians*, 72: 7-33.

Singh, R., A. Letai, and K. Sarosiek. 2019. 'Regulation of apoptosis in health and disease: the balancing act of BCL-2 family proteins', *Nat Rev Mol Cell Biol*, 20: 175-93.

Singh, S., and B. B. Aggarwal. 1995. 'Protein-tyrosine phosphatase inhibitors block tumor necrosis factor-dependent activation of the nuclear transcription factor NF-kappa B', *J Biol Chem*, 270: 10631-9.

Soares-Silva, M., F. F. Diniz, G. N. Gomes, and D. Bahia. 2016. 'The Mitogen-Activated Protein Kinase (MAPK) Pathway: Role in Immune Evasion by Trypanosomatids', *Front Microbiol*, 7: 183.

Sommariva, M., L. De Cecco, M. De Cesare, L. Sfondrini, S. Menard, C. Melani, D. Delia, N. Zaffaroni, G. Pratesi, V. Uva, E. Tagliabue, and A. Balsari. 2011. 'TLR9 agonists oppositely modulate DNA repair genes in tumor versus immune cells and enhance chemotherapy effects', *Cancer Res*, 71: 6382-90.

Sreenivasan, Y., A. Sarkar, and S. K. Manna. 2003. 'Mechanism of cytosine arabinoside-mediated apoptosis: role of Rel A (p65) dephosphorylation', *Oncogene*, 22: 4356-69.

Stow, J. L., P. C. Low, C. Offenhauser, and D. Sangermani. 2009. 'Cytokine secretion in macrophages and other cells: pathways and mediators', *Immunobiology*, 214: 601-12.

Strieter, R. M., J. A. Belperio, and M. P. Keane. 2002a. 'Cytokines in innate host defense in the lung', *J Clin Invest*, 109: 699-705.

Strieter, Robert M., John A. Belperio, and Michael P. Keane. 2002b. 'Cytokines in innate host defense in the lung', *Journal of Clinical Investigation*, 109: 699-705.

Sun, A., J. Tang, Y. Hong, J. Song, P. F. Terranova, J. B. Thrasher, S. Svojanovsky, H. G. Wang, and B. Li. 2008. 'Androgen receptor-dependent regulation of Bcl-xL expression: Implication in prostate cancer progression', *Prostate*, 68: 453-61.

Sung, B., M. K. Pandey, K. S. Ahn, T. Yi, M. M. Chaturvedi, M. Liu, and B. B. Aggarwal. 2008. 'Anacardic acid (6-nonadecyl salicylic acid), an inhibitor of histone acetyltransferase, suppresses expression of nuclear factor-kappaB-regulated gene products involved in cell survival, proliferation, invasion, and inflammation through inhibition of the inhibitory subunit of nuclear factor-kappaBalpha kinase, leading to potentiation of apoptosis', *Blood*, 111: 4880-91.

Sung, H., J. Ferlay, R. L. Siegel, M. Laversanne, I. Soerjomataram, A. Jemal, and F. Bray. 2021. 'Global Cancer Statistics 2020: GLOBOCAN Estimates of Incidence and Mortality Worldwide for 36 Cancers in 185 Countries', *CA Cancer J Clin*, 71: 209-49.

Swatek, K. N., and D. Komander. 2016. 'Ubiquitin modifications', *Cell Res*, 26: 399-422.

Tai, H. C., and E. M. Schuman. 2008. 'Ubiquitin, the proteasome and protein degradation in neuronal function and dysfunction', *Nat Rev Neurosci*, 9: 826-38.

Tan, Y., Q. Chen, X. Li, Z. Zeng, W. Xiong, G. Li, X. Li, J. Yang, B. Xiang, and M. Yi. 2021. 'Pyroptosis: a new paradigm of cell death for fighting against cancer', *J Exp Clin Cancer Res*, 40: 153.

Tang, W., Y. Li, D. Yu, A. Thomas-Tikhonenko, V. S. Spiegelman, and S. Y. Fuchs. 2005. 'Targeting beta-transducin repeat-containing protein E3 ubiquitin ligase augments the effects of antitumor drugs on breast cancer cells', *Cancer Res*, 65: 1904-8.

Thomson, A. W., P. J. O'Connell, R. J. Steptoe, and L. Lu. 2002. 'Immunobiology of liver dendritic cells', *Immunol Cell Biol*, 80: 65-73.

Thuduppathy, G. R., O. Terrones, J. W. Craig, G. Basanez, and R. B. Hill. 2006. 'The N-terminal domain of Bcl-xL reversibly binds membranes in a pH-dependent manner', *Biochemistry*, 45: 14533-42.

Tong, W., X. Chen, X. Song, Y. Chen, R. Jia, Y. Zou, L. Li, L. Yin, C. He, X. Liang, G. Ye, C. Lv, J. Lin, and Z. Yin. 2020. 'Resveratrol inhibits LPS-induced inflammation through suppressing the signaling cascades of TLR4-NF-kappaB/MAPKs/IRF3', *Exp Ther Med*, 19: 1824-34.

Ugai, T., J. P. Vayrynen, K. Haruki, N. Akimoto, M. C. Lau, R. Zhong, J. Kishikawa, S. A. Vayrynen, M. Zhao, K. Fujiyoshi, A. Dias Costa, J. Borowsky, K. Arima, J. L. Guerriero, C. S. Fuchs, X. Zhang, M. Song, M. Wang, M. Giannakis, J. A. Meyerhardt, J. A. Nowak, and S. Ogino. 2022. 'Smoking and Incidence of Colorectal Cancer Subclassified by Tumor-Associated Macrophage Infiltrates', *J Natl Cancer Inst*, 114: 68-77.

Ulanja, M. B., C. Ntafam, B. D. Beutler, D. Antwi-Amoabeng, G. A. Rahman, R. N. Ulanja, T. Mabrouk, S. B. Governor, F. T. Djankpa, and O. B. Alese. 2023. 'Race, age, and sex differences on the influence of obesity on colorectal cancer sidedness and mortality: A national cross-sectional study', *J Surg Oncol*, 127: 109-18.

Umare, V., V. Pradhan, M. Nadkar, A. Rajadhyaksha, M. Patwardhan, K. K. Ghosh, and A. H. Nadkarni. 2014. 'Effect of proinflammatory cytokines (IL-6, TNF-alpha, and IL-1beta) on clinical manifestations in Indian SLE patients', *Mediators Inflamm*, 2014: 385297.

Underhill, D. M., M. Bassetti, A. Rudensky, and A. Aderem. 1999. 'Dynamic interactions of macrophages with T cells during antigen presentation', *J Exp Med*, 190: 1909-14.

Underhill, D. M., and H. S. Goodridge. 2012. 'Information processing during phagocytosis', *Nat Rev Immunol*, 12: 492-502.

Urban, M. B., and P. A. Baeuerle. 1991. 'The role of the p50 and p65 subunits of NF-kappa B in the recognition of cognate sequences', *New Biol*, 3: 279-88.

Vallis, J., and P. P. Wang. 2022. 'The Role of Diet and Lifestyle in Colorectal Cancer Incidence and Survival.' in J. A. Morgado-Diaz (ed.), *Gastrointestinal Cancers* (Brisbane (AU)).

van de Veerdonk, F. L., M. G. Netea, C. A. Dinarello, and L. A. Joosten. 2011. 'Inflammasome activation and IL-1beta and IL-18 processing during infection', *Trends Immunol*, 32: 110-6.

Vanden Berghe, W., S. Plaisance, E. Boone, K. De Bosscher, M. L. Schmitz, W. Fiers, and G. Haegeman. 1998. 'p38 and extracellular signal-regulated kinase mitogen-activated protein kinase pathways are required for nuclear factor-kappaB p65 transactivation mediated by tumor necrosis factor', *J Biol Chem*, 273: 3285-90.

Venderbosch, S., J. H. de Wilt, S. Teerenstra, O. J. Loosveld, A. van Bochove, H. A. Sinnige, G. J.

Creemers, M. E. Tesselaar, L. Mol, C. J. Punt, and M. Koopman. 2011. 'Prognostic value of resection of primary tumor in patients with stage IV colorectal cancer: retrospective analysis of two randomized studies and a review of the literature', *Ann Surg Oncol*, 18: 3252-60.

Vieira, S. M., H. P. Lemos, R. Grespan, M. H. Napimoga, D. Dal-Secco, A. Freitas, T. M. Cunha, W. A. Verri, Jr., D. A. Souza-Junior, M. C. Jamur, K. S. Fernandes, C. Oliver, J. S. Silva, M. M. Teixeira, and F. Q. Cunha. 2009. 'A crucial role for TNF-alpha in mediating neutrophil influx induced by endogenously generated or exogenous chemokines, KC/CXCL1 and LIX/CXCL5', *Br J Pharmacol*, 158: 779-89.

Wang, L., C. Yin, T. Liu, M. Abdul, Y. Zhou, J. L. Cao, and C. Lu. 2020. 'Pellino1 regulates neuropathic pain as well as microglial activation through the regulation of MAPK/NF-kappaB signaling in the spinal cord', *J Neuroinflammation*, 17: 83.

Wang, Q., X. Shen, G. Chen, and J. Du. 2022. 'Drug Resistance in Colorectal Cancer: From Mechanism to Clinic', *Cancers (Basel)*, 14.

Wang, X., C. Smith, and H. Yin. 2013. 'Targeting Toll-like receptors with small molecule agents', *Chem Soc Rev*, 42: 4859-66.

Warner, K. D., C. E. Hajdin, and K. M. Weeks. 2018. 'Principles for targeting RNA with drug-like small molecules', *Nat Rev Drug Discov*, 17: 547-58.

Webster, J. D., and D. Vucic. 2020. 'The Balance of TNF Mediated Pathways Regulates Inflammatory Cell Death Signaling in Healthy and Diseased Tissues', *Front Cell Dev Biol*, 8: 365.

Whitmarsh, A. J., and R. J. Davis. 1996. 'Transcription factor AP-1 regulation by mitogen-activated protein kinase signal transduction pathways', *J Mol Med (Berl)*, 74: 589-607.

Wi, S. M., G. Moon, J. Kim, S. T. Kim, J. H. Shim, E. Chun, and K. Y. Lee. 2014. 'TAK1-ECSIT-TRAF6 complex plays a key role in the TLR4 signal to activate NF-kappaB', *J Biol Chem*, 289: 35205-14.

Win, A. K., R. J. Macinnis, J. L. Hopper, and M. A. Jenkins. 2012. 'Risk prediction models for colorectal cancer: a review', *Cancer Epidemiol Biomarkers Prev*, 21: 398-410.

Wong, R. S. 2011. 'Apoptosis in cancer: from pathogenesis to treatment', *J Exp Clin Cancer Res*, 30: 87.

Wu, M. H., P. Zhang, and X. Huang. 2010. 'Toll-like receptors in innate immunity and infectious diseases', *Front Med China*, 4: 385-93.

Wu, Y., X. Li, J. Jia, Y. Zhang, J. Li, Z. Zhu, H. Wang, J. Tang, and J. Hu. 2018. 'Transmembrane E3 ligase RNF183 mediates ER stress-induced apoptosis by degrading Bcl-xL', *Proc Natl Acad Sci U S A*, 115: E2762-E71.

Wynn, T. A., A. Chawla, and J. W. Pollard. 2013. 'Macrophage biology in development, homeostasis and disease', *Nature*, 496: 445-55.

Xiao, H., W. Qian, K. Staschke, Y. Qian, G. Cui, L. Deng, M. Ehsani, X. Wang, Y. W. Qian, Z. J. Chen, R. Gilmour, Z. Jiang, and X. Li. 2008. 'Pellino 3b negatively regulates interleukin-1-induced TAK1-dependent NF kappaB activation', *J Biol Chem*, 283: 14654-64.

Xiao, Y., J. Jin, M. Chang, J. H. Chang, H. Hu, X. Zhou, G. C. Brittain, C. Stansberg, O. Torkildsen, X. Wang, R. Brink, X. Cheng, and S. C. Sun. 2013. 'Peli1 promotes microglia-mediated CNS inflammation by regulating Traf3 degradation', *Nat Med*, 19: 595-602.

Xie, Y. H., Y. X. Chen, and J. Y. Fang. 2020. 'Comprehensive review of targeted therapy for colorectal cancer', *Signal Transduct Target Ther*, 5: 22.

Xu, Y., H. B. Ma, Y. L. Fang, Z. R. Zhang, J. Shao, M. Hong, C. J. Huang, J. Liu, and R. Q. Chen. 2017. 'Cisplatin-induced necroptosis in TNFalpha dependent and independent pathways', *Cell Signal*, 31: 112-23.

Xu, Y., H. Ma, J. Shao, J. Wu, L. Zhou, Z. Zhang, Y. Wang, Z. Huang, J. Ren, S. Liu, X. Chen, and J. Han. 2015. 'A Role for Tubular Necroptosis in Cisplatin-Induced AKI', *J Am Soc Nephrol*, 26: 2647-58.

Xu, Y., H. Yan, X. Zhang, J. Zhuo, Y. Han, H. Zhang, D. Xie, X. Lan, W. Cai, X. Wang, S. Wang, and X. Li. 2022. 'Roles of Altered Macrophages and Cytokines: Implications for Pathological Mechanisms of Postmenopausal Osteoporosis, Rheumatoid Arthritis, and Alzheimer's Disease', *Front Endocrinol (Lausanne)*, 13: 876269.

Yamin, T. T., and D. K. Miller. 1997. 'The interleukin-1 receptor-associated kinase is degraded by proteasomes following its phosphorylation', *Journal of Biological Chemistry*, 272: 21540-47.

Yang, S., B. Wang, F. Humphries, A. E. Hogan, D. O'Shea, and P. N. Moynagh. 2014. 'The E3 ubiquitin ligase Pellino3 protects against obesity-induced inflammation and insulin resistance', *Immunity*, 41: 973-87.

Yang, S., B. Wang, F. Humphries, R. Jackson, M. E. Healy, R. Bergin, G. Aviello, B. Hall, D. McNamara, T. Darby, A. Quinlan, F. Shanahan, S. Melgar, P. G. Fallon, and P. N. Moynagh. 2013. 'Pellino3 ubiquitinates RIP2 and mediates Nod2-induced signaling and protective effects in colitis', *Nat Immunol*, 14: 927-36.

Yang, Z., J. Liao, K. J. Cullen, and H. Dan. 2020. 'Inhibition of IKKbeta/NF-kappaB signaling pathway to improve Dasatinib efficacy in suppression of cisplatin-resistant head and neck squamous cell carcinoma', *Cell Death Discov*, 6: 36.

Yaron, A., H. Gonen, I. Alkalay, A. Hatzubai, S. Jung, S. Beyth, F. Mercurio, A. M. Manning, A. Ciechanover, and Y. Ben-Neriah. 1997. 'Inhibition of NF-kappa-B cellular function via specific targeting of the I-kappa-B-ubiquitin ligase', *EMBO J*, 16: 6486-94.

Yesudhas, D., V. Gosu, M. A. Anwar, and S. Choi. 2014. 'Multiple roles of toll-like receptor 4 in colorectal cancer', *Front Immunol*, 5: 334.

Yu, G. H., S. F. Li, R. Wei, and Z. Jiang. 2022. 'Diabetes and Colorectal Cancer Risk: Clinical and Therapeutic Implications', *J Diabetes Res*, 2022: 1747326.

Yu, H., L. Lin, Z. Zhang, H. Zhang, and H. Hu. 2020. 'Targeting NF-kappaB pathway for the therapy of diseases: mechanism and clinical study', *Signal Transduct Target Ther*, 5: 209.

Yu, K. Y., H. J. Kwon, D. A. Norman, E. Vig, M. G. Goebl, and M. A. Harrington. 2002. 'Cutting edge: mouse pellino-2 modulates IL-1 and lipopolysaccharide signaling', *J Immunol*, 169: 4075-8.

Yu, P., X. Zhang, N. Liu, L. Tang, C. Peng, and X. Chen. 2021. 'Pyroptosis: mechanisms and diseases', *Signal Transduct Target Ther*, 6: 128.

Yu, T., Q. Lu, X. Ou, D. Cao, and Q. Yu. 2014. 'Association of sedentary behavior with the expression levels of biomarkers in colorectal cancer: clinical analysis of 228 patients', *Tohoku J Exp Med*, 232: 167-76.

Yuan, H., Q. Dong, B. Zheng, X. Hu, J. B. Xu, and S. Tu. 2017. 'Lymphovascular invasion is a high risk factor for stage I/II colorectal cancer: a systematic review and meta-analysis', *Oncotarget*, 8: 46565-79.

Zakeri, A., and M. Russo. 2018. 'Dual Role of Toll-like Receptors in Human and Experimental

Asthma Models', *Front Immunol*, 9: 1027.

Zaman, S., R. Wang, and V. Gandhi. 2014. 'Targeting the apoptosis pathway in hematologic malignancies', *Leuk Lymphoma*, 55: 1980-92.

Zhang, E., and X. Li. 2022. 'The Emerging Roles of Pellino Family in Pattern Recognition Receptor Signaling', *Front Immunol*, 13: 728794.

Zhao, W., L. Wang, M. Zhang, C. Yuan, and C. Gao. 2012. 'E3 ubiquitin ligase tripartite motif 38 negatively regulates TLR-mediated immune responses by proteasomal degradation of TNF receptor-associated factor 6 in macrophages', *J Immunol*, 188: 2567-74.

Zheng, C., J. Chen, F. Chu, J. Zhu, and T. Jin. 2019. 'Inflammatory Role of TLR-MyD88 Signaling in Multiple Sclerosis', *Front Mol Neurosci*, 12: 314.

Zheng, D., T. Liwinski, and E. Elinav. 2020. 'Inflammasome activation and regulation: toward a better understanding of complex mechanisms', *Cell Discov*, 6: 36.

Zheng, T., Y. Zhou, X. Xu, X. Qi, J. Liu, Y. Pu, S. Zhang, X. Gao, X. Luo, M. Li, X. Wang, L. Dong, Y. Wang, and C. Mao. 2022. 'MiR-30c-5p loss-induced PELI1 accumulation regulates cell proliferation and migration via activating PI3K/AKT pathway in papillary thyroid carcinoma', *J Transl Med*, 20: 20.

Zhou, H., D. M. Monack, N. Kayagaki, I. Wertz, J. Yin, B. Wolf, and V. M. Dixit. 2005. 'Yersinia virulence factor YopJ acts as a deubiquitinase to inhibit NF-kappa B activation', *J Exp Med*, 202: 1327-32.

Zhou, L., Q. Ma, H. Shi, and K. Huo. 2010. 'NUMBL interacts with TRAF6 and promotes the degradation of TRAF6', *Biochem Biophys Res Commun*, 392: 409-14.

Zhuang, L., C. S. Lee, R. A. Scolyer, S. W. McCarthy, X. D. Zhang, J. F. Thompson, and P. Hersey. 2007. 'Mcl-1, Bcl-XL and Stat3 expression are associated with progression of melanoma whereas Bcl-2, AP-2 and MITF levels decrease during progression of melanoma', *Mod Pathol*, 20: 416-26.

Ziegler, U., and P. Groscurth. 2004. 'Morphological features of cell death', *News Physiol Sci*, 19: 124-8.